Modulation of neuronal function by tau, alpha synuclein or carbon dioxide

by

Emily Hill

A Thesis Submitted

For the degree of Doctor of Philosophy in Neuroscience

School of Life Sciences,

University of Warwick

Coventry, United Kingdom

March 2021

Table of Contents

List of Figures

List of Tables

Acknowledgements

Firstly, I would like to thank my supervisor, Dr Mark Wall, whose knowledge, and passion for science is a constant source of inspiration. His friendly, supportive nature has allowed me to grow and develop into a confident researcher. I want to thank him for giving me the freedom to drive our projects off in different directions, to test my own ideas and for always motivating me to be my best. Here's to many more years of working together!

I would also like to thank my second supervisor Magnus Richardson for patiently explaining both maths and modelling to me slowly until my brain could keep up. Thank you for your support and guidance over the last 4 years. Further thanks go to the members of my advisory panel, Professor Nicholas Dale and Dr Yuriy Pankratov for their constructive feedback and for challenging me to ensure my work is as good as it can be. I would like to thank Professor Kevin Moffat and Dr Tommy Karikari for providing the first tau samples when I started in the lab. This initial idea for a collaboration has led to so many exciting discoveries over the last 3 years. I would also like to thank Professor Jaime McCutcheon who mentored my first PhD mini-project, giving me my first experience of life in the lab. Further thanks go to Ian Hands-Portman and Saskia Bakker for their training on the confocal and electron microscopes and to Sam Dixon, Sarah Stanley and the BSU staff for their friendly greetings and help with the animals.

I have been lucky enough to have the opportunity to establish many independent collaborations over the last 3 years which have allowed me both to expand my field of knowledge and to build my skillset further. I would like to thank Dr. George Tetz, Dr Joanna Collingwood, Jake Brookes, Dr Thomas Karikari, Professor Henrik Zetterberg, Professor Kaj Blennow and Professor Richard Napier for allowing me to join your teams and trusting me with your research projects.

I would also like to thank my funding body: The Biotechnology and Biological Sciences Research Council (BBSRC) for funding this research through their Midlands Integrative Biosciences Training Partnership (MIBTP) doctoral training programme and Alzheimer's research UK for supporting this work.

The last four years would not have been possible without the amazing group of both current and previous lab members in C116 and C117. A special thank you to Pippa, Mónica, Martina, Dan, Caitlin, and Emma for making the last 4 years lively and fun and for always being up for an emergency tea break when one of us was having a bad day or needed advice.

I also wish to thank my family and friends who have supported me every step along this crazy journey. Firstly, to my wonderful fiancé Marcus for always being there to celebrate the good days and cheer me up on the stressful ones. For putting up with me when I take on crazy challenges like writing an entire grant in 24 hours and for embracing the passion that I have for my work. Also, to Poppy, Fudge and Pepper for all the fluffy cuddles while writing this thesis and for keeping me sane on the tougher days. A further thank you to Hannah, Amy, Alice, Sarah, and Luke – thank you for always looking interested while you listen to me ramble on about neurons. I couldn't have completed this without your friendship, encouragement, and our impromptu cocktail evenings!

Finally, I want to thank my parents for being a constant source motivation, love, and support over the years. Thank you for always believing in me! To my dad who has bravely battled Parkinson's disease for 14 years now, you are the reason I am in research and fighting to try and uncover what's going on in these horrible diseases. Your determination and drive to beat it inspires me every day. This one's for you dad!

Declaration

I, Emily Hill, hereby declare that, to the best of my knowledge, the material contained I this thesis is original and my own unless otherwise indicated, cited, or commonly known. I confirm that this thesis has not been previously submitted for any degree at this or any other institution.

'Parts of this thesis have been published by the author':

1. **Hill, E.,** Karikari, T., Moffat, K., Richardson, M. and Wall, M. (2019). Introduction of Tau Oligomers into Cortical Neurons Alters Action Potential Dynamics and Disrupts Synaptic Transmission and Plasticity. eNeuro, 6(5), pp. eNEURO.0166-19.2019
2. **E. Hill,** C. Hickman, R. Diez, M. Wall (2020) Role of A1 receptor activated GIRK channels in the suppression of hippocampal seizure activity Neuropharmacology, 164, p. 107904
3. **Hill, E.,** Dale, N. and Wall, M., (2020). Moderate Changes in CO_2 Modulate the Firing of Neurons in the VTA and Substantia Nigra. iScience, 23(7), p.101343.
4. **Hill, E,** Gowers, R, Richardson, M.J., Wall. M. J, (2020) Alpha-synuclein aggregates increase the conductance of substantia nigra dopamine neurons, an effect partly reversed by the K_{ATP} channel inhibitor glibenclamide. eNeuro.0330-20.2020
5. **Hill, E.,** Wall, M., Moffat, K. and Karikari, T., (2020). Understanding the Pathophysiological Actions of Tau Oligomers: A Critical Review of Current Electrophysiological Approaches. Frontiers in Molecular Neuroscience, 13.
6. **Hill, E**., Dale, N. and Wall, M., (2020). Detecting CO_2-Sensitive Hemichannels in Neurons in Acute Brain Slices. Star Protocols.

7. Karikari, T., Keeling, S., **Hill, E.,** Lantero Rodriguez, J., Nagel, D., Becker, B., Höglund, K., Zetterberg, H., Blennow, K., Hill, E. and Moffat, K., (2020). An extensive plasmid library to prepare tau protein variants and study their functional biochemistry. ACS Chemical Neuroscience.

Submitted (in review/press)

8. Wall, M., **Hill, E.,** Huckstepp, R., Deganutti, G. *et al.* (2020) A biased adenosine A1R agonist elicits analgesia without cardiorespiratory depression BioRxiv 10.1101/2020.04.04.023945 (in review)
9. **Hill, E**., Moffat, K, G., Wall, M, J., Zetterberg, H., Blennow, K., Karikari, T, K., (2021a) 'Functional applications of stable tau oligomers in cell biology and electrophysiology studies', *Methods in Mol Biology*. (in review)
10. **Hill, E**., Moffat, K, G., Wall, M, J., Zetterberg, H., Blennow, K., Karikari, T, K., (2021b) 'A validated method for producing stable tau oligomers, *Methods in Mol Biology,* Springer protocols. (in review)
11. **Hill, E.,** Karikari, T, K., Lantero-Rodriguez, J., Zetterberg, H., Blennow, K., Richardson, M. J., Wall, M. J. (2021) Truncating Tau Reveals Different Pathophysiological Actions of Oligomers in Single Neurons. (in review)
12. **Hill, E**., Dale, N. and Wall, M., (2021). CO_2 sensitive connexin hemichannels in neurons and glia: three different modes of signalling? (in review)

Abstract

The misfolding and aggregation of protein is a characteristic hallmark of neurodegenerative disorders, most notably of amyloid beta and tau in Alzheimer's disease and alpha synuclein in Parkinson's disease. There is gathering evidence that early soluble aggregates of these proteins are the most toxic species. In this thesis I have used whole-cell patch clamp recording to quantitively analyse the cellular and sub-cellular effects of introducing tau or alpha synuclein aggregates on neuronal or synaptic function in single neurons.

I have demonstrated that full-length tau oligomers (oTau) induce marked changes to action potential dynamics, synaptic transmission and plasticity that were not observed with monomeric tau. Consistent with these electrophysiological changes, oTau could diffuse from the injection site (soma) to synaptic sites within 30 minutes of recording. This study had provided valuable new insight into the actions of tau oligomers within single neurons. I then looked to define the mechanisms underlying these changes using tau truncations. C^{FRAG} (aa124-444) oTau caused a shift in the spike-initiation threshold, mediating the increase in excitability. While N^{FRAG} (aa1-123) tau aggregates and monomers both resulted in comparable changes to AP waveform as full length-oTau. Recording isolated voltage-gated sodium channels highlighted a tau-mediated reduction in both the half-activation and maximal sodium channel conductance.

Using the same method, I have demonstrated that introduction of aggregated αSyn into dopaminergic neurons in the substantia nigra significantly increased conductance and decreased excitability, an effect which could be partially prevented by pre-incubation of the slices with Glibenclamide. While evaluating these neurons, I discovered that they have an unexpected connexin hemichannel-mediated CO_2-sensitivity phenotype. These cells are located in regions of the brain that are involved in movement, reward, and arousal behaviour. Physiological changes in PCO_2 markedly altered whole-cell conductance and excitability. This work suggests a mechanism by which CO_2, could alter complex goal-directed behaviours.

Abbreviations

αSyn – Alpha synuclein

AADC - Aromatic Amino Acid Decarboxylase

aCSF – Artificial cerebral spinal fluid

AD – Alzheimer's disease

AMPA - α-Amino-3-hydroxy-5-methyl-4-isoxazolepropionic acid

AP – Action potential

APOE – apolipoprotein-E

APP – Amyloid precursor protein

ATP - Adenosine triphosphate

Aβ – Amyloid Beta

BNST - Bed Nucleus of the Stria Terminalis

C – Capacitance

CA1 - Cornu Ammonis 1

CA2 - Cornu Ammonis 2

CA3 - Cornu Ammonis 3

cAMP – Cyclic Adenosine Monophosphate

CBF - 5(6)-Carboxyfluorescein

CCD - charge-coupled device

CDNF - Cerebral dopamine neurotrophic factor

CeA - Central Nucleus of the Amygdala

C^{FRAG} – N-terminal truncation (aa 124-441)

CM – Centromedian nucleus

CO_2 – Carbon dioxide

COMT - Catechol-O-methyltransferase

COPD - Chronic obstructive pulmonary disease

CREB - cAMP-response element binding

CSF - Cerebral spinal fluid

Cx26 – Connexin 26

Cx30 – Connexin 30

Cx32 – Connexin 32

DDS – Drug Delivery system

ΔT – Spike-onset sharpness

DG – Dentate Gyrus

DHPG - 3,5-Dihydroxyphenylglycine

DIV – Dynamic IV

DN – Dopaminergic Neuron

DRN – Dorsal Raphe Nucleus

DTT - Dithiothreitol

E (mV) – Resting membrane potential

EC - entorhinal cortex

EIF – Exponential Integrate and Fire

EM – Electron Microscopy

EPSP – Excitatory Post Synaptic Potential

ER – Endoplasmic Reticulum

fAHP – Fast Afterhyperpolarisation Potential

FISH - Fluorescence in situ hybridization

FITC - Fluorescein isothiocyanate

FL – Full Length

FR – Firing Rate

FSCV – Fast Scan Cyclic Voltammetry

GABA - Gamma aminobutyric acid

GDNF - Glial Cell-Derived Neurotrophic Factor.

GFAP - Glial fibrillary acidic protein

GFP – Green Fluorescent protein

GIRK - G protein-coupled inwardly rectifying potassium channel

GPe - Globus pallidus, external segment

GPi - Globus pallidus, internal segment

HRP - Horseradish Peroxidase

IH - hyperpolarization-activated current

IPTG – Isopropyl β- d-1-thiogalactopyranoside

K_{ATP} - ATP-sensitive potassium channel

KLD – Kinase-Ligase-DpnI

KO – Knockout

LB – Lewy body

LB – Luria Broth

L-DOPA - l-3,4-dihydroxyphenylalanine

LH – Lateral Hypothalamus

LhB - Lateral Habenula

LTD – Long-term depression

LTP – Long- term potentiation

MAO - Monoamine oxidase

MAPT- Microtubule associated protein tau

MCI – Mild Cognitive Impairment

MF – Mossy Fibres

mGLuR - Metabotropic Glutamate Receptors

MML – Middle molecular layer

MPTP - 1-methyl-4-phenyl-1,2,3,6-tetrahydropyridine

MSK1 - Mitogen- and stress-activated protein kinase 1

mTau – tau monomers

MWCO – Molecular Weight Cut Off

NAc – Nucleus Accumbens Core

NAs - Nucleus Accumbens Shell

N^{FRAG} - C-terminal truncation (aa 1-123)

NFTs – Neurofibrillary tangles

NMDAR - N-methyl-D-aspartate receptor

NT – Noisy Trace

OD – Optical Density

oTau – tau oligomers

PAG - Periaqueductal Gray

PC – Pyramidal Cell

PCO_2 - Partial Pressure of Carbon Dioxide

PD – Parkinson's disease

PET – Positron emission tomography

PFC - Prefrontal cortex

PFFs – Pre-formed Fibrils

PP – Perforant Pathway

PPN - Pedunculopontine nucleus

PS – Presenilin

PSD95 - Postsynaptic density protein 95

RT-PCR - Reverse transcription PCR

rEIF – Refractory Exponential Integrate and Fire

RFP – Red Fluorescent Protein

Rin – Input resistance

ROS – Reactive Oxygen Species

Rs – Series resistance

SC – Schaffer collaterals

SDM – Site-Directed Mutagenesis

SDS-PAGE - Sodium Dodecyl Sulphate-Polyacrylamide Gel Electrophoresis

SIV – Standard IV

SNARE - SNAP Receptor

SNpc – Substantia Nigra pars compacta

SNpr – Substantia Nigra pars reticula

STN - Subthalamic nucleus

STP – Short-term potentiation

TA - Temperoammonic

TBST - Tris-buffered saline Tween

TEM – Transmission Electron Microscopy

TH – Tyrosine Hydroxylase

UPDRS – Unified Parkinson's Disease rating scale

UPR – unfolded protein response

VA/VL - Ventral anterior/ ventral lateral nucleus

VGAT - Vesicular GABA transporter

VP - Ventral Pallidum

VT – Spike threshold

VTA – Ventral Tegmental area

WT – Wild type

Introduction

Neurodegenerative disorders such as Alzheimer's disease (AD) and Parkinson's disease (PD) are both characterised pathologically by the misfolding and aggregation of native proteins. In AD, amyloid beta aggregates to form plaques and tau aggregates to form neurofibrillary tangles. In PD, alpha synuclein aggregates and accumulates within Lewy Body inclusions. While the presence of these large inclusions is well documented, there is gathering evidence that early soluble aggregates of these proteins are the most toxic species in pathology. There is relatively little understanding of the mechanisms of action of these small, soluble aggregates on neuronal function early in disease. In this thesis I have used whole-cell patch clamp recording to quantitively analyse the cellular and sub-cellular effects of introducing tau into cortical neurons (Chapter 3 and 4) or alpha synuclein aggregates into dopaminergic neurons (Chapter 5) on neuronal or synaptic function. While evaluating these dopaminergic neurons, I discovered that they, along with a neighbouring population of GABAergic neurons are unexpectedly sensitive to physiological changes in the level of CO_2. I have therefore gone on to characterise this phenotype and explored the underlying mechanisms (Chapter 6).

Parts of this chapter have been published previously: (Hill et al, 2020, Review)

1.1 Tau and associated tauopathies

1.1.1 Tau - physiology and pathology

Tau is a native human protein that is encoded by the microtubule associated protein tau (MAPT) gene. There are six isoforms in the human brain which are differentially expressed during development (Goedert et al., 1989, 1988; Goedert and Jakes, 2005). The N-terminal region can have 0, 1 or 2 inserts between amino acids 45 and 103, which results in 0N, 1N or 2N tau (Fig 1.1). The mid-region of tau is rich in prolines, as well as serine and threonine residues, which are strong targets for phosphorylation and have been linked to many physiological and pathophysiological cellular processes (Hampel et

al., 2010; Hanger et al., 2007; Stoothoff and Johnson, 2005; Wang et al., 2013). At the C-terminus of tau there are four pseudo-repeat domains, often referred to as R1-R4 (Fig 1.1), which form the microtubule binding domain. In its monomeric form, full length (2N4R) tau is intrinsically disordered with little to no secondary structure (Barghorn et al., 2004; Cleveland et al., 1977; Mirbaha et al., 2018; Mukrasch et al., 2009).

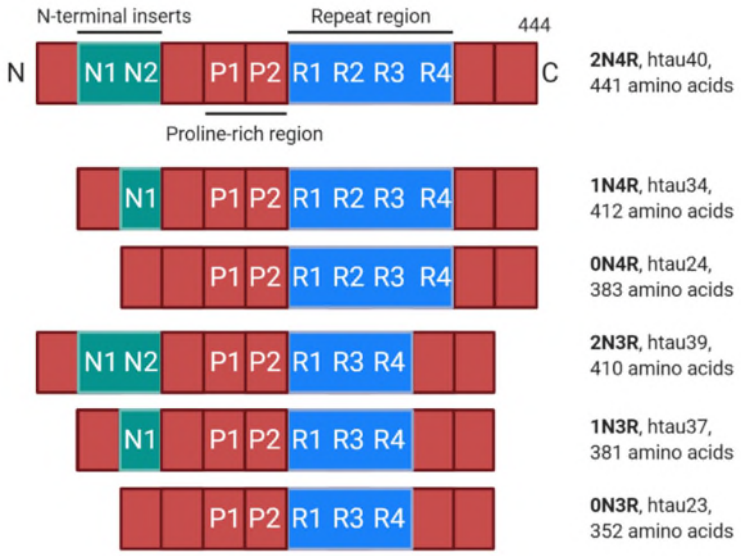

Figure 1.1: The six isoforms of tau protein in the human brain.
Alternative splicing produces six different isoforms of tau which differ by their composition of N and C terminal inserts (0N3R, 1N3R, 2N3R, 0N4R, 1N4R, 2N4R). 2N4R tau represents the full-length protein, also referred to as htau40 or tau441, and is the most commonly found isoform in the human brain. Figure adapted from (Karikari, 2017).

1.1.2 Physiological functions of tau

Primarily tau associates with the labile domain of microtubules, modulating their stability (Tracy and Gan, 2018; Fig 1.2) with a reduction in binding leading to enhanced rigidity, poorer flexibility and control (Qiang et al., 2018). Tau also regulates axonal transport (Fig 1.2), both from the axon to the soma (retrograde; Dixit et al, 2008) and from the soma to the axon (anterograde; Stamer et al., 2002). It can either act as a competitor for the binding sites of kinesin or dynein on the microtubules or it can bind directly to dynein (Magnani et al., 2007) or to the N-terminus of kinesin and modulate their activity directly (Kanaan et al., 2011). Tau can also be found in the nucleus and in the

dendrites. In dendrites it can assist with the spine remodelling that occurs during synaptic plasticity (Frandemiche et al., 2014; Regan et al., 2015; Fig 1.2). In the nucleus of human neuroblastoma cells, tau has been shown to contribute to the regulation of the integrity of genomic DNA (Loomis et al., 1990; Fig 1.2).

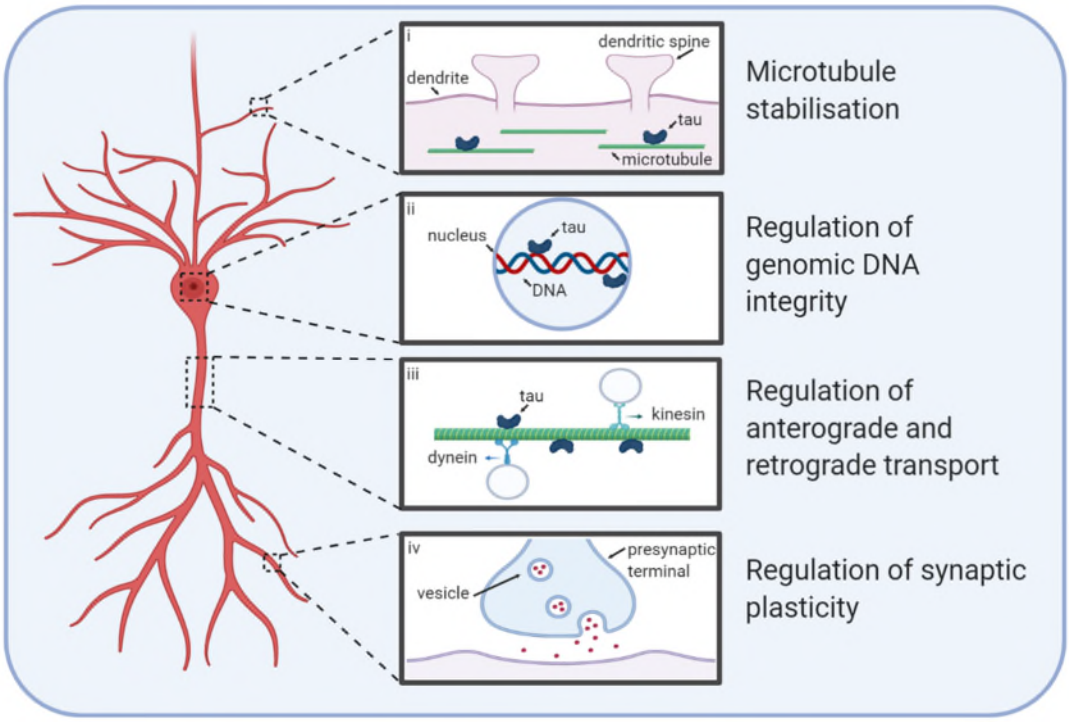

Figure 1.2: Tau in neuronal physiology.

The most prominent function is its modulation of microtubule stability (i). (ii) Tau regulates the integrity of genomic DNA in the nucleus by binding to different chromosomal regions. (iii) It also regulates axonal transport between the axon and soma by interfering with the binding of motor proteins kinesin and dynein to microtubules (iv) Finally, tau plays important roles in the regulation of synaptic plasticity at both pre- and postsynapses, for example by its contribution to the process of spine remodeling. Design concept from Wang and Mandelkow (2016).

1.1.3 Pathological cascade leading to tangles.

Physiologically, tau can undergo different post-translational modifications including phosphorylation, acetylation, and ubiquitination (Alonso et al., 2016; Beharry et al., 2014). The targeted binding and un-binding of tau to microtubules is mediated by the level of phosphorylation and must be finely

balanced in order to regulate its function (Fig 1.3). This balance is maintained by the counter-activity of kinases and phosphatases on specific residues of the tau protein and a number of these phosphorylation residues have been linked to tau functionality (Stoothoff and Johnson, 2005).

In disease states, the balance between phosphorylation and de-phosphorylation becomes dysregulated, leading to increased abnormal 'hyper' phosphorylated tau (Köpke et al., 1993). This hyperphosphorylated tau dissociates from microtubules and can sequester other monomeric tau molecules away from tubulin, disrupting microtubule function (Qiang et al., 2018). This disassociated monomeric tau is initially aggregation incompetent (Mirbaha et al., 2018) and has to undergo monomer-monomer interactions either via disulphide bonding or via its hexapeptide motifs to drive a conformational change from an unfolded, disordered structure to a new structured conformation that is rich in beta-sheets and aggregation-competent (Congdon et al., 2008; Friedhoff et al., 1998). This marks the beginning of the conventional pathological cascade starting with the aggregation to small soluble oligomeric structures, through to fibrils and then on to neurofibrillary tangles (NFTs; Avila et al., 2006; Maeda et al., 2006; Fig 1.3). This pathological cascade for tau is common to several disorders, collectively termed tauopathies. Until relatively recently, NFTs were thought to be the major toxic species, as their presence correlates well with disease progression and they are the most well characterised form of brain tau pathology (Braak and Braak, 1991). However the initial soluble tau oligomers (oTau), which are formed much earlier in the aggregation process, have been highlighted as more potent drivers of toxicity (Andorfer et al., 2003; Cowan et al., 2010; Lee et al., 2001; Spires et al., 2006; Tanemura et al., 2002; Tatebayashi et al., 2002; Wittmann et al., 2001; Yoshiyama et al., 2007). This theory is supported by the discovery of certain forms of tau that can form pathological (soluble) oligomers with functional implications but cannot aggregate any further into fibrils and NFTs (Karikari et al., 2019; Lasagna-Reeves et al., 2014, 2010).

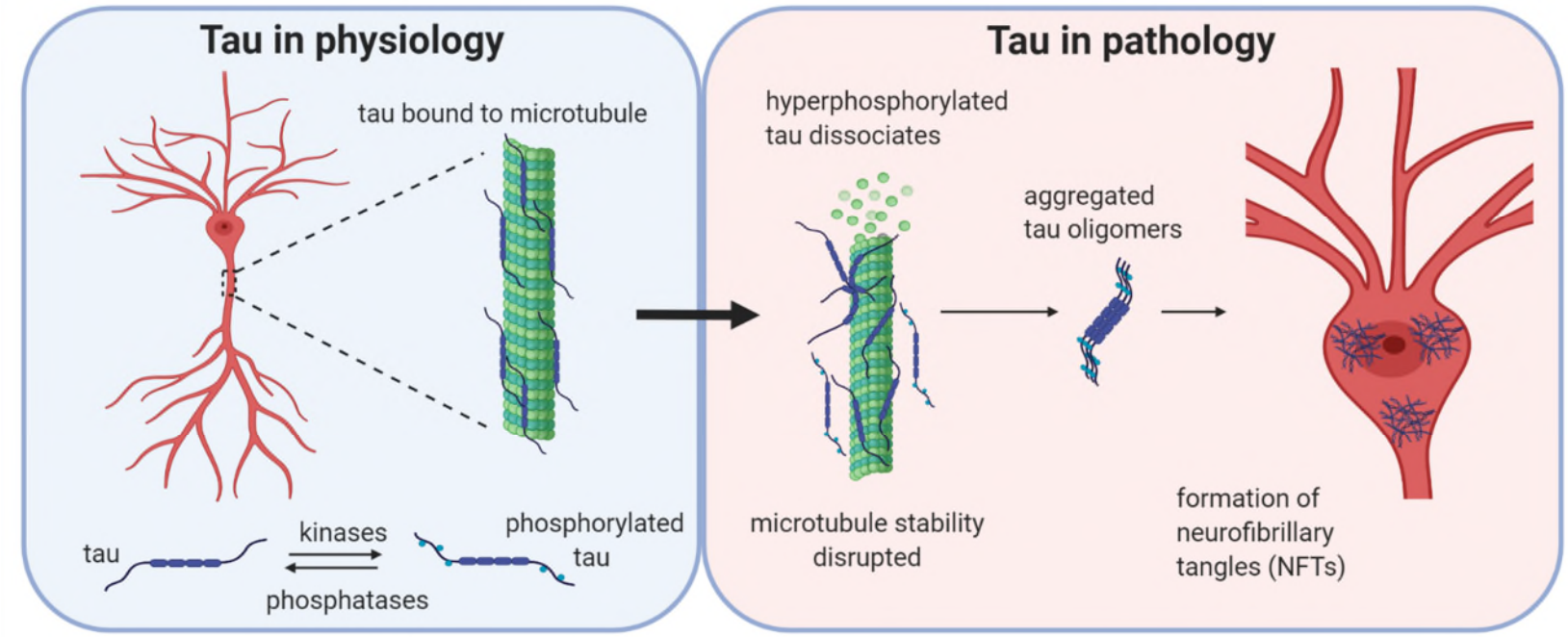

Figure 1.3: Tau in physiology and pathophysiology.

Under physiological conditions, tau is bound to microtubules and the stability is maintained by the balanced activities of kinases and phosphatases acting to regulate the binding of tau to the microtubules. If the balance is altered in favour of increased kinase activity, then tau can become hyperphosphorylated and detach from the microtubules. Initially, monomers are aggregation incompetent and have to undergo a conformational change using interactions via their hexapeptide motif or by disulphide bonding. Tau can then form aggregates, firstly small soluble oligomers which are β-sheet-rich and are thought to be the smallest toxic species. Subsequently, these species aggregate further into protofibrils, fibrils and finally into neurofibrillary tangles (NFTs).

1.1.4 Pathological actions of tau

Pathologically tau can cause cellular disruption by a host of mechanisms, depending on its cellular location. Tau can undergo a range of post-translational modifications including ubiquitination, acetylation or truncation. All of which can enhance detachment from microtubules and impairment of function. Once detached the pathological tau can mislocalise around the cell.

Tau can disrupt long term plasticity (both long-term potentiation and long-term depression) by its actions at postsynaptic sites. Hoover et al., (2010) demonstrated that this synaptic dysfunction precedes any visible neurodegeneration and that these are amongst the earliest detectable changes in many tauopathies. Post-synaptic mislocalisation of tau aggregates occurs much earlier than the loss of spines. In the P301L (human tau) mutant mouse, tau mislocalisation could be observed at post synaptic compartments and at pre-synapses by as early as 3-months, it was only at 18 months that synaptic loss begins. Pickett et al., (2017) further demonstrated that there is spread of the human tau between neurons of the middle molecular layer (MML) of the dentate gyrus at this stage – highlighting that this mislocalisation, and synaptic spread will occur in the early stages of the disease. Tau-mediated postsynaptic dysfunction has been confirmed both in *in vitro* and *in vivo* studies (Hill et al., 2019; Hoover et al., 2010; Lasagna-Reeves et al., 2012; Mondragón-Rodríguez et al., 2018; Ondrejcak et al., 2018; Puzzo et al., 2017; Rocher et al., 2010; Tai et al., 2014; Tamagnini et al., 2017; Thies and Mandelkow, 2007).

Although the postsynaptic roles of tau are more established, emerging evidence has also highlighted its roles in the disruption of presynaptic function. Tau accumulates in presynaptic terminals and can lead to a reduction in the number of vesicles available for release, inducing synaptic dysfunction and eventually leading to the loss of synapses (Decker et al., 2015). Tau can bind by its N-terminus to vesicles and by its C-terminus to actin filaments, cross-linking them and slowing down their movement. This leads to a reduction in presynaptic vesicle release (Fig 1.4). This could be reversed by removing the N-terminal region or by targeting with a peptide to bind and block the binding

site on the vesicles (McInnes et al., 2018; Zhou et al., 2017). Although phosphorylated tau cannot enter the nucleus, it can interact directly with the nuclear pore complex and disrupt nuclear transport (Eftekharzadeh et al., 2018; Fig 1.4). The sequestration of physiological tau into pathological aggregates will also limit the availability of normal tau to enter the nucleus and fulfil its roles in maintaining DNA integrity (Sultan et al., 2011). In cell culture experiments, it has been shown that small soluble tau oligomers are applied onto stem cell-derived cortical neurons or human neuroblastoma cells, some oligomers can be taken up into the nuclei so they may also have inter-nuclear effects (Evans et al., 2018; Karikari et al., 2019b, 2019a; Puangmalai et al., 2020; Usenovic et al., 2015; Wegmann et al., 2016).

1.1.5 Tau in co-operation with other proteins

Amyloid beta (Aβ) is produced by the proteolytic cleavage of amyloid precursor protein (APP), which is synthesised in the cell body and then conveyed by vesicular axonal transport to presynaptic terminals. APP is normally inserted into the presynaptic membrane and removed by endocytosis; in the endosome it is cleaved to make Aβ by secretases. There are two main forms of Aβ which differ depending on the patten of secretase activity that cleave the APP to produce them. Gamma secretase will always cleave APP first. If this is followed by alpha secretase, the non-amyloidogenic form of Aβ (Aβ40) will be produced. However it is followed by beta secretase, then the amlyoidogenic form of Aβ (Aβ42) will be produced instead (Cai et al., 1993; Citron et al., 1992; Suzuki et al., 1994). Both forms of Aβ (Aβ40/ Aβ42) are found in AD patients and healthy controls, but the ratio of Aβ42 to Aβ40 can be used as a maker of disease progression. (Haass et al., 1992; Seubert et al., 1992; Shoji et al., 1992). In healthy individuals, CSF has soluble Aβ of which 90% is Aβ40 and the remaining 10% is Aβ42 (more hydrophobic and more prone to aggregation). As plaques are formed, soluble Aβ42 levels drop in the CSF can be used as a biomarker for AD. Aβ will aggregate through a similar cascade to tau, through fibrils to large insoluble aggregates called plaques (Masters et al., 1985) which are largely not expected to be toxic due to their folded nature rendering the reactive surfaces inaccessible. An early intermediary to this aggregation

process is oligomers, which like tau, are soluble and highly toxic (Walsh et al., 2002).

Aβ can accelerate the phosphorylation of tau in the early stages, causing its dissociation and aggregation (Lewis et al., 2001). However, in the later stages of tau pathology (NFTs) this is independent of Aβ pathology and in fact NFT pathology tracks with disease progression much better than Aβ pathology (Lue et al., 1999; McLean et al., 1999; Näslund et al., 2000; Wang et al., 1999).

Tau can act together with amyloid beta (Aβ) oligomers to disrupt synaptic function. Co-treatment with Aβ oligomers and tau aggregates leads to tau mis-sorting to dendrites which triggers the translocation of tubulin tyrosine ligase-like enzyme 6 (TTLL6) into dendrites, which subsequently leads to the degradation of microtubules by Spastin, further damaging their integrity (Zempel et al., 2013). Dendritic aggregated tau can also act as a scaffold for the non-receptor-associated tyrosine kinase FYN. FYN is responsible for phosphorylating subunit 2 of the NMDA receptor (NMDAR), which leads to the stabilisation of the interaction between PSD95 and the NMDAR. By binding, it will enhance signalling and could contribute to the excitotoxicity that is reported with Aβ oligomers. Thus, the excitotoxicity caused by Aβ oligomers could depend on the co-presence of tau oligomers (Ittner et al., 2010; Roberson et al., 2007; Fig 1.4)

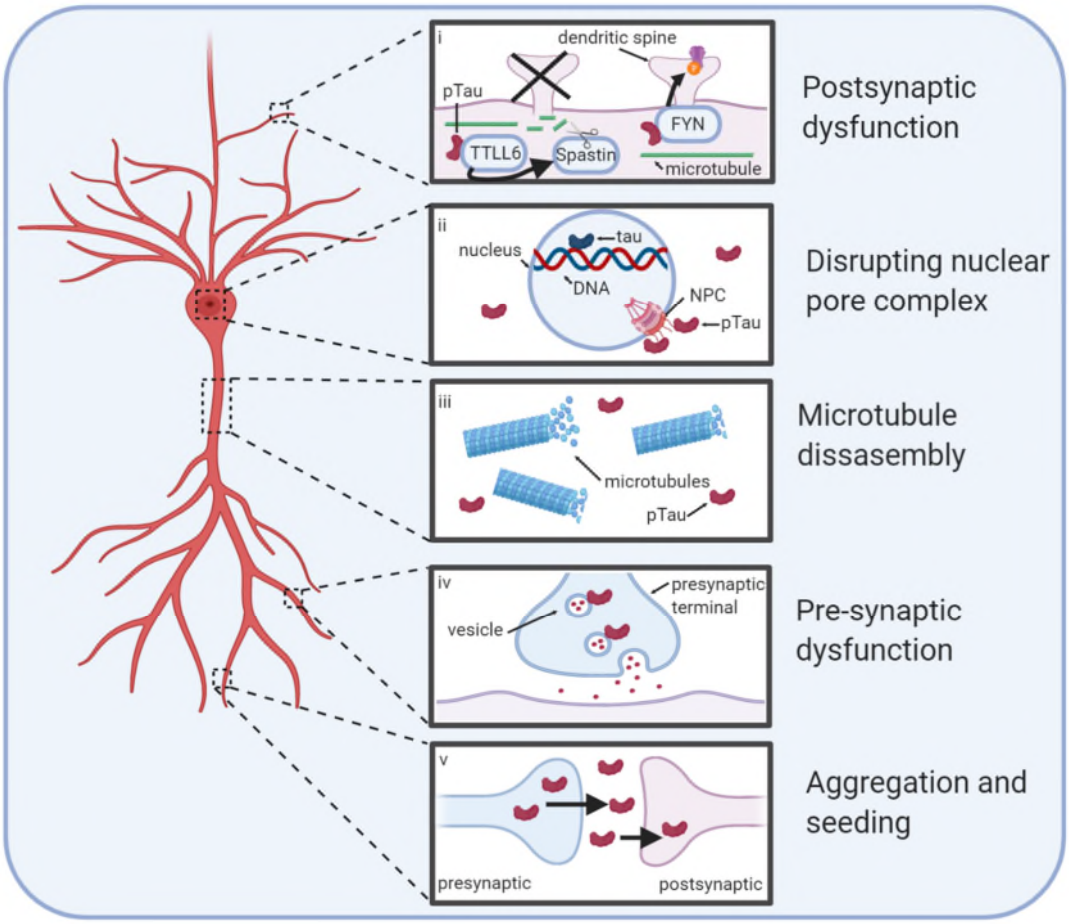

Figure 1.4: Functions of tau in pathology.

Tau can cause disruption to a wide range of cellular processes, depending on its localisation within the affected cell. If it reaches the dendrites, it can induce the loss of dendritic spines leading to postsynaptic dysfunction (i). Although phospho-tau cannot enter the nucleus, it can bind and disrupt the function of the nuclear pore complex (ii). The most prominent and well described consequence of aggregated tau is the disassembly of microtubules (iii) and the consequent alterations in their stability, function, and ability to assist in trafficking and cell transport. (iv) Pathological tau can also mislocalise to presynaptic terminals, whereby it binds to vesicles and slows down their rate of release and restock, thus limiting output. Finally, pathological tau in one neuron can act as a seed to transmit the pathology to neighbouring neurons (v), thus enabling the progression of the disease.

1.1.6 Tau propagation

Tau pathology originates in a single region and then spreads methodically through defined pathways that are individual to the tauopathy of interest (Braak and Braak, 1991). Tau can seed the spread of pathology between neurons, enabling transfer between different brain regions. Over time tau oligomers (oTau), both brain-derived and recombinantly sourced, can be internalised into neurons following extracellular application. Once inside, oTau can interact with endogenous tau and induce it to misfold and aggregate (Gibbons et al., 2019; Walsh and Selkoe, 2016). Some of this newly misfolded tau complex is then secreted to initiate a new cycle of propagation and associated toxicity in healthy neurons (Gibbons et al., 2019; Walsh and Selkoe, 2016). This initiates the cascade of intracellular toxicity that then transmits throughout the network. This cycle of propagation is often referred to as the transneuronal spread model (Fig 1.5a) and has been demonstrated in animal studies using both transgenic and wild type animals as well as basic cell models (Boluda et al., 2015; Clavaguera et al., 2009; Evans et al., 2018; Guo and Lee, 2011; He et al., 2020; Iba et al., 2013; Karikari et al., 2019a; Narasimhan et al., 2017; Puangmalai et al., 2020; Usenovic et al., 2015; Wegmann et al., 2016)

A second model for propagation is that of selective vulnerability, whereby some neurons are more susceptible to pathology than others, perhaps due to the presence of misfolded tau protein. In response to neuronal stress, a presynaptic ‘affected’ neuron will release diffusible metabolic factors which can then target these ‘vulnerable neurons’, transducing the stress and inducing the process of protein aggregation in the postsynaptic target cell. In the early stages of disease, only the ‘vulnerable’ neurons will be affected, but as disease progresses, aggregates are also able to transfer from cell to cell via a direct internalisation and release mechanism (Walsh and Selkoe, 2016; Fig 1.5b).

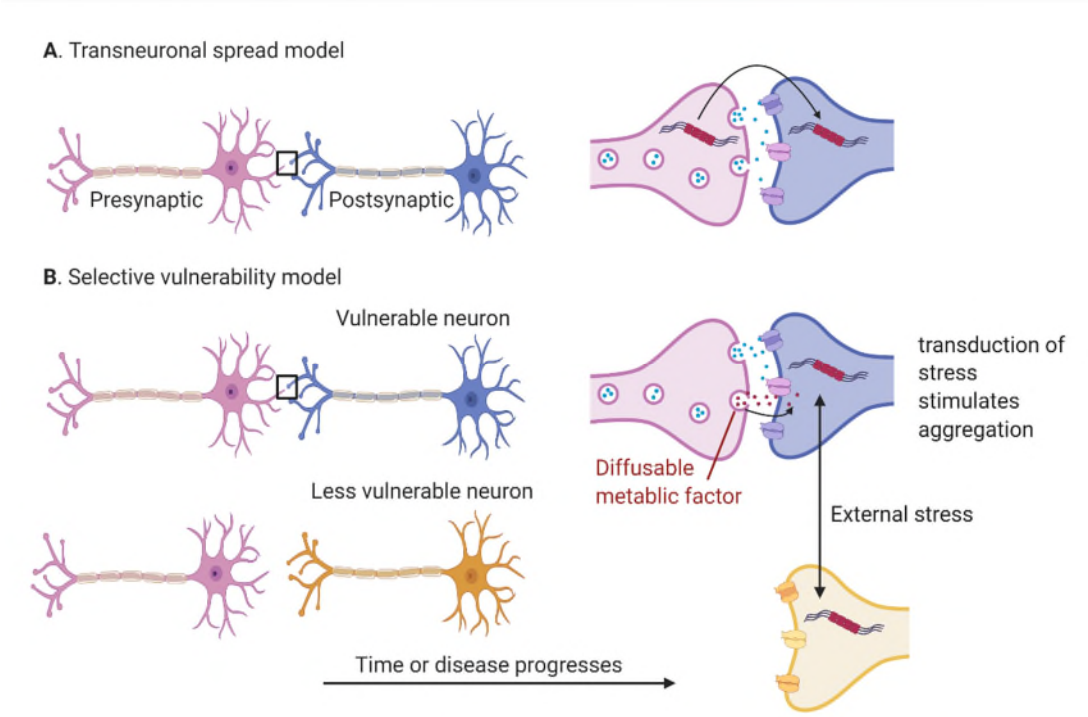

Figure 1.5: Methods of neuronal vulnerability to tau propagation.

A) The trans-neuronal spread model describes the direct physical transfer between neurons that make a synaptic connection. oTau is released into the extracellular space, internalised by the postsynaptic cell, and then stimulates the aggregation of endogenous tau. B) The selective vulnerability model describes a paradigm in which some neurons are more susceptible to damage (vulnerable neurons; purple), perhaps due to the presence of misfolded tau protein. Here in response to neuronal stress, diffusible metabolic factors are released and transferred across the synapse, inducing aggregation in the target cell. As disease progresses further, eventually the aggregates will be able to transmit from cell to cell via internalisation and release and even the less vulnerable neurons can be affected (yellow) (Walsh and Selkoe, 2016).

1.1.7 Alzheimer's disease and other tauopathies

Tauopathies are a group of diseases in which misfolded or aggregated tau plays a key role in mediating neuronal dysfunction and subsequent loss. They can be sub-categorised broadly by whether tau plays a primary role, these are termed 'primary tauopathies', or whether tau contributes in combination with other proteins such as Aβ or alpha synuclein (αSyn), these are termed 'secondary tauopathies'. Although tauopathies share some common mechanisms, they can be distinguished by the isoforms and ultrastructure of the tau aggregates (Dickson et al., 2011; Rademakers et al., 2012).

Alzheimer's disease (AD), a secondary tauopathy, is the most prevalent neurodegenerative disorder. AD has two major pathological hallmarks; extracellular amyloid beta and intracellular neurofibrillary tangles (NFTs) (Jack et al., 2013). AD is characterised by progressive and irreversible neuronal atrophy. Acetylcholine neurons are predominantly affected, initially in the entorhinal cortex, but as the disease progresses also the hippocampus and the cortex are affected with tau pathology. AD pathology then progresses progressively around the brain following the pathways described in Braak and Braak (1991; Fig 1.6).

1.1.8 Causes of Alzheimer's disease

Only ~1 % of cases of AD are inherited, with the remaining majority idiopathic, occurring as the result of a combination of genetic and environmental factors (Mayeux, 2003). There are four genes responsible for a large proportion of the mutations seen in AD: APP, presenilin 1 and 2 and apolipoprotein-E (APOE; Bekris et al., 2010). Mutations in APP alter the activity of the secretases responsible the production of Aβ, resulting in increased production of the toxic form of Aβ. Although excess Aβ can be cleared from the brain by transport across the vascular endothelium or by degradation by proteases or microglia, the clearance rate declines over time and this results in a build-up. Presenilin (PS) is part of the gamma secretase, therefore mutations in PS1 or PS2 also increase the production of the toxic form of Aβ (Citron et al., 1997; De Strooper et al., 1998; Scheuner et al., 1996). While APP mutations will not always result in AD, mutations in PS1 or PS2 will always result in fully penetrant early onset

AD (Raux et al., 2005). APOE is found in the extracellular space as a component of high-density lipoproteins and is involved in lipid and cholesterol transport. Its risk is determined by the combination of E2, E3 and E4 alleles held (Corder et al., 1993; Huang, 2006). Although, to date, there have been no reported mutations in MAPT (the gene encoding tau) that are related to Alzheimer's disease, there are a number reported for other tauopathies including frontotemporal dementia (Strang et al., 2019). These mutations have been used to generate transgenic tauopathy models to explore the pathology of dysfunctional tau on a general level (Ren et al., 2015). There are many other risk factors for tauopathies including diet, exercise and environmental factors (Barnard et al., 2014), which in combination with the genetic architecture will dictate whether someone will develop the disease, the age of onset and speed of progression.

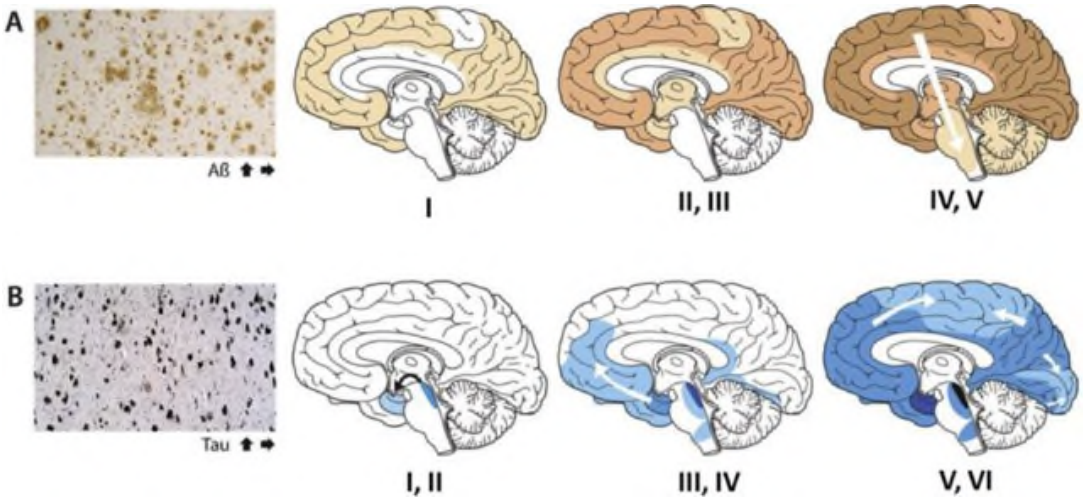

Figure 1.6: Progression of AD pathology throughout the brain.

A) Amyloid beta pathology as described by Thal and Braak (Thal et al., 2002). Progression from the neocortex to the entorhinal area and the hippocampus, then onto the cerebellum and brainstem. B) Tau NFT pathology as described by Braak (Braak and Braak, 1991). Progression starting in the entorhinal region, spreading to the hippocampus and then later onto the neocortex. A difference in the starting regions and pattern of spread can be observed. Amyloid pathology is more widespread in earlier stages than tau pathology, which is typical of the biomarker presentation clinically. Figure reproduced from (Jouanne et al., 2017).

1.1.9 Symptoms

Patients with Alzheimer's disease can present with a range of symptoms and the average life span post diagnosis is around 10 years (Fig 1.7). In the preclinical stages, they may display mild cognitive difficulties but not enough to affect their day-to-day functioning. This then develops further into mild cognitive impairment (MCI) in the 'prodromal stage' where the presence of AD biomarkers can be detected (Albert et al., 2011; Parnetti et al., 2019; Winblad et al., 2004). MCI/prodromal AD is an ideal stage to target therapeutically before widespread pathology spread, but is hindered by the fact very few cases are diagnosed at this early stage (Petersen, 2004). As the disease progresses to different brain regions, patients can suffer from severe loss of cognitive function which then results in major changes to behaviour as well as loss of functionality such as language and motor skills. In the late stages of the disease, symptoms become more varied and patients can also suffer from anxiety and depression (Atri, 2019).

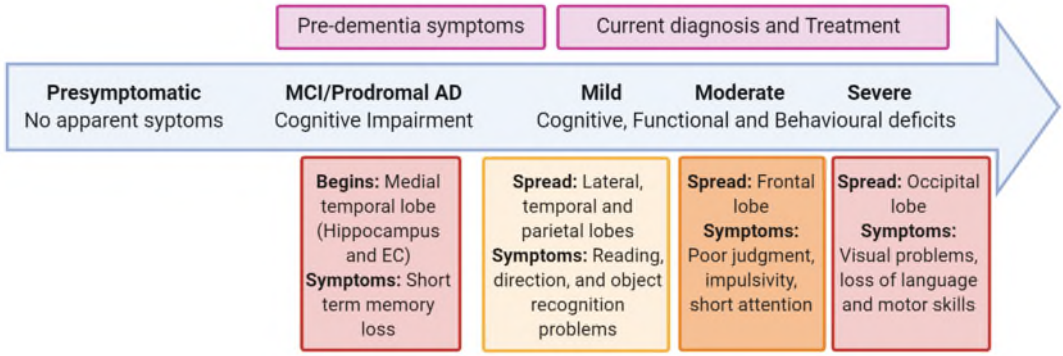

Figure 1.7: Timeline of AD progression paired with clinical presentation.

Details the progression from pre-symptomatic to MCI, through to mild, moderate, and severe AD. In most cases, AD is only clinically observable from the orange (moderate) stage, however this might be too late to act for treatment due to the widespread pathology by this stage.

1.1.10 Diagnosis and biomarkers

It can be difficult to diagnose AD with certainty due to the overlap of symptoms with other neurodegenerative diseases. The presence of amyloid-beta aggregates and phosphorylated tau aggregates (NFTs) are used for pathological confirmation of AD diagnosis post-mortem and correlate well with disease progression (Nelson et al., 2012). However, Aβ and tau pathology also precede the onset of cognitive impairment in AD by as much as 15-20 years before clinical loss of function or changes to brain structure so provide attractive targets for clinical biomarker development for early stage AD (Fig 1.8; Bateman et al., 2012; Buchhave et al., 2012; Fagan et al., 2014; Villemagne et al., 2013).

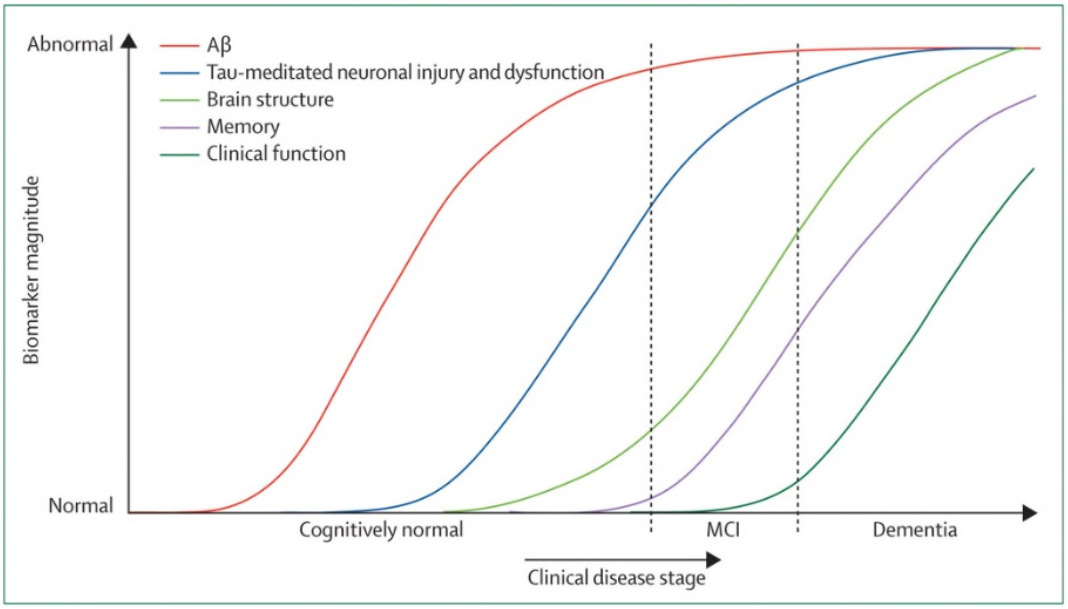

Figure 1.8: A schematic to show the best diagnostic biomarkers for Alzheimer's disease.

Clinical presentation of symptoms such as memory loss, loss of clinical function and changes to brain structure are preceded by changes to amyloid beta and tau pathology. This gives a window in which treatment can be administered before extensive pathology spreading, if successfully diagnosed in time (Jack et al., 2010).

Clinical biomarkers are molecules that can provide a ‘measurable indicator of pathology’, allowing the detection of disease at earlier stages. They can both aid diagnosis of diseases like AD but also assist in predicting the underlying pathologies (Zetterberg, 2019; Zetterberg and Burnham, 2019). The use of 11C Pittsburgh Compound B, florbetapir and florbetaben positron emission tomography (PET) imaging for Aβ pathology are well validated for Alzheimer’s disease and can provide 85–95% sensitivity and specificity (Zetterberg and Bendlin, 2021). It is worth noting that not all AD patients will have amyloid pathology and not all people with amyloid positive PET scans go on to develop the disease. It is therefore needed in combination with other tests in order to make an accurate diagnosis. CSF biomarkers for amyloid beta 1-42 (Aβ42), total tau (T-tau) and phosphorylated tau181 (P-tau181) can also be used for AD and provide similar sensitivity to PET scans (Zetterberg and Bendlin, 2021). Although showing a good level of accuracy, the collection of CSF samples involves minor surgery and PET scans need expensive brain imaging techniques, so cheaper less invasive methods are required.

Blood-based biomarkers allow for the possibility of screening for the same pathological markers but using a quick, relatively cheap and less-invasive assay (Toombs and Zetterberg, 2020). For example, using specific targeted biomarkers, such as P-tau181, a similar level of specificity and sensitivity as CSF Aβ42/Aβ40 and CSF T-tau can be achieved when comparing cohorts of Alzheimer’s disease patients to those that are cognitively normal (Janelidze et al., 2020; Karikari et al., 2020; Mielke et al., 2019; Thijssen et al., 2020). For example, plasma P-tau181 correlates well with CSF P-tau181 (Mattsson et al., 2016) with Aβ PET and tau PET (Mielke et al., 2019; Thijssen et al., 2020) and with Braak stage (Karikari et al., 2020), whilst not with neurofilament light (NFL; a common marker of neurodegeneration) (Thijssen et al., 2020).

1.1.11 Treating tauopathies: Alzheimer's disease

Brain atrophy cannot be reversed and so treating AD at the earliest possible stage is imperative. Alzheimer's disease and dementia are distinct from one another. People who have clinical Alzheimer's disease can develop dementia and the majority do although there are people who, despite having amyloid pathology, will never go on to develop Alzheimer's dementia within their lifetime. This provides a challenge for accurate diagnosis. Given the small proportion of cases that are heritable, mass genetic screening is unlikely to be an effective solution.

Initially, it was thought that by introducing small compounds termed 'plaque busters' or synthetic peptides, amyloid beta deposition in plaques could be reversed and that it may be possible to drive down amyloid pathology in the brain (Soto, 1999). Although initially promising, in some cases these peptides were found to brake the plaques down into small soluble toxic aggregates, and, even in cases where they were successful in driving down the levels of soluble amyloid beta, this did not correlate with an improvement in cognitive function (Mullane and Williams, 2020).

Another idea for targeting tau pathology is the use of peptides that prevent aggregation. Tau has two hexapeptide motifs with enhanced β-propensity that make it more likely to form beta sheets. By generating a peptide that binds and blocks this region, aggregation can be reduced (Pir et al., 2019). However, the problem with peptide-based therapy that there is a low level of blood-brain-barrier permeability and a high likelihood of degradation by proteases. There are a number of other approaches for targeting tau pathology that are also emerging including anti-aggregation agents (Bulic et al., 2010; Jouanne et al., 2017; Wischik et al., 2014) and antisense therapies for tauopathies with targetable mutations such as frontotemporal dementia (Schoch et al., 2016).

Perhaps the most promising of all treatment approaches over the last decade has been immunotherapy, for both Aβ and tau. By introducing antibodies targeting Aβ in rodent models, protein deposits were reduced, and cognitive function improved. Solanezumab, an example of immunotherapy targeted at Aβ failed in phase III trials in 2018 after not significantly altering cognitive

decline (even though it had shown promise in animal and early human trials) (Honig et al, 2018). Solanezumab is one example of many immunotherapy trials for Aβ; all have failed at the clinical trial stage to meet their endpoints (Wang et al, 2017; Panza et al, 2020). This may be because the administration is too late in the course of disease progression or that not enough of the dose enters the brain. However, it might still be a good approach if delivered to pre-symptomatic patients, dependent on advancements and availability of biomarker technology. The field is now shifting to also explore the possibility of anti-tau-based immunotherapy. There are a range of trials which aim to neutralise either monomeric (Boutajangout et al., 2011; Yanamandra et al., 2015, 2013), phosphorylated, mutated (Boutajangout et al., 2011; Chai et al., 2011; Congdon et al., 2013; d'Abramo et al., 2013; Kontsekova et al., 2014) or aggregated versions of the tau protein (Castillo-Carranza et al., 2014). When choosing an immunotherapy target there are many considerations, including, but not limited to, the epitope, the isotope of tau that it targets, the charge of the antibody and whether a whole or fragment of antibody is used (Sigurdsson, 2018). These factors will all alter the efficiency of the immunotherapy.

Immunotherapy must be targeted at a certain epitope of the protein and the target will determine the effects on tau function. This highlights the importance of understanding the underlying biological basis. It also means that just because a trial fails for one disease, it does not mean that it cannot be repurposed for another pathology with the same proteinopathies. For example, the Gosuranemab (Biogen) antibody failed at stage 2 in progressive supranuclear palsy but is now repurposed for tau targeting in AD. It is unlikely that one form of immunotherapy will be sufficient to work across all pathologies of tau or of amyloid beta (Sigurdsson, 2018). Basic science underpins the understanding of the mechanisms of protein-mediated degeneration and needs to guide the development of potential treatment strategies, to facilitate their timely success.

1.2.1 Parkinson's disease

Parkinson's disease (PD) was initially named 'The Shaking Palsy' by James Parkinson in 1817 when he observed, weakened muscle tone, resting tremor and stooping in his patients (Parkinson, 1817). It was later renamed by Jean-Martin Charcot to reflect its discoverer James Parkinson (Charcot, 1877). As scientists and clinicians began to understand more about the symptoms and the progression of this disease, a better understanding and methodology for diagnosis emerged. The discovery of Lewy bodies as a key pathology was first reported by Lewy (1912) and they are now known to be one of the major hallmarks of PD, as well as in Lewy body dementia and Parkinson's disease dementia. PD is a disorder that follows a typical spreading pattern around the brain and can be categorised by the location of pathology and clinical symptoms to give a measure of the stage of disease. These stages were outlined by Braak (Braak et al., 2003, 2002). PD is a disorder affecting many areas of the brain but one of the predominant and most susceptible to damage is the basal ganglia. The substantia nigra (SN) is a region within the basal ganglia and is an integral part of the circuitry. It is an area that suffers substantial neuronal loss throughout the disease and is well characterised as a key target for degeneration (Gibb and Lees, 1991; Paulus and Jellinger, 1991). The SN is home to one of the key populations of dopaminergic neurons in the brain and these are primarily lost over the course of the disease. Dopamine is a monoamine neurotransmitter involved in the processes of movement, reward and emotion, amongst many others. It was first discovered to be a neurotransmitter in the late 1950's (Bertler and Rosengren, 1959; Carlsson, 1959). The dopamine circuitry in the basal ganglia is complex and its projections need to be finely managed in order to be able to perform movements. Loss of dopaminergic neurons over the course of the disease lead to this balance being compromised and thus patients have difficulty controlling movement and co-ordination. The main changes to the pathway circuitry during PD are highlighted in Figure 1.9. They demonstrate the shift in the balance of the direct and indirect pathways, and the resulting effects on both the basal ganglia itself and the surrounding regions of the cortex, the brain stem, and the thalamus (Fig 1.9).

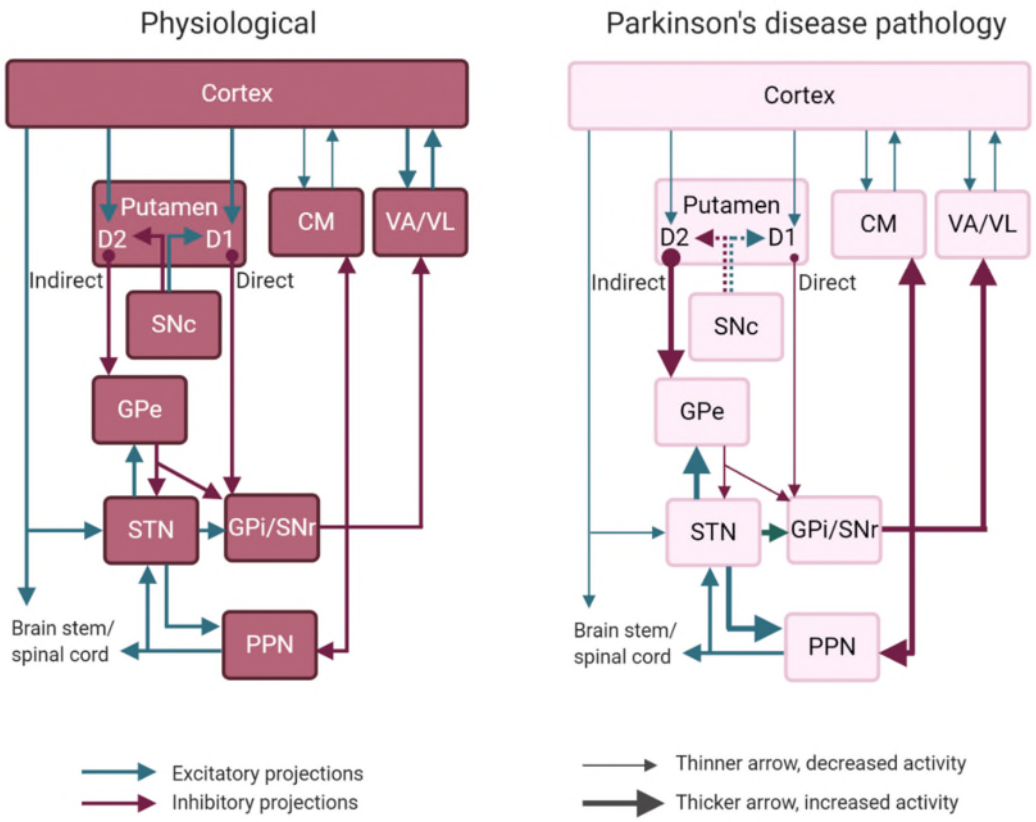

Figure 1.9: Schematic of the changes to basal ganglia circuitry that occur during Parkinson's disease.

Illustrated are the main regions of the basal ganglia, as well as the cortex, the brainstem, and the thalamus. The circuitry is complicated and can be divided into two pathways, the direct (through D1 dopamine receptors) and the indirect (through D2 dopamine receptors). The left-hand side demonstrates the physiological condition, with teal arrows representing excitatory projections and magenta representing inhibitory projections. The right-hand side demonstrates the changes that occur in Parkinson's disease, starting from the loss of dopaminergic neuron projection from the substantia nigra pars compacta (SNpc) and the subsequent changes to the strength of connections across the circuit. Thinner arrows represent a decrease in the activity of the projection compared to physiology. Thicker arrows, on the other hand represent an increase in activity of that projection compared to the physiological circuit. CM, centromedian nucleus; VA/VL, ventra; anterior/ ventral lateral nucleus; SNc, substantia nigra pars compacta; GPe, globus pallidus, external segment; STN, Subthalamic nucleus; GPi, globus pallidus, internal segment; SNr, substantia nigra pars reticula; PPN, pedunculopontine nucleus. (Figure concept from Smith et al., 2012).

1.2.2 Parkinson's disease - causes

Parkinson's disease has a complex aetiology, with a lifetime incidence of around 2% (Polymeropoulos et al., 1997). The biggest risk factor for developing PD is age (Eriksen et al., 2009; Hindle, 2010; Morgan and Finch, 1988; Niccoli and Partridge, 2012; Samii et al., 2004). Dopaminergic neurons are lost naturally over time and around 1 % of people over the age of 60 and 4 % of people over the age of 80 are affected (de Lau and Breteler, 2006). There is a slightly higher prevalence of disease in men than women (Haaxma et al., 2007; Shulman, 2007; Van Den Eeden et al., 2003), which might be due to oestrogen-mediated increase in dopamine release in the striatum (Haaxma et al., 2007). There is, however, no discrimination in prevalence across ethnicities (Van Den Eeden et al., 2003).

Parkinson's disease can be hereditary, and this accounts for between 5 and 10 % of cases. Mutations in the genes SNCA, which encodes alpha synuclein, or LRRK2, which encodes Leucine-rich repeat kinase 2, are known to be linked to the autosomal dominant form of familial PD. The link between SNCA and alpha synuclein was established in 1997 (Spillantini et al., 1997). Mutations lead to the misfolding and aggression of alpha synuclein protein which cannot be degraded by the ubiquitin-proteasomal-pathway and hence alpha synuclein is accumulated into inclusions. These toxic inclusions affect basic cellular functions, trafficking and transmission, eventually leading to cell death (Winner et al., 2011). LRRK2 harbours the most common familial mutations for PD and encodes a kinase that controls the phosphorylation of alpha synuclein and tau. LRRK2 mutations cause disruption to the level of phosphorylation and increase the amount of pathologically aggregated alpha synuclein and tau within neurons (Zimprich et al., 2004). A second set of genes PARK2, PINK1, DJ-1 and ATP13A2 are all linked to the autosomal recessive forms of familial Parkinson's disease and affect various other cellular processes (Lesage and Brice, 2009).

For the other 90% of cases, there are numerous risk factors, including genetic risk factors which have been highlighted using genome-wide-association-studies (Klein and Westenberger, 2012) as well as lifestyle factors including

smoking, caffeine and vitamin C and E intake; all of which are reported to reduce the risk of developing PD and thus could be neuroprotective (Checkoway et al., 2002; de Lau et al., 2005; Hantikainen et al., 2021; Hernán et al., 2003, 2002; Quik et al., 2012; Zhang et al., 2002). The mechanisms underlying these inverse relationships are yet to be established. For example, in meta-analysis studies, smoking has been associated with a significantly lower risk of developing PD (Li et al., 2015; Chen et al., 2010), however it is not clear which element of cigarette smoking is responsible for this reduction in risk. Studies have demonstrated that the reduced risk is also present in cases of smokeless tobacco use over non-smokers (O'Reilly et al., 2005), as well as those who have been exposed to environmental tobacco smoke (Nielsen et al., 2012). For example, nicotine, which is found in tobacco smoke can bind to and activate nicotinic acetylcholine receptors on dopaminergic terminals and modulate dopamine release and striatal activity (Ma et al., 2017; Quik et al., 2012, 2009). Nicotine has been shown to have protective effects in the 1-methyl-4-phenyl-1,2,3,6-tetrahydropyridine (MPTP) animal model of PD; reducing striatal damage and improving motor function (Bordia et al., 2006; Janson et al., 1992; Parain et al., 2001). It also reduced levodopa-induced dyskinesias in rodents and monkeys (Quik et al., 2013a, 2013b; Zhang et al., 2014a, 2014b). However clinical trials in humans have yielded inconsistent results (Lemay et al., 2004; Mitsuoka et al., 2002; Villafane et al., 2007).

Systemic analysis of over 100 observational studies of human caffeine intake confirms that it also confers a reduction in the risk of developing PD (Bakshi et al., 2020; Grosso et al., 2017; Hong et al., 2020; Li et al., 2012). In the MPTP (PD) animal model, caffeine consumption can reduce degeneration when given before treatment with MPTP (Xu et al., 2002), but can also confer neuroprotection when administered after the MPTP treatment (Sonsalla et al., 2012). Caffeine acts mainly at the adenosine A_{2A} receptor ($A_{2A}R$) as an antagonist to promote wakefulness (Huang et al., 2005). Studies to block A_{2A} receptors or genetically deleting them have demonstrated protection of dopaminergic neurons in PD animals (Chen and Schwarzschild, 2020; Ferreira et al., 2017; Kachroo and Schwarzschild, 2012). The action on A_{2A} receptors is of particular interest in PD as they are highly expressed in the striatum of

neurons in the indirect pathway (Figure 1.9). Here the A_{2A} receptors are co-localised with D2 receptors allowing dopamine and adenosine to have antagonistic effects on the same neurons (Cieślak et al., 2008). Activation of A_{2A} receptors therefore reduces the affinity of D2 dopamine receptors for dopamine and therefore reduces the ability to control movement (Cieślak et al., 2008; Popoli et al., 1994). It is also known that A_{2A} receptor activation inhibits the release of GABA in the striatum while enhancing GABA transmission in the globus pallidus, which also disrupts the balance of the direct and indirect dopaminergic pathways (Cieślak et al., 2008). Thus, it was proposed that A_{2A}R antagonists could provide a viable treatment option for PD (Berger et al., 2020; Munoz and Fujioka, 2018). Over 25 clinical trials in humans have been carried out to assess the efficacy of A_{2A}R antagonists in PD (Ren and Chen, 2020), culminating in the FDA approval of Istradefylline (an A_{2A}R antagonist) which is now prescribed as a combination therapy levodopa/carbidopa to help to manage 'off' periods (Berger et al., 2020).

Another confounding factor in PD pathogenesis is mitochondrial dysfunction and the subsequent accumulation of reactive oxidative species (ROS; Lesage and Brice, 2009). The high levels of ROS in PD are thought to result from a combination of high levels of iron in the SNpc and from dopamine metabolism. Dopamine undergoes oxidation to form dopamine quinones and free radicals (Muñoz et al., 2012). Dopamine levels are normally regulated through by the neuronal enzyme MAO-A, however in PD, the glial enzyme MAO-B becomes the primary dopamine metabolising enzyme (Riederer et al., 1987). A by-product of MAO-B-mediated dopamine metabolism is H_2O_2 which can enter dopaminergic neurons, react with iron, and form hydroxyl radicals (Kumar and Andersen, 2004; Nagatsu and Sawada, 2006). This explains the rationale behind the addition of MAO-B inhibitors as a clinical PD treatment in humans (Binde et al., 2020).

The MPTP primate model is one of the most commonly used PD animal models and works by blocking mitochondrial complex one, increasing ROS and leading to similar degeneration patterns to those observed in PD (Sian et al., 1999). Environmental stress in the form of pesticides found in drinking water or on farms has been correlated with risk due to a higher reported

prevalence in rural areas of the United States (Lai et al., 2002). There is also evidence that exposure to certain metals like iron and copper can increase risk due to their ability to bind to and disrupt alpha synuclein's function (Bush, 2000; Dexter et al., 1991, 1989; Gorell et al., 1997).

1.2.3 Parkinson's disease – diagnosis and symptoms

Diagnosis of PD is challenging as several the symptoms overlap with those of other neurodegenerative disorders. The Unified Parkinson's Disease Rating Scale (UPDRS) is a series of questions and tasks designed to characterise if a patient displays characteristic PD phenotypes and is then used post-diagnosis to track progression. The UPDRS scale is used internationally across clinical trials and for diagnoses allow worldwide uniformity (Fahn and Elton, 1987). Symptoms of PD only present clinically when 70-80 % of the dopamine input to the striatum is lost (Bernheimer et al., 1973). Motor deficiencies are the most common early symptoms, resulting from the reduction of dopamine in the substantia nigra, including a unilateral resting tremor, increased rigidity and a loss of postural control (Hisahara and Shimohama, 2011; Fig 1.10). Sometimes if the balance of medication is not correct, patients can experience bradykinesia (slow movement) or tardive dyskinesia (unwanted jerks or movement). As the disease progresses, finer motor control becomes affected leading to further symptoms including micrographia (progressively small handwriting) and loss of control over facial expressions (Lesage and Brice, 2009). One of the most disabling symptoms of PD, which tends to occur in the later stages of disease is freezing of gait, where there is a delay between deciding to move and initialising the movement (Schapira et al., 2009; Fig 1.10). Patients can also develop mental health complications such as depression and anxiety as PD progresses. However, it is unclear whether these are part of the pathology or a consequence of the effects the other symptoms on quality of life. As patients become more heavily medicated over time, medication-induced side effects can present and can be as, if not even more, disabling as the pathology itself (Chaudhuri et al., 2006).

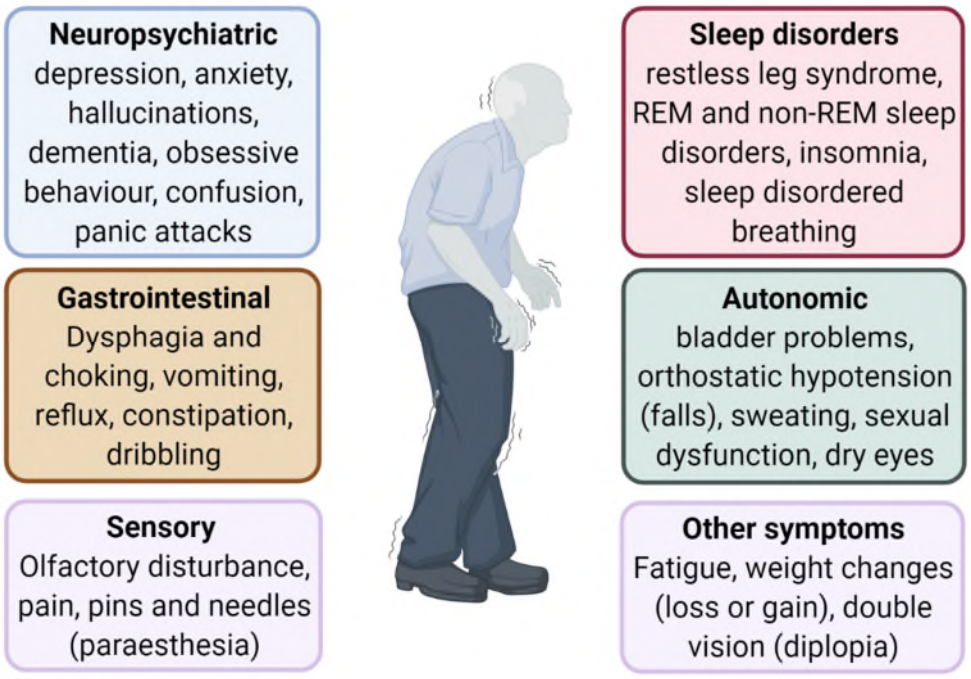

Figure 1.10: The non-motor symptoms of Parkinson's disease (PD).

Parkinson's disease is often miscategorized as just a movement disorder, affecting posture, movement control and gait problems as the image in the center shows. However, often overlooked, there are also widespread non-motor symptoms that can have a large effect on patients' quality of life, some of the main symptoms are categorized and listed. A number of these side effects will occur in the later stages of the disease and may be a result of the drug regime rather than as a direct result of the pathology.

1.2.4 Parkinson's disease - spread of disease pathology

The early stages (1 and 2) of PD are known as the 'pre-symptomatic stages and represent the time period before patients present with a substantial clinical motor deficit but do exhibit pathology in the form of inclusion bodies in the brainstem. PD is believed to originate in the dorsal motor nucleus of the vagus nerve (Del Tredici et al., 2002), however at this stage, Lewy body pathology can also found in the olfactory bulb (Barz et al., 1997; Fig 1.11). By stage 2 the pathology has also spread to the medulla and pons. One of the first symptoms of PD that is almost universal (~90%) across patients is olfactory loss and this tends to occur in these early stages of the disease (Haehner et al., 2007; Ross et al., 2008; Sommer et al., 2004). Stages 3 and 4 are the first symptomatic stages and these are characterised pathologically by the spread of Lewy bodies to the basal ganglia, specifically into the substantia nigra pars compacta (SNPc; Eriksen et al., 2009; Fig 1.11), which is the primary site for dopaminergic cell loss in PD. Dopaminergic neurons can be located by their neuromelanin content which appears as a black pigment. Lewy bodies when they form tend to displace neuromelanin within dopaminergic neurons. Dopaminergic neuronal loss is accelerated in stage 4. Other affected regions include the basal forebrain and the hippocampus (Dickson et al., 1991; Divac, 1975). Stage 5 and 6 are the final stages of the disease and represent the advanced stages of the disease where patients begin to suffer from a range of non-motor and autonomic deficits alongside their symptoms.

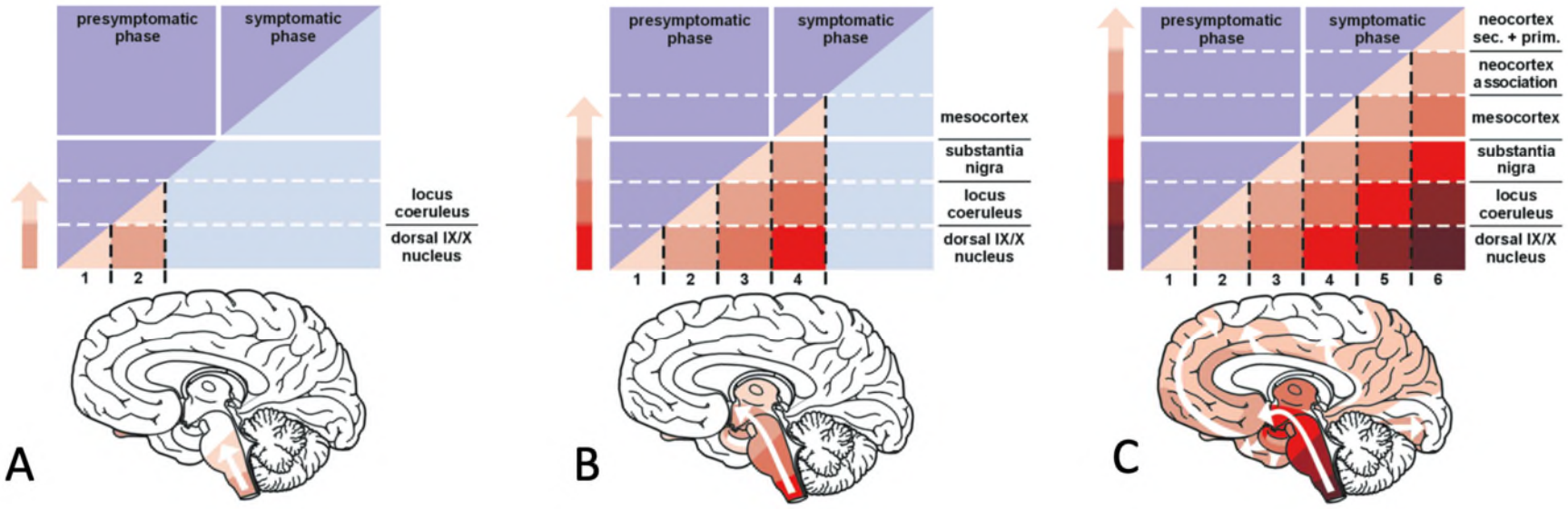

Figure 1.11: Illustration of the pathological spread in cases of idiopathic Parkinson's disease.

A) In stages 1 and 2, pathology is found in the olfactory bulb and the medulla oblongata. B) By stages 3 and 4, the substantia nigra and areas of the basal forebrain start to become affected, first mildly, but then progressing to more severe. This is where the symptomatic clinical presentation usually arises. By stage 5 and 6, pathology has spread further into the neocortex and surrounding regions and symptoms increase in severity (Braak et al, 2002).

1.2.5 Alpha-synuclein - physiology and pathology

Alpha synuclein (αSyn) is a small intracellular protein of only 140 amino acids that is abundantly expressed throughout the brain. It is found primarily at presynaptic terminals where it plays a role in vesicle trafficking and recycling via interactions with SNARE proteins (Fig 1.12 and 1.13; Lashuel et al., 2013) but can also be found in the mitochondria and nucleus. Like tau, monomeric αSyn is an intrinsically disordered protein (IDP). IDPs do not show a well-defined three-dimensional structure, often due to having a high proportion of charged or polar amino acids in their sequence (Skrabana et al., 2006). This structural flexibility allows them to carry out their roles within neurons and is lost upon aggregation when the protein becomes ordered and rigid. Pathological αSyn was first discovered in the amyloid beta inclusions of Alzheimer's patients (Uéda et al., 1993) and only later was its role in PD uncovered. Aggregation is commonly induced by reactive oxygen species (ROS) following damage to the structure of αSyn and follows a similar pattern of aggregation to tau, starting with accumulation into soluble oligomers, then to fibrils and through to Lewy bodies and Lewy neurites.

Oligomers of αSyn cause toxicity by a range of cellular mechanisms (Fig 1.12). αSyn aggregates decrease the ability of the ubiquitin proteasome pathway (UPP) to remove abnormal proteins, so ubiquitin-bound proteins are often found as a component of Lewy bodies (Alves-Rodrigues et al., 1998; Dehay et al., 2015). They can also induce mitochondrial dysfunction by depolarising mitochondria, which results in intracellular calcium retention and cell swelling (Luth et al., 2014), or by targeting the mitochondria itself, accumulating on the outer membrane and making it permeable which leads to mitochondrial fragmentation and mitophagy. αSyn aggregates can directly interact with complex 1 to increase the levels of reactive oxygen species which then in turn increase the oxidative damage within the cell. Extracellularly applied oligomers of αSyn can also impair LTP by binding and activating NMDA receptors (Diógenes et al., 2012). At presynaptic terminals, oligomeric αSyn can induce synaptic dysfunction by disrupting vesicle trafficking (Jakes et al., 1994). It can also interfere with synaptobrevin in the SNARE complex, which is vital for the fusion of vesicles with the membrane ready for neurotransmitter release (Burré

et al., 2010; Choi et al., 2013; Lashuel et al., 2013; Murphy et al., 2000; Figure 1.13)

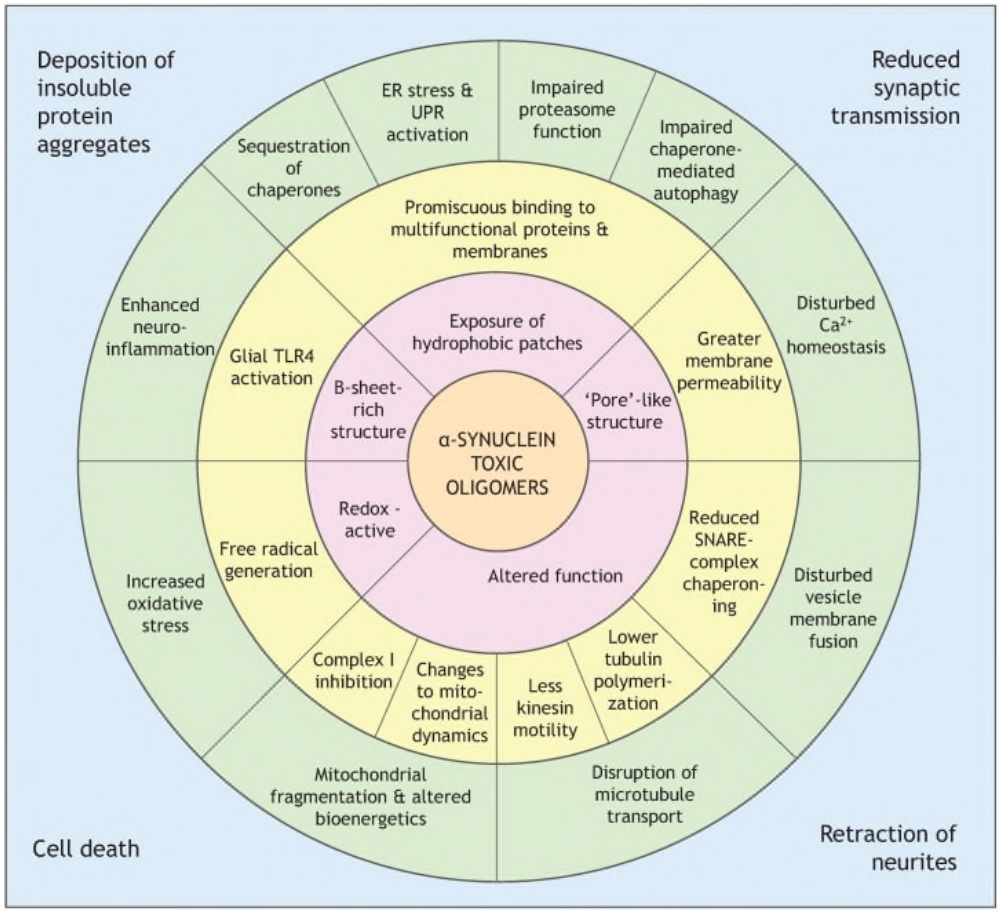

Figure 1.12: Effects of alpha synuclein aggregates within individual neurons
Pink shell: details the proposed mechanisms of toxicity of the oligomers. Yellow shell: examples of some of the effects that the oligomers have within neurons. Green shell: disruption caused to cellular systems by the accumulation of aggregates. Blue outline: pathological outcomes. ER—endoplasmic reticulum. UPR—unfolded protein response. Figure reproduced from (Roberts and Brown, 2015).

Toxic αSyn oligomers can be transmitted between cells, providing a possible mechanism for disease progression. When autophagy fails, exosomes are used to release the oligomers into the extracellular space (Danzer et al., 2012). Rostami et al., (2017) demonstrated that the cellular distress induced by aggregates causes tunnelling nanotubes to form. These are utilised by neighbouring astrocytes to send mitochondria as an additional energy source. At the same time, the aggregates can travel down these microtubules to neighbouring astrocytes, transferring the pathology.

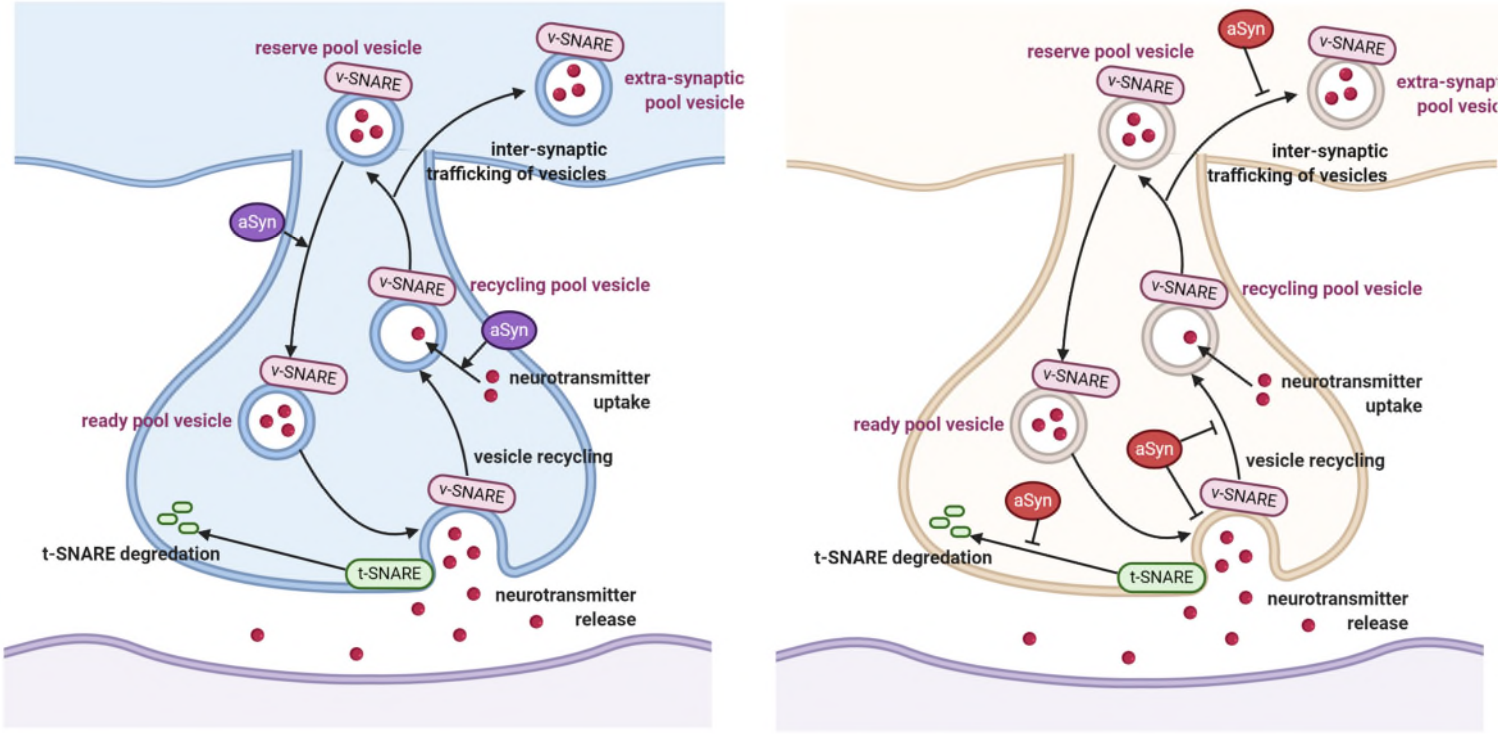

Figure 1.13: Presynaptic roles of alpha synuclein in physiology and pathology.

Physiologically, alpha synuclein (αSyn, purple; left panel) assists in the trafficking of vesicles via their interactions with the vesicle-associated SNARE (v-SNARE) and the target membrane associated SNARE (t-SNARE). It also assists in the refilling of neurotransmitters into vesicles after release. Pathologically, when aggregated (red; right panel), it can impair neurotransmitter release in a number of ways, it can directly inhibit release, alter vesicle trafficking, and also slow the recycling process by inhibiting vesicle refilling (Figure concept from Lashuel et al, 2013).

1.2.6 Treatments for Parkinson's disease

All current pharmacological treatments for Parkinson's disease act by relieving symptoms rather than by targeting the underlying cause. Having established that a loss of dopaminergic signalling is central to disease progression, researchers searched for a method to boost the dopamine signal that declines in the brains of PD patients. This came in the form of levodopa (L-3,4-dihydroxyphenylalanine; L-DOPA), which is then converted into dopamine via DOPA decarboxylase dopamine and noradrenaline neurons (Cotzias et al., 1969, 1967; Yahr et al., 1969; Fig 1.14). This was a revolutionary discovery in its time and is still the current frontline treatment for newly diagnosed Parkinson's disease patents. The rate limiting step in the production of dopamine lies between tyrosine and L-DOPA and so the administration allows this to be bypassed and a quicker boost to dopamine levels. Unfortunately, only 1% of the dose that is taken orally will reach the target site in the brain. As with many pharmaceutical therapies the issue is tolerance and over time patients develop tolerance and need to increase their levels of medication. At the peak of the dose of L-DOPA, patients can sometimes suffer from motor overload, which is referred to as dyskinesia, unwanted jerk movements (Schapira et al., 2009). There is therefore a ceiling to which the dose can be increased as all of these medications have side effects that have to be managed. This means that as the disease progresses, patients need to supplement L-DOPA with various other drugs (Fig 1.14). As the disease progresses, patients can suffer from 'on' and 'off' periods. 'On' periods refer to a period of time in which the anti-parkinsonian dopaminergic medications are working, and symptoms are improved. 'Off periods' refer to a worsening of symptoms despite continued anti-parkinsonian medication, which can manifest as a delay to symptom alleviation after a dose of levodopa, a decline in benefit of the treatment (at the end of a dose) or the complete lack of efficacy of a therapeutic dose altogether (Swope, 2004).

To prevent loss of orally administered L-DOPA in the periphery, DOPA decarboxylase inhibitors can be prescribed which prevent the breakdown to dopamine. They cannot pass the blood brain barrier, so they only prevent peripheral breakdown. This means that instead of only 1% of the dose reaching

the brain, up to 10% can. Dopamine agonists can also be used which mimic the activity of dopamine at dopamine receptors without the need for the dopa decarboxylase step needed for L-DOPA (Schapira et al., 2009). MAO and COMT inhibitors can also be used to supplement drug regimens when patients develop tolerance to L-DOPA (Hammond et al., 2007).

Long-term pharmacological therapy results in decreased efficacy and can induce complex side effects (Poewe et al., 2017). In these cases, deep brain stimulation can be considered. Candidates must have had PD for a minimum of 5 years and must have originally responded to L-DOPA treatment to be considered for deep-brain stimulation. Microelectrodes are implanted surgically into one of the following regions STN, GPi or *Ventralis intermedius (*VIM) and connected to a pulse delivery device to target the overactive indirect pathway.

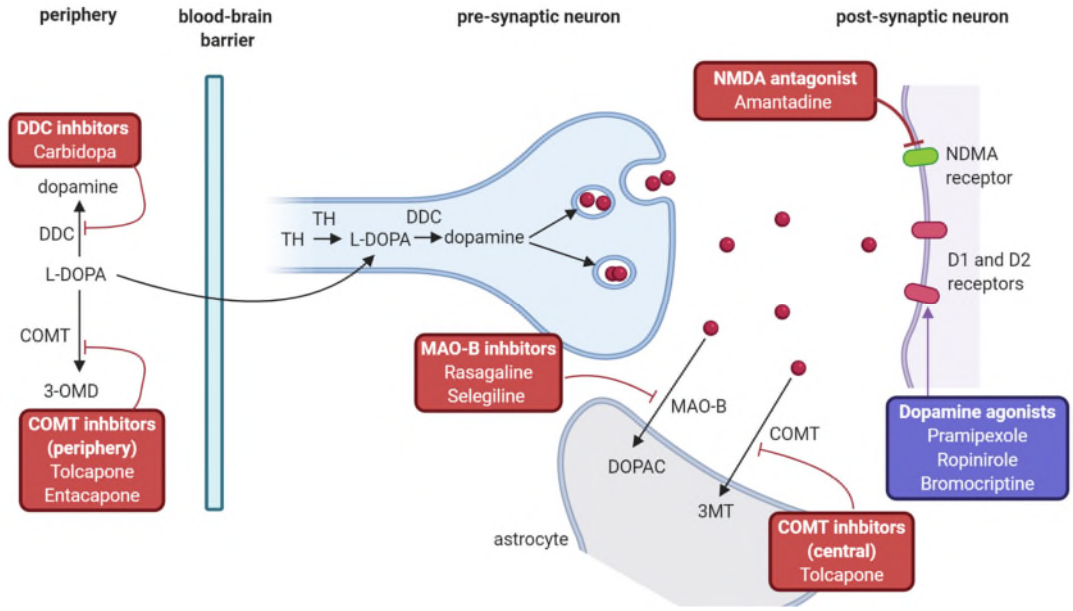

Figure 1.14: Pharmacological approaches to treating Parkinson's disease.
The symptoms of Parkinson's disease can be managed using a variety of drugs. The drugs increase dopamine signalling by regulating various components of dopamine metabolism, synthesis, release, and signal transduction. The frontline treatment is L-DOPA; however, this often needs to be supplemented with dopamine agonists, MAO-B and COMT inhibitors as the disease progresses.

1.2.7 Gene therapy

There are several potential ways to utilise gene therapy to help patients suffering from PD (Chen et al., 2005). Firstly, via increasing the production of dopamine, thus improving quality of life through symptom reduction. This can be done by delivering a combination of three different enzymes aminoacid decarboxylase (AADC), tyrosine hydroxylase (TH) and GTP-cyclohydrolase 1 (GCH-1). Tyrosine hydroxylase converts tyrosine to DOPA, AADC (DOPA decarboxylase) converts DOPA to dopamine and GCH-1 is the rate limiting step in the synthesis of tetrahydrobiopterin, which acts as a cofactor for tyrosine hydroxylase. In human trials, bilateral intra-striatal delivery of a combination of these three enzymes (a treatment called ProSavin) into the putamen was well tolerated and significantly improved motor symptoms by 1 year compared to baseline (Palfi et al., 2014). Moderate improvements could still be observed at the 5-year follow up stage (Palfi et al., 2018). There is evidence that level of dopamine replacement achieved, although enough to give significant reduction in symptoms, could be enhanced further. Parallel trials are now underway to discover different viral options that could increase efficiency, such as OXB-102 which is currently in pre-clinical trials (Badin et al., 2019).

The second is to introduce adeno-associated viral vectors (AAV) encoding glutamic acid decarboxylase (GAD), the enzyme which is the rate limiting step in the synthesis of GABA, into the subthalamic nucleus (STN). Increased GABA transmission in the STN inhibits glutamatergic neurons, thus increases movement (Emborg et al., 2007). Results from Phase I (Luo et al., 2002) and Phase II clinical trials (LeWitt et al., 2011) showed that bilateral delivery of AAV-GAD into the STN was safe and tolerable and that there was significant improvement in motor impairment, with little off-target effects.

A third approach would be to deliver neurotrophic factors such as glial derived neurotrophic factor (GDNF) or cerebral dopamine neurotrophic factor (CDNF) (Coune et al., 2012). This approach is hindered by these factors being too large to readily cross the blood brain barrier (Boado and Pardridge, 2009; Wang et al., 2012). Recent trials have shown promise in the delivery of GDNF

directly into the brain. Dopamine activity was increased by 54 %, although no corresponding change to UPDRS score meant that they did not successfully meet their clinical endpoints (Whone et al., 2019). This may be due to the length of the study period. For GDNF, the drug can be delivered via bilateral intraputamenal implanted catheters which are connected to a port which is fixed behind the patient's ear (Fig 1.15). This overcomes the lack of access across the blood brain barrier and the surgery itself proved successful, safe and effective (Fig 1.15; Whone et al., 2019).

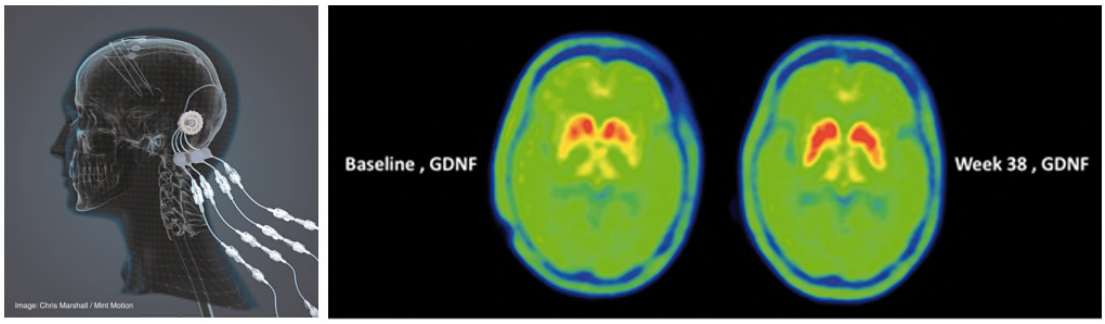

Figure 1.15: GDNF trial using the new investigational drug delivery system.
(Left) Schematic of the delivery system designed for this trial. Four catheters are implanted to deliver intermittent bilateral intraputamenal infusions of GDNF. The catheters are attached to an external pump which is fitted behind the patient's ear to allow delivery (Marshall, 2019). (Right) ^{18}F-DOPA images (PET imaging) to assess whether GDNF can increase the levels of L-DOPA in the striatum. A significant increase from baseline levels was seen in GDNF but not placebo receiving patients (Whone et al, 2019).

There are now 2 clinical trials underway (by Herantis Pharma) utilising the same delivery system to deliver a different neurotrophic factor called CDNF (Phase I/II trial; NCT03295786). Early results after 6 months show that delivery is safe and tolerable. The same company is also working on a non-invasive fragment of CDNF (xCDNF) which is able to cross the blood brain barrier, clinical trials for this are due to begin in 2023 (Herantis Pharma, 2020).

1.2.8 Stem cells

The DNs that are lost during PD progression cannot be naturally regenerated. As the neuronal loss is selective to midbrain dopaminergic neurons in PD, targeted cell replacement has been an attractive strategy for a number of decades (Backlund et al., 1985; Freed et al., 1992; Lindvall et al., 1990; Widner et al., 1992). There are two options to produce stem cells: those that originate from embryos and then differentiate, and those that come from adult cells and are reprogrammed. In the 1990's DNs were generated from embryonic stem cells (from foetal mesencephalic tissue) and grafted into the striatum of PD patients. Although successfully boosting levels of dopamine (for ~20 years), the grafted neurons were still susceptible to the pathology (Barker et al., 2015; Kefalopoulou et al., 2014; Li et al., 2016). There are also ethical issues surrounding the use of embryonic stem cells, making tissue acquisition challenging for the current TRANSEURO trial (Fan et al., 2020).

The second option is to harvest adult stem cells from the patient, which ensures that there will be no immunorejection and reduces the risk of tumorigenesis. Using Yamanaka transcription factors (Oct4, Sox2, Klf4 and c-Myc) pluripotency can be induced into adult stem cells (iPSCs) and they can then be differentiated into midbrain dopaminergic neurons (Kirkeby et al., 2012; Kriks et al., 2011). Editing tools like CRISPR/Cas9 can then be used generate isogenic cell lines of patient mutations. This is as close as *in vitro* biology can get to modelling human disease cells (Soldner et al., 2011). It is a costly and time consuming process so generating a way to produce HLA-homozygous 'universal stem cells' that can match large groups of the population rather than be individualised to the patient is the next step (Fan et al., 2020; Taylor et al., 2012).

The next challenge is to develop cells to graft that are resistant to degeneration. There is growing evidence that endogenous alpha synuclein is needed in order for Lewy pathology propagation and so generating graft cells with alpha synuclein knocked out is an attractive prospect for generating pathology-resistant midbrain DNs (Abeliovich et al., 2000; Chen et al., 2019; Luk et al., 2009).

1.3 Electrophysiological evaluation of oligomer pathology

Electrophysiology provides a valuable tool for evaluating the effects of aggregated proteins on neuronal function. Given that changes on this cellular level likely precede symptom development, it can give valuable insights into the early changes and how they might be able to be targeted to alter the progression of pathology. This thesis will deal only with *in vitro* electrophysiology in acute brain slices, but these electrophysiological techniques can also be used *in vivo* under different circumstances. *In vivo* experiments would give a greater level of translatability as the whole brain remains intact. However, I used *in vitro* experiments as they allow much greater control over the structure and concentration of aggregates and allow for fine pharmacological manipulations. *In vitro*, there are two commonly used electrophysiology techniques which can be implemented (Fig 1.16). The first is extracellular field recording which can provide an overview of the local network in the area of recording, detailing changes on a circuit level (Fig 1.16A). This can be useful for the study of synaptic transmission and synaptic plasticity and sample many synapses, providing an average response. Field recordings can be performed in a number of regions but are commonly performed in the hippocampus by stimulating Schaffer collateral/commissural fibres where they make synapses onto CA1 pyramidal cells, and recording excitatory postsynaptic potentials (EPSPs) in the CA1 region (Zhang et al., 2014).

The second, more targeted, technique is patch clamp recording which can provide access to specific changes within a single neuron (Fig 1.16B). The technique was developed by Neher and Sakmann (1976) in order to record the current flowing through single channels on a small patch of membrane. It was then later extended to measure from channels distributed across whole-cell membranes (Hamill et al., 1981). It can provide high resolution measurements from single neurons including sub-threshold information (such as changes in membrane potential and input resistance) which is not obtainable from extracellular field recordings. It works by forming a high resistance seal between the end of a glass recording pipette and the cell of interest. Negative pressure is then applied which ruptures the membrane and allows the contents

of the patch pipette to dialyse the cell. This type of recording is known as 'whole-cell' recording and allows for simultaneous current and voltage measurements to be taken from the cell. There are other forms of patch clamp recording which differ slightly in the initial patch protocol (inside out, outside out, cell attached, nucleated patch), with the form of recording defined by the experimental question (Van Hook and Thoreson, 2014). Once in whole-cell configuration, recordings can be made in one of two ways, either using the current clamp or voltage clamp configuration (Van Hook and Thoreson, 2014). In voltage clamp, the voltage across the cell membrane is clamped (usually around -60 mV) and the current needed to maintain this voltage level can be recorded. In current clamp, the cells resting membrane potential (mV) can be measured. This method allows the membrane potential to fluctuate in response to synaptic inputs or other membrane currents. Current can be injected (via the patch pipette) in order to elicit and record a voltage response.

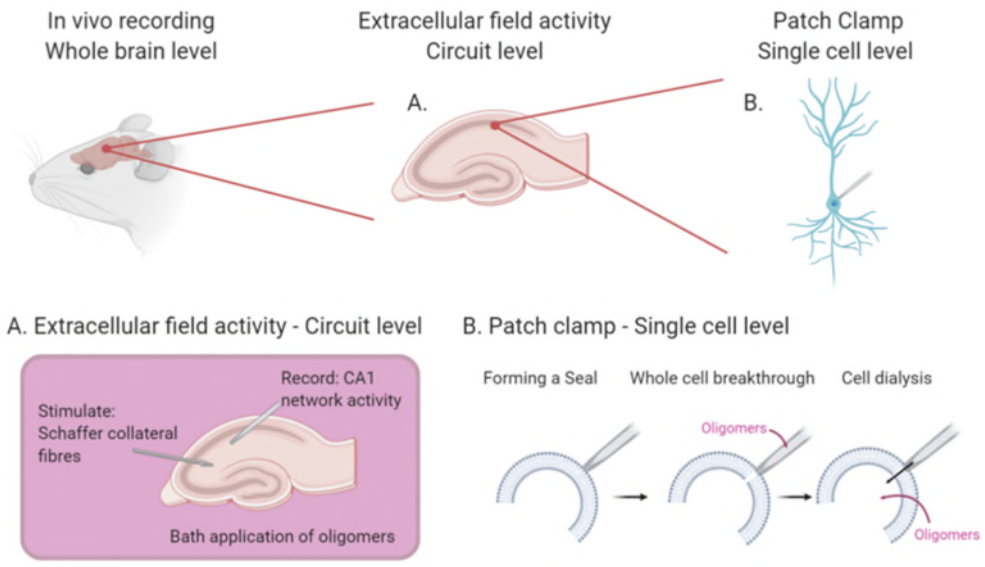

Figure 1.16: Electrophysiological approaches to measuring neuronal function. *A schematic to demonstrate the two most used in vitro approaches to evaluate the effect of tau dysfunction on neuronal activity. A) Extracellular field recordings in the CA1 region of the hippocampus use an electrode to stimulate the Schaffer collateral fibers and recording where they synapse onto CA1 pyramidal neurons. Recording field excitatory post-synaptic potentials (fEPSPs) allows the study of circuit activity. B) Whole-cell patch clamp recording allows for the parameterisation of single neurons and the study of the intracellular effects of structure and concentration-defined protein aggregates.*

There are three main delivery approaches used to evaluate the effects of protein aggregates, these are: transgenic mice, extracellular bath application/ viral infection, or delivery into single cells via the patch pipette.

1.3.1 Transgenic models

A classic approach to study physiological protein function is to generate transgenic mouse models and compare them to their wild-type littermates. This approach has several limitations, including compensation from other proteins during development. For example, in *MAPT* $^{-/-}$ mouse models there are limited functional effects observed, as other axonal proteins such as microtubule-associated protein 1A (MAP1A) can compensate to perform the microtubule-stabilization functions of tau (Dawson et al., 2001; Fujio et al., 2007; Harada et al., 1994; Tucker et al., 2001). Most studies of oligomer pathology using transgenic models depend upon promoting the overexpression of protein or by enhancing the level of aggregation and measuring the electrophysiological or behavioural phenotypes (Andorfer et al., 2005, 2003; Cowan et al., 2010; Lee et al., 2001; Polydoro et al., 2009; Spires et al., 2006; Tanemura et al., 2002; Tatebayashi et al., 2002; Wittmann et al., 2001; Yoshiyama et al., 2007). Another limitation in this case is that it is hard to quantify the exact form of protein responsible (e.g., small soluble oligomer, fibrils, insoluble aggregates, tangles), or the concentration of protein needed to see these effects. This introduces variation into data and makes equating changes in neuronal properties with tau aggregate structure and concentration difficult.

1.3.2 Extracellular bath application or viral injection

A different approach to study oligomer pathology is to perfuse the protein aggregates (recombinant or isolated from patient samples) onto the acute brain slices or by injecting them *in vivo* (Lasagna-Reeves et al., 2012). This method will circumvent the challenges of compensation observed with transgenic models and has been used successfully to elucidate many elements of aggregate pathology (Acquarone et al., 2019; Fá et al., 2016; Lasagna-Reeves et al., 2012; Ondrejcak et al., 2018). It does however have similar limitations in that the pathological effects cannot be easily attributed to the structure or concentration of protein aggregate. It can be hard to know how

much of the aggregate has been taken up into each neuron as in both cases they are applied extracellularly and thus they cannot determine whether the effects observed are due to the internalisation of aggregates or indirectly through the proteins acting extracellularly or indirectly through other cells, such as glia and astrocytes.

1.3.3 Delivery via patch-pipette

The lab of Dr Wall (where the work for this PhD thesis was undertaken), developed a novel approach utilising structurally defined, concentration-controlled preparations of oligomers, delivered via the patch pipette to characterise changes in neuronal function using whole-cell patch clamp recording (Kaufmann et al., 2016). Utilising a single-neuron approach allows one cell to be targeted in a network free from pathology, thus allowing direct time- and concentration- dependent effects of protein aggregates to be measured. This technique permits the targeting to pre- or post-synaptic cells to study synaptic transmission and plasticity as well as tracking of aggregate movement through the cell from the soma to processes. This technique provides an unparalleled level of mechanistic detail and will be implemented throughout this thesis to study aggregate-induced pathology. This technique does have a number of limitations including that the maximum recording timescale is defied by the lifetime of the slice and that the timescale from the introduction of aggregates to effects can vary from cell to cell. It can also be challenging to translate the single cell findings into an in vivo functional assay (for example behavioural tests) as only on neuron is targeted rather than the network.

1.4 Carbon dioxide in health and disease

1.4.1 Carbon dioxide

Carbon dioxide (CO_2) is excreted by breathing and its regulation is vital for life. The levels of CO_2 in the blood fluctuate around the physiological normal level of 40 mm Hg (Huckstepp et al., 2010b). If the level of blood CO_2 rises and the lungs can't remove it quickly enough then respiratory acidosis will occur, this is normally characterised by blood pH falling below 7.35 (normally the pH is between 7.35 and 7.45). In severe cases, this can lead to heart failure or death (Patel and Sharma, 2021). CO_2 levels can be altered by many situations, for example they will be increased in people who suffer from asthma, sleep apnoea or chronic obstructive pulmonary disease (COPD)(Owens and Malhotra, 2010). On the contrary, levels can be lowered when people hyperventilate (Brown, 1953; Wilson et al., 1991).

The ventilatory response to changes in the levels of PCO_2 consists of both a peripheral and a central response. The central CO_2 chemoreceptors are responsible for around 60-70% of the hypercapnic respiratory response, while the peripheral CO_2 chemoreceptors are responsible for the remaining 30-40 % of the response. The ventilatory response to PCO_2 changes can be modelled using a two component model, whereby the peripheral and central chemoreceptor responses (components) can be separated by the differences in their time constants (Dahan et al., 2007; Pedersen et al., 1999). In humans, when PCO_2 levels are increased from 44 to 55 mm Hg CO_2 and ventilation was measured, the peripheral chemoreceptors correspond to the fast component of the response (time constant ~ 3-10 s) whereas central chemoreceptors correspond to the slower component of the response (time constant ~ 2 mins; Dahan et al., 2007)). Central chemoreceptors are mainly localised on the surface of the ventral medulla but also on the nucleus of the solitary tract, locus coeruleus, caudal medullary raphe and the fastigial nucleus of the cerebellum. There will be some degree of temporal specificity depending on the site of CO_2 detection (Nattie, 1999).

1.4.2 Connexins

Connexins are a family of proteins that are embedded in cell membranes and can form large-pored channels. They assemble in groups of six into large conductance hexameric channels called connexons (Fig 1.17). Assembly of connexons occurs before delivery to the plasma membrane (Goodenough et al., 1996; Kumar and Gilula, 1996; Willecke et al., 2002) and once formed may either be delivered to the membrane or maintained in intracellular stores for a later timepoint (George et al., 1999). Two connexons on plasma membranes of neighbouring cells can then co-assemble to form a 'gap junction'. These channels allow the passage of both ions and other small molecules such as glucose and lactate. This inter-neuron connection is a key form of cell-to-cell communication. If there is just the one connexon that opens into the extracellular space and is not docked to an adjacent cell, they are known as a 'hemichannels' and have functions that are distinct from those of gap junctions. (Dale, 2008; Huckstepp et al., 2010b; Pearson et al., 2005; Stout et al., 2002; Weissman et al., 2004). Hemichannels can release adenosine triphosphate (ATP) to signal via ionotropic P2X and metabotropic P2Y receptors to mediate intracellular communication (Huckstepp et al., 2010b; Pearson et al., 2005). They can also, through opening, drastically alter both neuronal excitability and whole-cell conductance (Moore et al., 2014). Hemichannels can be homomeric if they consist of six of the same connexin proteins or heteromeric if they consist of a combination of different connexins and can have varying different effects to the homomeric channels. This is a complicating factor when studying the functional effects of specific connexins.

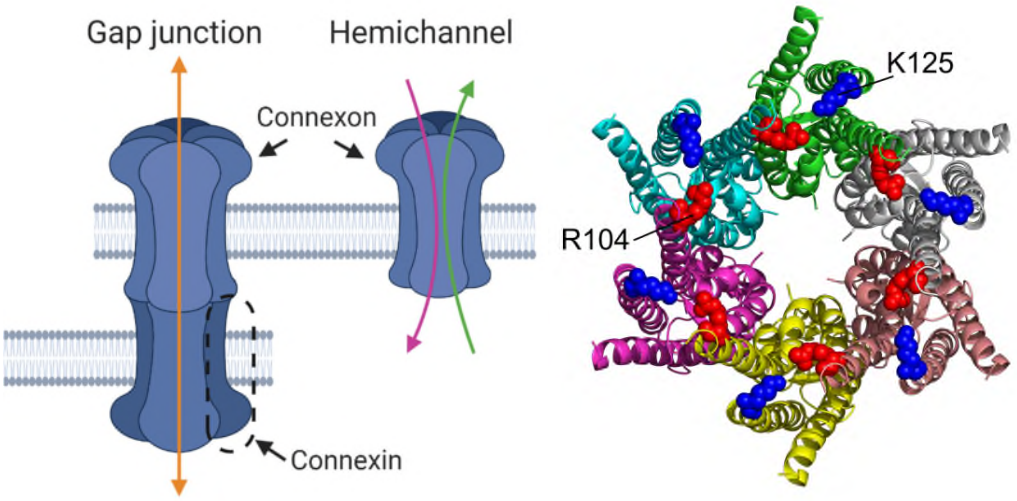

Figure 1.17: Connexin assembly into gap junctions and hemichannels.
(Left) Connexin channels assemble in groups of 6 to form connexons. These then either co-assemble with another connexon on a neighbouring neuron and form a 'gap junction' or remain as a single connexon open to the extracellular space, in which case they are known as 'hemichannel'. (Right) Structure of Cx26 showing the position of residues K125 (blue) and R104 (red) that form the carbamate bridge under alterations of CO_2 levels. Mutations of these two important residues abolishes the sensitivity to CO_2 (Adapted from Nijjar et al., 2021).

1.4.3 Carbon dioxide and connexins

There are 21 connexin genes in the human genome. There are a subfamily of these connexins that have evolved to be directly sensitive (not through a pH change) to CO_2 (connexin 26 (Cx26), connexin 30 (Cx30) and connexin 32 (32)) (de Wolf et al., 2016; Huckstepp et al., 2010b, 2010a; Meigh et al., 2013). Of these, Cx26 shows the strongest sensitivity and this is known to be mediated directly via the carbamylation of lysine residue 125 (Huckstepp et al., 2010b; Meigh et al., 2013). This is supported by compelling evidence that if this carbamylation motif is inserted into a CO_2-insensitive connexin (connexin 31), then CO_2 sensitivity can be induced in these channels (Meigh et al., 2014). Further evidence of this direct action through the carbamylation site comes from mutation studies: if either K125R or R104A are mutated within connexin 26, the CO_2 sensitivity is abolished (Meigh et al., 2014). If K125 is mutated to C125 instead then the hemichannel instead becomes sensitive to NO or NO_2

(Meigh et al., 2015). There is also no evidence of connexin 26 sensitivity to carbon monoxide (personal communication, Dale 2020). Finally, there are now cryoEM structures of gap junctions that support the carbamylation of K125 at different levels of PCO_2 (Brotherton et al., 2020). Since the physiological midpoint for Cx26 hemichannel opening is ~40 mm Hg CO_2, there will be a proportion of Cx26 hemichannels that are open at rest.

There is substantial additional functional research to support the direct interaction between CO_2 and Cx26 hemichannels. Firstly, in early patch clamp experiments, clear conductance changes were observed when the level of CO_2 was altered in cell lines (expressing Cx26; Fig 1.18). Raising the level of CO_2 to 55 mm Hg caused an increase in whole-cell conductance and in contrast, reducing to 20 mm Hg caused a decrease in whole-cell conductance. These effects are completely independent of any changes to pH (as all experiments were performed with isohydric solutions) (Huckstepp et al., 2010a, 2010b).

Connexin 26 is capable of forming heteromeric hemichannels or gap junctions with a number of other connexins, including Cx32, which is also sensitive to CO_2, although at higher levels (~ 70 mm Hg; Koval et al., 2014). Both Cx26 and Cx32 are expressed on the surface of the ventral medulla and thus it is feasible that they could form heteromeric channels, but the function of these channels is currently unknown.

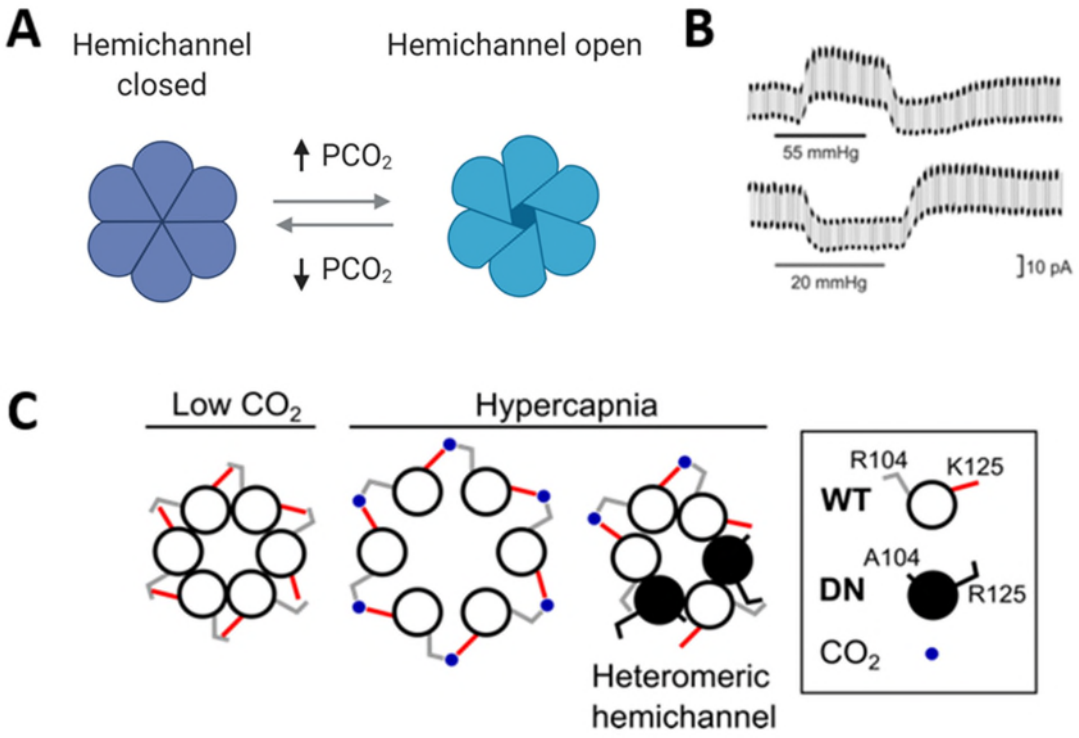

Figure 1.18: The results of changing the level of PCO_2 on connexin 26 hemichannels, effects on conductance.

(A) Through direct interactions between CO_2 and then connexins themselves, open probability can be shifted. Increasing the level of PCO_2 results in the opening of more hemichannels. Decreasing the level of PCO_2 results in the closing of more hemichannels. (B) Initial patch clamp recordings (Huckstepp et al, 2010) in cell lines expressing connexin 26 hemichannels. Altering the level of CO_2 (under isohydric conditions), results in changes to channel open probability and consequently to conductance changes. (C) Schematic to demonstrate how the dominant negative version of Cx26 allows hemichannel responses to be evaluated. This innovative method uses two mutations (K125R and R104A) to the connexin 26 gene that result in a subunit that can assemble with wild type connexin 26 subunits to form hemichannels but these resulting hemichannels are unable to change conformation and open in response to CO_2.

1.4.4 Physiological consequences of CO_2 sensitivity on breathing

Altering the level of CO_2 (without compensation) will result a change in pH which has been linked in a number of studies to the regulation of control of breathing (Gourine et al., 2010; Hosford et al., 2018; Kumar et al., 2014; Loeschcke, 1982; Trapp et al., 2008; S. Wang et al., 2013). There is also compelling evidence that CO_2 can have direct effects on breathing (Eldridge et al., 1985; Shams, 1985).

Raised CO_2 levels trigger the release of ATP from glial cells in the brainstem and this has direct effects on breathing (Gourine et al., 2005; Huckstepp et al., 2010a). Over many years, increased understanding of the direct mechanism of CO_2 interaction with connexin 26 has allowed the development of genetic tools with which to understand the physiological functions that this sensitivity contributes to. By generating a dominant negative subunit of Cx26, the functional effects of the sensitivity can be studied. This innovative method uses two mutations (K125R and R104A) to the Cx26 gene that result in a subunit that can assemble with wild type Cx26 subunits to form hemichannels, but the resulting hemichannels are unable to change conformation and open in response to CO_2 (Fig 1.18). In initial *in vivo* experiments, the dominant negative subunit of Cx26 was expressed in the glial cells within the medulla oblongata. It was demonstrated that CO_2 binding to Cx26 contributes to roughly half of the adaptive ventilatory response to hypercapnia that is controlled by central chemosensors (van de Wiel et al., 2020).

1.4.5 Conservation of Cx26-mediated CO_2 sensitivity across species

CO_2-sensitive Connexin 26 homologs are found in humans, rats, chickens, and naked mole rats. However, the level of CO_2 needed to open the channels differs across species. In humans and in rats the resting pCO_2 is ~ 40 mm Hg CO_2 and a shift to 55 mm Hg CO_2 is sufficient to significantly open the channels. However, in chickens, Cx26-mediated CO_2 sensitivity is lower, and they show significant channel opening at 35 mm Hg CO_2. The mole rat, in contrast is only CO_2 sensitive if the level is increased to 70 mm Hg CO_2 (de

Wolf et al., 2017). These distinctions are particularly interesting when one considers the environments in which these species reside and how this could be beneficial for respiratory chemoreception. Naked mole rats reside underground in burrows, with low gas permeability, therefore, will be rebreathing air and will thus experience hypoxia and hypercapnia. They are therefore adapted to survive better and maintain body weight in these conditions than standard laboratory rats (Arieli et al., 1977). It has further been shown that the level of CO_2 equilibrated in subepidermal gas pockets of the mole rat is considerably higher than that of the standard laboratory rat, thus suggesting that the resting pCO_2 may be higher (Ar et al., 1977). Whereas birds need to be able to fly at high altitudes. At higher altitudes, the birds will breathe more frequently and thus lower their pCO_2. Therefore, they need to be able to tolerate much lower pCO_2 levels than mammals in order to regulate their breathing (Osborne et al., 1977; Osborne and Mitchell, 1978) and maintain blood flow (Faraci and Fedde, 1986). They have adapted to have a lower resting pCO_2 of ~30 mm Hg, for example in chickens it is reported to be ~33 mm Hg CO_2 (Calder and Schmidt-Nielsen, 1968; de Wolf et al., 2017).

1.4.6 Not just a glial connexin

Although widely considered to be a primarily glial connexin (Nagy et al., 2011), connexin 26 is also expressed in a small number of neuronal populations throughout the brain. DN coupling via gap junctions was first described by Grace and Bunney (1983). A study by Vandecasteele et al. (2005) confirmed the presence of functional gap junctions between pairs of neighbouring DNs in the SNpc (Vandecasteele et al., 2007; Fig 1.19). They followed this with a second study to look at which connexins were present in the dopaminergic neurons (Fig 1.19). At postnatal day (P)7-10, connexins 26, 30 36, 23 and 43 are expressed (mRNA, from single cell RT-PCR). There is then a developmental shift and by P17-21 there is expression instead of Cx31.1, 36 and 43 (Vandecasteele et al., 2006). This is of particular interest given that connexins 26 and 30 are known to be directly sensitive to changes in CO_2 levels. Note that this demonstration of the mRNA being present does not mean that there are functional hemichannels. They performed dye loading experiments with luciferase yellow to look for functional hemichannels. By

lowering the calcium, hemichannels should open and allow the dye to be taken up, however they did not find evidence of this. This may have been because the connexins assemble as heteromers and this prevents the uptake.

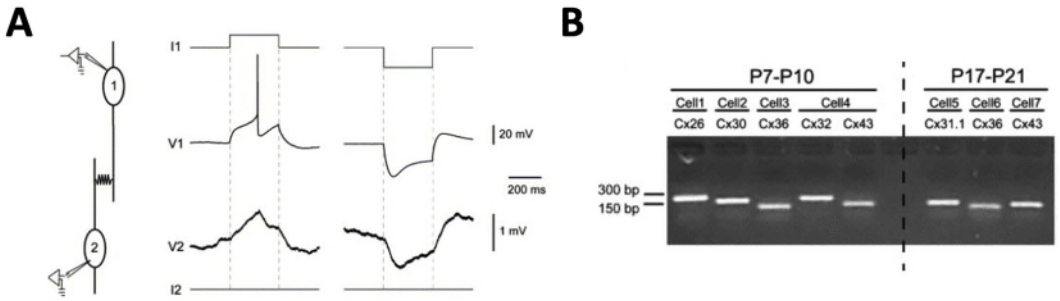

Figure 1.19: Demonstration of functional gap junctions between neighbouring dopaminergic neurons of the substantial nigra and the corresponding connexin expression

A. Whole-cell patch clamp recording of pairs of neighbouring dopaminergic neurons demonstrating functional gap junctions (electrical coupling) between cell 1 and cell 2. By injecting current (either +100 pA or -200 pA) only into one cell, a voltage response can be elicited in both cells. (Vandecasteele et al., 2005) B. A follow up study in which single cell RT-PCR was used to establish which members of the connexin subfamilies are expressed (mRNA) in representative example dopaminergic neurons within the substantia nigra. At postnatal day (P)7-10, connexins 26, 30 36, 23 and 43 can be found. There is then a developmental shift and by P17-21 there is expression instead of Cx31.1, 36 and 43. (Vandecasteele et al., 2006).

1.5 Recording regions and their physiological functions

1.5.1 Hippocampus – structure and connectivity

The hippocampus is divided into 4 main subfields CA1, CA2, CA3 and the dentate gyrus (DG). It is a region of the brain that is well characterised, and the circuitry of innervation is well established (Figure 1.20A). Input arrives to the hippocampus from the entorhinal cortex (EC) via two pathways, the perforant pathway (PP) and the temporoammonic (TA) pathway. The PP is the main input to the hippocampus, and it encompasses the traditional excitatory tri-synaptic pathway (Knierim, 2015). Axons from layer II of the EC project to the granule cells in the dentate gyrus (DG). DG axons are known as Mossy Fibres (MF) and they relay the signal from the DG to CA3 neurons. Then the signal is relayed along CA3 axons, which are known as Schaffer Collaterals (SC) to CA1 neurons. Finally, CA1 neurons can the relay the signal back to the EC, which forms the major output pathway of the hippocampus (Anderson et al., 2009; Neves et al., 2008). There are also additional projections from the EC directly to CA3 through the PP and also from the EC directly to CA1 through the TA pathway (Deng et al., 2010; Kajiwara et al., 2008; Figure 1.20A).

The CA1 layer of cells was chosen for my experiments as it contains pyramidal cells that are easy to locate and characterise (Figure 1.20B, C) and are easy to parameterise due to existing models developed and already implemented in the lab (Badel et al., 2008a, 2008b).

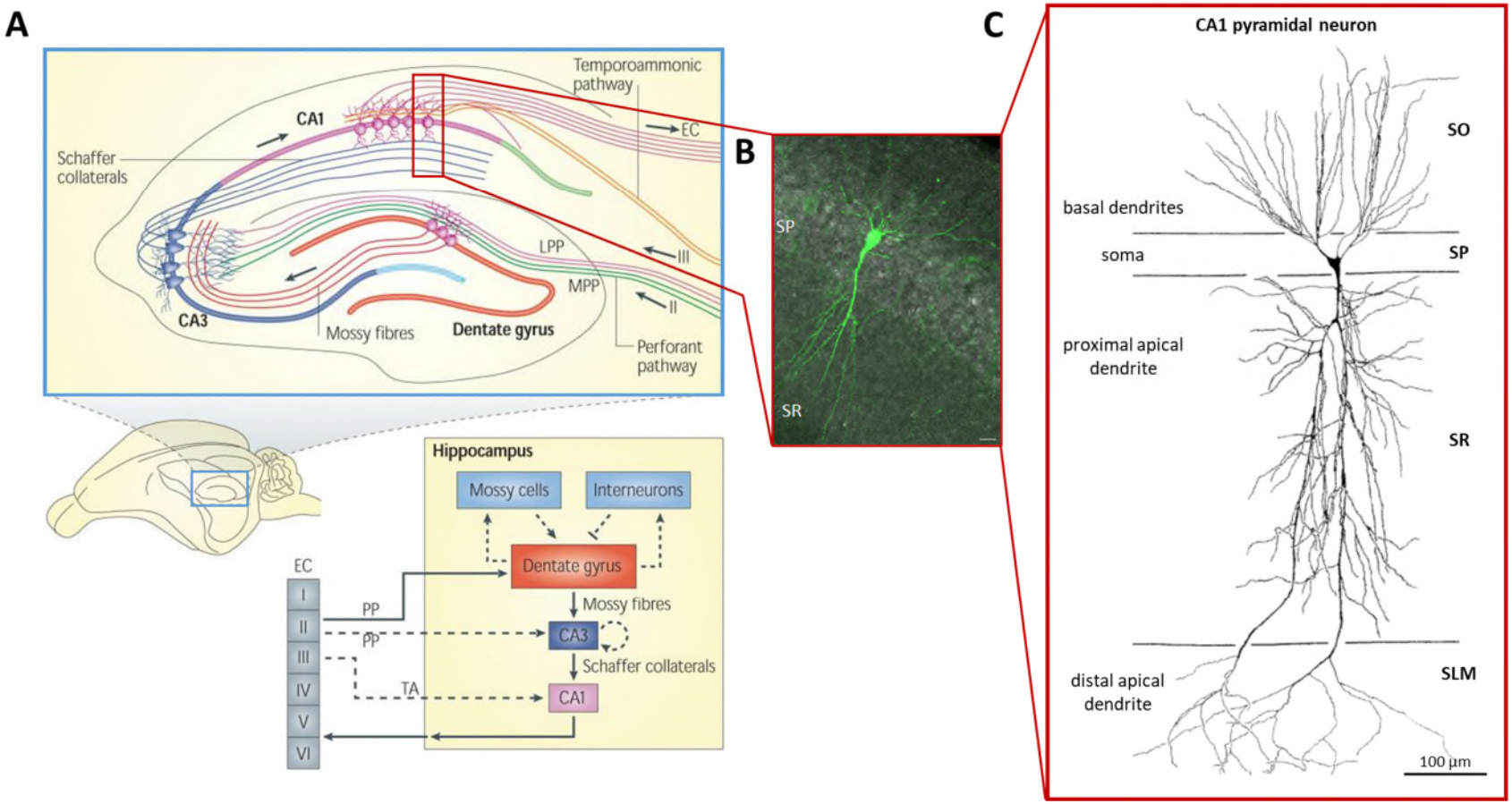
A
Temporoammonic pathway
CA1
EC
Schaffer collaterals
LPP
III
MPP
II
CA3
Mossy fibres
Dentate gyrus
Perforant pathway
Hippocampus
Mossy cells
Interneurons
Dentate gyrus
Mossy fibres
CA3
Schaffer collaterals
CA1
EC
I
II
III
IV
V
VI
PP
PP
TA
B
SP
SR
C
CA1 pyramidal neuron
SO
basal dendrites
soma
SP
proximal apical dendrite
SR
distal apical dendrite
SLM
100 µm

Figure 1.20: Structure and connectivity at the level of the hippocampus and a detailed example of CA1 neuron morphology

A. A schematic to demonstrate the circuitry of the hippocampus. There are two main input pathways from the entorhinal cortex (EC) - the perforant pathway (PP) and the temporoammonic (TA) pathway. The traditional excitatory tri-synaptic pathway runs from layer II of the EC to the dentate gyrus, then project to the pyramidal neurons in CA3 through the Mossy fibers (MF). These neurons then relay the message onto CA1 neurons through the Schaffer collaterals (SC). Followed by a projection back to the EC. There are additional projections from the EC directly to CA3 through the PP and also from the EC directly to CA1 through the TA pathway. The hippocampal recordings in this thesis were made from CA1 neurons in acutely prepared slices. Figure adapted from (Deng et al., 2010). B. Representative example of a recorded CA1 neuron that was filled with Alexa Fluor 488 to allow its morphology and localization to be examined. Imaged using Leica 770 confocal microscopy over bright field to highlight its position in the slice, scale bar = 14 µm. C. An illustration of the morphology of a CA1 pyramidal neuron. Its soma is in the stratum pyramidale (SP) and basal dendrites project into the stratum oriens (SO). Its apical dendrite is long and through the stratum radiatum (SR; where the proximal apical dendrites are found) to the stratum lacunosum-moleculare (SLM, where the most distal apical dendrites are located). Both the basal and apical dendrites display branches of projections. Figure adapted from (Ishizuka et al., 1995).

1.5.2 Hippocampus – role in learning and memory

The hippocampus is a region of the brain with important physiological roles in learning and memory (Ballard et al., 2019; Knierim, 2015; Scoville and Milner, 1957; Squire, 2009; Squire et al., 2015). It is also one of the key sites of pathology in Alzheimer's disease, where atrophy results in impaired cognition, working and episodic memory (Jack et al., 1999; O'Shea et al., 2016).

Synaptic plasticity in the form of long-term potentiation (LTP) and long-term depression (LTD) are key processes involved the in the storage and maintenance of memory (Abraham et al., 2019; Nabavi et al., 2014; Neves et al., 2008; Ryan et al., 2015). The CA1 region of the hippocampus provides a good site for studying synaptic plasticity as its circuitry is well characterised and it readily displays both long term potentiation (LTP) and long term depression (LTD) (Bliss and Gardner-Medwin, 1973; Bliss and Collingridge,

1993; Bliss and Lømo, 1973; Dhuriya and Sharma, 2020; Lüscher and Malenka, 2012; Malenka and Bear, 2004).

1.5.3 Neocortex

A subset of my experiments were performed in the neocortex, which has roles in memory storage and reasoning as well as perception and the generation of motor command. The structure and inter-layer connectivity is well conserved across species (Kozloski et al., 2001; Silberberg et al., 2002) which has allowed for effective characterisation in animal models. The layered columnar structure of the sensory cortices was first proposed by Vernon Mountcastle, in 1957 following initial characterisation in cats, but recent work (for ethical and practical reasons) tends to use rodent models instead (Mountcastle, 1998). The neocortex has a layered structure, with layer one at the outer edge of the slice, then layer II/III, layer IV, layer V and finally layer VI towards the border before the hippocampus. Neurons within each layer vary in size and project to different brain regions including the thalamus, the striatum and other areas of the cortex (Fig 1.21). Attempts have been made to use modelling approaches alongside electrophysiology to digitally reconstruct this network to understand its function better (Markram et al., 2015). In layer V, there are two subgroups of neurons, thick and thin tufted, which differ by the morphology of their apical dendrites and their neuronal inputs. In this study I targeted the thick tufted group, which are located deeper into layer V and whose axons project to the striatum, the pons, and the spinal cord. Thick tufted neurons are easily identifiable by their thicker apical dendrites and extensive branching in layer 1 of the cortex and burst firing on whole-cell breakthrough (Romand et al., 2011). Neurons in layer V are able to form synaptic connections with neighbouring neurons (Markram et al., 1997; Ramaswamy et al., 2015) and therefore provide a useful tool for studying synaptic transmission. This was the rationale behind using this brain region, as the synaptic connection rate (between pairs of neurons) was higher than in the hippocampus. Thick-tufted neurons in layer V were targeted as they have a connection rate of 1 in 10 pairs (Markram et al., 1997). These neurons have also been shown previously to work well with the dynamic IV extraction method which our lab have used previously to

parameterise neurons (Badel et al., 2008a, 2008b; Harrison et al., 2015; Kaufmann et al., 2016).

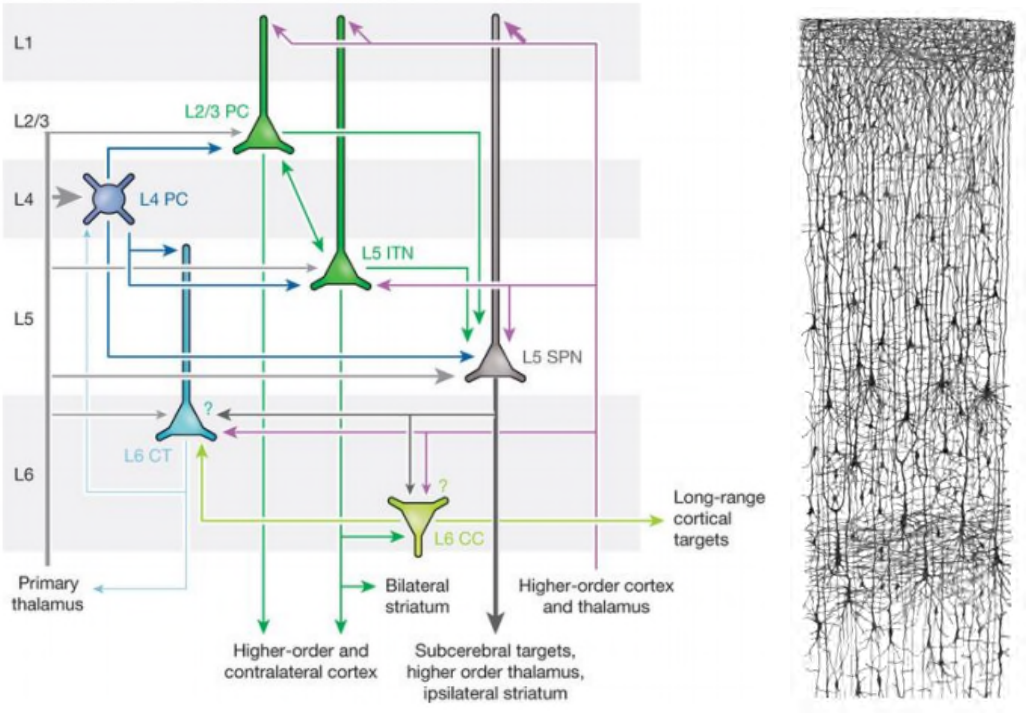

Figure 1.21: A simplified schematic of the microcircuitry of the neocortex.
A) The layers of excitatory neurons and their projection pathways are indicated (Figure reproduced from Harris and Mrsic-Flogel, 2013). B) Golgi stain of the neurons in the neocortex, demonstrating their elaborate axonal and dendritic ramifications and columnar structure (adapted from Ramón y Cajal, 1911).

Although the neocortex is not the most recognised region of pathology in PD and AD, Lewy body pathology can develop in the cortex and this is often paired with the loss of cholinergic input from the basal forebrain to the cerebral cortex and consequent neurodegeneration (Bohnen and Albin, 2011; Müller and Bohnen, 2013; Sugiyama et al., 1994). It is therefore a useful target region for evaluating protein aggregate pathology for my studies.

1.5.4 Pyramidal neurons

Layer V neurons in the cortex and CA1 neurons in the hippocampus are both examples of pyramidal neurons, which have a characteristic structure (Spruston, 2008). Pyramidal neurons are extensively studied and therefore provide an attractive target, both for electrophysiological characterisation and for modelling studies. Their structure is well conserved across brain regions (Fig 1.22) and consists of a soma with a single projecting axon which projects via collaterals both locally and to long range targets. Their dendrites consist of both short (basal) and a long projecting apical dendrite. Both sets of dendrites are highly specialised and able to receive synaptic inputs (London and Häusser, 2005). They express several different types of ion channels, including GIRK and HCN channels and the number of channels increases with distance from the soma. This means that they can be activated and inhibited by a range of neuromodulators (Berger et al., 2001; Takigawa and Alzheimer, 1999).

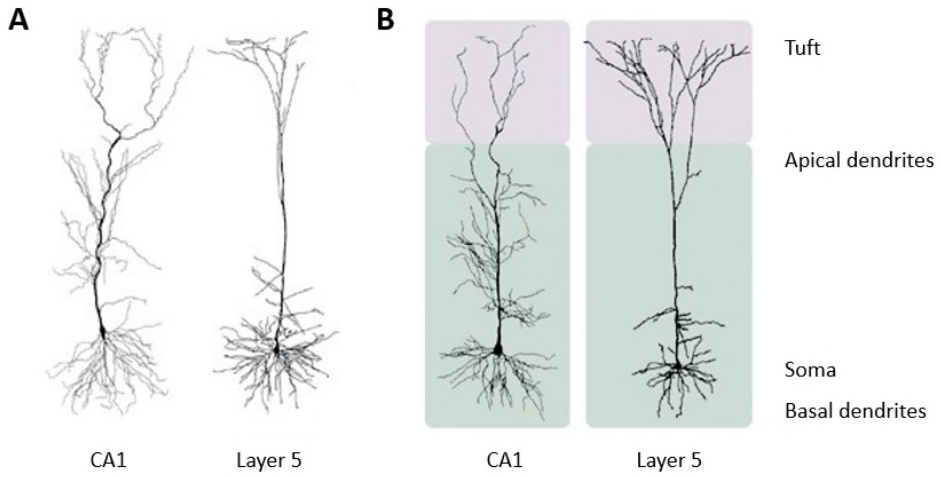

Figure 1.22: A comparison of the structure of pyramidal neurons in Layer of the neocortex and the CA1 region of the hippocampus.

A) Both examples of pyramidal neurons, they demonstrate considerable similarity in structure but differ in length of their apical dendrite and number of oblique dendrites. B) The apical tuft (purple) receives excitatory inputs that can differ from those targeting proximal apical dendrites or basal dendrites. For example, for in CA1 pyramidal neurons, the dendrites in the apical tuft located receive synaptic input directly from the entorhinal cortex, whereas the basal and proximal apical dendrites

in the stratum radiatum receive input primarily from CA3 cells via the Schaffer Collaterals. (Amaral and Lavenex, 2007; Figure adapted from Spruston, 2008).

1.5.5 Basal ganglia

The basal ganglia is a region near the base of the brain that encompasses different sub-regions including the substantia nigra (pars compacta and pars reticulata), the striatum (caudate nucleus and putamen), the globus pallidus (external GPe and internal GPi) and the subthalamic nucleus (STN). The substantia nigra pars compacta (SNpc) is a one of the key dopaminergic nuclei in the brain and its neurons play important roles in the control of movement, reward, and sleep. Glutamatergic transmission into the basal ganglia is received from the neocortex. From the SNpc, the basal ganglia circuitry has two major pathways of dopaminergic innervation (Figure 1.9; Lanciego et al., 2012).

Dopamine is a small molecule excitatory neurotransmitter widely distributed throughout the brain. Dopamine receptors belong to the G-protein coupled receptor (GPCR) subfamily and can be classified into receptor families D1 and D2 by their physiology and pharmacology (Bhatia et al., 2021). Dopamine receptors from the D1 family (D1 and D5) are coupled to Gαs. When dopamine binds to a D1 family dopamine receptor, the *globus pallidus interna/substantia nigra pars reticular* (GPi/SNr) is inhibited directly and this results in the upregulation of the glutamatergic output from thalamus to neocortex, thus increasing movement (Bhatia et al., 2021; Keeler et al., 2014). Thus, when neurons are lost from the SNpc, there results a lack of regulation, a loss of excitation to the neocortex and thus impaired motor control.

The D2 receptor family is comprised of receptors D2, D3 and D4, which couple to Gαi. When dopamine binds to a D2 receptor, it inhibits the subthalamic nucleus (STN) via a pathway through the *globus pallidus externa* (GPe). The STN can then send excitatory projections back to the GPi/SNR (Keeler et al., 2014). The binding of dopamine to D2 family receptors has also been shown to decrease the activity of tyrosine hydroxylase by modulating its level of phosphorylation (Kehr, 1974; Roth, 1984; Wolf and Roth, 1990). A reduction in D2 receptors (after neurons are lost), will lead to less inhibition of movement

and dystonia (DeLong and Wichmann, 2007; Galvan and Wichmann, 2008; Keeler et al., 2014).

There are two D2 receptor variants, D2S and D2L which are produced by alternative splicing, with the long version harbouring an extra 29 nucleotide cytoplasmic loop. D2S and D2L localise to the presynaptic and postsynaptic membranes respectively (Hisahara and Shimohama, 2011). Some populations also have local D2 autoreceptors which respond to dopamine and modulate the neuronal resting potential. These D2S receptors are found at pre-synapses and acts as a negative feedback loop so when dopamine is released, it binds and prevents further release of dopamine via hyperpolarisation of the membrane potential and thus a decrease in firing rate and excitability (Mercuri et al., 1997; Silva and Bunney, 1988). This occurs via activation of a GIRK conductance (Cathala and Paupardin-Tritsch, 1999; Lacey et al., 1987).

1.5.6 Ventral tegmental area

The ventral tegmental area (VTA) is a group of neurons located close to the midline on the floor of the midbrain and is one of the core regions of dopaminergic signalling in the brain. Several recent studies have shown that the VTA is highly heterogeneous containing different subtypes of neurons and many projection sites (Fig 1.23). Between 65-70 % of neurons are dopaminergic, with most of the remaining neurons (~35%) GABAergic and a small percentage being glutamatergic. In this thesis, I focus on the GABAergic neurons, of which ~32% are both VGAT- (vesicular transporter) and GAD67-positive, ~67% are VGAT-positive and only 1% are positive for GAD67 but not for VGAT, highlighting the heterogeneity even within the GABAergic subgroups of the VTA (Chowdhury et al., 2019).

Some of the GABAergic neurons can also co-release other transmitters such as glutamate and dopamine (Bouarab et al., 2019; Morales and Root, 2014; Root et al., 2018; Takata et al., 2018; Yoo et al., 2016; Fig 1.24). Although it is important to distinguish that dopaminergic neurons that co-release GABA cannot be identified by conventional markers as they synthesise their GABA using ALDH1a1 rather than GAD (Kim et al., 2015) and they load vesicles with VMAT2, independent of VGAT (Tritsch et al., 2012).

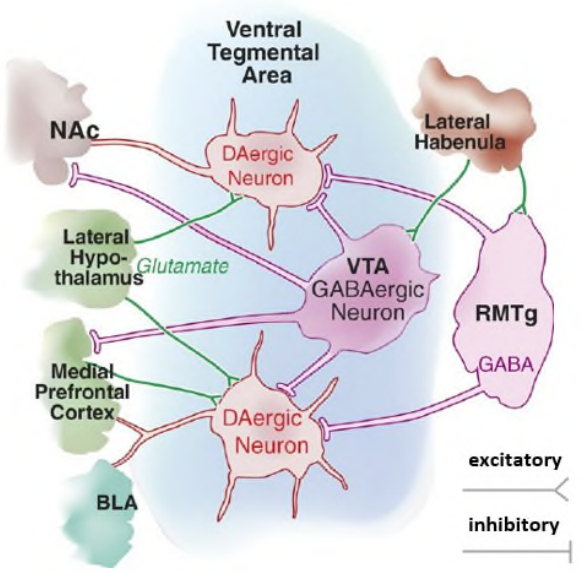

Figure 1.23: A simplified schematic of the complex circuitry of the ventral tegmental area and surrounding brain regions.

Dopamine neurons receive excitatory inputs from a number of regions including the lateral hypothalamus, medial prefrontal cortex (mPFC) and the pedunculopontine tegmental nucleus/ laterodorsal tegmental nucleus. They then project to the basolateral amygdala, medial prefrontal cortex, and the nucleus accumbens (NAc). GABAergic neurons receive excitatory inputs from the lateral habenula and inhibit both the mPFC and the NAc as well locally inhibiting dopamine neurons in the VTA. Figure adapted from Stuber et al., (2012).

VTA dopaminergic neurons have well-defined roles in motivation, reinforcement learning and reward processing (Holly and Miczek, 2016; Lammel et al., 2014; Morales and Margolis, 2017). GABAergic neurons play a modulatory role, with both local and long range projections (Bouarab et al., 2019) and are believed to encode the prediction of reward (Eshel et al., 2015; Tan et al., 2012; van Zessen et al., 2012). Long-term potentiation of local GABAergic synapses onto VTA DA neurons, greatly increases the inhibition of DA neurons (Simmons et al., 2017) and this can be blocked by a single administration of drugs of abuse such as morphine, ethanol or cocaine (Guan and Ye, 2010; Niehaus et al., 2010; Nugent et al., 2009, 2007). Long range GABAergic projections from the VTA to the dorsal raphe nucleus (DRN) are involved in the encoding of both aversion (activation of rostral VTA neurons that project to DRN serotonergic neurons) and reward (activation of caudal VTA neurons that project to DRN GABAergic neurons (Li et al., 2019).

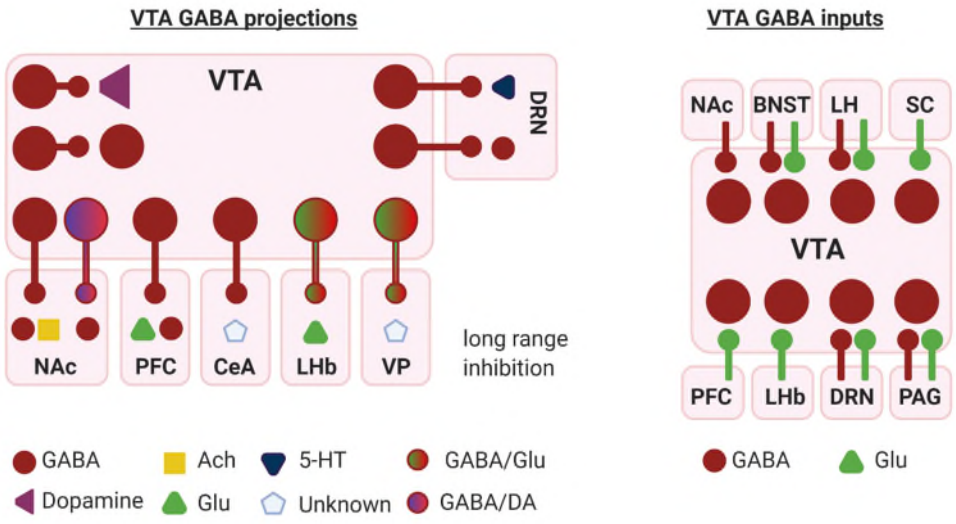

Figure 1.24: Complex heterogeneity of GABAergic inputs and outputs from the ventral tegmental area

The VTA has a complex input and output pattern GABA neurons from a wide range of brain regions. It is complicated further by the presence of synapses that can co-release combinations of other neurotransmitters too (e.g., dopamine and glutamate or GABA and glutamate). Abbreviations: BNST, bed nucleus of the stria terminalis; CeA, central amygdala; DRN, dorsal raphe nucleus; LHb, lateral habenula; LH, lateral hypothalamus; NAc, nucleus accumbens; PAG, periaqueductal gray; PFC, prefrontal cortex; SC, superior colliculus; VP, ventral pallidum; VTA, ventral tegmental area. (Adapted from Bouarab et al., 2019)

Although this role in aversion and reward is well characterised, more recently the VTA has also been found to also have important roles in other behaviours. For example, it has been demonstrated that the VTA is a key component of the sleep/wake circuitry, with VTA-dopaminergic neuron activation sufficient to drive wakefulness and necessary for the maintenance of wakefulness (Eban-Rothschild et al., 2016; Fifel et al., 2018). It has been shown that VTA GABAergic neurons can also mediate changes in activity across the sleep/wake cycle and their activation can alter the sleep/wake state (Takata et al., 2018; Yu et al., 2019) and that disruption of these GABAergic neurons can lead to mania (Yu et al., 2020). Given the important and varied roles of these neuronal populations in a wide range of behaviours, any factors that modulate their function and excitability could potentially also influence these behaviours.

1.6 PhD Aims

1. To use whole-cell patch clamp recording to introduce oligomeric forms of tau protein into hippocampal neurons to evaluate its effects on neuronal function: **(Chapter 3)**
    a. Firstly, on action potential dynamics and subthreshold neuronal properties in single cells
    b. Then using synaptically connected pairs of cortical cells, to establish whether there are specific pre- or postsynaptic effects of oligomeric tau protein on synaptic transmission and plasticity (both short- and long-term)
    c. Finally using high-resolution imaging techniques to study oTau localisation
2. To use truncations of the full-length tau protein to test if there are specific regions of the tau molecule that are responsible for the observed changes in neuronal properties, and to begin to decipher the mechanisms underlying these changes. **(Chapter 4)**
3. To introduce alpha synuclein monomers and oligomers into identified dopaminergic cells in the substantia nigra and observe the time dependent electrophysiological effects, then to assess how they are mediated. **(Chapter 5)**
4. To use electrophysiology, pharmacology and immunohistochemistry to evaluate the CO_2 sensitivity of dopaminergic neurons in the substantia nigra and GABA neurons in the VTA. **(Chapter 6)**

Methods and Materials

Parts of this chapter have been published previously:

- *Hill et al., 2020, Star protocols*
- *Hill et al, 2021a, b (Invited book chapters, in press).*

2.1 Tau production

I generated tau oligomers following the protocols published in Karikari et al., (2017; Fig 2.1). Some of the preparations were maintained unlabelled and some were labelled with a fluorescent dye to allow monitoring of cellular localisation following injection into neurons. Alongside the tau production, I also generated control samples which were not inoculated with a tau plasmid in stage 2.1.1. These controls (both labelled and unlabelled) were interleaved with the testing of the tau samples for comparison.

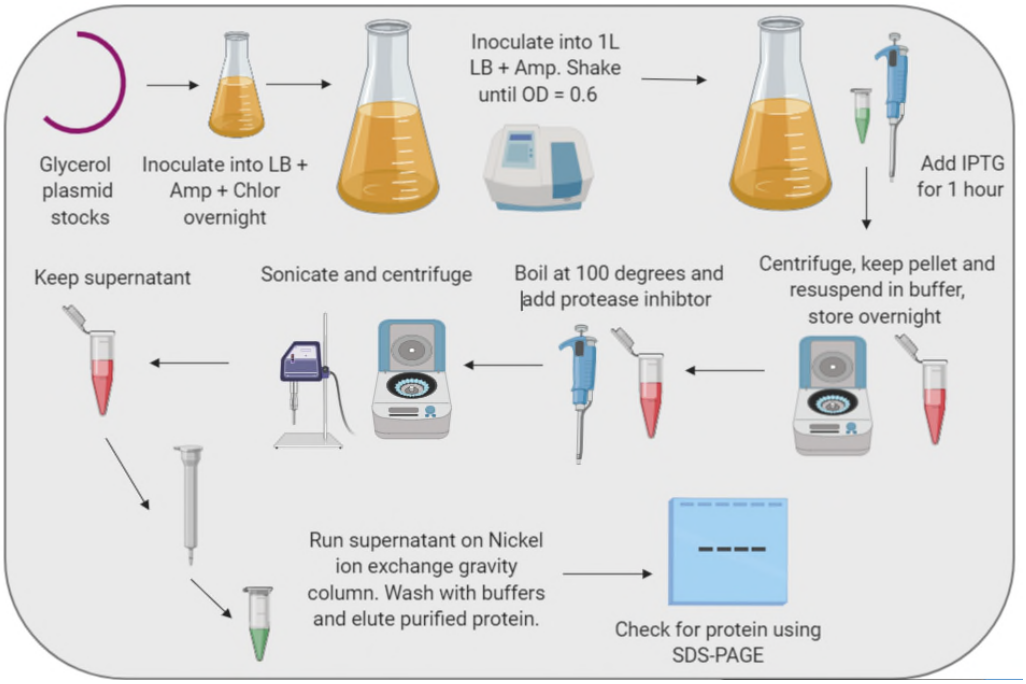

Figure 2.1: A simplified diagram of the tau production protocol

A schematic displaying the key stages from initial glycerol stocks of plasmids through expression and purification stages to detection of the purified protein via SDS-PAGE. Detailed methods follow (2.1.1-2.1.3)

2.1.1 Protein expression

Escherichia coli BL21 (DE3) carrying pProEX plasmids (Promega, Fig 2.2) coding for wild-type full-length tau-441 (Uniprot ID: P10636-8; appendix ref) with N-terminal 6xHis and FLAG tags and cysteine modifications (C291A/C322A/I260C), were inoculated into Luria broth (15 ml) containing ampicillin (100 mg/ml) and chloramphenicol (35 µg/ml) and incubated at 37 °C at 180 rpm overnight. Cultures were then added to 750 ml LB broth with ampicillin (100 mg/ml) and returned to the shaking incubator for 90 minutes. When the OD600 reached 0.6, 0.5mM isopropyl β-D-1 thiogalactopyranoside (IPTG) was added for 1 hour. Samples were centrifuged for 10 minutes at 4 °C at 9800 g. The supernatant was removed, and pellets washed with 10 mM 7.4 buffer Na_2HPO_4 twice before being re-dissolved in 10 mM sodium phosphate buffer (pH 7.4) and stored at -20 ºC until use.

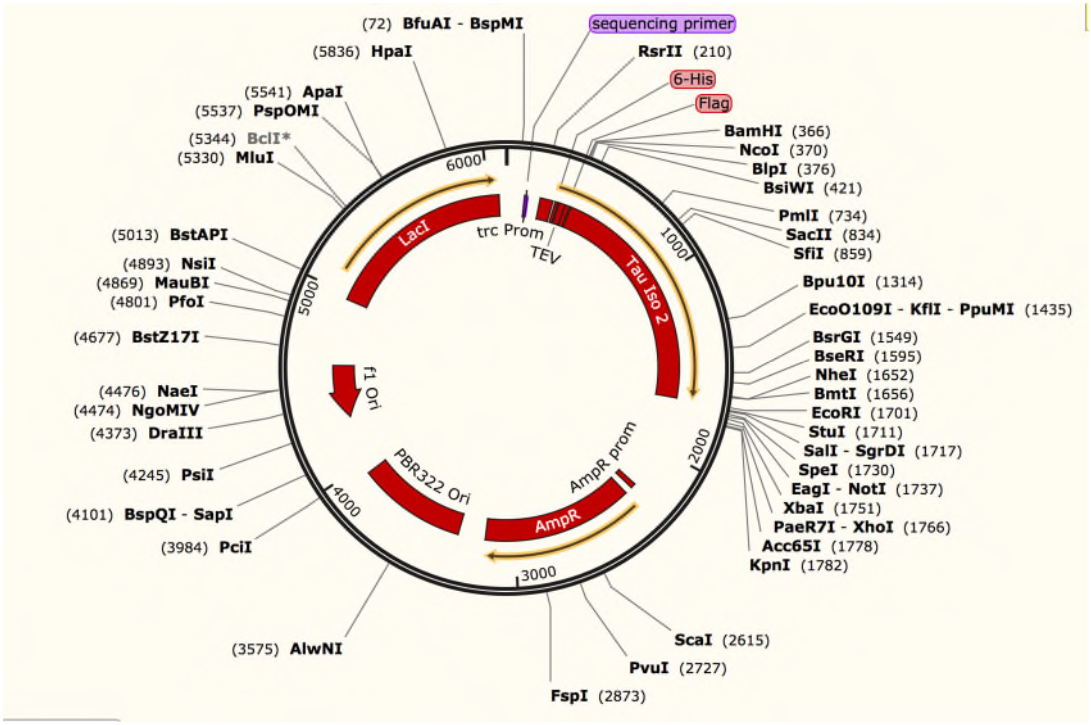

Figure 2.2: pProEXHTA-Flag-Mtau40 plasmid structure.

Escherichia coli BL21 (DE3) carrying pProEX plasmids (Promega) coding for wild-type full-length tau-441 (Uniprot ID: P10636-8) with N-terminal 6xHis and FLAG tags and cysteine modifications (C291A/C322A/I260C).

2.1.2 Protein purification

Samples were defrosted on ice and boiled for 10 minutes at 100 °C. A protease inhibitor cocktail tablet was added (Thermofisher Scientific, #A32963) and left to dissociate for 1 hour at room temperature. Each sample was then sonicated at 70% power for 1 minute and centrifuged at 4 °C, at 48000 g for 15 minutes. The supernatant containing the crude extract was kept and purified using an immobilised metal affinity chromatography (IMAC) A Ni-NTA column.

Buffer A: 50 mM Na_2PO_4 pH 7.0, 500 mM NaCl, 10 mM Imidazole

Buffer B: 50 mM Na_2PO_4 pH 7.0, 500 mM NaCl, 25mM Imidazole

Buffer C: 50 mM Na_2PO_4 pH 7.0, 500 mM NaCl, 500 mM Imidazole

The column was first washed with 70% ethanol. The chelating sepharose resin, added to the column (GEHealthcare, UK), was charged with 10 mM $NiCl_2$/CH_3COONa pH 4.0 and equilibrated with buffer A followed by the addition of the crude extract. The column was then washed once with buffer A, twice with buffer B (increased imidazole concentration for washing) and finally then washed once with buffer C to elute the purified protein from the column in 1 ml fractions. Eluted fractions were frozen at -20 ˚C until use.

2.1.3 Concentrating the tau protein

Collected 1 ml fractions of eluted protein were run on six percent hand-cast non-denaturing sodium dodecyl sulphate polyacrylamide gel electrophoresis (SDS-PAGE) gels (Table 2.1) to find those with the highest yields.

Resolving gel:	**Stacking gel:**
5.2 ml H_2O	2.975 ml H_2O
2 ml bis-acrylamide (Sigma Aldrich #A3574)	0.67 ml bis-acrylamide
2.6 ml 1.5M Tris/HCl pH 8.8	1.25 ml 0.5M Tris/HCl pH 6.8
100 ml 10% SDS (Sigma Aldrich #L3771)	50 ml 10% SDS
100 ml 10% APS (Sigma Aldrich #A3678)	50 ml 10% APS (made fresh)
10 ml TEMED (Sigma Aldrich #T-7024)	5 ml TEMED

Table 2.1: Recipe for six percent hand-cast non-denaturing sodium dodecyl sulphate polyacrylamide gel electrophoresis (SDS-PAGE) gels.

APS and TEMED were added immediately before use. Resolving gel was allowed to set for 30 minutes before stacking was added and then allowed to set for a further 30 minutes. Gels were then used immediately.

After running the gels, they were stained with Instant Blue (Expedeon, #ISB1L) for 1 hour at room temperature. Fractions that contained high protein yields were then pooled together for concentrating. Vivaspin falcons (5000 MWCO; Sigma Aldrich, #VS2011) were washed with 1 ml NaH_2PO_4 buffer pH 7.4 and then defrosted samples were added and centrifuged for 30 minutes x 2600 xg x 4 °C until ~80 % had gone through. A bicinchoninic acid (BCA, G-Biosciences, #786-570) curve was used to calculate the concentration and where needed the remaining liquid concentrated with further spins and concentration recalculated until all samples reached 1 mg/ml.

2.1.4 Labelling of tau protein oligomers

One of the aims of this project was to monitor the localisation of the introduced tau within neurons. A label that binds to cysteine residues (Alexa Fluor 488 C5-maleimide (Molecular Probes, #A10254)) was chosen for this in order to reduce aggregation and maintain the tau at a low molecular weight. The initial tau plasmid had 3 cysteine modifications in order to maintain function and allow this labelling. These modifications have previously been shown to have no detrimental effects on tau function (Karikari et al., 2019a; Kumar et al., 2014; Michel et al., 2014; Shammas et al., 2015). Samples were adjusted to 1 mg/ml, with 1 ml tris(2-carboxyethyl)phosphine (TCEP, Sigma Aldrich, #C4706), and Buffer NA_2HPO_4 pH 7.4 and left for 1 hour to allow the 5 x molar excess of TCEP to reduce the protein down to monomers. The label (1.5 ml, 4x molar excess) was then added, and the samples allowed to reform oligomers overnight. Samples were freeze-dried on dry ice before being stored at -80 °C.

The following day samples were defrosted on ice and the label dialysed out using dialysis buffer (50 mM Tris HCl pH 7.5, 100 mM NaCl) in a Slide-A-LyzerTM MINI Dialysis device (10K MWCO, Thermofisher Scientific, #69570). The buffer was changed 4 times over 12 hours and the sample recovered at the end of the day. Unlabelled controls were prepared following the same protocol but with equal volume of 10 mM NA_2HPO_4 pH 7.4 instead of the maleimide label. The entire labelling process was performed at room temperature.

2.1.5 Structural characterisation of oTau using transmission electron microscopy

Transmission electron microscopy was used to confirm the aggregated nature of the protein. Formvar/carbon-coated 300-mesh copper grids (Agar scientific, #162) were glow-discharged using the ELMO system from Cordouan Technologies. Samples (5 µl) of labelled or unlabelled tau-441 preparations were pipetted onto the grid and allowed to bind for 1 minute. Filter paper was then used to remove any excess liquid and 5 µl of 2 % uranyl acetate was added for 1 minute. Filter paper was then used to remove any excess uranyl

acetate stain and the grids were imaged using a JEOL-2100F transmission electron microscope.

2.1.6 Preparation of tau monomers

In order to confirm that any observed effects on neuron electrophysiology were specifically the result of oligomeric tau protein, the oligomeric samples were broken down into monomers and then tested. To do this, 5 mM of reducing agent dithiothreitol (DTT, Sigma Aldrich, #10197777001) was added to the samples which were then incubated at 60 ˚C for 30 minutes. This was sufficient to break the tau oligomers down to monomers (Fá et al., 2016). This was confirmed using hand-cast non-denaturing SDS-PAGE 6% and staining with Instant blue (Expedeon, #ISB1L). I then validated that the monomers would remain monomeric for a 3-hour period following breakdown, if stored on ice, thus providing a period in which experiments could be carried out. A confirmatory gel was run at the end of the experiments to demonstrate that a partner sample, treated with this monomerisation protocol also remained monomeric after 3 hours.

2.2 Tau N-terminal mutant production

2.2.1 Plasmid modification and primer design

A New England Biolabs Q5 site-directed mutagenesis kit (NEB, #E0554S) was used to generate the deletion of the N-terminal region of the tau protein from the original full-length plasmid (Appendix; 8.3). I left the first methionine amino acid in place for structural integrity and designed the primers to cut out amino acids 2-122 (pink region, Fig 2.3; Table 2.2).

Primer:	**Sequence (5' to 3'):**
Forward Reverse	AGCCTGGAAGACGAAGCT CATGGATCCCTTATCGTCATC

Table 2.2: Primers for plasmid modification

i500 mM primer stocks in EB buffer and stored at -20 degrees. Working stocks of 10 mM were made fresh with nuclease-free water for each SDM protocol.

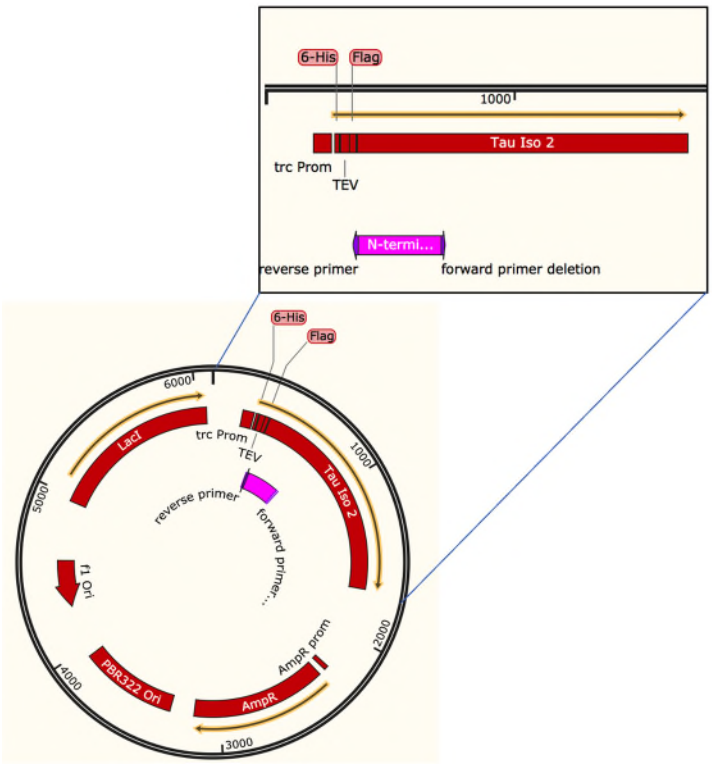

Figure 2.3: pProEXHTA-Flag-Mtau40 plasmid with deletion and primers marked.

Plasmid encodes full length human wild type 441- Tau, preceded by His and Flag tags upstream. The pink region marks the proposed deletion of t77he N-terminal region (2-122). Purple arrows represent the forwards and reverse primers used to complete the site directed mutagenesis.

2.2.2 Site directed mutagenesis

Site directed mutagenesis was carried out using the template plasmid DNA and primers detailed in 2.2.1. For full protocol details please see kit, but briefly:

	Volume	**Final concentration**
Master Mix	12.6 ml	1x
10 mM forward primer	1.25 ml	0.5 mM
10 mM reverse primer	1.25 ml	0.5 mM
Template DNA	0.5 ml	1-25 ng
Nuclease-free water	9.5 ml	

The following cycle conditions were used to carry out the initial mutagenesis:

	Temperature	**Time**
Initial denaturing	98 degrees	30 seconds
25 cycles	98 degrees	10 seconds
	56 degrees	20 seconds
	72 degrees	20 seconds per kb (6.5kb)
Final extension	72 degrees	2 minutes
Hold	4 degrees	

The PCR product was used to set up three KLD reactions using 1 - 3 ml starting material:

PCR product	1 ml	2 ml	3 ml
2 x KLD reaction buffer	5 ml (1x FC)	5 ml (1x FC)	5 ml (1x FC)
10 x KLD Enzyme mix	1 ml (1x FC)	1 ml (1x FC)	1 ml (1x FC)
Nuclease free water	3 ml	2 ml	1 ml

2.2.3 Transformation into competent cells

5 ml of the KLD product was added to 50 ml of competent cells (from the NEB SDM kit, #E0554S), incubated on ice for 30 minutes and heat shocked at 42˚C for 30 seconds. After a 5-minute incubation on ice, 950 ml SOC medium (Sigma Aldrich, #S1797) was added to each sample and placed in a shaking incubator at 37 ˚C for 1 hour. Dilutions of 50, 100 and 850 ml were plated onto LB + ampicillin (100 mg/ml) plates and allowed to incubate and grow overnight at 37 ˚C in a shaking incubator. The following day, 12 colonies were picked, and added to 5-10 ml fresh LB buffer + ampicillin (100 mg/ml). Samples were incubated shaking at 37 ˚C overnight.

2.2.4 Miniprep and DNA double digest

A Monarch Plasmid Miniprep Kit (NEB, #T1010) was used to isolate the plasmid DNA from *E.Coli* and stored at 4˚C. A DNA double digest of the isolated plasmid DNA was carried out using 2 ml DNA, restriction enzymes BamHI and EcoRI (0.5 ml each), chosen as they cut either side of tau (Fig 2.3), CutSmart buffer (NEB, #B7204S) 2 ml and 15 ml Nuclease-free water. Reactions were left at 37 ˚C in water bath overnight. Undigested full-length samples should give a 1.4kb fragment and successful mutagenesis should give a 1.1kb fragment. DNA gel electrophoresis was used to confirm the presence of the truncated fragment. Proteins were separated using SDS-PAGE electrophoresis in a 1 % gel. A protein ladder was used for size reference (#P7712 or #P7712S from New England BioLabs, size range = 11 – 245 kDa). 25 ml of each sample was loaded and ran for 1 hour (120 V, 200 mA, 50 W). Gel detection performed using an ImageQuant™ LAS4000 biomolecular imaging system (GE Healthcare).

2.2.5 Sequencing

Sequencing was performed to check that the mutagenesis had been successful for all samples that showed deletions on gel electrophoresis (5 ml DNA 80-100 ng, 5 ml primer). Sequencing primers were made up to 500 mM stock in EB buffer and stored at -20 ˚C. A working stock was created in water and used for the sequencing preparations. Sequencing was outsourced to Eurofins. Snap gene was used to evaluate the sequencing data.

2.2.6 Transformation of successful colonies

1 ml DNA was added to 100 ml competent cells (thawed on ice) and incubated for 40 minutes on ice. Heat shock was performed for 90 seconds at 43 ˚C and then 1 ml SOC medium (Sigma Aldrich, #S1797) added. Samples were incubated for 1 hour at 37 ˚C and then 10 ml and 100 ml spread onto LB + ampicillin (100 mg/ml) plates for each of the samples. The remaining sample was spun for 5 minutes at 13000 g to pellet, the supernatant removed, and pellet resuspended in 100 ml LB. 100 ml was then plated onto a LB + ampicillin (100 mg/ml) plate and all plates were incubated at 37 ˚C overnight. The following morning colonies were inoculated into LB + ampicillin (100 mg/ml) and left to grow overnight. After 24 hours, samples were either used to make 50% glycerol stocks and frozen at -80 ˚C or inoculated into larger 750 ml cultures of LB + ampicillin (100 mg/ml) and the protocol for producing full-length tau was initiated (as in 2.1.1-2.1.3).

2.2.7 Western blot protocol

Blocking solution: TBS + Tween 20 with 2 % dried skimmed milk (Marvel, UK)

Transfer solution: 200 ml blocking x10, 400 ml methanol, 1400 ml water

Following purification, to ensure that the observed bands on SDS-page were tau-positive, a western blot was used. The resolving gel was washed in transfer solution to remove SDS and then was transferred to an ECL nitrocellulose membrane (Amersham Biosciences, #10600002). The gel was packed into a Mini Trans-Blot Cell (Bio-Rad) and submerged in transfer solution at 4 °C. Electrophoresis was used to enable transfer to the membrane at 200 mA for 2.5 hours. The membrane was then removed and blocked with TBS + Tween 20 (TBST) containing 2 % dried skimmed milk (Marvel, UK) for 1 hour to prevent non-specific binding. The primary antibody was added against tau (HT7, ThermoFisher, 1:1000, #MN1000) for 2 hours and the washed 4 times with TBST. The secondary antibody (horseradish peroxidase (HRP)-conjugated anti-mouse antibody, 1:1000 dilution; ThermoFisher #61-6520) was then added for 1 hour at room temperature. Finally, the membrane was washed a further 4 times with TBST and then imaged using an electrochemiluminescent detection kit (BIORAD Clarity Western ECL, #170-

5060). Gel detection performed using an ImageQuant™ LAS4000 biomolecular imaging system (GE Healthcare).

2.3 Methods: Alpha Synuclein preparation

2.3.1 Alpha synuclein sonication to produce oligomers

Due to time constraints, alpha synuclein aggregates were bought from Abcam (ab218819) in the form of pre-formed fibrils. In order to introduce alpha synuclein as oligomers into neurons (as with the tau protein), the pre-formed fibrils were added to a 500 µl vial of intracellular solution (to produce the correct final concentration, always after filtration) then sonicated on full power for 15 minutes in an ultrasonic water bath. Samples were then kept on ice until use.

2.3.2 Structural confirmation

Confirmation the proteins were in oligomeric form was completed with negative stain transmission electron microscopy.

2.4 Methods: Electrophysiology

2.4.1 Preparation of tissue

C57/Bl6 wild type mice (2-4 weeks) were used for experiments. The precise postnatal age of the mice used can be found in individual Chapters. Mice were killed by cervical dislocation and then decapitated in accordance with the U.K. Animals (Scientific Procedures) Act (1986). All experiments were approved by the University of Warwick local Animals Welfare and Ethics Board (AWERB).

2.4.2 Solutions

Solution	Contains (mM):
Cutting aCSF	127 NaCl, 1.9 KCl, 8 $MgCl_2$, 0.5 $CaCl_2$, 1.2 KH_2PO_4, 26 $NaHCO_3$, 10 D-glucose (pH 7.4 when bubbled with 95% O_2 and 5% CO_2, 300 mOSM)
Recording aCSF	127 NaCl, 1.9 KCl, 1 $MgCl_2$, 2 $CaCl_2$, 1.2 KH_2PO_4, 26 $NaHCO_3$, 10 D-glucose (pH 7.4 when bubbled with 95% O_2 and 5% CO_2, 300 mOSM)
Intracellular patch solution	135 Potassium gluconate, 7 NaCl, 10 HEPES, 0.5 EGTA, 10 Phosphocreatine, 2 MgATP, 0.3 NaGTP (293 mOSM, pH 7.2) (to allow identification of the recorded cells, in a subset of experiments, Alexa Fluor Hydrazide dyes (488 or 594) were added to intracellular solution to a final concentration of 0.05 mM final concentration

Table 2.3: Recipes for the solutions needed for whole-cell patch clamp recording in mouse brain slices

2.4.2 Sub-dissection and slicing

The brain was rapidly removed and submerged in cold (2-4°C) high Mg^{2+}, low Ca^{2+} cutting aCSF (Table 2.3). Specific dissections were carried out depending on the regions of interest:

Hippocampus: The cerebellum was removed, and a cut made down the midline to separate the hemispheres. These were glued midline down onto a metal stage to allow the cutting of parasagittal hippocampal slices.

Neocortex: The cerebellum was removed, and a cut made down the midline to separate the hemispheres. These were glued midline down onto a metal stage which was tilted by +15˚, such that the blade started cutting from the surface (layer 1) of the neocortex towards the caudal border of the neocortex. This ensured the integrity of layer V pyramidal cell dendrites in slices close to the midline (Kerr et al., 2013).

Substantia nigra and ventral tegmental area: The cerebellum and a small rostral section were removed and then the brain was glued onto a metal stage rostral end facing downwards to allow the cutting of coronal slices.

Dorsal striatum for fast scan cyclic voltammetry recording: The cerebellum and a small rostral section were cut off and then the brain was glued onto a metal stage rostral end facing upwards to allow the cutting of coronal slices.

350 µM slices were cut using a Microm HM 650V microslicer and transferred into a Gibbs chamber filled with oxygenated recording aCSF (Table 2.3). The slices were stored at 34 °C in until they were used for recording or dye loading (between 1 and 8 hours after slicing).

2.4.3 Preparation of pipettes

Glass pipettes were pulled with a micropipette puller (Sutter Instruments P1000) using borosilicate glass capillary tubes (Multichannel systems, #300057, OD=1.5 mm, ID=0.86 mm). Pipette resistance was between 5 and 10 mΩ for all experiments.

2.4.4 Whole-cell patch clamp recording

A slice was transferred to the recording chamber, perfused with recording aCSF (rate: 2-3 ml/minute) and oxygenated at 30 °C. Slices were visualized using IR-DIC optics with an Olympus BX151W microscope (Scientifica) and a CCD camera (Hitachi). Whole-cell current clamp recordings (Fig 2.4) were made from pyramidal cells in area CA1 of the hippocampus, layer V thick-tufted neurons in the somatosensory cortex, dopaminergic neurons in the substantia nigra and GABAergic neurons in the ventral tegmental area using patch pipettes (5–10 MΩ) manufactured from thick-walled glass (Multichannel systems, #300057). Cells were identified by their position in the slice which was confirmed from their electrophysiological properties and their morphology visualised with fluorescence imaging. Recordings of voltage responses were made at several different time points in current clamp using an Axon Multiclamp 700B amplifier (Molecular Devices, USA) and digitised at 20 kHz. Axon pClamp 10 software (Molecular Devices) was used for data acquisition and to perform analysis. For all recordings, only cells that had resting membrane potentials of between -60 mV and -75 mV at whole-cell break through were analysed. Bridge balance was monitored throughout and any cells that had changes of more than 20 % over the course of the experiments were discarded.

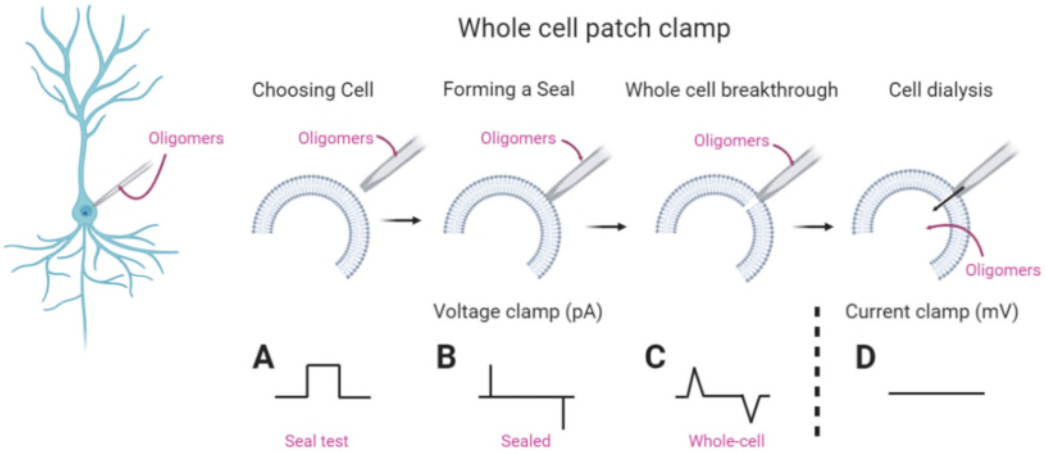

Figure 2.4: Simplified schematic of the whole-cell patch clamp protocol.
Neurons are identified using brightfield imaging. A) Then using a glass pipette (5-10 MΩ resistance), the neuron is approached with positive pressure to dimple the membrane. A square current step is applied of 5-10 mV (as shown in A) as it makes the sealing process easier to monitor. B) Once the dimple is observed, pressure is released, and this allows a high resistance seal to form between the end of the pipette and the cell membrane. This seal needs to be at least 1 GΩ. At this point the trace will appear flat with only fast electrode capacitance transients visible these can be zeroed off at this step. C) Gently applied negative pressure ruptures the membrane and this allows breakthrough into whole-cell mode at which point the capacitance is now greater as it reflects the capacitance of the whole-cell. Recording can then be moved from voltage clamp into current clamp mode (D) to start the experiment, during which time the contents of the patch pipette will start to dialyse the cell. Oligomeric protein can be introduced via the patch pipette for efficient dialysis into the recorded neuron.

2.4.5 Dot blots to determine filtration effects

Intracellular patch solution is usually filtered before use to prevent debris from blocking the patch pipettes. However, the filtering may remove the added tau protein and thus dot blots were performed to determine whether tau protein should be added to the intracellular solution before or after filtration (Fig 2.5). For each sample, 2 ml was spotted onto nitrocellulose membrane, allowed to dry for 15 minutes, and then blocked with 10 % non-fat milk in TBST for 1 hour. The membranes were then washed 5 times with TBST and incubated for 2 hours with primary antibodies diluted in TBST: T22 (Merck; 1:1000 dilution), HT7 (ThermoFisher; 1:1000 dilution), K9JA (Dako; 1:5000 dilution). The membranes were washed 5 times with 10 % TBST and then treated for 2 hours with secondary antibody (anti-rabbit IgG or anti-mouse IgG, Thermofisher, #31460, #61-6520). Following further washes, the membranes were developed with an electrochemiluminescent detection kit (BIORAD Clarity Western ECL #170-5060). Gel detection performed using an ImageQuant™ LAS4000 biomolecular imaging system (GE Healthcare).

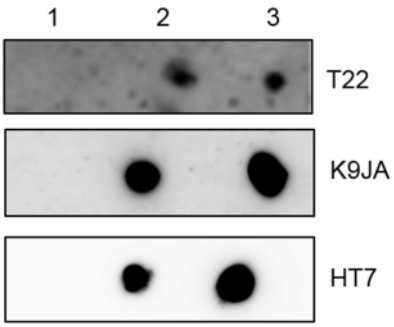

Figure 2.5: Dot blot analysis to confirm when the most effective time is to add oTau to the intracellular recording solution.

Samples (2 µl) were blotted onto a nitrocellulose membrane, blocked, and treated with one of the primary antibodies (T22, K9JA or HT7), followed by their respective secondary. Three different conditions were tested: 1) Control: filtered intracellular solution 2) Intracellular solution with oTau added and then filtered and 3) Filtered intracellular solution with oTau added after the filtering. It is clear that some oTau is lost in condition 2 and therefore condition 3 was used for all experiments.

Blots confirmed the tau was oligomeric (T22, oligomer specific), and showed that the tau reacted strongly with HT7 and K9JA antibodies, which bind to the mid-region and microtubule binding region of tau respectively (Chen et al, 2019). There was loss of oTau when it was added pre-filtration. oTau was therefore added after the solutions had been filtered. For individual experiments, tau oligomers from a 22 mM stock (monomer concentration) were added to filtered patch solution to give a final concentration of either 44 nM, 133 nM or 444 nM (2, 6 and 20 µg/ml tau) for CA1 neurons and 666 nM for layer V cells to account for their increased size (30 µg/ml tau).

2.4.6 Stimulation protocols

All cells were allowed to stabilise for a few minutes after breaking through into whole-cell mode before data was acquired. A range of different stimulation protocols have been used across experiments.

Standard IV protocol

The standard current-voltage relationship was constructed by injecting step currents (1 s) from -200 pA (CA1 pyramidal cells), -600 to -400 pA (layer V pyramidal cells) and -300 pA (dopaminergic neurons) incrementing by 100 pA until a regular firing pattern was induced (Fig 2.6). A plot of step current against voltage response around the resting potential was used to measure the input resistance (gradient of the fitted line).

Hyperpolarising step protocol

Hyperpolarising step currents (50 pA, 100 ms) were injected at 1 Hz with the corresponding voltage responses recorded (Fig 2.6). This allowed quantification of the time course of changes in input resistance/conductance. For analysis, average voltage responses can be constructed for 10-minute periods.

Dynamic IV protocol

The dynamic-IV current provides a more naturalistic current to the neurons (Badel et al., 2008b, 2008a). It is generated using the summed numerical output of two Ornstein–Uhlenbeck processes (Uhlenbeck & Ornstein, 1930) with time constants τ_{fast} = 3 ms and τ_{slow} = 10 ms. This current waveform, which mimics the stochastic actions of AMPA and $GABA_A$ receptor channel activation, is injected into cells and the resulting voltage recorded (a fluctuating noisy trace) (Fig 2.6). The current trace is the same for all recordings to allow a comparison over time, however the amplitude of the current (gain) can be altered to achieve a consistent firing rate across recordings. The voltage trace was used to measure the frequency of action potential firing and to construct a dynamic-IV curve. The firing rate was measured from voltage traces evoked by injecting a current waveform of the same gain and offset for all timepoints (to achieve a firing rate ~1-3 Hz). Action potentials were detected by a manually set threshold and the interval between action potentials measured.

The dynamic membrane current (I_{ion}) can be calculated using:

$$I_{ion}(V,t) + I_{noise} = I_{inj}(t) - C\frac{dV}{dt}$$

for which the injected current (I_{inj}) is known, the derivative (dV/dt) can be calculated from the experimentally measured voltage response, and the capacitance (C) is calculated as in (Badel et al., 2008b). A scatter plot of the transmembrane current against voltage (Fig 2.6D) illustrates the dynamic relationship between the two, with the effects of weak background synaptic activity and other sources of high-frequency variability being accounted for as intrinsic noise (I_{noise}) (Badel et al., 2008b). Averaging the transmembrane current in 1 mV bins removes the time dependence of I_{ion} (V, t) to yield the typical ionic current at a particular voltage, and thus defines the dynamic I–V curve (I_{dyn}):

$$I_{dyn}(V) = Mean\,[I_{ion}(V,t)]$$

The exponential integrate-and-fire model (Fourcaud-Trocmé et al., 2003) provides an excellent fit to the dynamic I-V curve (Badel et al., 2008b, 2008a;

Harrison et al., 2015; Fig 2.6E). The exponential integrate-and-fire (EIF) model is characterized by a voltage forcing term F(V) that is related to the I_{dyn} as:

$$F(V) = \frac{-I_{dyn}(V)}{C}$$

where the steady state forcing function F(V) for the EIF model is given as:

$$F(V) = \frac{1}{\tau}\left(E - V + \Delta_{\tau exp}\left(\frac{V - V_T}{\Delta_T}\right)\right) = -\frac{I_{dyn}(V)}{C}$$

By fitting the dynamic curve to the EIF model, I could then extract four parameters: membrane time constant (τ), resting potential (E), spike-initiation threshold (V_T) and spike-onset sharpness (Δ_T), which describes the voltage range over which an AP initiates (Badel et al., 2008a, 2008b; Harrison et al., 2015; Kaufmann et al., 2016). Dynamic *I–V* curves are constructed from the pre-spike voltage response (subthreshold and run up to spike) with all data falling within a 200 ms window after each spike being excluded from analysis. All analysis of the Dynamic IV traces was completed using MATLAB and Julia software platforms (Bezanson et al., 2017).

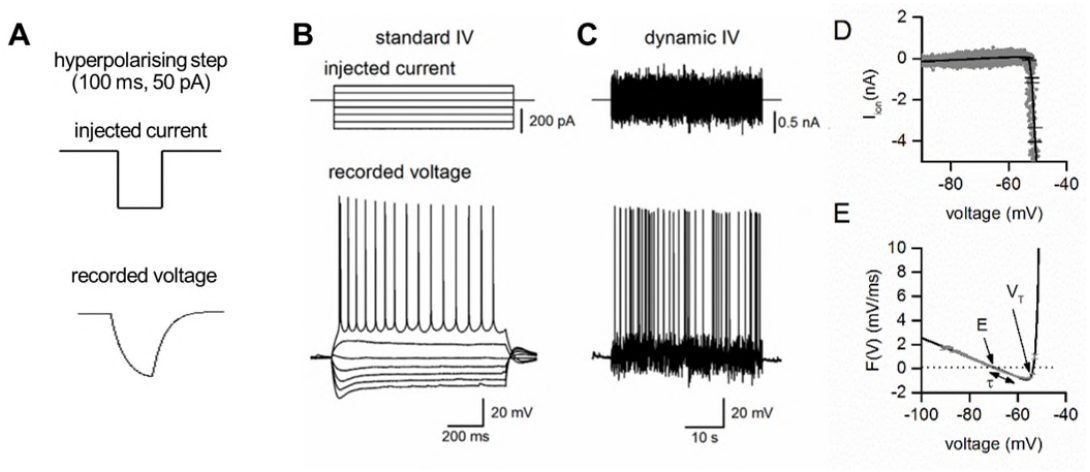

Figure 2.6: Extraction of electrophysiological parameters

A number of different techniques are used in this thesis in order to parameterise neurons electrophysiologically. A) The simplest is the continuous injection of a 100 ms 50 pA hyperpolarizing current step delivered every 1 s. The resulting voltage response time course is recorded and can be used as a measure of input resistance change over time. (B) The next is the standard IV protocol used to extract neural parameters. In this example, current steps (1 s long) start at -300 pA and are increased by 50 pA (top panel) until a regular firing pattern is induced (bottom panel). Current steps around the resting potential can be used to extract the input resistance. (C) The third current injection protocol (dynamic IV) injects a naturalistic current into the cell (top panel) and the voltage recorded (bottom panel) can be used to determine the firing rate under a naturalistic state, and it can also extract a number of other parameters (Badel et al, 2008, Harrison et al, 2015). (D) From the voltage response, the mean ionic current I_{ion} is plotted against membrane potential (grey). The black line is the dynamic IV curve generated by the average current at a particular voltage (in 1 mV time bins). (E) The negative of I_{ion}/C is then plotted (grey) along with the EIF (exponential integrate-and-fire) computational model fit (black line). From this curve subthreshold parameters can be extracted (such as resting potential E, time constant T, spike-onset sharpness, capacitance, and spike-threshold voltage V_T).

Synaptic transmission

To measure synaptic transmission between connected neighbouring neocortical thick-tufted layer-V pyramidal cells, 3 simultaneous whole-cell current-clamp recordings were made in somatosensory cortex (Markram et al 1997; Kerr et al 2013). Recordings were made from neurons in slices from P12-18 mice since unitary EPSPs from younger mice have a larger amplitude than unitary EPSPs in slices from older mice, and younger mice show marked short-term depression (Reyes and Sakmann 1999; Kerr et al 2013) which can be used to measure the effects of oligomeric tau (oTau) on release probability. Once synaptic connectivity was confirmed, 6 action potentials were evoked in the presynaptic neuron (5 at 20 Hz followed by a single recovery action potential after a 1 second interval) using 5 ms current steps. The amplitude of the current steps was carefully monitored throughout experiments to ensure they reliably induced the firing of single action potentials. These stimulus trains were separated by 10 seconds and repeated for the duration of recordings. The amplitude of overlapping unitary EPSPs was accurately measured using voltage deconvolution (Kerr et al., 2013; Richardson and Silberberg, 2008a).

Long term synaptic plasticity

To measure long-term potentiation (LTP), whole-cell current-clamp recordings were made from CA1 hippocampal pyramidal cells in the presence of 50 µM picrotoxin (to block $GABA_A$ receptors). Schaffer collaterals were stimulated with a concentric bipolar electrode (FHC, Maine USA) every 20 s. The stimulation strength was set to evoke reliable and robust synaptic transmission (EPSP amplitude ~ 3 mV) without producing action potential firing in the postsynaptic cell. Stimulations of the theta-frequency (4-12 Hz) are commonly used to induce LTP (Grover, Kim, Cooke and Holmes, 2009; Bland, 1986; Buzsáki, 2002). After a 15-minute baseline with stable EPSP amplitudes, LTP was induced by theta-burst stimulation (10 trains of 10 stimuli (100 Hz) separated by 100 ms) and EPSPs were recorded for at least 30 minutes. Theta-burst stimulation is a robust and commonly used approach to generate LTP (Larson and Munkácsy, 2015).

To measure metabotropic glutamate receptor (mGluR) -mediated long-term depression (LTD), whole-cell current-clamp recordings were made from CA1 hippocampal pyramidal cells in the presence of 50 µM picrotoxin (to block $GABA_A$ receptors) and 5 mM L689,500 to block NMDA receptors. Schaffer collaterals were stimulated (as above) to evoke reliable and robust synaptic transmission (EPSP amplitude ~ 3 mV) without producing action potential firing in the postsynaptic cell. After a 10-minute baseline, LTD was induced by 100 µM of the mGluR5 agonist DHPG for 10 minutes and EPSPs were recorded for 30 minutes further following wash.

Recording isolated voltage-gated sodium currents

To record voltage-gated sodium channel currents in isolation, the intracellular and extracellular solutions used were modified from Milescu, et al (2010) (Fig 2.7). The extracellular solution contained the following (in mM): 124 NaCl, 25 $NaHCO_3$, 3 KCl, 1.5 $CoCl_2$, 1.0 $MgSO_4$, 0.5 NaH_2PO_4, and 30 D-glucose, equilibrated with 95% O_2 and 5% CO_2 (pH 7.4). Calcium chloride was replaced with cobalt chloride in order to block the voltage-gated calcium channel currents. Experiments were performed at room temperature (~ 22ºC to improve the quality of the voltage clamp, (Milescu et al., 2010)). To reduce the amplitude of the sodium channel currents, 50 mM Na^+ was present in the intracellular solution: 70 Cs-gluconate, 30 Na-gluconate, 10 TEA-Cl, 5 4-AP, 10 EGTA, 1 $CaCl_2$, 10 HEPES, 4 Mg-ATP, 0.3 Na_3-GTP, 10 Na_2-phosphocreatine. Series resistance (R_s) was measured throughout the recording and were typically in the range of 6-12 MΩ. Cells with R_s over 15 MΩ or those that varied by more than 20 % over the period of recording were discarded. R_s was not compensated, but the liquid junction potential of ~ 8 mV was corrected for. Leak currents were subtracted using a standard P/N protocol (Bezanilla and Armstrong, 1977), where a scaled down version of the protocol is given (in this case ¼ of the size) in order to measure the passive (leak) current. This response is assumed to be linear, so can be scaled and subtracted from the recorded trace to display only active changes (voltage-gated sodium currents).

The stimulation protocol was adapted from Milescu et al., (2010) to allow fully clamped somatic Na^+ channel currents to be recorded. Neurons were held at

-80 mV. A depolarising pre-pulse was given (5 ms, -40 mV) to activate axonal, but not somatic, sodium channels. This was followed by a 1 ms step to -55 mV and then voltage steps (from -60 to 60 mV, 5 ms duration) were used to elicit controlled Na^+ channel current responses. The inter-sweep interval was 2 s. From the current responses, plots of current vs voltage or conductance vs voltage were calculated. Conductance is given by the following equation:

$$Conductance\ (g) = I_{Na}/(V_{Step} - V_{Reversal})$$

The plot of conductance vs voltage was fitted with a Boltzmann equation:

$$y = \frac{A_1 - A_2}{1 + e^{(x-x_0)/dx}} + A_2$$

and then the half activation voltage and the rate constant of activation were extracted and compared between control and oTau introduced neurons.

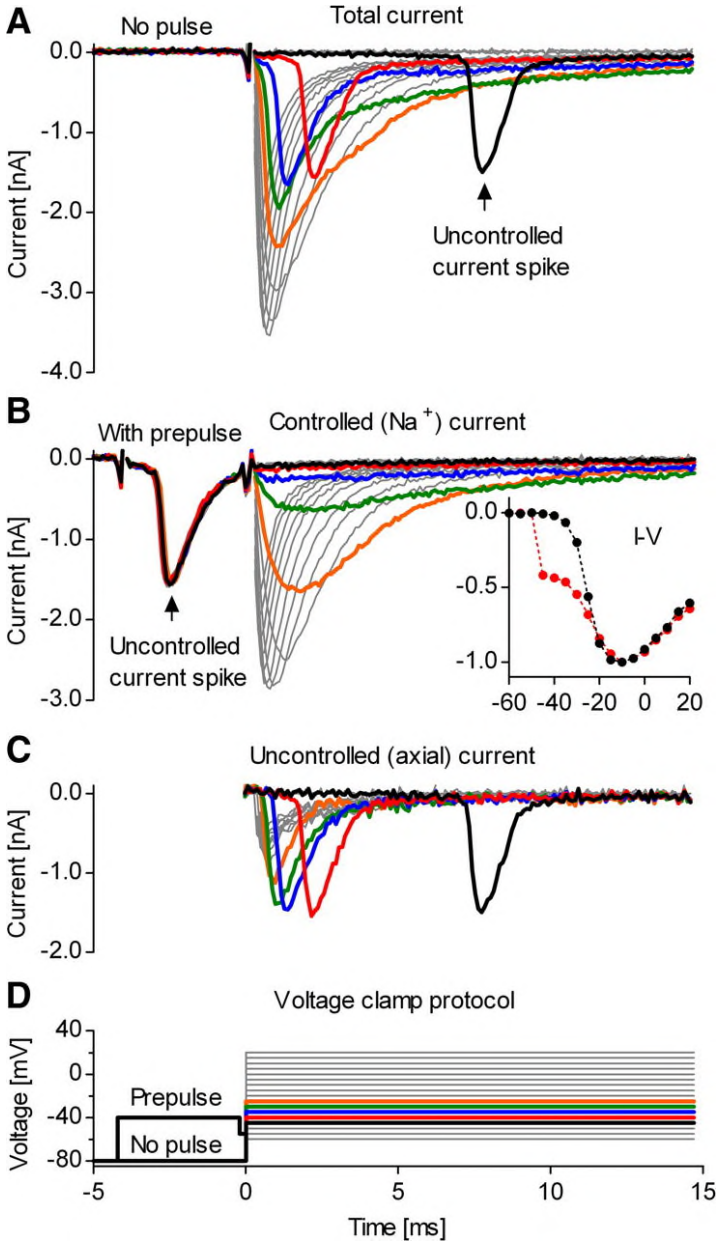

Figure 2.7: Protocol for recording voltage-gated sodium currents in acute slices

Recording voltage-gated sodium currents in acute slices is complicated by the inability to efficiently voltage clamp them, and this arises due to their size and multicompartment nature. In this protocol developed by Milescu et al., (2010), a solution is described. A) The result of attempting to record the currents with no additional intervention; the currents are uncontrolled due to inefficient clamp. B) Introducing a pre-pulse ahead of the current steps activates the axonal but not somatic sodium channels, allowing for controlled (well-clamped) recordings to be made of somatic voltage-gated sodium channels. C) Subtraction of trace B from A to give the uncontrolled axial current D) Protocol for stimulation to perform the pre-pulse

and recording steps in voltage clamp. Specific stimulation and response pairs are indicated via colour coding.

Hodgkin Huxley modelling

The Hodgkin-Huxley (HH; Hodgkin & Huxley, 1952) model provides a unified framework for modelling the ionic conductances that generate APs. The HH model can be applied to study voltage-gated sodium and potassium channels. It proposes that each sodium channel contains a set of 3 identical, rapidly responding, activation gates (the m-gates), and a single, slower-responding, inactivation gate (the h-gate) (Hodgkin & Huxley, 1952).

The membrane current is given by:

$$I = C_m \frac{dVm}{dt} + g_K(V_m - V_k) + g_{Na}(V_m - V_{Na}) + g_l(V_m - V_l)$$

Where I is the total membrane current and C_m is the membrane capacitance, g_K, g_{Na} and g_l are the potassium, sodium and leak conductances per unit area, and V_k , V_{Na} and V_l are reversal potentials.

The sodium conductance can be given by:

$$I_{Na}(t) = \bar{g}_{Na} m(V_m)^3 h(V_m)(V_m - E_{Na})$$

Where $\bar{g}_{Na}$ is the maximal sodium conductance and *m* and *h* are quantities between 0 and 1 that are associated with sodium channel activation and inactivation, respectively. V_m is the membrane potential and E_{Na} is the reversal potential for sodium.

Initial parameters were assigned as follows: $\bar{g}_{Na}$: $120\ mS/cm^2$, $\bar{g}_K$: $36\ mS/cm^2$, g_l: $0.3\ mS/cm^2$, C_m: $1\ \mu F/cm^2$, Vm: $-70\ mV$, E_{Na}: $60\ mV$, E_K: $-88\ mV$, E_l: $-54.4\ mV$ in line with Hodgkin and Huxley 1952; for the squid giant axon).

2.5 Methods specific to connexin hemichannel measurements

2.5.1 Isohydric solution preparation

Solutions with different bicarbonate content were used to alter the levels of CO_2 perfusing the brain slices under isohydric conditions (constant pH, as in de Wolf et al, 2006). The standard baseline solution is 35 mm Hg CO_2 aCSF. This is then either increased to 55 mm Hg CO_2 to raise CO_2 levels or decreased to 20 mm Hg CO_2 to lower CO_2 levels. The composition of these aCSF recipes is given in Table 2.4 and differ in their concentrations of NaCl and $NaHCO_3$.

Solution	Contains (mM):
Control (35 mmHg CO_2) aCSF	124 NaCl, 26 $NaHCO_3$, 1.25 NaH_2PO_4, 3 KCl, 10 D-glucose, 1 $MgSO_4$, 2 $CaCl_2$, (pH 7.4 when bubbled with 95% O_2 and 5% CO_2)
Hypercapnic (55 mmHg CO_2) aCSF	100 NaCl, 50 $NaHCO_3$, 1.25 NaH_2PO_4, 3 KCl, 10 D-glucose, 1 $MgSO_4$, 2 $CaCl_2$, (pH 7.4 when bubbled with 95% O_2 and 5% CO_2)
Hypocapnic (20 mmHg CO_2) aCSF	140 NaCl, 10 $NaHCO_3$, 1.25 NaH_2PO_4, 3 KCl, 10 D-glucose, 1 $MgSO_4$, 2 $CaCl_2$, (pH 7.4 when bubbled with 95% O_2 and 5% CO_2)

Table 2.4: Recipes for the solutions needed for isohydric aCSF buffers for altering the level of CO_2 at a constant pH.

To ensure that the solutions remain isohydric (constant pH) then the pH was adjusted by perfusing with different CO_2/O_2 mixtures to match the pH of the 35 mm Hg CO_2 solution (Fig 2.8):

For 20 mm Hg CO_2, two 0-10 cc/MIN AIR x 100 (6831) mixers were used, one for the 100 % O_2 line and one for the 95% O_2/5% CO_2 line to mix the two gases in a roughly 1:1 proportion.

For 55 mm Hg CO_2, one 0-250 cc/MIN AIR x 100 (6831) mixer was used for the 95% O_2/5% CO_2 line and one 0 -10 cc/min AIR (6387) mixer was used for the 100 % CO_2 line, to mix the gases in a roughly 0.96 to 0.04 proportion.

Throughout the day, pH was monitored to ensure that it did not change.

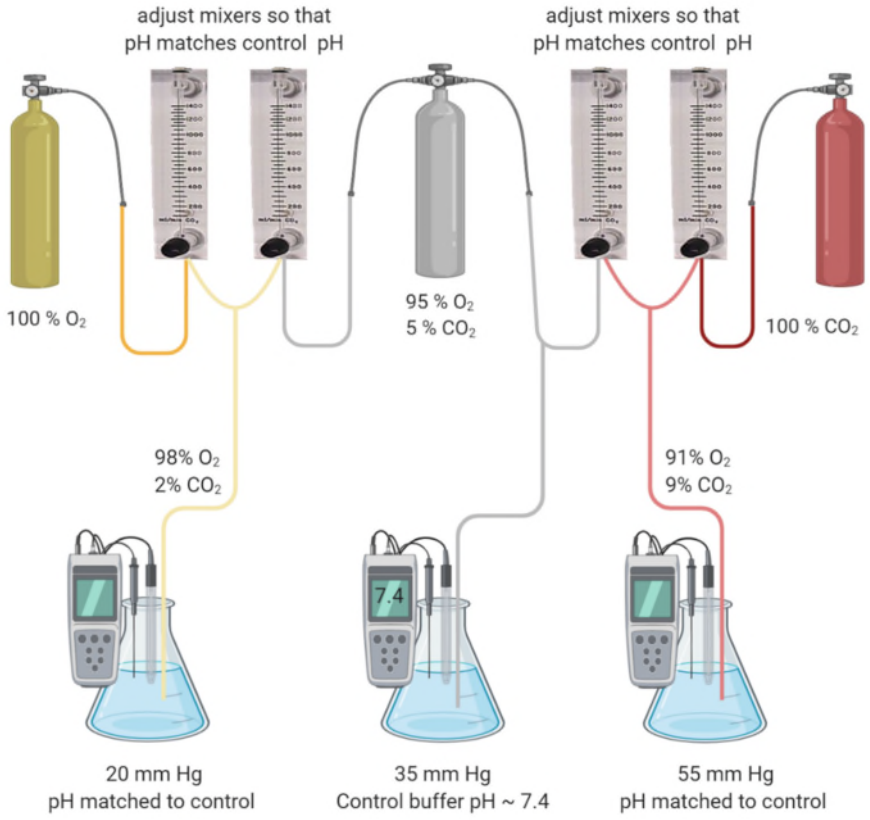

Figure 2.8: Mixer set up to enable smooth isohydric CO_2 level change.

The 35 mm Hg CO_2 buffer was bubbled with 95% O_2 5% CO_2. The pH of this buffer was ~7.4. The 55 mm Hg CO_2 buffer was saturated with 9% CO_2 (with the balance being O_2) with pH maintained to match control (35 mm Hg). This was achieved by mixing the 95% O_2 5% CO_2 line with a 100 % CO_2 line (adjustments were made using the mixer dials). The 20 mm Hg CO_2 buffer was saturated with 2% CO_2 (with the balance being O_2), with pH maintained to match control (35 mm Hg). This was achieved by mixing the 95% O_2 5% CO_2 line with a 100 % O_2 line (adjustments were made using the mixer dials).

2.5.2 Dye loading

The methods were based on the protocols published in Huckstepp et al., (2010). Whole-cell patch clamp recordings were first used to confirm that the dye loading was performed in the correct regions (substantia nigra pars compacta and ventral tegmental area). Slices were then incubated in 35 mmHg CO_2 aCSF for 20 minutes. The perfusion solution was changed over to the 55 mmHg CO_2 (high CO_2, hypercapnic) solution containing 5(6)-carboxy-fluorescein dye (CBF, 100 µM, Novabiochem, #8.51082.001) for 20 minutes. This allowed any CO_2-sensitive hemichannels to open and the CBF dye to diffuse into the cells. The perfusion solution was then changed to 35 mmHg CO_2 solution containing CBF, to allow the CO_2-sensitive hemichannels to close, trapping the dye within the cells (Fig 2.9). The slice was washed for 3 hours to reduce background staining before imaging. Images were rapidly acquired using the CCD camera (Hitachi) with 488 nm fluorescence (CoolLED) since CBF bleaches quickly and cannot be fixed with PFA.

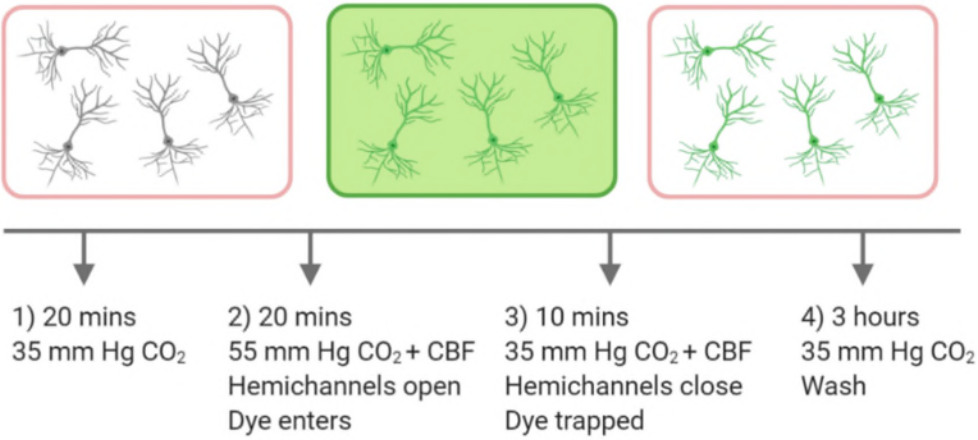

Figure 2.9: Simplified schematic of the dye loading protocol.

A schematic to demonstrate the dye loading protocol. The slice is equilibrated for 20 mins in control aCSF (35 mmHg CO_2) at 30 °C. 55 mmHg CO_2 aCSF (hypercapnic) containing 5(6)-carboxy-fluorescein (CBF, 100 µM) was then applied for 20 mins to allow CO_2 sensitive-hemichannels to open. Then 35 mmHg CO_2 aCSF containing CBF (100 µM) was applied for 5 minutes to allow the hemichannels to close. Finally, the slice was washed with 35 mmHg CO_2 aCSF for 3 hours to reduce the background staining before imaging. The dye loading method is based on that described in Huckstepp et al., (2010).

2.6 Immunohistochemistry

Mice (P7-10 and P17-20) were either cardiac perfused with 4% PFA and then post-fixed overnight at 4 ˚C (Chapter 6) or slices were cut as normal then fixed with 4% PFA for 1 hour at room temperature (Chapters 3 and 5). For the cardiac perfused mice, an overdose via intraperitoneal injection of sodium pentobarbital (>100 mg/kg) was given, followed directly by transcardial perfusion with non-heparinized PFA (4%; made in PBS). All cardiac perfusions were kindly performed by appropriate licence holders (Dr Huckstepp, Dr Bhandare or Dr Van de Wiel). If cardiac perfused, the tissue was washed thoroughly with PBS and then sliced coronally (350 µm). All slices were washed 5 times with PBS and then blocked for an hour (1% BSA, 0.4% Triton 100X in PBS, 400 µl per slice), then washed 3 times for 5 minutes with PBS. The relevant primary antibodies were applied (200 µl per slice, see individual chapters for details) for an hour at room temperature and then kept at 4 - 8 ˚C overnight. Slices were washed 5 times for 5 minutes with PBS and the corresponding secondary antibody (200 µl per slice) added for 4 hours at room temperature. Slices were then washed 5 times for 5 minutes with PBS and mounted on glass slides with Vectashield (Vector laboratories, #H-5000). All imaging was carried with confocal microscopy (Leica 710 and Zen Black for image acquisition and processing, respectively). Controls were carried out without the primary antibodies and showed no fluorescence.

2.7 Transmission electron microscopy

Formvar/carbon-coated 300-mesh copper grids (#S162, Agar Scientific) were glow-discharged using the ELMO system from Cordouan Technologies. Five microliters of labelled or unlabelled tau-441 preparations were pipetted onto the grid and allowed to bind for 1 min. Excess samples were removed with a strip of filter paper, and 5 µl of 2% uranyl acetate added for 1 min. After removing the excess stain with a strip of filter paper, the grids were imaged using a JEOL-2100F transmission electron microscope.

2.8 Statistical analysis and software

All statistical analysis was performed in GraphPad Prism using non-parametric methods: Kruskal–Wallis analysis of variance (ANOVA), Mann Whitney and Wilcoxon signed-rank tests as required for non-parametric data.

Parametric tests such as t-tests or ANOVAs assume that the data is normally distributed (Hodges Jr and Lehmann, 1956). However, tests for normality such as Kolmogorov-Smirnov or Shapiro-Wilk are only useful for large sample sizes. If it is not possible to assume normality, then the most conservative strategy is to use a nonparametric test designed for non-normal data (Ghasemi and Zahediasl, 2012; Morgan, 2017). Therefore, while non-parametric tests have lower statistical power than their parametric equivalents, they are the correct choice for these studies with low sample sizes (Sullivan et al., 2016). Non-parametric analyses were performed for all comparisons.

All data is represented as mean and standard error of the mean with individual experiments represented by single data points. Each recorded cell is one data point. All experimental conditions were measured using multiple animals and recording conditions were interleaved to remove bias introduced from individual animals. Data points for each experimental condition were derived from a minimum of 4 individual animals. No experimenter blinding was performed as the same quality control criteria was applied to all recordings.

Biorender.com was used for the generation of figures under an appropriate personal software license.

2.9 Drugs and pharmacological agents

Drugs were stored as stock solutions in dH_2O or DMSO as required (1-100 mM) and diluted freshly into aCSF on the day of use. See 8.1 (Appendix) for full materials and reagents list.

Chapter 3:

Oligomeric tau injection alters action potential dynamics and disrupts synaptic transmission *in vitro*

Parts of this chapter have been published previously (Hill et al., 2019):

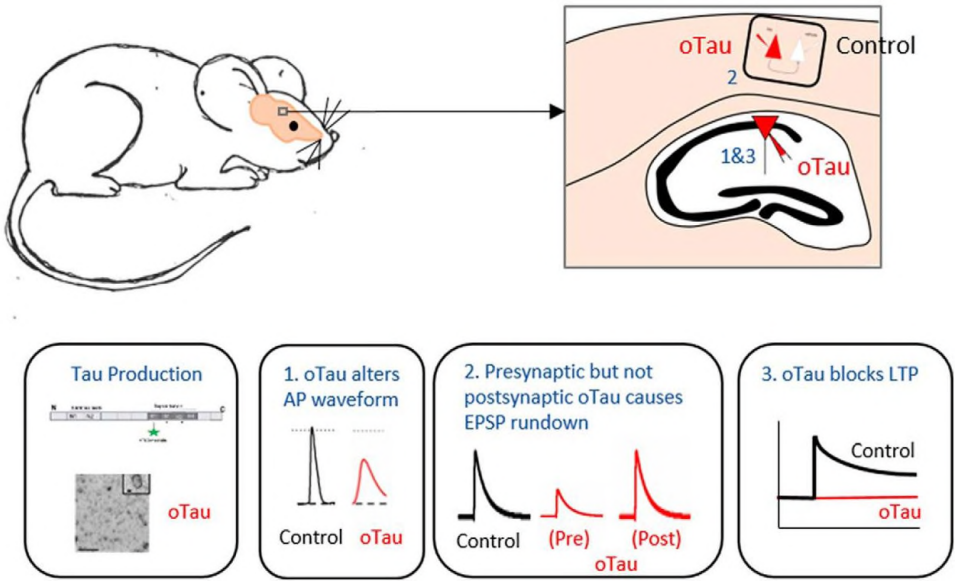

Figure 3.1: oTau mediated effects on neuronal function, synaptic transmission, and plasticity.

Visual abstract to represent the key findings of this results chapter. oTau introduced into single neurons alters action potential waveform, disrupts synaptic transmission (pre-synaptic action) and alters synaptic plasticity (post-synaptic action).

3.1 Introduction

Tau is a highly soluble microtubule-associated protein that acts within neurons to modify their stability (Baas and Qiang, 2019; Binder et al., 1985; Caceres and Kosik, 1990; Hirokawa et al., 1988). Aside from its role in stabilising axonal microtubules, physiologically tau is also found elsewhere in neurons. It is known to be expressed in the dendrites and plays important roles in regulating plasticity at the synapse. Endogenous (non-misfolded) tau has been recorded at both pre-synaptic terminals (Pooler et al., 2013; Sokolow et al., 2015;

Yamada et al., 2014) and post-synaptic boutons (Gómez-Ramos et al., 2009; Ittner et al., 2010; Regan et al., 2015; Tai et al., 2012). Pathologically, tau contributes to several diseases, commonly termed tauopathies. Here, abnormally phosphorylated tau can dissociate from microtubules to form oligomers and fibrils (Avila et al., 2006) which associate in the soma-dendritic compartment. Tau can aggregate further to form neurofibrillary tangles (NFTs) and, although their presence strongly correlates with disease progression (Nelson et al., 2009), it is the soluble oligomers that appear to be the toxic species in terms of disrupting neuronal function and these disruptions can occur in the absence of any NFT pathology (Andorfer et al., 2003; Cowan et al., 2010; Lee et al., 2001; Spires et al., 2006; Tanemura et al., 2002; Tatebayashi et al., 2002; Wittmann et al., 2001; Yoshiyama et al., 2007). Understanding which forms of the tau protein within the aggregation cascade are the most toxic will allow the generation of more targeted treatments for tauopathies in the future.

There is relatively little quantitative information on the concentration- and time-dependent actions of soluble tau oligomers (oTau) on the electrophysiological and synaptic properties of single neurons. To address this problem, in this Chapter, whole-cell patch clamp recording was used to introduce known concentrations of oligomeric full-length human tau-441 into mouse hippocampal CA1 pyramidal and neocortical layer-V thick-tufted pyramidal cells. A combination of standard electrophysiological profiling and detailed computational modelling was implemented to allow the full characterisation of the effects of oTau. Standard current-voltage relationships were constructed at regular time intervals (every 10 mins), to confirm the cell type, to monitor the quality of the recording and to provide an overview of electrophysiological deterioration in response to the introduced oligomers. This is a standard method for assessing neuronal responses, first described in Hodgkin and Huxley (1952). Working with my collaborators in the Zeeman Institute (Warwick), I also implemented a simplified reduced refractory integrate and fire (rEIF) model to enhance my analysis of the effects of oTau. Dynamic I-V curves were generated from the voltage responses to injected noisy fluctuating currents (see Methods for full details; (Badel et al., 2008a) at each of the

recorded time points (every 10 mins). These were then used to fit to the rEIF model and allowed full parameterisation of changes in the electrophysiological properties over time.

3.2 Results

3.2.1 Preparation of tau oligomers (oTau)

The recombinant tau used for this project was generated under the guidance of Dr Karikari. This allowed me to fully characterise the structure of the protein and the stage of aggregation, ensuring consistency across the range of my experiments. Recombinant full-length human tau-441 was expressed in *E. coli*, purified and aggregated following the protocols outlined in Karikari et al., (2019b, 2017). This is the longest of the six isoforms of tau found in humans (2N4R; Fig 3.2) and harbours no disease-related mutations or additional post translational modifications such as phosphorylation.

Figure 3.2: Structure of the full-length human tau used in this study.
Based on full-length human wild type tau, this construct has both N-terminal repeats (N1 and N2) and 4 microtubule binding repeat domains (R1, R2, R3 and R4). Also known as Tau-441, it is the longest isoform of the six commonly found in humans. To allow visualisation, oTau was labelled with an Alexa Fluor 488 maleimide dye which binds to cysteine residues. As there are two native cysteines within important microtubule binding regions, these were modified to alanine (C291A and C322A, shown as black dots below R2 and R3) and replaced with one at the edge of this region (residue 260 (I260C) in R1). This tau construct has been used previously (Karikari et al., 2017).

Tau was labelled with an Alexa Fluor maleimide dye (488) that binds to cysteine residues to allow localisation and to maintain the oligomeric species at a low molecular weight. Three mutations were introduced into tau to ensure that this labelling did not disrupt function: two cysteines that normally reside in

the microtubule binding region were modified to alanines (C291A and C322A), and a cysteine was introduced to allow binding at the edge of the repeat region (I260C). Labelling limits aggregation because tau can aggregate via the formation of disulphide bonds; this aggregation is reduced by blocking cysteine residues with the label (Karikari et al., 2017).

3.2.2 Electron microscopy to characterise the oTau

This study focussed on oligomeric tau, which is known to disrupt neuronal function (Fá et al., 2016; Ondrejcak et al., 2018). As transmission electron microscopy (TEM) allows the identification and quantification of the size and shape of protein species, I used negative-stain TEM to analyse the aggregation state. My observations confirmed that the oTau had a spherical granular form, typical of oligomeric species, that were of similar size and profile to previous preparations using the same protocol (Karikari et al., 2017; Fig 3.3A). No protein aggregates were observed in the control sample (Fig 3.3B).

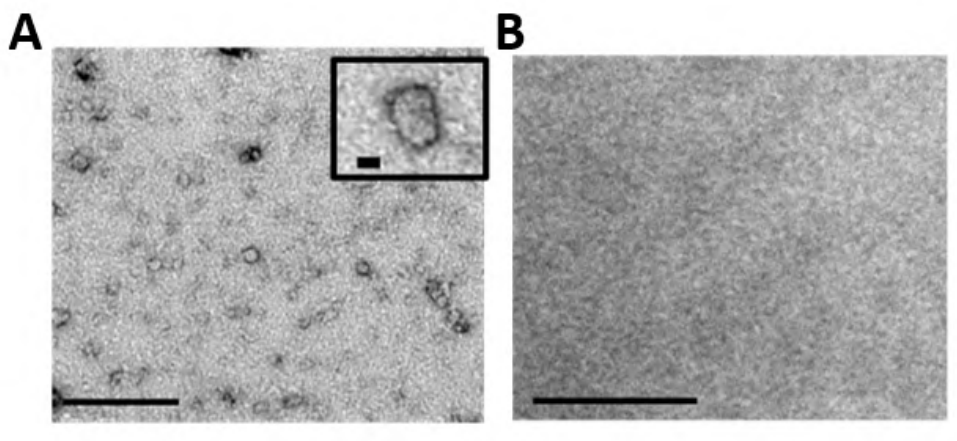

Figure 3.3: Characterisation of the aggregation level of the recombinant tau samples using negative-stain transmission electron microscopy.

A. Example negative-stain electron micrograph of oTau to assess the state of aggregation. Clear granular structures can be observed which indicate oligomeric form. Scale Bar = 200 nm. Insert, a higher magnification of a single spherical oligomer structure. Scale bar = 20 nm. B. Example negative-stain electron micrograph of labelled control (buffer and label only) shows no oligomeric protein present. Scale bar = 200 nm.

3.2.4 Immunohistochemistry to monitor localisation of oTau

The fluorescent labelling of oTau allows it to be visualised within neurons following its introduction via the patch pipette. This allowed me to determine where oTau could diffuse within the period of recording, and if it became concentrated in specific regions of the cell. This could then be correlated with any changes seen in the neuron's electrophysiology (Figure 3.4A). As a marker for the recorded cells, and to ensure being able to locate them with confocal microscopy, recorded neurons were also filled with Alexa Fluor 594 dye (red; Figure 3.4B). This, in combination with the labelled oTau (green), facilitated the imaging of oTau localisation. For these studies, neurons were recorded from for at least 20 minutes, the pipette carefully removed, and the slice fixed in 4% PFA, washed and mounted. Initially standard confocal imaging was used using a Leica 710 and Zen software for acquisition and processing, respectively. Constructing a Z-stack for the whole neuron confirmed that the oTau (green) was emerging from the pipette and entering the soma of the recorded cell, where it appeared to aggregate. This imaging method was unable to detect tau outside of the cell body, likely due to the low resolution of imaging and low concentration of oligomer.

I therefore repeated the experiments but imaged this time with the Airy Scan module of the Leica 880 in combination with Zen software for acquisition and processing, respectively. This allowed me to observe a diffuse spread of tau throughout the recorded neuron in both the axon and in the dendrites. Within the dendrites oTau could be observed parallel to the dendritic bifurcation and at localised in regions that could be postsynaptic sites (Figure 3.4C). This is the first time such widespread diffusion of oTau has been documented in such a short timeframe, facilitated by the introduction via patch-pipette (30 minutes, Fig 3.4B, C).

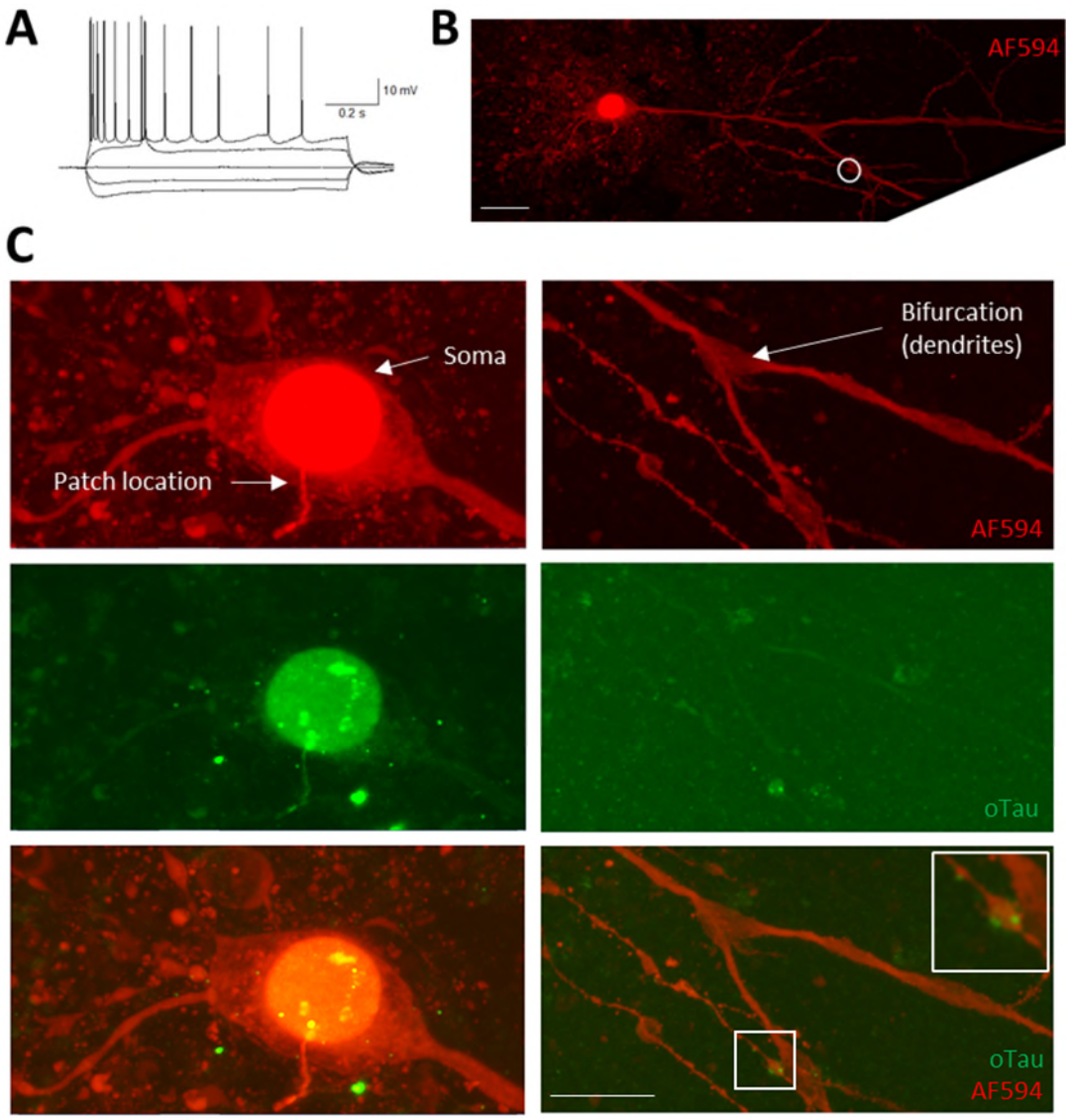

Figure 3.4: Localisation of oTau within a CA1 neuron after 30 minutes after introduction at the soma

A. SIV response for the recorded CA1 PC (steps from -200 pA, by +100 pA). The SIV trace clearly fits the profile of a CA1 pyramidal neuron. B. Alexa Fluor dye was introduced (in the patch solution) to allow the neuron and its processes to be identified. The AiryScan module of the Leica 880 was used to perform a tile-scan of Z-stacks (28 tiles, 258 Z-planes) to image the entire neuron. The Z-stacks were then processed and stitched using the Zen software suite. The neuronal morphology matches that of a CA1 pyramidal neuron (Figure 1.20). Scale bar = 20 µm. C. oTau (labelled green) was introduced via at the soma. Clear aggregation in the soma can be observed (left). However, oTau was also observed to have spread throughout the processes, including down a dendrite adjacent to the bifurcation. Scale bar = 10 µm.

3.2.5 Electrophysiological effects of oTau introduction on CA1 pyramidal cell subthreshold properties

The aim of the next stage of the project was to fully characterise the effects of oTau on CA1 pyramidal neurons in the hippocampus. To ensure the validity of my observations, I carried out several interleaved control experiments. Firstly, alongside tau production, I generated labelled and unlabelled control samples (no inoculation with tau plasmids, using the same volume of sodium phosphate buffer pH 7.4 in its place). oTau or the control samples were added each day in the same volume to intracellular solution to ensure that there was no effect on cell properties from the dilution of the intracellular solution. Secondly, to ensure that the observed effects were not the results of the non-specific actions of introducing any aggregation-competent molecule, I used bovine serum albumin (BSA). BSA has a similar molecular weight to tau. I used it at a much higher concentration than oTau (20 µM compared to 44-666 nM) and did not observe any significant differences from vehicle introduced recordings. This observation is further complimented by my results in Chapter 5 where introduction of alpha synuclein aggregates produces very different changes in electrophysiological properties.

During these experiments, I wanted to extract a full set of electrophysiological parameters over the time course of the recordings. For this I used two different stimulation protocols (see Methods for full details). The first, a step current injection, is used to develop a standard current-voltage relationship plot. From which, voltage steps close to the resting membrane potential were used to calculate input resistance manually using the gradient of the fitted line. The second stimulation protocol was the dynamic current-voltage relationship, which is generated from the voltage response to a fluctuating noisy current input that mimics native channel activity, providing a more natural stimulus for the neuron allowing a more thorough parameterisation. Using both standard and dynamic IV protocols, several concentrations of oligomeric tau were tested (44 nM, 133 nM and 444 nM oTau) to determine concentration-dependent effects. These oTau tests were interleaved with both control (vehicle) and BSA solutions. I had originally hoped to use both standard and dynamic relationships over the whole period of recording, but while the dynamic IV

parameter extraction was effective for all conditions at 0 mins (mean spike match of 72.2 ± 1.7 %, predicted vs experimental data), for the cells with oTau introduced, by 40 mins the model predictions were unable to accurately match the experimental spike data (mean spike match of 46.1 ± 5.5 %) (Fig 3.5). Therefore, this method was not used to extract parameters at later time points. The poor spike match could be due to the altered action potential waveform or a hidden threshold within the code, this needs to be investigated further. Despite not being able to use the dynamic current-voltage protocol to compare over time, the step current-voltage responses could be used to examine changes to resting membrane potential and input resistance.

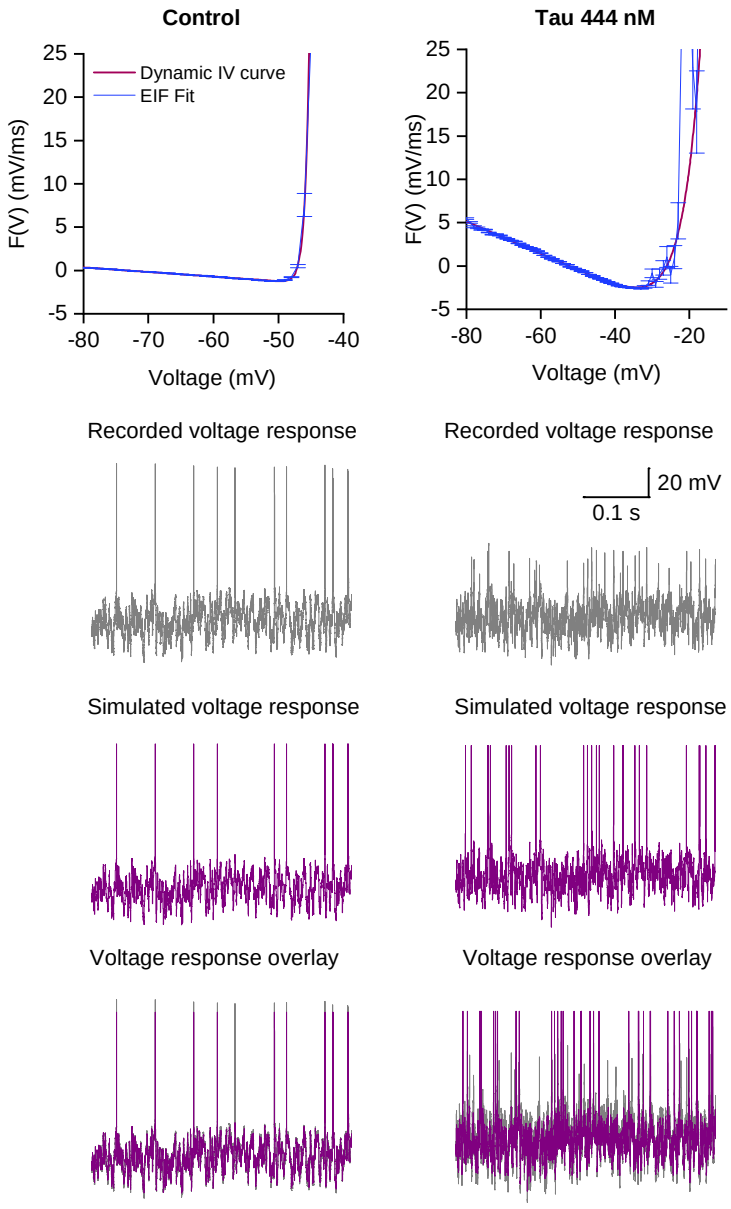

Figure 3.5: Analysis using the dynamic IV method at 40 mins.

Dynamic IV curve (pink) and EIF computational model fit (blue) for a control (left) and 444 nM oTau (right) cell after 40 minutes of recording. From this curve a number of subthreshold parameters can be extracted (such as resting potential E, time constant τ, and spike-threshold voltage VT; see Methods for more details). Recorded (grey) and simulated (purple) voltage traces are overlaid. (Left) For the control cell, the experimental and simulated traces are well matched (85%). (Right) For the oTau introduced cell however, the experimental and simulated traces are poorly matched (29%) and therefore the EIF model cannot be used to parameterise the oTau induced neurons over time.

The introduced oTau took varying lengths of time to have its effects in each cell. This could be due to several factors including cell size, morphology and series resistance. Regardless of the observed effects of oTau, recordings were maintained as long as they remained stable (defined as: membrane potential that did not depolarise above -50 mV and less than 20% alteration in series resistance). The average recording time was 40 minutes and so this was chosen as the final time point to be compared with the results at 0 mins (whole-cell breakthrough).

There was no significant difference in any of the extracted parameters (resting membrane potential, capacitance, cell time constant, spike-onset sharpness, spike threshold) at 0 mins (0-5 minutes after whole-cell breakthrough) across all of the experimental treatments as determined with Kruskal-Wallis tests (n = 10 for vehicle, n = 5 for BSA, n = 9 for oTau 44 nM, n =11 for oTau 133 nM and n =10 for oTau 444 nM, Table 3.1). Although for most conditions, there were no significant changes to most of the measured parameters over the period of recording, 444 nM oTau significantly increased input resistance (0 mins, 176.8 ± 4.7 mΩ, 40 mins, 239.3 ± 36.3 mΩ, p = 0.002) and depolarised the resting membrane potential (from -68.0 ± 1.7 mV at 0 mins to -61.8 ± 1.7 mV at 40 mins, p = 0.050; Fig 3.6C). This is consistent with previously reported data from the rTg4510 mouse model, which expresses human tau variant P301L, where the pyramidal cells are depolarised by ~ 8 mV compared to wild type littermates (Rocher et al., 2010). These changes were not observed with the introduction of vehicle, BSA, 44 or 133 nM oTau. Consistent with this increase in input resistance and depolarisation, there was also a significant increase in the action potential firing rate in cells injected with 444 nM oTau (p = 0.025, measured from the voltage response to dynamic noisy current input at time 0 and after 40 mins) and although not reaching significance, six out of seven cells injected with 133 nM oTau also had an increased firing rate (Table 3.4).

	Vehicle		BSA		44 nM oTau		133 nM oTau		444 nM oTau	
Parameter	**Mean**	**SEM**	**Mean**	**SEM**	**Mean**	**SEM**	**Mean**	**SEM**	**Mean**	**SEM**
Capacitance (pF)	121.8	± 12.56	125.6	± 14.17	132.55	± 17.65	105	± 8.04	125.3	± 14.31
Rin (MΩ)- steady state	164.4	± 12.22	183.6	± 21.13	157.9	± 23.01	180.4	± 20.4	176.8	± 4.74
Time constant (ms)	20.7	± 1.75	15.72	± 0.89	16.7	± 1.86	15.2	± 1.4	19.63	± 2.25
RMP (mV)	-67.2	± 1.16	-68.5	± 1.34	-69.6	± 0.91	-66.2	± 1.06	-64.95	± 2.0
VT (mV)	-50.1	± 0.68	-52.7	± 1.26	-54.8	± 0.98	-50.7	± 1.35	-50.92	± 1.49
ΔT (mV)	0.77	± 0.036	0.82	± 0.063	0.97	± 0.15	0.87	± 0.1	0.89	± 0.08
AP Amplitude (mV)	75.8	± 4.87	83.6	± 1.84	86.11	± 1.59	77.91	± 2.82	82.66	± 1.9
AP duration (ms)	1.42	± 0.093	1.48	± 0.07	1.28	± 1.31	1.41	± 0.07	1.44	± 0.053
AP rise (mV/ms)	249.4	± 30.54	288.4	± 17.8	318.8	± 26.55	252.7	± 23.68	282.11	± 21.85

Table 3.1: Electrophysiological parameters for all conditions made at time 0 (whole-cell breakthrough) for CA1 neurons.

All recordings are made from hippocampal CA1 neurons. There was no significant difference between any of the measured parameters at time 0 minutes (whole-cell breakthrough), using Kruskal Wallis ANOVAs. Data shown as mean and SEM for each experimental condition.

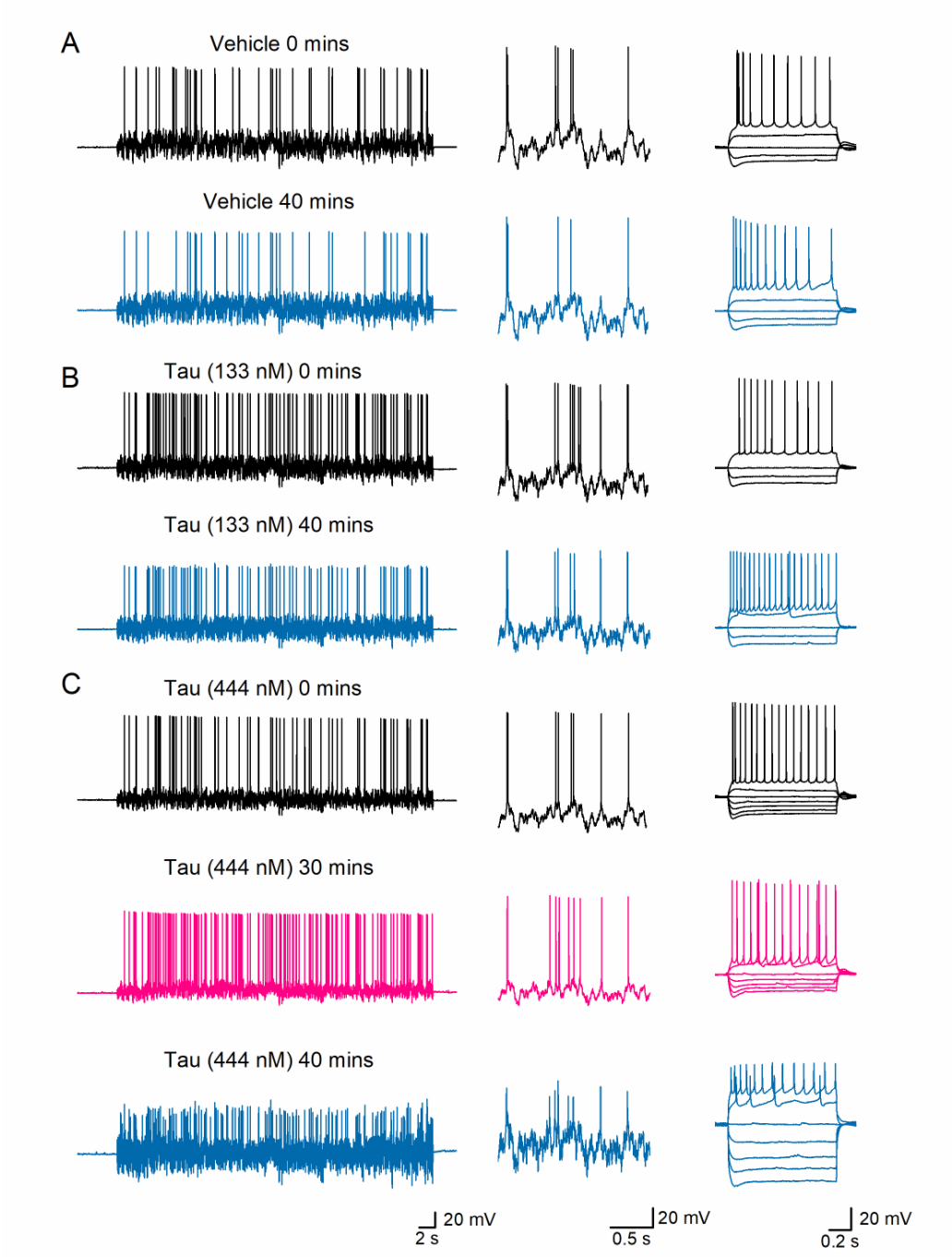

Figure 3.6: oTau introduction into CA1 hippocampal neurons has little effect on sub-threshold electrophysiological properties at low concentrations and at early time points (up to 30 minutes).

A. (Left) Example voltage response of a CA1 hippocampal neuron in response to a standard fluctuating noisy current injection in a cell injected with vehicle solution at time 0 mins (breakthrough, top) and after 40 mins of recording (bottom). (Middle, top, and bottom) Middle column demonstrate the voltage response over identical time periods on an expanded time base, showing that there is no change over time. Right panel shows the voltage response to stepwise current injections for 0 and 40 mins.

The voltage response also does not change over time. B. (Left) Example voltage response of a CA1 hippocampal neuron in response to a fluctuating noisy current injection in a cell injected with 133 nM oTau at time 0 mins (breakthrough, top) and after 40 mins of recording (bottom). (Middle, top, and bottom) Insets demonstrate the same voltage response on an expanded time base, demonstrating that there is little change to the voltage response over time, but that the action potential amplitudes are smaller. (Right) shows the voltage response to stepwise current injections for 0 and 40 mins. The voltage response does not change over time C. (Left) Example voltage response of a CA1 hippocampal neuron in response to a fluctuating noisy current injection in a cell injected with 444 nM oTau at time 0 mins (breakthrough, top) and after 30 (middle) and 40 mins of recording (bottom). (Middle, top and bottom) Insets demonstrate the same voltage response on an expanded time base, demonstrating that there is little change to the voltage response over time at 30 minutes but significant changes at 40 mins. (Right) Similarly, there are clear changes at 40 minutes, to the current-voltage relationship for the stepwise current injections to action potential amplitude and input resistance.

3.2.6 oTau markedly slows action potential dynamics and reduces action potential amplitude

To establish why there is a marked reduction in the spike match efficiency (Fig 3.5) for cells where oTau was introduced using the dynamic current-voltage protocol, I investigated whether there were changes to the action potential waveform (amplitude, duration, rate of rise and decay). Significant changes were observed at the 40-minute time-point for all concentrations of oTau (Fig 3.7) but were not observed when neurons were injected with either vehicle or BSA (Fig 3.7). For all three concentrations of oTau (44, 133, and 444 nM), there was a significant decrease in action potential amplitude, speed of rise and speed of decay at 40 minutes compared to time 0 mins (Fig 3.7). The time-course for these changes in action potential parameters (amplitude and rate of rise) were examined for the different concentrations of oTau. The effects of 444 nM oTau were significantly different from time 0 (whole-cell breakthrough) earlier than for 44 and 133 nM oTau (10 vs 20 minutes), characteristic of a concentration-dependent effect (Fig 3.7C).

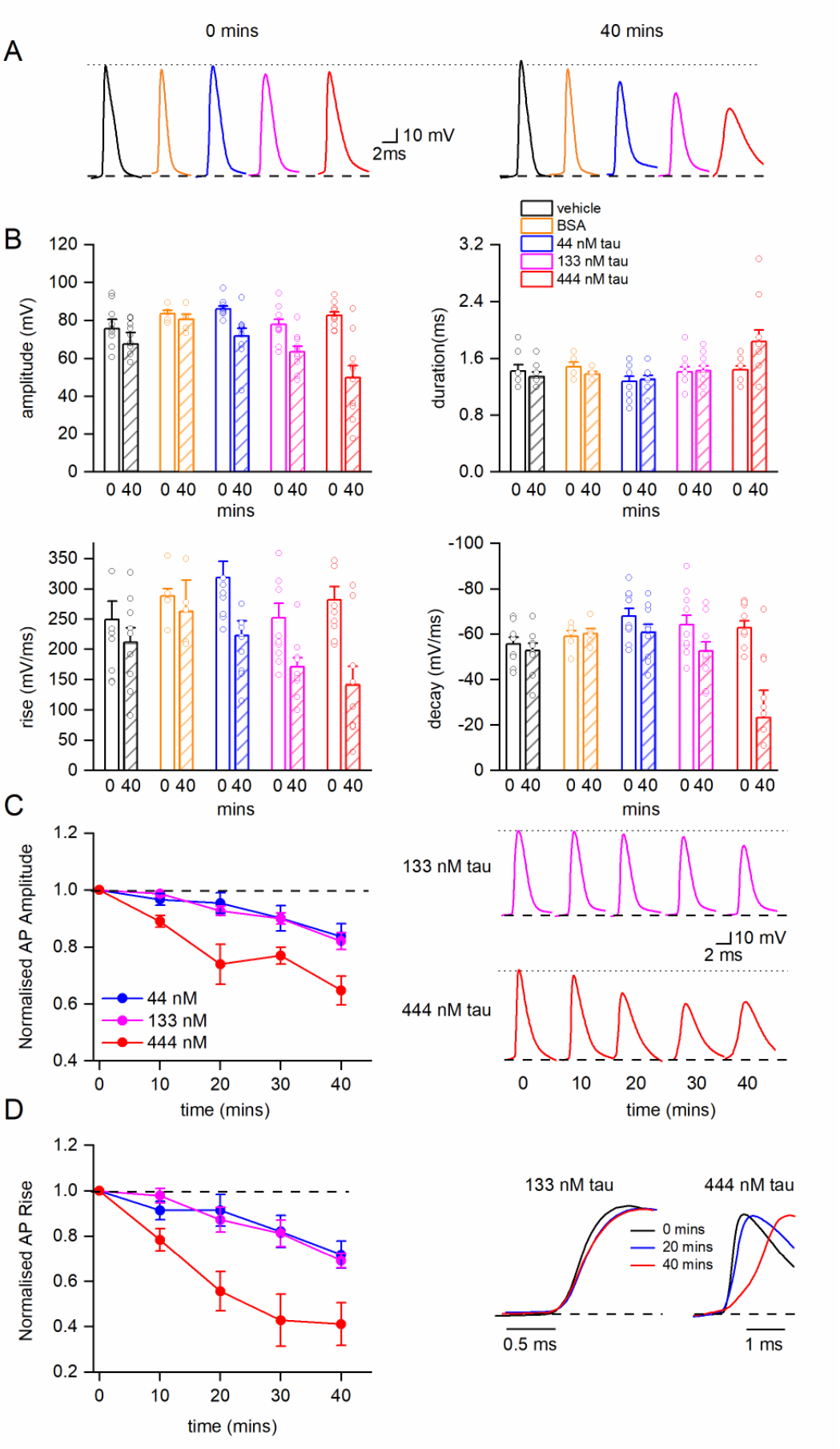
A
0 mins
40 mins
10 mV
2ms
B
vehicle
BSA
44 nM tau
133 nM tau
444 nM tau
amplitude (mV)
duration(ms)
rise (mV/ms)
decay (mV/ms)
0 40
mins
C
Normalised AP Amplitude
44 nM
133 nM
444 nM
time (mins)
133 nM tau
444 nM tau
10 mV
2 ms
D
Normalised AP Rise
0 mins
20 mins
40 mins
0.5 ms
1 ms

Figure 3.7: Introduction of oligomeric tau causes a significant change to action potential dynamics.

A. Representative voltage traces of a single action potential from single experiments at 0 mins (left) and 40 mins (right) for all conditions (vehicle, BSA, 44 nM oTau, 133 nM oTau and 444 nM oTau). B. Mean data for analysis of changes to action potential waveform for each of the conditions (vehicle, BSA, 44 nM oTau, 133 nM oTau and 444 nM oTau). Parameters measured were amplitude, duration, rate of rise and rate of decay. Bar charts displaying the mean and SEM data for each condition at the two timepoints (clear bar 0 mins, striped bar 40 mins), with individual data points overlaid. Action potential amplitude was decreased significantly from 0 minutes to 40 minutes with all concentrations of oTau tested (44 nM p = 0.004, 133 nM p = 0.002, 444 nM p = 0.002). Only the highest concentration of oTau (444 nM) gave a significant increase in action potential duration (p = 0.016). Rate of rise and decay was significantly slower for all three concentrations of introduced oTau (rise: 44 nM p = 0.004, 133 nM p = 0.002 and 444 nM p = 0.004; decay: 44 nM p = 0.008, 133 nM p = 0.002 and 444 nM p = 0008). C. Action potential amplitude evaluated over 10-minute time intervals. The left panel shows the mean amplitude normalised to the baseline (0 mins) for the three different concentrations of oTau (44 nM, 133 nM, and 444 nM). This demonstrates the drop in amplitude for all three concentrations of oTau over time. The right panel shows action potential waveforms from individual representative experiments at time points from 0 mins to 40 mins for 133 nM or 444 nM oTau introduction demonstrating the decrease in amplitude and which also highlights the concentration-dependent effect. D. Rate of rise evaluated over 10-minute time intervals. The left panel shows the mean rate of rise normalised to the baseline (0 mins) for the three different concentrations of oTau (44 nM, 133 nM, and 444 nM). This demonstrates the slower rate of rise for all three concentrations of oTau over time. The right panel shows normalised and superimposed examples of action potentials to demonstrate the effect on oTau introduction on action potential rate of rise over the period of recording.

3.2.7 The changes in action potential kinetics do not occur with monomeric tau

Given that some species of monomeric tau (seed-competent) can trigger intracellular tau aggregation (Mirbaha et al., 2018), it was important to distinguish whether the effects that I observed were specific to tau oligomers or just the result of increasing the concentration of tau in the cells. Oligomeric tau was monomerised using DTT and heat (see Methods) and maintained on ice to prevent re-aggregation while the experiments were carried out (Fig 3.8A). This monomeric tau (mTau; 444 nM) was introduced into hippocampal pyramidal cells to evaluate whether it gave similar effects to oTau. There was no significant change in the current-voltage relationship over-time (Fig 3.8B, C) and no change in action potential amplitude (at 40 mins the mean amplitude was 98.6% of the amplitude at time 0, Fig 3.8C). Therefore, it is only the oligomeric forms of tau that give rise to the observed changes to action potential waveform and input resistance over the 40-minute time period of my recordings.

3.2.8 The changes to action potential waveform are not due to changes in series resistance

oTau was delivered into cells through a glass pipette with a small tip with relatively high resistance (5-10 MΩ). As the tau is aggregated, it is feasible that it could block the pipette tip and impede the correct measurement of voltage. To check that this was not the case, series resistance was monitored throughout the experiments and any recordings where it altered by more than 20 % throughout the duration of the recording were excluded from analysis. There was no influence of the experimental condition on stability of series resistance throughout the recording. In general, I observed no significant change to series resistance over time and there was also no difference in the series resistance measurements for each of the conditions at 0 mins (Fig 3.8D).

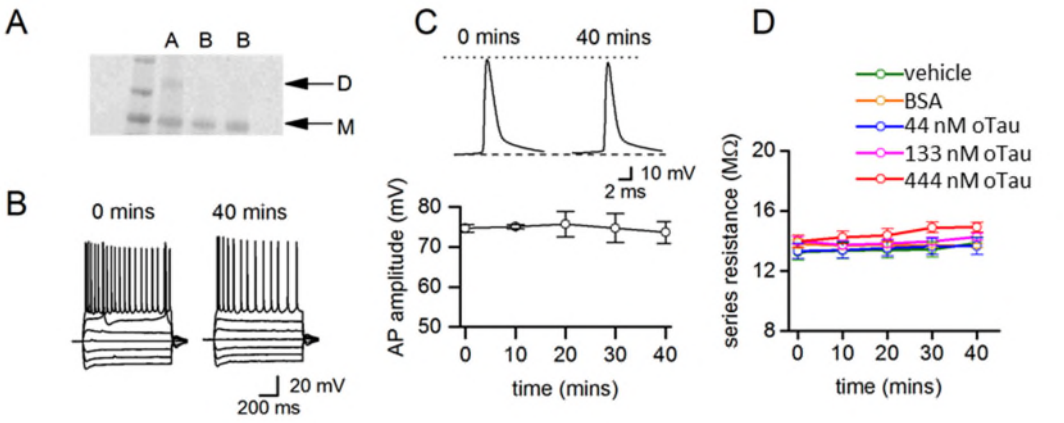

Figure 3.8: Evaluation of the effect of mTau on AP waveform showed no effect. *A. SDS-Page gel demonstrating dimeric tau protein (lane A) and tau protein converted to monomers (mTau, lanes B), stained with Instant Blue, and imaged using Image Quant (see Methods). B. There were no significant differences between current-voltage responses from a hippocampal CA1 neurons injected with 444 nM of mTau measured at 0 mins and after 40 mins of recording. C. (Top panel) Examples of action potential waveforms recorded at 0 mins and after 40 mins of recording from a neuron injected with 444 nM mTau. mTau does not change the amplitude or kinetics of the action potential waveform. (Bottom panel) summarises data from 5 neurons, showing that action potential amplitude does not change over time when neurons are injected with 444 nM mTau. D. The mean series resistance plotted against time for neurons injected with vehicle, BSA or oTau (44, 133, or 444 nM). There was no significant difference in series resistance between treatments and the series resistance did not significantly alter during recordings.*

3.2.9 Re-patching experiments confirm observations result from the introduction of oTau into the cell

I used an experimental design, termed ‘re-patching’ previously published by (Qui et al., 2014) to further exclude the possibility that tau was blocking the pipette tip or accumulating inside the cell impeding voltage measurement. oTau was introduced into CA1 pyramidal cells and recordings (step and dynamic current inputs) taken for ~ 20 mins until the change in AP waveform phenotype was observed. The pipette was then carefully removed from the cell and the cell ‘re-patched’ with a fresh pipette containing only vehicle solution. If the action potential waveform remained altered, then it was the result of the oTau and not simply a blockage of the pipette (n= 3 oTau; Fig 3.9 A-C) There was no significant difference in the first and re-patch for double vehicle injected cells (n= 4 control, Fig 3.9 D-F).

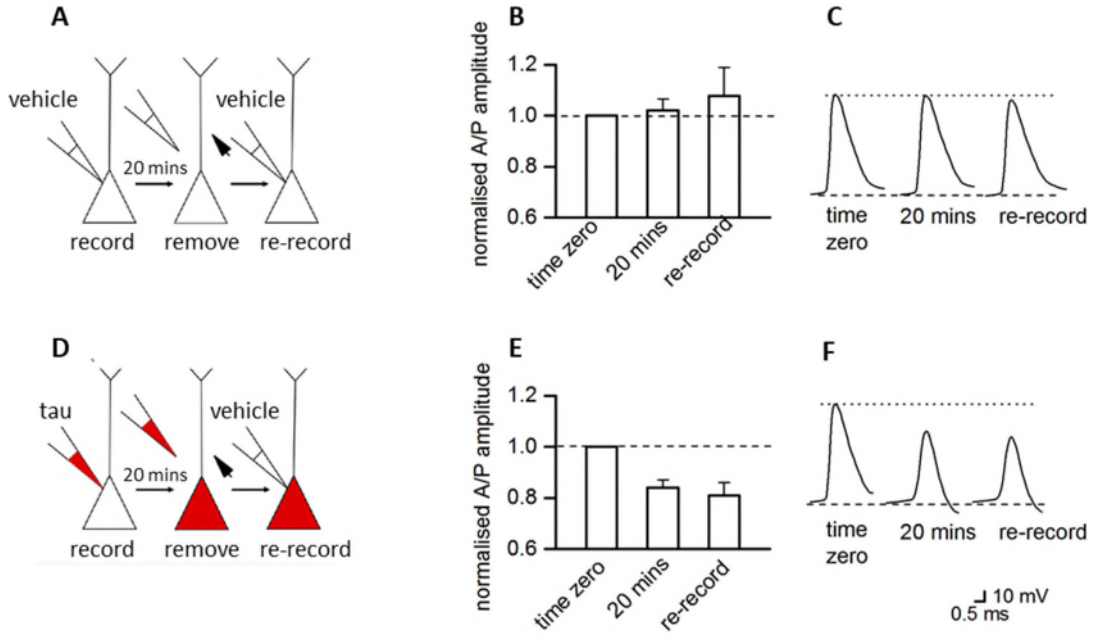

Figure 3.9: Re-patching experiments confirm that the observations are not due to blockage of the pipette tip.

A. Schematic to illustrate the protocol for repatching experiments. Recordings were made in CA1 pyramidal neurons of the hippocampus for 20 minutes using a pipette filled with intracellular solution and vehicle. The pipette was then carefully removed and then the cell was immediately re-patched with a clean pipette containing intracellular solution + vehicle. B. In the control (vehicle) cells, there was little change over time (at 20 mins, it was 102.0 ± 4.0 % of the amplitude at time 0) and very little

change to action potential amplitude was observed between patches 1 and 2 (108.0 ± 11.0 % of amplitude at time zero, n = 4 neurons) suggesting that the re-patching protocol is stable. C. Example traces shown for the initial patch at time zero, 20 minutes into the patch and then the re-recorded pipette for vehicle injected cells. D. A schematic to illustrate the protocol for repatching experiments with oTau injection. Recordings were made in CA1 pyramidal neurons of the hippocampus for 20 minutes using a pipette filled with intracellular solution + 444 nM oTau. The pipette was then carefully removed and then the cell re-patched with a clean pipette containing intracellular solution + vehicle. E. In cells injected with oTau (444 nM), action potential amplitude decreased over the course of 20 minutes (at 20 mins, it was 84.0 ± 3.1 % of the amplitude at time 0) and then remained reduced when the cell was re-patched with a separate pipette + vehicle (81.0 ± 5.0 % of amplitude at time zero, n = 3). F. Example traces shown in (F) for the initial patch at time zero, 20 minutes into the patch and then the re-recorded pipette.

3.2.10 Introduction of oTau into presynaptic neurons markedly impairs basal synaptic transmission

Given the marked effects of oTau on action potentials, I next investigated whether this translated into deficits in synaptic transmission. Such deficits have been reported previously, usually by using a stimulating electrode to activate many synaptic pathways in transgenic mice or mice that have had oTau perfused extracellularly. There are many limitations to these approaches. Firstly, using a stimulating electrode, it is not possible to know how many cells are being activated, whereas with paired recordings I could measure the effect of activating a single cell. Secondly, these methods expose every cell to the effects of tau to varying degrees which may lead to adaptation as the circuit could be changed. Using paired recordings, I was able to target oTau to either the pre- or post-synaptic cell and introduce the oTau into a small number of cells, which is unlikely to change the circuit. I initially considered studying the connection between CA1 and CA3 pyramidal cells (PCs) of the hippocampus, as I had already detailed the effects of oTau in CA1 PCs. However, the connection rate is low - between 1 and 5% (Debanne et al., 2008), which means large numbers of recordings will have to be made to find enough synaptic connections for significance. In contrast, neighbouring thick-tufted PCs in Layer V of the neocortex have a higher connection rate of ~ 10 %

(Markram et al., 1997). I located the somatosensory region of the neocortex under low magnification relative to the position of the hippocampus. I then identified thick-tufted layer V PCs using two methods. Firstly, I introduced dye via the intracellular solution to examine cellular morphology. Thick-tufted layer V PCs are large in size and have a distinct apical dendrite, projecting from layer Vb and bifurcating within layer II/III. Secondly, they have a distinct electrophysiological phenotype, as can be examined from the stepwise current-voltage relationship, typically exhibiting burst-firing action potentials (Kasper et al., 1994; Ramaswamy et al., 2015). Neurons that did not fit with expected morphological and electrophysiological phenotype were discarded from analysis (thin-tufted layer V PCs and interneurons). As I had moved to a new cell type, it was firstly important to validate that the results observed in the hippocampus were comparable to that of thick-tufted layer V PCs in the neocortex. In order to achieve similar results on a comparable timescale, the concentration of oTau was increased from 444 nM to 666 nM to account for the larger size of these cells relative to CA1 neurons (mean capacitance in CA1 neurons: 121.0 pF ± 6.2, in thick-tufted layer V PCs: 191.3 pF ± 20.8). There was no change in action potential amplitude for thick-tufted layer V PCs that were injected with vehicle (mean of 80.9 mV ± 1.8 vs 77.9 mV ± 2.1, p = 0.134, *n* =10). Action potential amplitude was significantly reduced from 74.45 ± 2.1 mV at time zero to 60.1 ± 6.3 mV after 40 minutes (p = 0.014) in cells where oTau was injected (*n* = 8, Fig 3.10A). There was no change to input resistance for vehicle injected cells (90.1 ± 12.0 MΩ vs. 92.2 ± 13.0 MΩ, p = 0.672), but for cells in which 666 nM oTau was introduced, the input resistance did increase over the course of 40 minutes of recording (from 92.5 MΩ ± 7.58 at time zero to 108.2 ± 8.1 MΩ at 40 minutes p = 0.045, Fig 3.10A).

In order to determine whether pairs of neighbouring thick-tufted layer V PCs were synaptically connected (Fig 3.10B-C), a stimulus train of 5 action potentials (20 Hz) was given with a one second pause and then a 6th recovery action potential (as in Kerr et al., 2013; Fig 3.10D). This allowed the effects on amplitude and latency of EPSPs along with the degree of depression and recovery to be examined. I performed these experiments in young (P12-P21 mice as their unitary EPSPs have a larger amplitude than those from older

mice and show marked short-term depression (Kerr et al., 2013; Reyes and Sakmann, 1999), which can be used to measure the effects of oTau on release probability. For each synaptically connected pair, oTau was either introduced into the pre- or the postsynaptic cell or neither (vehicle introduced instead) (Fig 3.10C) Once a connection was found, the stimulus protocol was repeated every 10 seconds for the duration of the recording. Due to the small amplitude of many of the EPSPs, (average amplitude ~ 0.8 mV, in line with Markram et al., 1997), averages of the sweeps were taken at 10-minute time intervals (30-50 sweeps per average). To establish whether there were changes to synaptic depression, the amplitude of each EPSP across the train needed to accurately be determined. This can be confounded as the EPSPs are superimposed on the decay (or tail) of the previous EPSP. Deconvolution and re-convolution of the traces allowed for the amplitude to be accurately measured (Richardson and Silberberg, 2008b). Briefly, EPSPs were averaged (after correcting for baseline drift) and then deconvolved. Each deconvolved EPSP was cropped and then reconvolved so that the individual average EPSPs were no longer superimposed on the decay of the previous EPSP (Fig 3.10 E-F). With assistance from collaborators at the Zeeman Institute, I wrote the code to perform this in Julia (available on request). The accuracy of the program was confirmed by reconvolving the uncropped EPSPs and the comparing the resulting waveform to the untransformed EPSPs. There were a small number of EPSPs that were still too small to run the re-convolution, so these were used solely for the measurements based on the first EPSP but not used for synaptic depression.

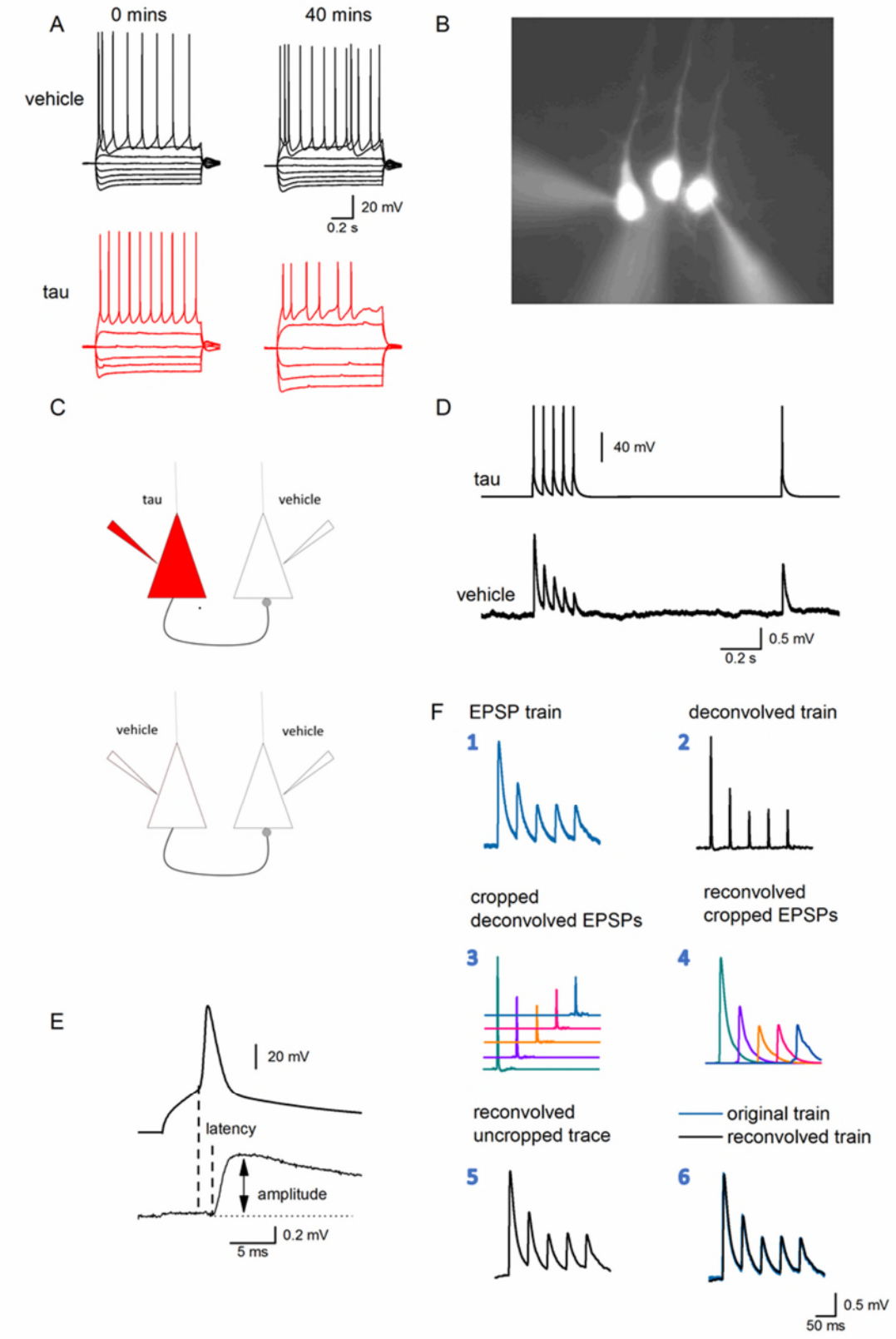
A
0 mins
40 mins
vehicle
20 mV
0.2 s
tau
B
C
tau
vehicle
vehicle
vehicle
D
tau
40 mV
vehicle
0.5 mV
0.2 s
E
20 mV
latency
amplitude
0.2 mV
5 ms
F
EPSP train
deconvolved train
1
2
cropped
deconvolved EPSPs
reconvolved
cropped EPSPs
3
4
reconvolved
uncropped trace
original train
reconvolved train
5
6
0.5 mV
50 ms

Figure 3.10: Protocols for testing the effect of oTau on membrane properties and synaptic transmission in layer V pyramidal neurons.

A. Voltage response to stepwise current injection protocol at 0 and 40-minute timepoints for control cells injected with vehicle (top) or 666 nM oTau (bottom). There was no significant change in the control cells but a reduction in action potential amplitude and an increase in input resistance. B. Micrograph of three Layer V PCs labeled with Alexa Fluor 488. Recordings were routinely made from three neighboring pyramidal cells to increase the probability of finding synaptically connected cells. C. Diagram of the protocol used to record pairs of synaptically coupled thick-tufted layer V PCs. Either both pipettes contained vehicle (bottom), or tau was targeted at the pre- or post-synaptic cell of the pair (top). D. Diagram to represent the stimulus delivered to the pairs of connected cells. A train of 5 action potentials (20 Hz) were stimulated in the presynaptic oTau cell using short depolarising current steps followed by a 1 second gap and then a recovery action potential. EPSPs resulting from APs were then recorded in the postsynaptic vehicle cell. E. Example AP and corresponding EPSP to illustrate the recorded parameters (EPSP amplitude and latency). F. Method of accurately measuring the amplitude of the 2nd to 5th EPSPs in the train. EPSPs were averaged (after removing any baseline drift; 1) and then deconvolved (top right; 2). The deconvolved EPSPs were cropped (3) and then reconvolved so that individual average EPSPs were not superimposed on the decay of the previous EPSP average (4). The accuracy of the deconvolution method was confirmed by reconvolving the uncropped EPSPs (5) and comparing the resultant waveforms to the original untransformed EPSPs (6).

3.2.11 Introduction of oTau into the presynaptic cell of a connected pair impairs the synaptic transmission

In total, 230 pairs of thick-tufted layer V PCs were recorded from, of which 24 were connected synaptically. This gave an overall connection probability of 1 in 9.6 pairs, comparable with the 1 in 10 pairs that were synaptically connected in a previous study of these neurons (Markram et al., 1997). In 10 control pairs, vehicle was introduced into both the presynaptic and postsynaptic cells in the pair. For the remaining recordings, oTau was introduced in one pipette and vehicle in the other pipette. Therefore, once a connection was found, the tau would be in either the presynaptic or the postsynaptic cell. In 10 of the pairs

oTau was introduced into the presynaptic cell and vehicle into the postsynaptic cell. In the remaining 4 pairs, oTau was targeted to the postsynaptic cell, with vehicle introduced into the presynaptic cell. At early time points (0-10 minutes) there was no significant difference in the amplitude of the first EPSP in the train ($p = 0.510$) or its latency ($p = 0.581$) when either vehicle or oTau were introduced into the presynaptic cell (mean unitary EPSP amplitude: vehicle 0.8 ± 0.1 mV; oTau 0.6 ± 0.1 mV; latency: vehicle 2.2 ± 0.0002 ms, oTau 2.1 ± 0.0001 ms). In control pairs (both vehicle), the amplitude of the EPSP remained stable throughout the recording (the amplitude of the first EPSP after 40-50 minutes of recording was 80.5 ± 14.0 % ($n = 10$) of the EPSP amplitude at 0-10 minutes of recording, $p = 0.375$). However, when oTau was introduced into the presynaptic cell, at 40-50 minutes, the amplitude of the first EPSP was significantly reduced in 7 out of 10 of the paired recordings to 30.0 ± 10.0 % of the amplitude of EPSPs at 0-10 minutes ($p = 0.034$, $n = 10$, Fig 3.11 A-B). This was not a result of the recordings becoming unstable as the mean membrane potential at time zero, -67.5 ± 1.5 mV, was not significantly ($p = 0.095$) different from the membrane potential 40 minutes, -62.5 ± 1.3 mV. To ensure that the decrease in EPSP amplitude was not due to failure of action potential firing, every sweep was reanalysed and any with failed AP firing were removed from analysis (46 out of 3900 sweeps, ~ 1.2 %).

3.2.12 Deficits in synaptic transmission are associated with increased short-term depression

Changes to short term synaptic plasticity were measured using the train of 5 AP (20 Hz, 50 ms interval) and evaluating the degree of depression across conditions. For analysis, the amplitude of EPSPs in the train (2^{nd}- 5^{th} EPSP) were measured relative to the amplitude of the first EPSP. In 9 out of 10 recordings (in one recording the connection was too weak to accurately measure the amplitude of the 2^{nd} -5^{th} EPSPs) with vehicle introduced into both the pre- and postsynaptic cells, there was little change in the degree of short-term depression over the duration of the recordings (Fig 3.11C, D). There was a small (but significant) increase in depression and a decrease in the paired-pulse ratio (second EPSP/first EPSP amplitude) from 0 to 30 minutes (Fig 3.11G). In the recordings (8 out of 10, two connections were too weak to

accurately measure) where oTau was introduced into the presynaptic cell there was an increase in the degree of short-term depression (Fig 3.11E, F). If the reduction in EPSP amplitude induced by oTau was a consequence of a fall in the probability of neurotransmitter release, then short-term depression would have been expected to reduce (equivalent to the activation of presynaptic receptors such as adenosine A_1, as in Kerr et al., 2013). This was not the case with oTau introduction and therefore the changes to short term plasticity are unlikely to be due to a fall in release probability. In 4 out of the 8 connections there was a complete failure of transmission during the train: the 2^{nd}-5^{th} EPSPs were absent (Fig 3.11E). Changes to AP waveform were not characterised from the pairs data due to the waveform being contaminated by the stimulus used to evoke the APs. All sweeps were, however, manually checked for AP failures and any sweeps that did have action potential failures were removed from analysis. Finally, paired-pulse ratio (amplitude of first EPSP/ amplitude of second EPSP) was calculated. Although there was a significant decrease in the ratio over time it is comparable between oTau and control.

The recovery EPSP (evoked 1 s after the train of EPSPs) was used to determine the duration of the enhanced depression observed with oTau. The amplitude of the recovery EPSP was measured relative to the first EPSP in the train. Even though the degree of depression was significantly higher in the oTau introduced pairs, the recovery (amplitude of recovery EPSP/ amplitude of first EPSP) was not different between the conditions. Therefore 1 s is a long enough time for recovery of the enhanced depression and shows the depression is reversible.

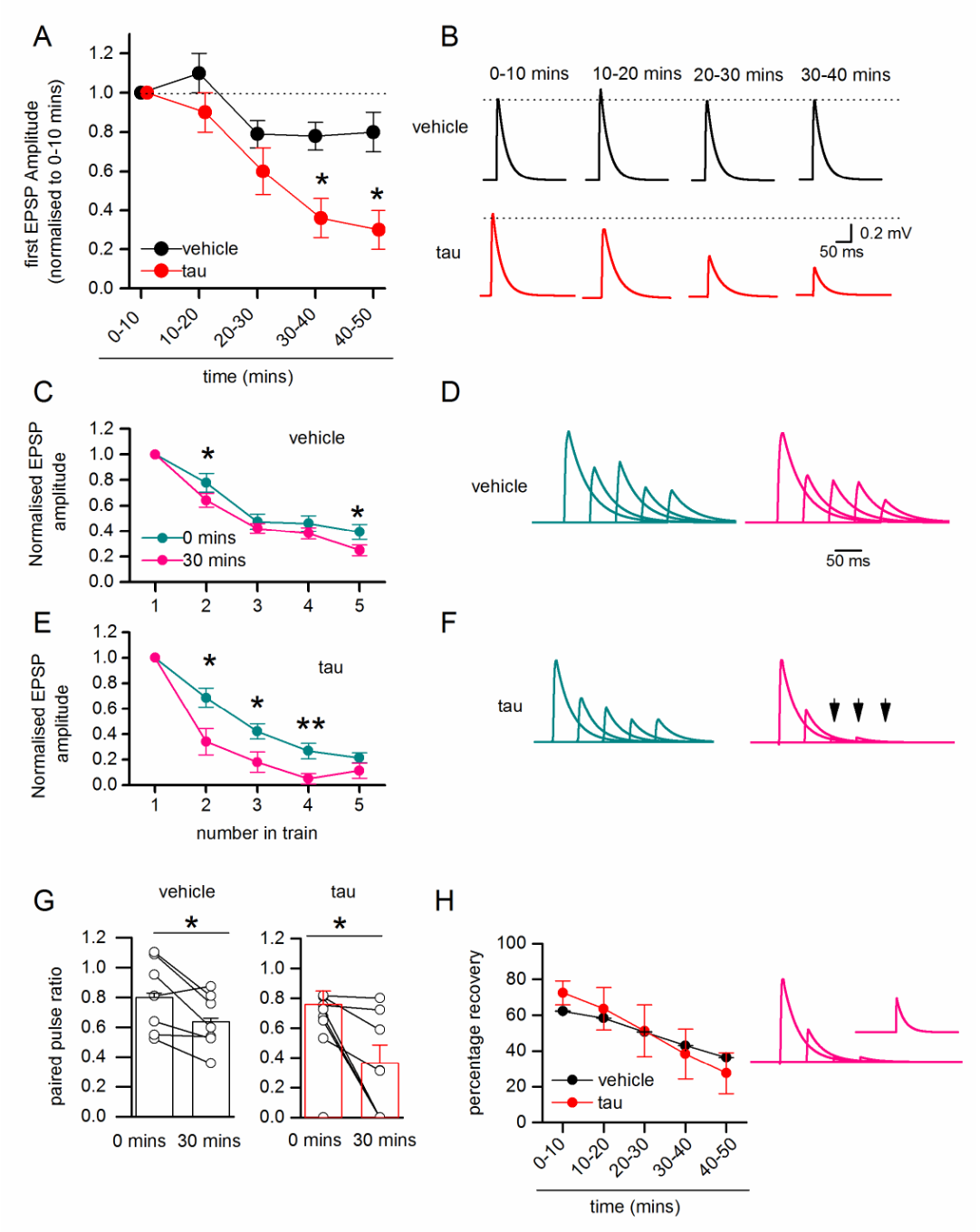

Figure 3.11: Introduction of oTau into the presynaptic cell of a connected pair impairs the synaptic transmission.

A. Mean normalised amplitude of the first EPSP in the train (normalised to the EPSP at 0-10mins). Each timepoint is an average of EPSPs across the 10-minute time window (~50 sweeps). The black line represents the pairs with vehicle in both pipettes and the red line represents pairs in which oTau (666 nM) was introduced into the presynaptic cell of the pair. For the control pairs there was no significant change over time (p = 0.375). However, for those with oTau introduced, there was a significant

decline in amplitude over time (control vs oTau 30-40 mins p = 0.029, 40-50 mins p = 0.034). B. At each timepoint, representative EPSP averages are shown for vehicle and oTau introduced pairs. They have been deconvolved, cropped and re-convolved so that the full rise and decay of each EPSP can be observed. A clear reduction can be observed for oTau introduced pairs. C. The 2nd to 5th EPSP amplitudes were also analysed following the deconvolution and reconvolution process. They are presented normalised to the first EPSP in the train's amplitude in vehicle. Data is shown for 0-10 minutes and at 30-40 minutes. There was a small but significant increase in depression between 0 mins and 30-40 mins for the 2nd EPSP (p = 0.032) and the 5th EPSP (p = 0.041). D. A representative single recording to show the average EPSP waveforms in vehicle for all 5 EPSPs in the train after vehicle introduction. Averages are shown for 0-10 mins and 30-40 mins of recording. The EPSP traces were normalised so the amplitude of the first EPSP remains the same, to highlight changes in depression. E. The 2nd to 5th EPSP amplitudes were also analysed following the deconvolution and reconvolution process. They are presented normalised to the first EPSP in the train's amplitude when oTau has been injected into the presynaptic cell. Data is shown for 0-10 minutes and at 30-40 minutes. There was a significant increase in depression between 0-10 and 30-40 mins for the 2nd EPSP (p =0.0347), 3rd EPSP (p = 0.037) and 4th EPSP (p = 0.009). F. A representative single recording to show the average EPSP waveforms in vehicle for all 5 EPSPs in the train after oTau (666 nM) introduction. Averages are shown for 0-10 mins and 30-40 mins of recording. The EPSP traces were normalised so the amplitude of the first EPSP remains the same, to highlight changes in depression. Although it is clear that the 3rd, 4^{th,} and 5th EPSPs are absent, this was not a result of failed action potentials. G. Graphs to demonstrate the paired pulse ratio for cells with vehicle or oTau introduced (amplitude of the second EPSP/ amplitude of the first EPSP). The points are means from single experiments and the bars show the overall mean and SEMs for all recordings. For both conditions, there was a significant fall in the paired-pulse ratio over the duration of the recording (vehicle p = 0.032 and oTau p = 0.035). H. Following a 1 second recovery period a final EPSP was evoked (left). The amount of recovery (recovery EPSP/ first EPSP) decreases over time and is similar for cells for both conditions. Waveforms after 30-40 minutes (right, same recording as in F) showing the absence of the 3rd-5th EPSPs, but there is some recovery after the 1s interval (inset).

3.2.13 Introducing oTau into the postsynaptic cell does not impair basal synaptic transmission

In the remaining 4 pairs of synaptically connected thick-tufted layer V PCs, where the oTau was introduced only into the postsynaptic cell, there was no significant reduction in EPSP amplitude over the recording period (average EPSP amplitude after 40 minutes was 91.8 % of the EPSP recorded at 0-10 minutes) and there was no change to the degree of short-term depression (Fig 3.12). Therefore, introduction of oTau over ~40 mins results in significant changes to basal synaptic transmission specifically at presynaptic sites.

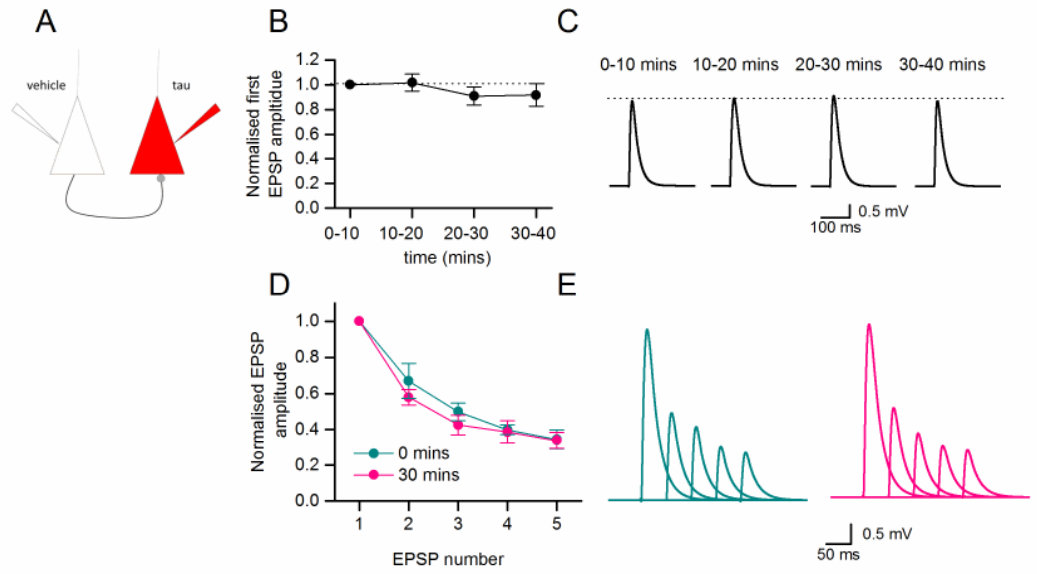

Figure 3.12: Introduction of oTau into postsynaptic neurons has no significant effect on basal synaptic transmission

A. Using a similar protocol as was used for measuring the pre-synaptic effects of oTau, oTau (666 nM) is introduced to only the postsynaptic cell. Diagram illustrates the experimental setup. B. Normalised first EPSP amplitude (1st in the train of 5) at 10 minute-averaged timepoints between 0 and 40 mins after tau (666 nM) introduction. Normalisation is done at each time point to the amplitude of the EPSP over the first 0-10 minutes of recording. There was no significant change over the period of recording. C. Representative examples of EPSPs from single experiments. The EPSPs were averaged over 10 minutes and have been deconvolved, cropped and re-convolved to show the full-time course for each EPSP waveform. Traces are shown for each of the averaged timepoints. D. The 2nd to 5th EPSP amplitudes were also analysed following the deconvolution and reconvolution process. They are presented

normalised to the first EPSP in the train's amplitude. Data is shown for 0-10 minutes and at 30-40 minutes. There is no significant change over the period of recording. E. A representative single recording to show the average EPSP waveforms for all 5 EPSPs in the train after oTau (666 nM) introduction. Averages are shown for 0-10 mins and 30-40 mins of recording. The EPSP traces are not normalised.

3.2.14 Post-synaptic oTau disrupts long term potentiation

It has previously been demonstrated that extracellular application of oTau, but not monomeric (m)Tau can impair synaptic plasticity, both long-term potentiation (LTP) and long-term depression (LTD), (Fá et al., 2016; Lasagna-Reeves et al., 2012). Ondrejcak et al., (2018) demonstrated that for a subset of AD brain extracts that produced an amyloid beta-independent reduction in LTP, immunodepletion of the extract with the Tau5 monoclonal antibody prevented the impairment of LTP, suggesting the importance of tau in mediating the changes to synaptic plasticity. However, from these experiments, it is not clear what the actual concentration of oTau is inside the cells or whether the actions on plasticity are pre- or postsynaptic.

To investigate this, I made whole-cell current clamp recordings from CA1 hippocampal neurons and stimulated the Schaffer collateral fibres (Fig 3.13A). oTau, vehicle or mTau were introduced into the postsynaptic neuron and the effects on long-term potentiation (LTP, induced with theta burst stimulation TBS) measured. There was no significant difference in the amplitude of EPSPs across all of the conditions at 0 mins (one-way ANOVA, $p = 0.148$). Although there was considerable variability between cells regarding the response to the TBS, there was no significant difference in the area under the curve (of the response to TBS) across conditions ($p = 0.787$). When vehicle was introduced into the postsynaptic cell, theta-burst stimulation (TBS) induced robust potentiation (30 minutes after the stimulation, EPSP amplitude was 3.9 ± 1.2 x the baseline amplitude, n = 7, Fig 3.13A). This potentiation was NMDA receptor dependent as it was abolished by the NMDA receptor antagonist L689,560 (5 µM, 0.4 ± 0.1 x the baseline EPSP amplitude after 30 minutes, n = 3, Fig 3.13B). In initial experiments I found that oTau (444 nM) abolished both STP and LTP (n = 7 slices, Fig 3.13C). The experiments were then repeated with a 10-fold reduction in the concentration of oTau (44 nM) which

also abolished LTP but did not completely prevent STP (n = 5, Fig 3.13D). Monomeric tau (444 nM) had little effect on the degree of potentiation compared to control (LTP p = 0.151 or STP p = 0.429, n = 5, Fig 3.13E, F). Therefore, even though there were no effects on basal synaptic transmission when oTau was introduced into the postsynaptic cell, it abolishes LTP, a measure of synaptic plasticity which could be one of the mechanisms underlying the learning and memory deficits in diseases involving tau oligomers such as Alzheimer's disease.

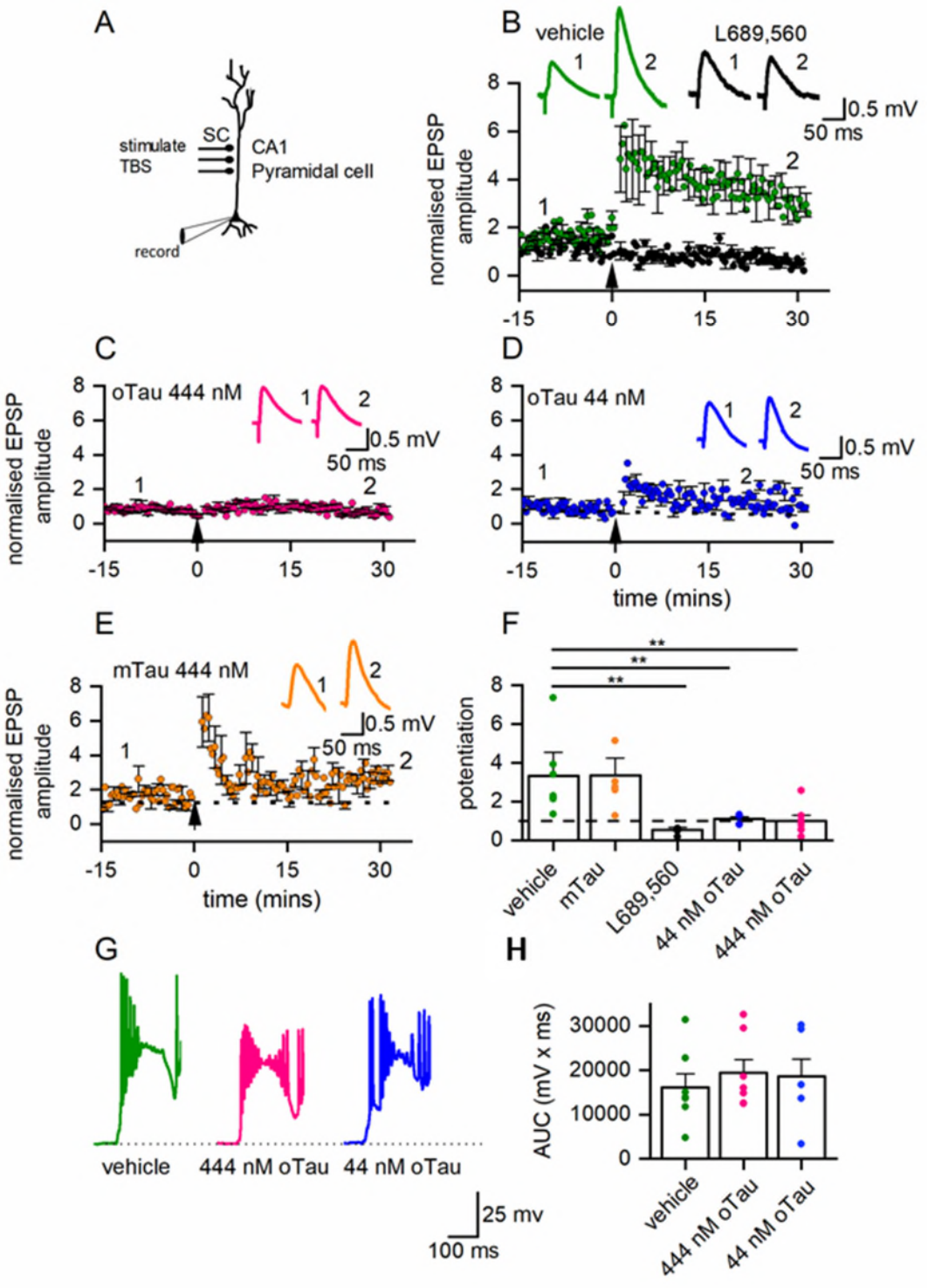
A
stimulate
TBS
SC
CA1
Pyramidal cell
record
B
vehicle
L689,560
1
2
0.5 mV
50 ms
normalised EPSP amplitude
C
oTau 444 nM
D
oTau 44 nM
time (mins)
E
mTau 444 nM
F
potentiation
**
vehicle
mTau
L689,560
44 nM oTau
444 nM oTau
G
vehicle
444 nM oTau
44 nM oTau
25 mv
100 ms
H
AUC (mV x ms)
30000
20000
10000
0

Figure 3.13: Introduction of oTau into the postsynaptic neuron blocks the induction of long-term potentiation

A. Illustration of the protocol used to measure long-term potentiation (LTP). Stimulation of the Schaffer collaterals evoked EPSPs in CA1 hippocampal cells. LTP was induced by theta burst stimulation (TBS). Vehicle or oTau were introduced via patch pipette to the CA1 neuron being recorded. B. Mean EPSP amplitude against time for vehicle controls (n = 7) and for 3 slices where 5 µM L689,560 was added to block NMDA receptors. The TBS protocol evoked robust potentiation which was abolished by the NMDA antagonist. Inset shows example average waveforms before TBS (1) and 30 mins after TBS (2) for both control and 5 µM L689,560. C. Mean EPSP amplitude against time for 444 nM oTau introduced cells (n = 7). STP and LTP were completely abolished by oTau. Inset shows example average waveforms before TBS (1) and 30 mins after TBS (2). D. Mean EPSP amplitude against time for 44 nM oTau introduced cells (n = 5). LTP was completely abolished by oTau. However, there was some short-term potentiation. Inset shows example average waveforms before TBS (1) and 30 mins after TBS (2). E. Mean EPSP amplitude against time for monomeric 444 nM tau (mTau) introduced cells (n = 5). LTP was induced with mTau. Inset shows example average waveforms before TBS (1) and 30 mins after TBS (2). F. A summary graph demonstrating the mean potentiation. In control conditions (vehicle in the intracellular solution) after 30 minutes following TBS, EPSP amplitude was potentiated to 331.0 ± 132.0 % of the baseline amplitudes (n = 7). This potentiation was lost in the presence of L689,560 (53.0 ± 14.0 % of the baseline amplitude, n = 3), with oTau 444 nM in the intracellular solution (99.0 ± 31.0 % of the baseline amplitude p = 0.042, n = 7, control vs 444 nM) and with 44 nM oTau in the intracellular solution (111.0 ± 10.0 % of the baseline amplitude, n = 5). In contrast potentiation persisted with mTau (444 nM) in the intracellular solution (335.0 ± 90.0 % of the baseline amplitudes, n = 5). A Kruskal Wallis one-way ANOVA gives a significant effect of treatment condition against vehicle (p = 0.003) and Dunn's post hoc analysis shows significant differences between the potentiation of cells injected with vehicle and L689,560, 44 nM or 444 nM oTau (p = 0.006, p = 0.008 and p = 0.002 respectively) compared to control. G. Example voltage responses to the TBS used to induce potentiation for a vehicle, 444 nM oTau and a 44 nM Tau introduced neuron. H. Mean voltage responses to TBS (measured as area under the curve; AUC) for a vehicle, 444 nM oTau and a 44 nM oTau introduced neuron. Graph shows mean and SEM data with individual data points overlaid. There was no difference across experimental group in response to TBS.

3.2.15 Post-synaptic oTau disrupts long term depression

In preliminary experiments, I also began to evaluate the effects of post-synaptic oligomeric tau on metabotropic glutamate receptor (mGluR)-mediated long-term depression (LTD) with whole-cell current-clamp recordings from CA1 hippocampal pyramidal cells in the presence of 50 µM picrotoxin (to block GABAA receptors) and 5 µM L689,500 (to block NMDA receptors). As with the LTP protocol, the Schaffer collaterals were stimulated every 20 seconds to evoke reliable and robust synaptic transmission (EPSP amplitude ~ 3 mV). After a 10-minute baseline, LTD was induced by 100 µM of the mGluR5 agonist DHPG for 10 minutes and EPSPs were recorded for 30 minutes further following induction (Fig 3.14A). When oTau (444 nM) was introduced into the CA1 neuron, the mean LTD at 30-minutes post induction was 56.0 ± 0.1% of baseline (n=6) in control cells and 106.0 ± 0.2 of baseline (n=5) in oTau cells (Fig 3.14B-D). Although only a preliminary study, this a significant reduction in depression at 30 mins following induction (Kruskal Wallis ANOVA, control vs oTau, $p = 0.028$).

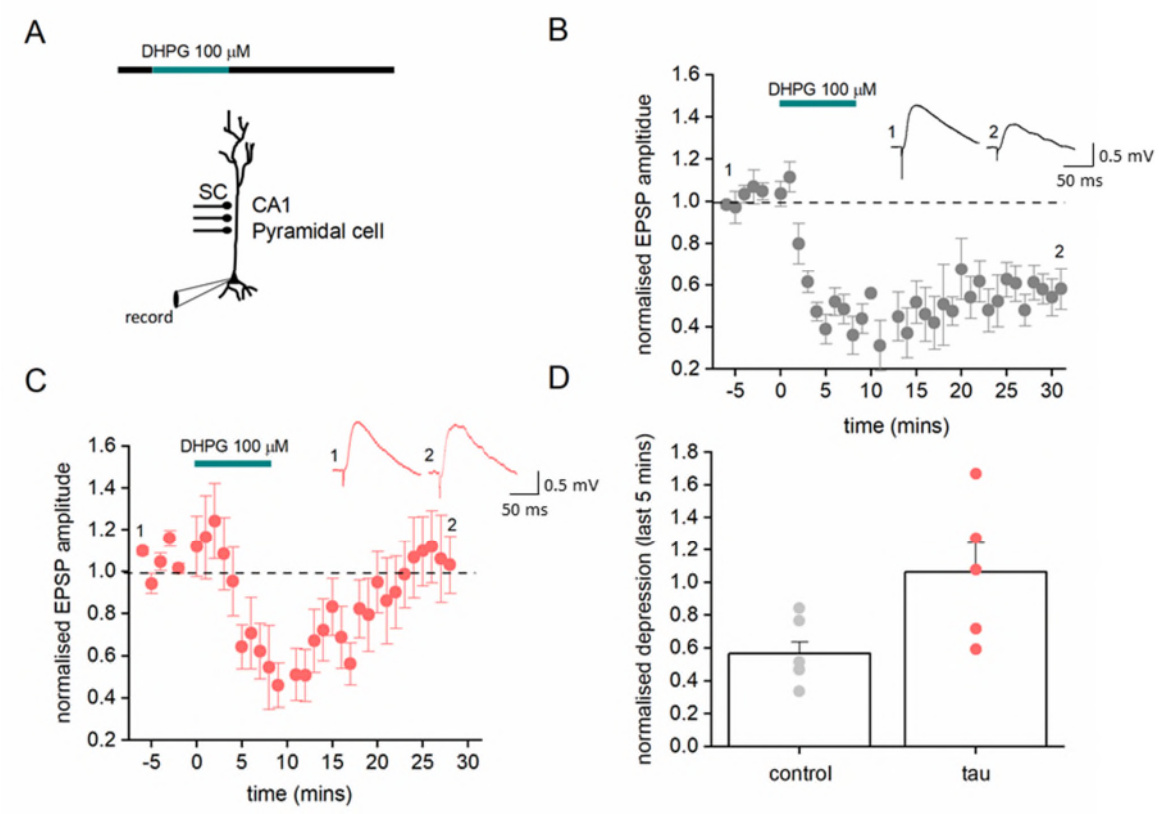

Figure 3.14: Introduction of oTau into the postsynaptic neuron reduced long-term depression.

A. Illustration of the protocol used to measure long-term depression (LTD). Stimulation of the Schaffer collaterals evoked EPSPs in CA1 hippocampal cells. LTD was induced by application of 100 µM of the mGluR5 agonist DHPG for 10 minutes. Vehicle or oTau were introduced via the patch pipette to the CA1 neuron being recorded. B. Mean normalised EPSP amplitude against time for 444 nM oTau introduced cells (n = 6). LTD was completely abolished by oTau. Inset shows example average waveforms before DHPG application to induce LTD (1) and 30 mins after induction (2). C. Mean normalised EPSP amplitude against time for control cells (n = 5). LTD was reliably achieved in controlled cells. Inset shows example average waveforms before DHPG application to induce LTD (1) and 30 mins after induction (2). D. Mean depression (normalised to baseline) for control and Tau introduced cells at 30-minutes post induction. Graph shows mean and SEM, data points are individual experiments overlaid. A significant reduction in depression can be observed in the oTau cells compared to control (p = 0.028).

3.3 Conclusion

The aim of the work in this Chapter was to provide further understanding of the role of tau oligomers in the disruption of neuronal function. This field of research is important given the ageing global population and an increased pressure to understand neurodegenerative conditions like Alzheimer's disease, in which tau is a key pathological player. Previous studies have utilised transgenic animal models of tauopathies (Booth et al., 2016; McInnes et al., 2018; Rudinskiy et al., 2014; Zhou et al., 2017), but it is difficult to determine the concentration or the form of tau that is responsible for the toxicity. Other approaches use extracellular bath-application of tau oligomers (Fá et al., 2016; Lasagna-Reeves et al., 2012; Puzzo et al., 2017) but it is difficult to know how much of the applied tau oligomers are taken up into neurons and then act directly inside the cells or whether the tau oligomers have indirect effects. It is also impossible to quantify the exact concentration of oligomers within the recorded cells. For both transgenic animals and extracellular application methods, it is not possible to say whether any effects synaptic transmission or plasticity are pre- or postsynaptic. Using my method, introducing tau through the patch pipette, I can directly target the characterised oTau into single neurons in a network that is free from pathology and allowing targeting of oTau to pre- or post-synaptic cells. In comparison with the other methods, I have outlined that: i) my method requires a much lower quantity of oligomer per experiment; ii) each cell acts as its own control (upon whole-cell breakthrough) and iii) effects can be observed in real time; allowing for a direct correlation between the observed effects and the different concentrations of injected oligomer. I have demonstrated in this study comparable concentration-dependent effects for oTau introduction into CA1 neurons in the hippocampus and Layer V pyramidal neurons in the cortex. Marked changes to action potential dynamics, synaptic transmission and plasticity were mediated by oligomeric, but not monomeric, tau protein. Consistent with these electrophysiological changes, I have also demonstrated that oTau can diffuse from the injection site (soma) to synaptic sites within 30 minutes of recording. This study provides valuable new insight into the actions of tau oligomers within single neurons. It answered questions that have never before been

possible to explore with traditional methods. Though this study greatly enhances the field of knowledge regarding the actions of oligomeric tau in neurons, there are many unanswered questions regarding underlying mechanisms that will need to be investigated in future experiments (see Chapter 4).

Chapter 4:

Truncating Tau Reveals Different Pathophysiological Actions of Oligomers in Single Neurons

Results of this chapter have been published previously: (Hill et al., 2021, in review)

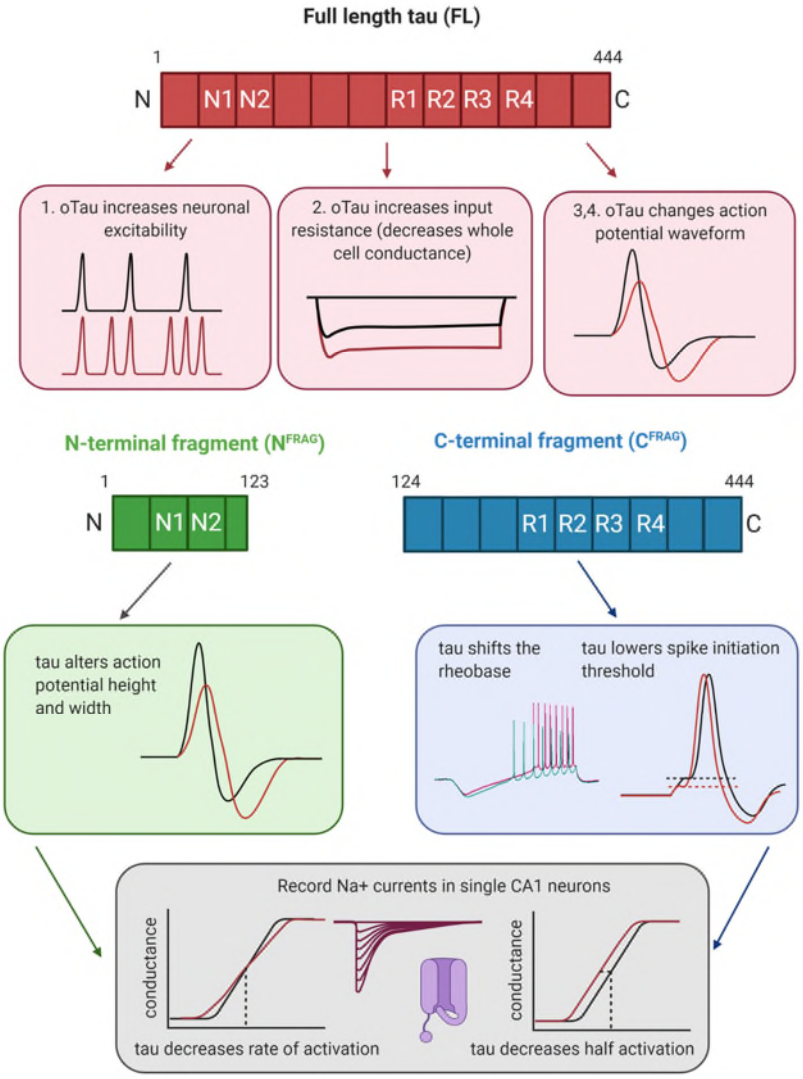

Figure 4.1: Tau truncations can dissect apart the effects on action potential and neuronal excitability, a summary of identified mechanisms

4.1 Introduction

In Chapter 3, in order to study the acute effects of tau oligomers, I used whole-cell patch-clamp recording to introduce known concentrations of structurally defined oligomeric full-length human tau-441 (oTau) into mouse hippocampal CA1 pyramidal and neocortical layer-V thick-tufted pyramidal cells (Hill et al., 2019). In this study, I have begun determining the mechanisms underlying these changes to excitability, conductance and action potential waveform. My strategy was to use recombinantly produced tau truncations to determine whether specific regions of tau are responsible for the observed effects. Identifying the regions of tau mediating neuronal dysfunction will assist in tracking down protein-protein interactions, help design assays for interacting partners and provide a mechanistic framework for drug development.

To decide on the truncations to use, I considered two factors. Firstly, to find tau fragments that exist in the human brain, as this will also provide information on the pathological actions of these truncated tau molecules. A fraction of the toxic oTau pool in human AD brains is released into cerebrospinal fluid (CSF) in a manner that associates with pathological AD markers. The majority of this tau appears as fragments or truncations, for example as N-terminal fragments of amino acids 1-123 or 1-224 (Cicognola et al., 2019). I then investigated if any of these fragments had already been evaluated in previous studies. Zhou et al., (2017) had used a similar N-terminal truncation of tau (to the 1-123 fragment) to identify synaptic transmission deficits in cell culture models. Taking these two factors together, I decided to study the N-terminal truncation of amino acids 124-444 (C^{FRAG}) and the resulting fragment of amino acids 1-123 (N^{FRAG}).

I have implemented the same single-cell approach in combination with detailed computational modelling to start to determine the underlying mechanisms of the changes to excitability, conductance and action potential waveform. This approach provides a simple, yet highly effective way to generate detailed quantitative information on the functional effects of different mutations and truncations of tau oligomers, as well as to test pharmacological drugs and interventions. Understanding the direct actions of tau oligomers will lead to

better understanding of the disease process and provide new avenues for diagnostics and therapeutics.

4.2 Results

4.2.1 Structural characterisation of the tau samples

In this study, the actions of oligomeric full length (FL) tau were compared to the effects of oligomers formed from two truncated forms of tau. The first is an N-terminal truncation (C^{FRAG}) consisting of amino acids 124-444 (Fig 4.2A). The second is the N-terminal fragment that is removed by this truncation (N^{FRAG}) and consists of amino acids 1-123 (Fig 4.2A).

One of the goals of my previous study (Hill et al, 2019), was to visualise the localisation of the introduced tau oligomers in the recorded neuron. To achieve this, the tau oligomers were labelled (Alexa Fluor maleimide 488 bound to cysteine residues). This required the introduction of mutations to the tau molecule, to move the cysteine residues to enable efficient label binding without impeding tau function (Hill et al, 2019). In this study, I have used tau that was not labelled and therefore does not require these cysteine modifications. It therefore represents full length tau in its native state (Fig 4.2A).

The recombinant full length and truncation of tau used in the study were initially going to be produced by myself but due to time constraints were produced by collaborators at the University of Gothenburg.

All three samples (FL, C^{FRAG} and N^{FRAG}) were examined in both aggregated and monomeric form. Negative-stain transmission electron microscopy (TEM) was used to evaluate the samples. TEM confirmed that all the oligomeric species were in the form of small aggregates rather than longer fibrils and that none of the monomeric species showed aggregates (Fig 4.2B).

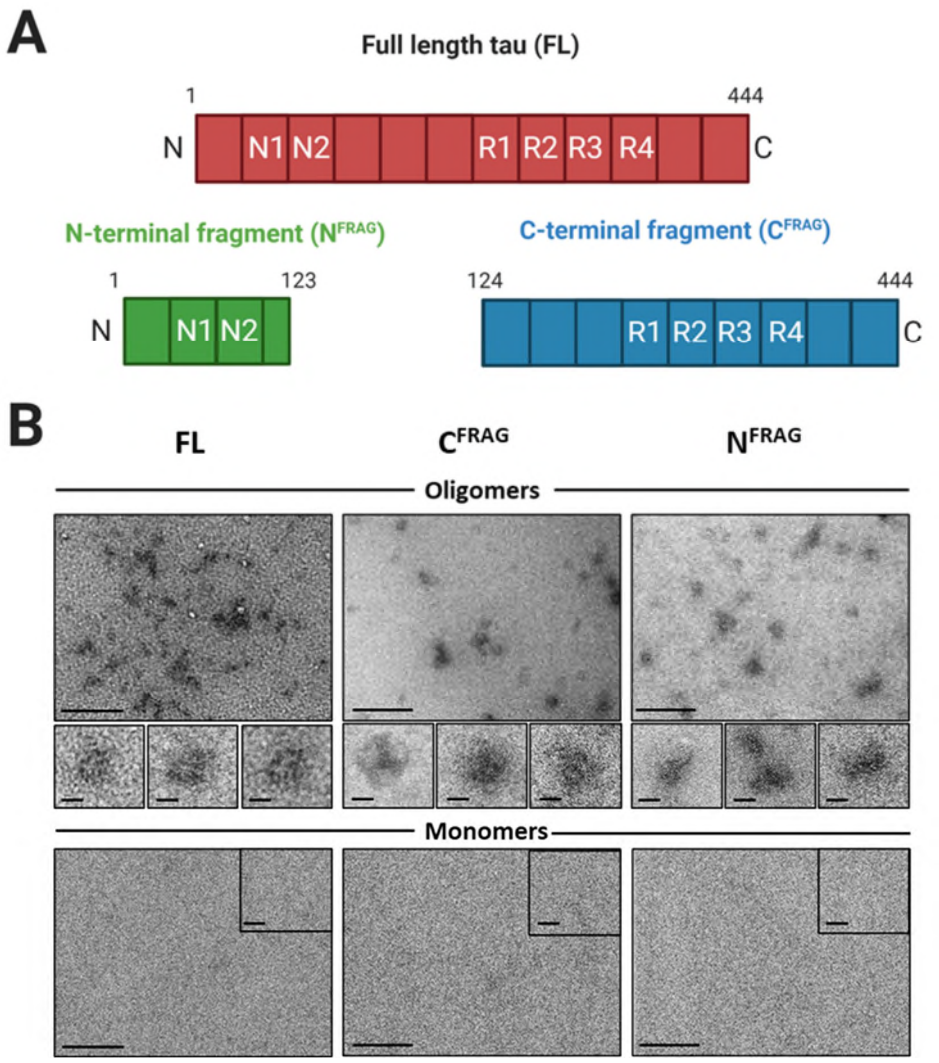

Figure 4.2: Structure and characterisation of the tau truncations

A) Schematic to illustrate the tau constructs used in this study. Full length (FL) tau has two N terminus repeats (N1, N2) and four microtubule-binding repeat domains (R1–R4). Two other truncations were tested. The first is an N-terminal truncation (termed C^{FRAG}) which consists of amino acids 124-444. The second, is the N-terminal fragment that is removed by the C^{FRAG} truncation (termed N^{FRAG}) which consists of amino acids 1-123. All three versions of tau (FL, C^{FRAG} and N^{FRAG}) were characterised as monomers and after undergoing the oligomerisation protocol. B) The structure of the aggregates formed will differ significantly due to the structure of the monomeric forms. However negative-stain transmission electron microscopy was used to confirm that the monomeric samples had no aggregation and the samples that had undergone aggregation process demonstrated small, aggregated forms (resembling oligomeric form rather than fibrils), scale bar = 200 nm, inset: higher magnification scale bar = 20 nm.

4.2.2 Using oligomeric C^{FRAG} to separate effects on whole-cell conductance, neuronal excitability and action potential waveform

I first compared the effects of oligomers made from N-terminal truncated tau (C^{FRAG}) to full length (FL) tau with vehicle (PBS) as the control. I used the same concentration (444 nM) of tau oligomers as in Hill et al., (2019) which gave reproducible results. This concentration is based on the molecular weight of the monomer, as oligomeric composition is heterogeneous. This will result in an overestimate of the actual concentration of oligomers introduced (see Hill et al 2020). Following their introduction into hippocampal pyramidal neurons, standard and dynamic IV protocols (see Methods) were used to extract electrophysiological parameters. There was no significant difference in the electrophysiological parameters at time 0 (whole-cell breakthrough) across the three conditions (Kruskal-Wallis One-Way ANOVAs resting potential $p = 0.139$, peak input resistance $p = 0.229$, firing rate $p = 0.644$, action potential amplitude $p = 0.753$ or action potential width $p = 0.910$, $n = 12$ for each condition, see Table 4.1). Therefore, the initial quality of recordings and neuronal properties were comparable across the experimental treatments.

In neurons with vehicle (control) introduced, there were no significant changes to any of the measured parameters over the 40-minute period of recording (0 vs 40 mins, peak input resistance $p = 0.146$, firing rate $p = 0.183$, action potential amplitude $p = 0.073$ or action potential width $p = 0.227$, see Table 4.1, Fig 4.3). There were also no changes to the resting membrane potential over the duration of the recordings for any of the experimental conditions (vehicle, full length tau and truncated tau, $p = 0.090$, 0.086 and 0.080 respectively, Fig 4.3A, B).

Unmodified FL oTau had comparable effects to labelled FL oTau (Hill et al., 2019): increased input resistance, increased neuronal excitability and changed the action potential waveform (reduced amplitude and increased width). This confirms that the effects of tau oligomers observed in my previous study were not altered by the cysteine mutations and label. I have previously demonstrated that the effects of FL tau were specific to oligomers and that monomeric versions had no significant effect on any of the neuronal properties

over the duration of the recordings, therefore I did not repeat this for the unmodified FL tau. I observed a significant increase in input resistance (Rin) upon introduction of FL tau (at 40 mins, the Rin was 130.0 ± 6.3 % of the resistance at time 0, whole-cell breakthrough, p = 0.001, Fig 4.3C). In contrast C^{FRAG} introduction did not significantly alter Rin (at 40 mins, the Rin was 100.0 ± 2.1 % of the input resistance at time 0, p = 0.926, Fig 4.3C). There was a significant increase in neuronal excitability mediated by FL Tau (at 40 mins, the firing rate, measured from the voltage response to naturalistic current injection, was 171.0 ± 19.3 % of that at time 0, p = 0.020, Fig 4.3 E, F). I had originally assumed that the FL oTau-mediated increase in neuronal excitability resulted from the increase in input resistance. Therefore, as C^{FRAG} had no effect on input resistance, I predicted that it would not affect neuronal excitability. However, surprisingly C^{FRAG} significantly increased excitability (at 40 mins, the firing rate was 164.0 ± 22.5 % of that at time 0, p = 0.013, Fig 4.3E, F). This suggests that the effects on neuronal excitability can occur independently of changes in input resistance.

As I previously reported for modified FL tau (Hill et al., 2019) native FL tau significantly changed the action potential (AP) waveform, with action potential amplitude at 40 minutes significantly (p = 0.001) reduced to 70.0 ± 7.4 % of that at time 0 minutes (Fig 4.3D, G) and action potential width at 40 minutes significantly (p = 0.035) increased to 134.0 ± 17.2 % of that at time 0 minutes (Fig 4.3D, H). Introduction of C^{FRAG} tau did not replicate the changes to action potential waveform observed with FL tau. Neither the action potential amplitude (at 40 minutes 91.0 ± 1.6 % of that at time 0 minutes, p = 0.079, Fig 51F) or action potential width (at 40 minutes 102.0 ± 3.0 % of that at time 0 minutes p = 0.475, Fig 4.3D, G, H) were significantly changed. This suggests that the effects of oligomeric tau on the action potential waveform could either be a direct result of the N-terminal sequence or could result from a specific structure of the oligomers, which will probably differ following truncation. Thus, removing amino acids 1-122 from full length tau resulted in the loss of effects on the action potential waveform and on the input resistance, although the increase in excitability remained.

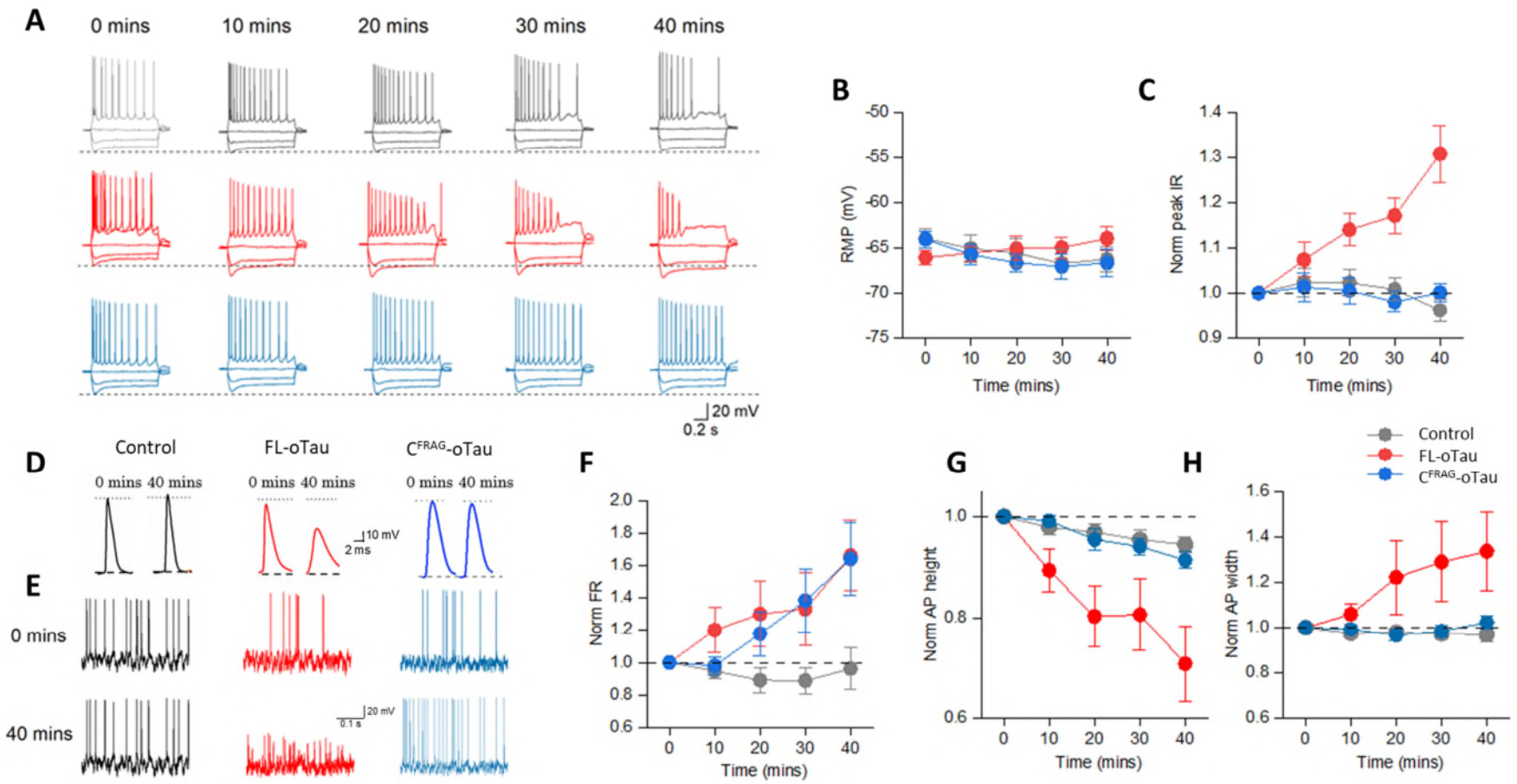
A
0 mins
10 mins
20 mins
30 mins
40 mins
20 mV
0.2 s
B
RMP (mV)
Time (mins)
C
Norm peak IR
Time (mins)
D
Control
FL-oTau
CFRAG-oTau
0 mins 40 mins
10 mV
2 ms
E
0 mins
40 mins
20 mV
0.1 s
F
Norm FR
Time (mins)
G
Norm AP height
Time (mins)
H
Norm AP width
Time (mins)
Control
FL-oTau
CFRAG-oTau

Figure 4.3: Tau effects on neuronal excitability, input resistance, and action potential waveform

A) Standard current−voltage response in control (vehicle) neurons (grey), FL tau (red) and C^{FRAG} tau (blue) over the 40-minute period of recording. B) Graph showing that there is no change to the resting membrane potential over the period of recording for any of the conditions. C) Graph plotting input resistance against time. FL tau significantly increased input resistance whereas control neurons and neurons with C^{FRAG} tau showed no significant changes. D) Representative examples of action potential waveforms for an individual neuron with one of the three conditions introduced (control, 444 nM FL-oTau, 444 nM C^{FRAG} oTau). There is no effect on AP waveform in the control or C^{FRAG} oTau cells, but a comparable effect on action potential height and width to Chapter 3 with FL-oTau is observed. E) Example membrane-potential responses to naturalistic current injection at time 0 (after whole-cell breakthrough, top) and after 40 min of recording for each of the three conditions (vehicle, FL tau and C^{FRAG} tau). There is a reduction in action potential amplitude with FL tau coupled with an increase in excitability. C^{FRAG} tau has no effect on action potential amplitude but increases excitability whereas vehicle has no effect. F) Graph plotting normalised firing rate (normalised to time 0) against time. Both FL and C^{FRAG} tau oligomers produce a significant increase in neuronal excitability that is not seen in vehicle cells. (G) Graph plotting action potential amplitude against time and (H) action potential width against time. A reduction in action potential amplitude (G) and increase in width (H) are only produced by FL tau and not by C^{FRAG} tau or vehicle.

	Vehicle/ control (n=12)				Full length tau (n=12)				C^{FRAG} (truncated tau) (n=12)			
	0 mins		40 mins		0 mins		40 mins		0 mins		40 mins	
Parameter	**Mean**	**SEM**	**Mean**	**SEM**	**Mean**	**SEM**	**Mean**	**SEM**	**Mean**	**SEM**	**Mean**	**SEM**
RMP (mV)	-64	± 1.07	-66	± 1.36	-66	± 0.75	-64	± 1.30	-64	± 0.92	-67	± 1.52
Peak Rin (MΩ)	204	± 18.6	197	± 20.1	165	± 6.29	218	± 16.1	178	± 13.4	177	± 11.7
Firing Rate (Hz)	1.73	± 0.4	1.63	± 0.45	1.25	± 0.3	1.73	± 0.3	1.1	± 0.19	1.5	± 0.21
AP Height (mV)	85	± 2.52	83	± 2.86	87	± 3.42	63	± 7.48	89	± 2.19	86	± 2.45
AP width (ms)	1.8	± 0.09	1.7	± 0.08	1.8	± 0.05	2.4	± 0.34	1.8	± 0.06	1.9	± 0.06
Rheobase (pA)	61	± 3.47	60	± 4.51	68	± 5.39	47	± 7.42	79	± 7.74	56	± 8.18

Table 4.1: Electrophysiological parameters measured for CA1 neurons with either vehicle, C^{FRAG} or N^{FRAG} introduced.

Recordings were made from hippocampal CA1 neurons. There was no significant difference between any of the measured parameters at 0 minutes (whole-cell breakthrough), using Kruskal Wallis ANOVAs (see text for p values). Comparisons were then made between 0 and 40 minutes for each of the conditions using non-parametric Wilcoxon-signed rank tests (see text for p values). Data shown as mean and SEM.

4.2.3 The increase in neuronal excitability by C^{FRAG} is confirmed by a reduction in the rheobase current.

To evaluate the effects on neuronal excitability in more detail I examined the rheobase, the minimum current required to elicit an action potential. I used a protocol (see Methods) where a current ramp (from – 50 pA to 100 pA over 1 s; Fig 4.4A) was injected every 10 minutes throughout the recording. There was no significant difference in the minimum current (rheobase) to evoke an action potential in control vs FL or C^{FRAG} neurons at time 0 (whole-cell breakthrough) using a Kruskal-Wallis One-Way ANOVA (at 0 mins, the mean rheobase in control was 61.0 ± 3.5 pA, with FL the mean rheobase was 68.0 ± 5.4 pA and with C^{FRAG} the mean rheobase was 79.0 ± 7.7 pA, $p = 0.129$, Table 4.1, Fig 4.4), thus the recordings are comparable. In control neurons, there was no significant difference in the rheobase current over the duration of the recording (at 40 minutes, the rheobase was 105.0 ± 3.0 % of the value at time 0 mins, $p = 0.083$, Table 4.1, Fig 4.4).

However, when full length and C^{FRAG} aggregated forms of tau were introduced, the rheobase was significantly reduced (reflecting an increase in excitability, Table 4.1, Fig 4.4). For FL tau, at 40 minutes the rheobase was 66.0 ± 7.0 % of the value at time 0 mins ($p = 0.002$). When C^{FRAG} tau was introduced, at 40 minutes the rheobase was 70.0 ± 5.0 % of the value at time 0 mins ($p = 0.001$, Table 4.1, Fig 4.4). A non-parametric two-way ANOVA was then used to evaluate whether the shift in rheobase was dependent solely on the treatment condition, on the timescale of recording, or a combination of both. A significant effect of time ($p < 0.0001$) and condition (vehicle or truncated tau; $p < 0.0001$) were observed to contribute to the alteration of rheobase, with significance observed from the 20-minute time-point onwards (as determined by Dunn's post-hoc analysis; 20 mins $p = 0.006$, 30 mins $p < 0.0001$, 40 mins $p < 0.0001$). This data is also consistent with the effect on the frequency of action potentials in response to fluctuating noisy current traces, where the action potential waveform is altered in the cells that had FL introduced, but not C^{FRAG} introduced (Fig 4.3F, G).

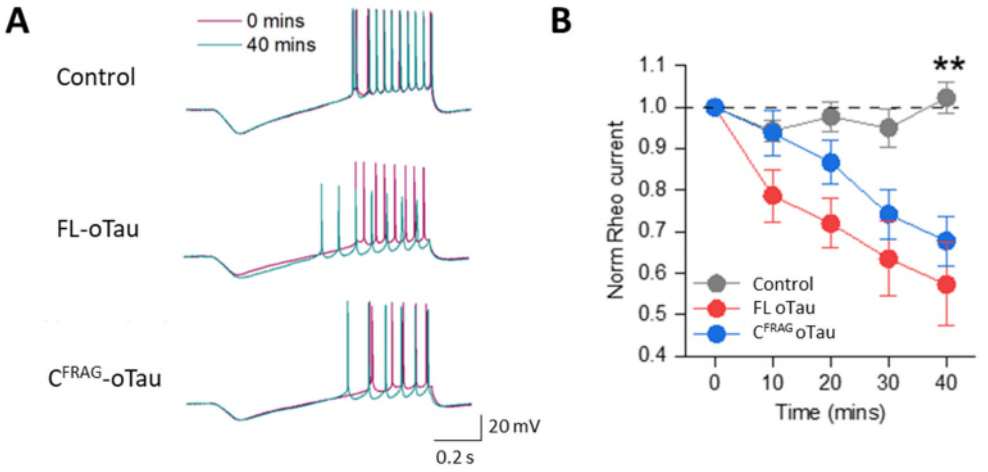

Figure 4.4: oTau alters the rheobase current.

A) Examples from representative cells (control, full length, and N-terminally truncated tau oligomers) demonstrating the effects on rheobase over time. B) Graph plotting mean and SEM for control (vehicle), full length and C^{FRAG} tau oligomers on rheobase over time. Both full length and C^{FRAG} tau oligomers significantly reduced the current needed to elicit an action potential, reflecting an increase in neuronal excitability.

4.2.4 C^{FRAG} truncated tau alters excitability by moving the spike initiation threshold

I then examined how oligomeric tau might be decreasing the rheobase current (increasing excitability) and hypothesized it might be because the difference between the resting membrane potential and spike initiation threshold is reduced. Since there is no change in resting membrane potential caused by oTau, this could only occur if there was a hyperpolarising shift in spike initiation threshold. The dynamic IV method (Badel et al., 2008b, 2008a) provides a method to accurately parameterise neurons (see Methods for more details). One of the parameters that it can extract is the spike initiation threshold. In my original study (Hill et al., 2019), I was unable to use this technique to map changes in neuronal parameters over time as the method is not very effective if there are significant changes in the action potential waveform. However, as the truncated form of tau has no effect on the action potential waveform (Figure 4.3), I was able to use the dynamic IV protocol to examine changes to the spike initiation threshold.

There was no significant difference between the spike initiation threshold in control vs C^{FRAG} neurons at time 0 (whole-cell breakthrough), thus the recordings were comparable (mean threshold in control neurons was -53.8 ± 1.5 mV, n=12, compared to the mean threshold in C^{FRAG} neurons which was – 51.0 ± 1.3 mV, n=12, p = 0.519). In control neurons, there was no significant difference in spike threshold over the duration of the recording (at 40 minutes, the spike threshold was -52.5 ± 1.6 mV, p = 0.477). Whereas for neurons where 444 nM C^{FRAG} oTau was introduced, the spike initiation threshold was significantly reduced (more negative) at 40 minutes as compared to 0 minutes (at 40 minutes, the spike threshold was -54.0 ± 1.3 mV, p = 0.001, Fig 4.5 A, B). A non-parametric two-way ANOVA was then used to evaluate whether the shift in threshold was dependent solely on the treatment condition, on the timescale of recording, or a combination of both. A significant effect of time (p = 0.013) and condition (vehicle or truncated tau; p = 0.0001) were observed to contribute to the alteration of spike initiation threshold, with significance observed from the 20-minute timepoint onwards (as determined by post-hoc analysis; 20 mins p = 0.008, 30 mins p = 0.047, 40 mins p = 0.020). Although a change in threshold of 4 mV might seem small, across a network this could cause a significant shift in network excitability.

I also noted an increase in spike-onset sharpness which is a measure of the time from a cell reaching the spike initiation threshold and the subsequent onset of the action potential (spike). This increase in spike-onset sharpness (sharper DIV curve, decrease in time) fits with the increase in neuronal excitability. There was no significant difference between the onset in control vs C^{FRAG} neurons at time 0 (whole-cell breakthrough), thus the recordings were comparable in quality and stability (mean spike-onset sharpness in control neurons was 0.74 ± 0.04 mV, n=12, compared to the mean threshold in C^{FRAG} neurons which was 0.9 ± 0.1 mV, n=12, p = 0.129, Fig 4.5C). In control neurons, there was no significant difference in spike-onset sharpness over the duration of the recording (at 40 minutes, the spike-onset sharpness was 0.81 ± 0.04 mV, p = 0.910). In contrast, for neurons where 444 nM aggregated C^{FRAG} tau was introduced, the onset was increased (steeper, reflecting increased excitability) at 40 minutes compared to 0 minutes (at 40 minutes,

the spike-onset sharpness was 1.18 ± 0.07 mV, p = 0.001). A non-parametric two-way ANOVA was then used to evaluate whether the shift in spike-onset sharpness was dependent solely on the treatment condition, on the timescale of recording, or an interaction between both. A significant effect of time (p = 0.005) and condition (vehicle or truncated tau; p = 0.0001) were observed to contribute to the alteration of spike-onset sharpness, with significance observed from the 30-minute timepoint onwards (as determined by post-hoc analysis; 30 mins p = 0.002, 40 mins p = 0.0001).

I then implemented a complimentary modelling approach to evaluate whether either of these effects, either on spike initiation threshold or on spike onset sharpness, could account solely for the increase in excitability observed. To do this I used the refractory integrate and fire (rEIF) model (see Methods for more details) to simulate a voltage response given the parameters extracted from the DIV curves at 0 mins (Fig 4.5E); the firing rate matched the experimental trace (Fig 4.5D). I manually shifted only the spike threshold by -4 mV (in line with the change in the experimental traces) and re-ran the simulation. Comparing this to the experimental trace at 40 minutes, it is clear the change in spike threshold alone is sufficient to mediate the increase in neuronal excitability (Fig 4.5E). I then repeated the same procedure but instead shifted the spike-onset sharpness, the simulation predicted little effect on neuronal excitability (Fig 4.5E), suggesting that the change is predominantly mediated by the change in spike threshold.

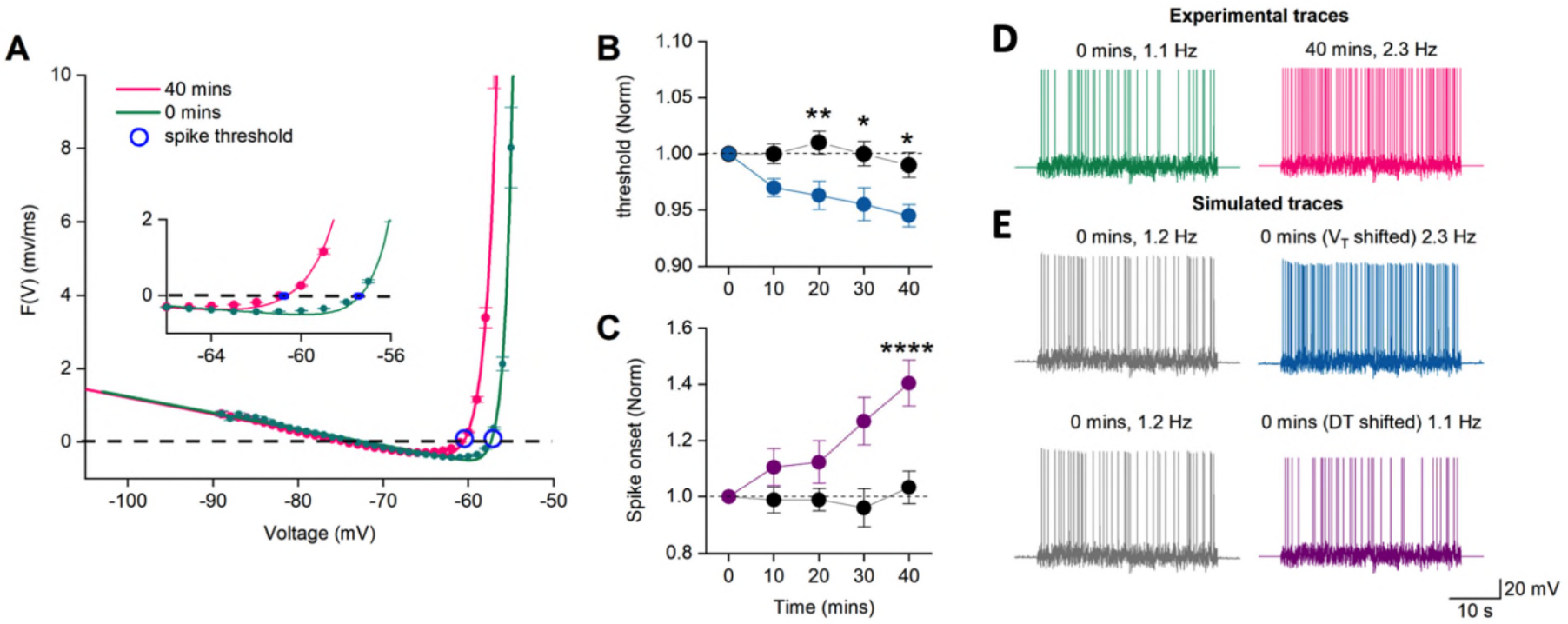
A
40 mins
0 mins
spike threshold
F(V) (mv/ms)
Voltage (mV)
B
threshold (Norm)
**
*
*
C
Spike onset (Norm)
****
Time (mins)
D
Experimental traces
0 mins, 1.1 Hz
40 mins, 2.3 Hz
E
Simulated traces
0 mins, 1.2 Hz
0 mins (V$_T$ shifted) 2.3 Hz
0 mins, 1.2 Hz
0 mins (DT shifted) 1.1 Hz
20 mV
10 s

Figure 4.5: oTau- mediates a shift in spike initiation threshold.

For the dynamic I-V protocol, a naturalistic current is injected into the cell and the voltage recorded is then used to extract a set of parameters (resting potential E, time constant τ, and spike-threshold voltage VT; see methods for more details). The second point where the DIV curve crosses 0 (mV/ms) represents the spike initiation threshold. A) Representative example of the dynamic IV curve for a neuron with the N-terminal truncation of tau introduced at 0 mins (green) and 40 mins (pink). A shift in spike initiation threshold (circled) of 4 mV (more negative) can be observed, thus the neurons are more excitable. B) The mean normalised spike threshold data is plotted against time (with SEM) to show the reduction in spike threshold in C^{FRAG} cells compared with cells where vehicle was introduced. Data is normalised to the spike initiation threshold at time 0 mins. C) Graph plotting spike-onset sharpness against time. There is an increase in spike-onset sharpness observed in neurons where C^{FRAG} was introduced, reflecting faster spike generation after reaching threshold, again fitting with the increase in excitability. (D) Membrane-potential responses to naturalistic current injection for the neuron modelled in (A) demonstrates the increase in neuronal excitability mediated by the introduction of C^{FRAG} tau oligomers. (E) Simulated membrane- potential response based on the extracted neuronal parameters at time 0 mins (left), using the refractory integrate and fire model. The neuronal firing rate matches the experimental trace well. The spike threshold was then manually shifted by -4 mV and the simulation re-run (right, blue), resulting in an increase in excitability, comparable with the experimental trace at 40 mins (D). The same procedure was performed, but only shifting spike-onset sharpness and re-simulating with little effect on excitability or firing rate (right, purple), thus confirming that the increase in excitability is predominantly mediated by a shift in spike threshold.

4.2.5 N^{FRAG} aggregate introduction generates a rapid onset increase in input resistance and decrease in action potential amplitude

As C^{FRAG} oligomers did not replicate the changes to input resistance and action potential waveform observed with FL tau oligomers, I next introduced N^{FRAG} tau (at 444 nM) into neurons and measured changes to neuronal parameters to investigate if this fragment of tau was responsible. Unexpectedly, in preliminary experiments, I observed a large increase in input resistance within

the first 5 minutes of recording. At 5 minutes the input resistance was 169.0 ± 24.2 % of that at 0 minutes (whole-cell breakthrough, *n* = 4, Fig 4.6A). I have previously shown through re-patching experiments that tau oligomers do not aggregate in the end of the pipette tip and impede voltage measurements (Hill et al., 2019 and Chapter 3). However, this rapid change could be due to the tau oligomers aggregating close to the introduction site in the soma and making the electrotonic size of the soma appear reduced (this would result in a smaller capacitance measurement at 5 minutes). To test this I extracted the time constant by fitting the voltage step (exponential) and used this to calculate cellular capacitance using the following equation:

$$Time\ constant\ (T) = Input\ resistance\ (R_{in})\ x\ Capacitance\ (C)$$

As well as the rapid increase in input resistance, by 5 minutes the time constant was reduced to 77.0 ± 3.2 % of that at 0 minutes (*n* = 4, Fig 4.6A). This change in time constant reflected a change in whole-cell capacitance (by 5 minutes the capacitance was reduced to 53.0 ± 5.4 % of that at 0 minutes (*n* = 4, Fig 4.6A). I considered whether this rapid change to whole-cell resistance and capacitance could be due to aggregation of the N^{FRAG} tau in the soma impeding current flow.

To test this possibility further, I performed a subset of experiments where two simultaneous whole-cell patch clamp recordings were made to the same CA1 pyramidal neuron (Fig 4.6B). In turn I injected a 200 pA hyperpolarising (1s) step via one of the pipettes and recorded the voltage response in both of the pipettes. (Fig 4.6C). As the current needs to flow to the 'recording only' pipette, the voltage response was always slightly smaller than the response at the 'inject and record' pipette as some of the current is lost. In cells where both pipettes were filled with vehicle, there was no change to the relative size of responses ($V_{rec}/V_{rec+inject}$) between 0 mins (whole-cell breakthrough) and 5 mins (the relative response was 97.0 ± 1.7 % of the response at 0 minutes, p = 0.148, n = 8, Fig 4.6D). However, when 444 nM of N^{FRAG} tau was introduced in the 'inject and record pipette', the same large rapid increase in input resistance (as in Fig 4.6A) was observed. This was not reflected in an increase in the voltage step as measured by the second 'recording only' pipette with, in fact, the response becoming considerably smaller (Fig 4.6 E, F). Thus, the ratio

of the responses would be expected to change. At 5 minutes the relative response was 58.4 ± 7.0 % of the response at 0 minutes, p = 0.008, n = 8, Fig 4.6 E, F).

A non-parametric two-way ANOVA was also used to evaluate whether the resistance change was dependent solely on the treatment condition, on the timescale of recording, or a combination of both. A significant effect of time (p = 0.049) and condition (vehicle or N^{FRAG}, p < 0.0001) were observed to contribute to the change in resistance. Thus, confirming that for this concentration of introduced N^{FRAG} aggregates, they must be accumulating around the introduction site, impeding the flow of current between the two pipettes, resulting in an 'artificial' increase in input resistance and decrease in the observed capacitance due to the cell appearing electrotonically smaller.

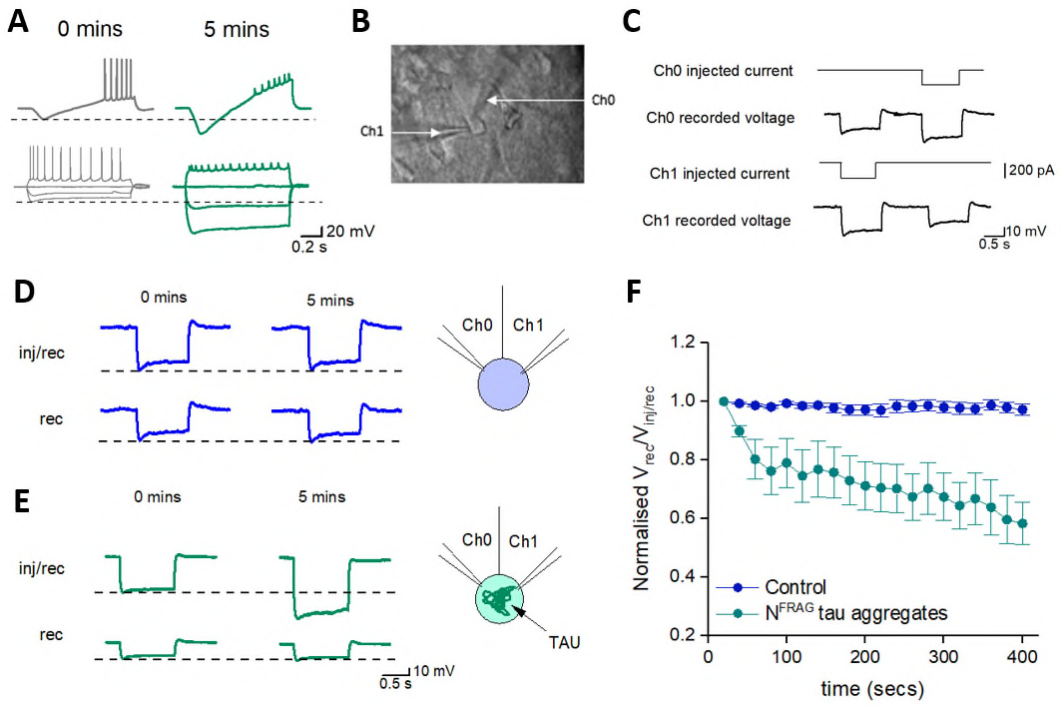

Figure 4.6: Rapid increase in input resistance mediated by 444 nM NFRAG aggregates is due to aggregation around the site of introduction impeding current flow.

A) Representative examples of rheobase and SIV protocols at 0 mins (whole-cell breakthrough) and after 5 mins, demonstrating a rapid, large increase in input resistance and reduction in spike amplitude. B) Bright-field image of a CA1 neuron in the hippocampus with two patch pipettes recording simultaneously at the soma. C) Schematic of the stimulation protocol used. A 200 pA hyperpolarising current step

was given to Ch0 or Ch1 in turn and the voltage response was recorded in both channels (Ch0 or Ch1). D) Representative example where both pipettes were filled with vehicle, and where there was no change to the relative size of responses between 0 mins (whole-cell breakthrough) and 5 mins. E) Representative example when 444 nM N^{FRAG} was introduced via the 'inject and record pipette'; the same rapid increase in input resistance (as in A) was observed. This is not reflected in an increase in the voltage step as measured by the second 'recording only' pipette, thus suggesting that the aggregates are impeding current flow between the pipettes. F) Mean and SEM data for control (n = 8) and 444 nM N^{FRAG} recordings (n=8). A clear reduction in the ratio of voltage of the 'record' pipette compared to the 'inject and record' pipette (where tau was introduced) can be observed.

4.2.6 At lower concentrations N^{FRAG} selectively changes the action potential waveform, an effect independent of the structural form

In my original study with full length tau (Hill et al., 2019; Chapter 3), the increase in input resistance and changes to action potential waveform occurred at much later time points than the 5 minutes into the recording I observed with N^{FRAG}. Thus, to examine the effects of N^{FRAG} in more detail I used a lower concentration of N^{FRAG} tau (133 nM). There was no N^{FRAG} tau-mediated change in RMP (at 40 mins, the RMP was 99.0 ± 1.0 % of that at time 0, p = 0.961, *n* = 12, Fig 4.7A) or input resistance (at 40 mins, the peak input resistance, measured from the voltage response to step current injection, was 102.0 ± 7.7 % of that at time 0, p = 0.953, Fig 4.7B). There was also no significant change in firing rate (at 40 mins, the firing rate, measured from the voltage response to naturalistic current injection, was 107.0 ± 13.6 % of that at time 0, p = 0.747, Figure 4.7C) or rheobase current (at 40 mins, the rheobase was 127.0 ± 11.9 % of that at time 0, p = 0.129, Fig 4.7D). However, the changes to action potential waveform (increased width and decreased amplitude) that were observed both in my original study (Hill et al, 2019; Chapter 3) and with the full-length tau in this Chapter were also observed with 133 nM N^{FRAG}. Action potential amplitude at 40 minutes was significantly reduced to 76.0 ± 2.9 % of that at time 0 minutes (p = 0.001, Fig 4.7 E, F) and action potential width at 40 minutes was significantly increased to 118.0 ± 7.4 % of that at time 0 minutes (p = 0.019, Fig 4.7 E, G). This was unexpected as

the N-terminal fragment will form structurally different aggregates to FL tau. I therefore wondered whether the effects on action potential waveform were independent of structure and related directly to the N-terminal sequence (amino acids 1-123).

As an initial test I repeated the same experiments with the monomeric version of the N^{FRAG}. There was no N^{FRAG} monomeric tau-mediated change in RMP (at 40 mins, the RMP was 104.0 ± 2.4 % of that at time 0, p = 0.094, *n* = 12, Fig 4.7A) or input resistance (at 40 mins, the peak input resistance, measured from the voltage response to step current injection, was 102.0 ± 4.1 % of that at time 0, p = 0.940, Fig 4.7B). There was also no significant change in firing rate (at 40 mins, the firing rate, measured from the voltage response to naturalistic current injection, was 106.0 ± 10.5 % of that at time 0, p = 0.507, Fig 4.7C) or rheobase current (at 40 mins, the rheobase was 116.0 ± 10.1 % of that at time 0, p = 0.240, Fig 4.7D). However, a comparable change to action potential waveform was observed with monomeric forms of N^{FRAG}. Action potential amplitude at 40 minutes was significantly reduced to 82.0 ± 2.6 % of that at time 0 minutes (p = 0.001, Fig 4.7E, F) and action potential width at 40 minutes was significantly increased to 123.0 ± 2.0 % of that at time 0 minutes (p = 0.030, Fig 4.7E, G).

Given that the oTau-induced changes to action potential waveform (reduced amplitude, increased width and increased rate or rise and decay) that occur with full length tau (Hill et al., 2019) also occurred with the N-terminal fragment (N^{FRAG}), both as a monomer and an oligomer, it is likely that there is a region in that 1-123 amino acid region that is directly interacting with an intracellular component or process, rather than being an effect due to the structure. Given that for N^{FRAG} both the rise and decay of action potentials are slower and for C^{FRAG} that the spike initiation threshold is also shifted, making the cells more excitable, I next decided to use FL oTau look at whether either of these changes were mediated by interactions with voltage-gated sodium channels.

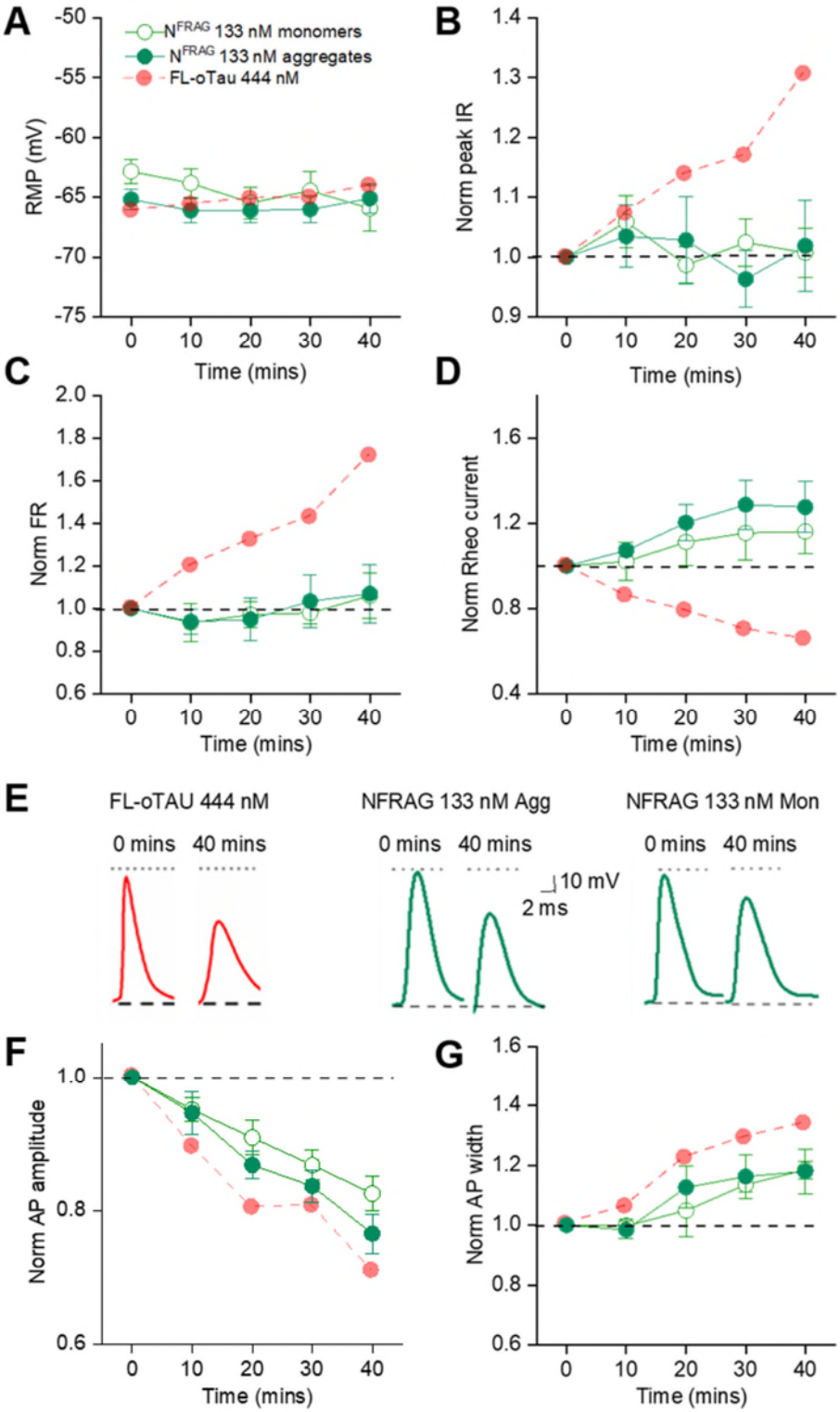
A
B
C
D
E
F
G
N^FRAG 133 nM monomers
N^FRAG 133 nM aggregates
FL-oTau 444 nM
RMP (mV)
Norm peak IR
Norm FR
Norm Rheo current
Norm AP amplitude
Norm AP width
Time (mins)
FL-oTAU 444 nM
NFRAG 133 nM Agg
NFRAG 133 nM Mon
0 mins
40 mins
10 mV
2 ms

Figure 4.7: The effects of FL-oTau on action potential waveform are maintained by N^{FRAG} aggregates and monomers.

(A) Graph showing that there is no change to the resting membrane potential over the period of recording for any of the conditions. (B) Graph showing that there is no change to the input resistance over the period of recording for 133 nM N^{FRAG} aggregates or monomers, whereas FL oTau increased input resistance (C) Graph showing that there is no change to firing rate over the period of recording for 133 nM N^{FRAG} aggregates or monomers, whereas FL oTau increased excitability (D) Graph showing that there is no change to the rheobase current over the period of recording for 133 nM N^{FRAG} aggregates or monomers, whereas FL-oTau reduced it (E) Representative examples of action potential waveforms for an individual neuron with one of the three conditions introduced (444 nM FL-oTau, 133 nM N^{FRAG} aggregates or monomers). A comparable effect on action potential height and width is observed. (F) Graph showing that there is a comparable change to action potential amplitude over the period of recording for 133 nM N^{FRAG} aggregates or monomers and FL-oTau. (G) Graph showing that there is a comparable change to action potential width over the period of recording for 133 nM N^{FRAG} aggregates or monomers and FL-oTau. *Pale dashed red lines demonstrate the effects of FL-oTau for comparison (from data presented in Figure 4.3) Action potential (AP), Firing rate (FR), Input resistance (IR), Resting membrane potential (RMP)*

4.2.7 Oligomeric tau alters reduces Na^+ channel half activation voltage and slows the rate of activation

Recording sodium channel currents in hippocampal neurons in acute brain slices is difficult as there are considerable problems with space clamp due to their size and the large amplitude and speed of the currents. One way to effectively clamp the currents is to electrotonically isolate the soma. To do this I followed the protocol outlined in Milescu et al., (2010), using a short depolarising pre-pulse to inactivate the axonal sodium channels, leaving only the somatic channels able to be activated. Sodium channel current amplitude was also reduced (by increasing intracellular Na^+ concentration) and recordings were carried out at room temperature to slow the currents (see Methods for details). It was then possible to achieve reasonable voltage clamp

(Fig 4.8A). Steps from -60 mV by 5 mV to 60 mV were used to evoke sodium channel currents.

Conductance was calculated using the following equation:

$$conductance\ (g) = current\ (I)/(V_{Step} - V_{reversal})$$

Conductance was plotted against voltage and a Boltzmann fit was applied. The fit (Fig 4.8B, C) can be used to extract the half activation and the rate of activation constant. The half activation was stable in control recordings. At 20 mins, the half activation was 98.0 ± 1.0 % of that at time 0, p = 0.203, Fig 4.8B, D). In contrast, in cells that had 444 nM FL tau oligomers introduced, by 20 minutes the half activation had shifted significantly to be more negative (activate earlier, reflective of an increase in excitability). At 20 minutes, the half activation was 150.0 ± 11.7 % of that at time 0, activating at ~4 mV earlier (p = 0.008, Fig 4.8C, D). This could explain the change in spike threshold that I observed. I also extracted the rate constant of activation (indicative of the rate of rise in conductance relative to change in voltage). The time constant was stable in control recordings: at 20 mins, it was 101.0 ± 3.6 % of that at time 0 (p = 0.938, Fig 4.8B, E), whereas in tau cells, by 20 minutes the time constant had increased significantly (flatter slope, reflective of slower channel activation). At 20 minutes, the rate of activation constant was 171.0 ± 15.4 % of that at time 0 (p = 0.008, Fig 4.8C, E). This could explain the slowing of the action potential rise observed in (Hill et al., 2019) and in this study.

I then implemented a simplified model of the neuronal action potential (AP) with general applicability (Hodgkin and Huxley, 1952) to evaluate whether the conductance changes mediated by FL-oTau could feasibly underlie the changes that I observed in AP waveform. My experimental voltage gated sodium current recordings showed that FL-oTau mediates a reduction of $\bar{g}_{Na}$ to by two thirds of the value at 0 minutes after 20 minutes (Fig. 4.8F-I). Therefore, I first simulated an AP with $\bar{g}_{Na} = 120\ mS/cm^2$ (Hodgkin and Huxley, 1952, Figure 4.8J, red) and then again with $\bar{g}_{Na} = 40\ mS/cm^2$ (Figure 56J, red trace). I found that this reduction in $\bar{g}_{Na}$ matches the experimental phenotype well (the changes in AP amplitude and speed of rise to threshold; Figure 4.8K).

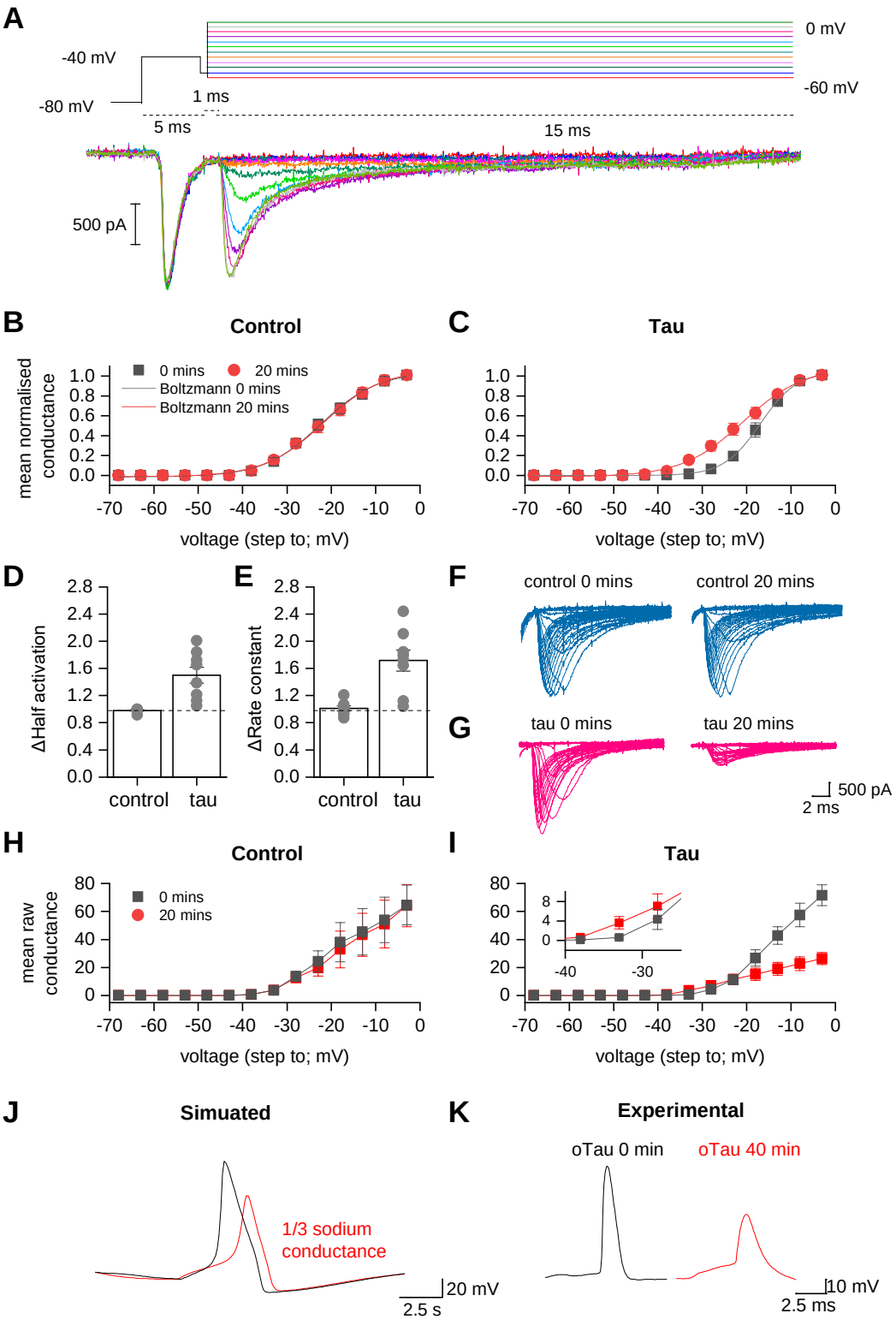
A
0 mV
-40 mV
-60 mV
-80 mV
1 ms
5 ms
15 ms
500 pA
B
Control
mean normalised conductance
0 mins
20 mins
Boltzmann 0 mins
Boltzmann 20 mins
voltage (step to; mV)
C
Tau
voltage (step to; mV)
D
ΔHalf activation
control
tau
E
ΔRate constant
control
tau
F
control 0 mins
control 20 mins
G
tau 0 mins
tau 20 mins
500 pA
2 ms
H
Control
mean raw conductance
0 mins
20 mins
voltage (step to; mV)
I
Tau
voltage (step to; mV)
J
Simuated
1/3 sodium conductance
20 mV
2.5 s
K
Experimental
oTau 0 min
oTau 40 min
10 mV
2.5 ms

Figure 4.8: Tau directly modifies somatic sodium currents in CA1 neurons, recorded using whole-cell voltage clamp in acute slices.

A) Example of the recording protocol (adapted from Milescu et al, 2010). A pre-pulse step of 5 ms from the holding value of -80 mV to -40 mV elicits a current response from axonal (but not somatic) Na^+ channels. A brief step to -55 mV (1 ms) follows before the step used to evoke the controlled sodium channel current (15 ms). The steps were given on consecutive sweeps from -60 V to + 60 mV with a 2 s gap between each sweep. Leak currents were subtracted with the P/N protocol (1/4) and the junction potential (+ 8 mV) was corrected for. B) Conductance was calculated using the following equation: conductance (g) = current (I)/ (Vstep –Vreversal). The conductance in response to steps up to 0 mV is plotted as a mean (and SEM) of all control cells (n=7). C) The conductance in response to steps up to 0 mV is plotted as a mean (and SEM) of all tau introduced cells (n=7). For B and C, the grey line is 0 mins and the red 20 mins. A Boltzmann fit allows half activation voltage and the time constant (measure of the speed of activation). D) Mean change from 0 mins to 20 mins for control and tau cells in half activation; data is given relative to the value at time 0. Mean and SEM are shown, and individual data points are overlaid on top. While control cells are stable over 20 mins, tau introduced cells see a significant decrease in half activation (activate at lower voltages; increase in excitability), but they also see a doubling of the time constant (reflecting a much slower activation – fitting with the slower rise time of action potentials observed in Chapter 3 (and Hill et al, (2019) and Chapter 3. D) Change in half activation, relative to the value at time 0. Mean and SEM are shown, and individual data points are overlaid on top. While control cells are stable over 20 mins, FL-oTau introduced cells see a significant decrease in half activation (activate at lower voltages; increase in excitability). I also see a doubling of the rate constant of activation (E). F, G) Representative example current sodium current recordings for control and FL-oTau at 0 mins and 20 mins demonstrating the reduction in peak current induced by FL oTau. H, I) Raw conductance data (averaged) for control (H) and FL-oTau (I) to highlight the reduction in maximal conductance for FL-oTau after 20 mins. Inset demonstrates the crossover at low voltages, where FL oTau at 20 mins has higher conductance, despite the maximal conductance being reduced at higher voltages. J) Implementing a simple Hodgkin Huxley model of action potential dynamics to predict the effect of reducing the maximal sodium conductance by 2/3 (as measured experimentally (I)). The simulated reduction in current amplitude and rise to threshold appears to match the experimental phenotype for FL-oTau (K).

4.3 Conclusion

I have used two fragments of tau to dissect the actions of full length (FL) tau oligomers on neuronal properties (Chapter 3; Hill et al., 2019), and have started to define the underlying mechanisms. Two different truncated forms of tau oligomers were introduced into CA1 hippocampal neurons via the patch pipette during whole cell recording. I found that both labelled (Hill et al 2019; Chapter 3) and unlabelled FL tau oligomers had very similar effects: they both increased input resistance, increased excitability, increased action potential width and reduced action potential amplitude. When the first 123 amino acids of tau were removed (124-444, termed C^{FRAG}) only the effects on excitability remained. If the first 123 amino acid fragment was introduced into neurons (1-123, N^{FRAG}), then depending on the concentration, there were changes to input resistance and action potential waveform. This work has shown that by modifying the tau molecule it is possible to dissect apart the multiple effects it has on neuronal function. Using truncations of tau as a tool to establish the pathological mechanisms of action will enhance the understanding of tau pathology and could lead to the discovery of new therapeutic targets and opportunities.

Chapter 5:

Alpha-synuclein aggregates increase the conductance of substantia nigra dopamine neurons, an effect partly reversed by the K_{ATP} channel inhibitor glibenclamide.

This chapter has been in part published previously: (Hill et al., 2021)

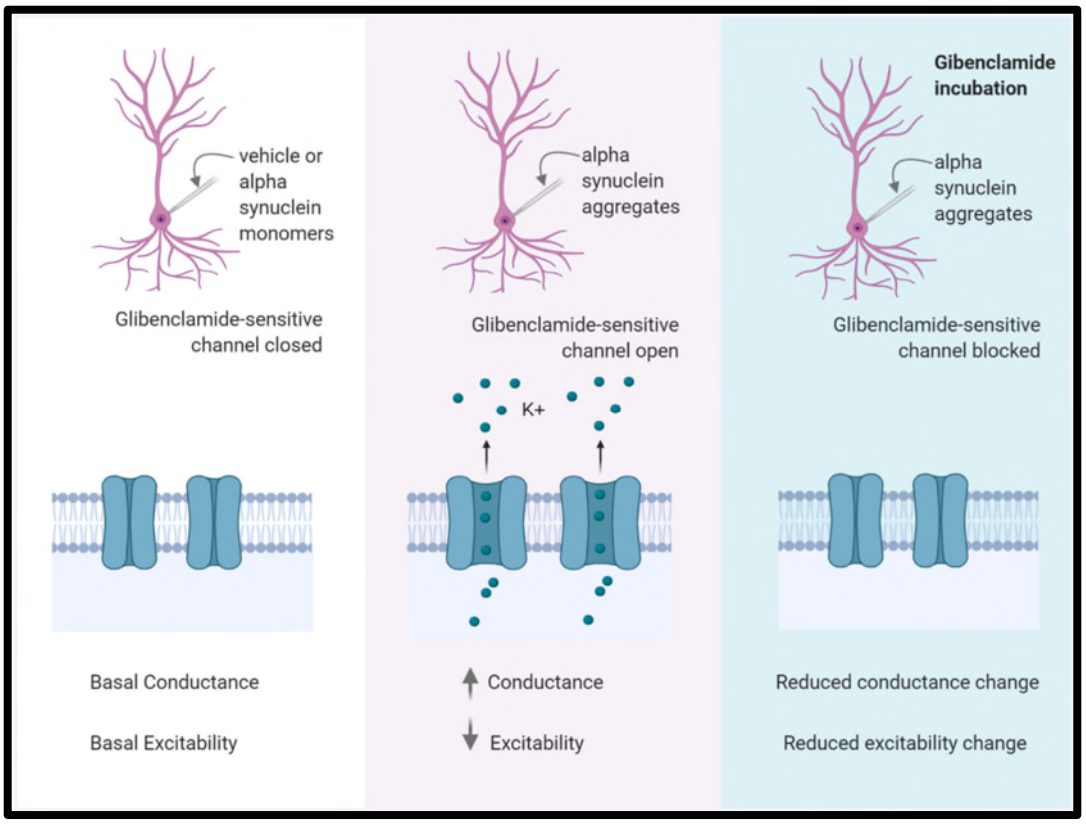

Figure 5.1 – Alpha synuclein aggregates induce a change in whole cell conductance and neuronal excitability via K_{ATP} channel activation

5.1 Introduction

Dopaminergic neurons (DNs) in the substantia nigra pars compacta (SNpc) form a key part of the basal ganglia circuitry and play important roles in modulating movement, emotion, arousal, and reward behaviour (Barter, 2015; Berker and Rutledge, 2014; Lavezzi et al., 2020; Pierce and Péron, 2020). They have large branches of projections, fire action potentials at rest (tonic pacemaker firing) and require large amounts of ATP to maintain function. This makes them particularly sensitive to damage from oxidative stress, which can lead to mitochondrial dysfunction (Muñoz et al., 2012). This vulnerability makes them amongst the most susceptible neurons to degeneration in Parkinson's disease (PD; Damier et al., 1999; Michel et al., 2014). DNs are lost over the progression of PD, primarily from the SNpc in the early stages, but later in the disease are also lost from the ventral tegmental area (VTA). When DNs degenerate in PD, it often leads to reduced control of movement (akinesia, bradykinesia) and the development of a resting tremor.

Alpha synuclein (αSyn) is a small, native intracellular protein. It is found primarily at presynaptic terminals where it contributes to neurotransmitter uptake and vesicle recycling (Figure 1.13; Iwai et al., 1995). Alpha synuclein is intrinsically disordered but becomes ordered upon aggregation (Alderson and Markley, 2013). This triggers the beginning of its pathological cascade from monomers through to Lewy bodies, of which soluble oligomers are believed to be amongst the most toxic of the intermediates (Burré et al., 2010; Jakes et al., 1994; Lashuel et al., 2013; Murphy et al., 2000). Alpha synuclein (αSyn), specifically in an oligomeric conformation, has a well-established role as a major pathological species in PD, with its deposition in Lewy bodies closely correlated with disease progression. However, there is currently very little quantitative information about the mechanisms underlying the pathological actions of αSyn on neuronal function. Understanding these early changes could provide insights into how treatments can be better targeted for PD.

In this study, I have used a combination of whole-cell patch-clamp recording and computational modelling to provide a detailed characterisation of the early

electrophysiological effects of acutely introducing oligomeric αSyn into single DNs in the SNpc. The same method of introducing the alpha synuclein oligomers as outlined in Chapters 3 and 4 was implemented (delivery through the patch pipette during whole-cell patch clamp recording). Thus, it has the same major advantages: no compensation within the circuit, removal of any slow uptake steps, control over the structure and concentration of the introduced oligomers, and each cell acts as its own internal control (at time zero after whole-cell breakthrough). By using a combination of standard and dynamic-IV protocols (Badel et al., 2008b, 2008a; Harrison et al., 2015), I have parameterised dopaminergic neurons and the effects of acute oligomeric αSyn exposure.

5.2 Results

5.2.1 Characterising dopaminergic neurons in the substantia nigra

Putative dopaminergic neurons (DNs) in the substantia nigra pars compacta (SNpc) were recorded from using whole-cell patch clamp. Neurons were identified initially by their morphology and position in the slice and were further confirmed to be dopaminergic by their characteristic electrophysiological profile including: their sensitivity to dopamine, display of pacemaker firing and a large hyperpolarising (I_H) current, as well as rebound firing in response to the injection of hyperpolarising current steps (Grace and Onn, 1989; Krashia et al., 2017; Richards et al., 1997; Fig 5.2). All recorded DNs were sensitive to dopamine (Figure 5.2A). Dopamine binds to D2 auto-receptors and prevents further release of dopamine via hyperpolarisation of the membrane potential and thus a decrease in firing rate and excitability (Mercuri et al., 1997; Silva and Bunney, 1988). This occurs via activation of a GIRK conductance (Cathala and Paupardin-Tritsch, 1999; Lacey et al., 1987). The application of 30 µM dopamine inducing a hyperpolarisation of the membrane potential by 7.4 ± 1.2 mV (n = 49; data not shown). Standard step and dynamic current injections were used to assess electrophysiological; properties of putative DNs (Figure 5.2B).

Most of the recorded DNs displayed spontaneous pacemaker firing (36 out of 49 neurons, 73 %, mean firing rate of 1.1 ± 0.1 Hz) which was abolished after

application of 30 µM dopamine, as is characteristic for DNs in the SNpc (Figure 5.2A; Grace and Onn, 1989; Lacey et al., 1989). In DNs, in response to the injection of negative current steps, a characteristic large sag can be observed (Neuhoff et al., 2002) and, following termination of the hyperpolarising step, rebound firing was observed in 33 out of 49 neurons (68 %) which are both characteristic of the presence of large I_H currents in DNs (Figure 5.2C). In response to the application of 30 µM dopamine, rebound firing was abolished and the voltage response to the injection of hyperpolarising current steps was reduced, reflecting an increase in whole-cell conductance (Figure 5.2D). Dopamine application also reduced the firing rate in response to positive current injection for both the current step (SIV) and naturalistic (DIV) protocols (firing rate reduced to 62.7 ± 0.2 % of that in control). Both the sag response and rebound firing could be abolished by applying 100 µM ZD7288, a pharmacological inhibitor of I_H in dopamine neurons (Figure 5.2E; Harris and Constanti, 1995; n=6), confirming that they were I_H-mediated. Finally, to confirm that the location of recording was being identified correctly, for a subset of neurons, immunohistochemistry was used to further confirm that the recorded neurons were dopaminergic (n = 9). Neurons were filled with AF594 (red) via the patch pipette and then immunohistochemistry was used to show co-localisation with tyrosine hydroxylase (TH; Figure 5.2F). All of the filled neurons (n=9) correctly co-localised with TH.

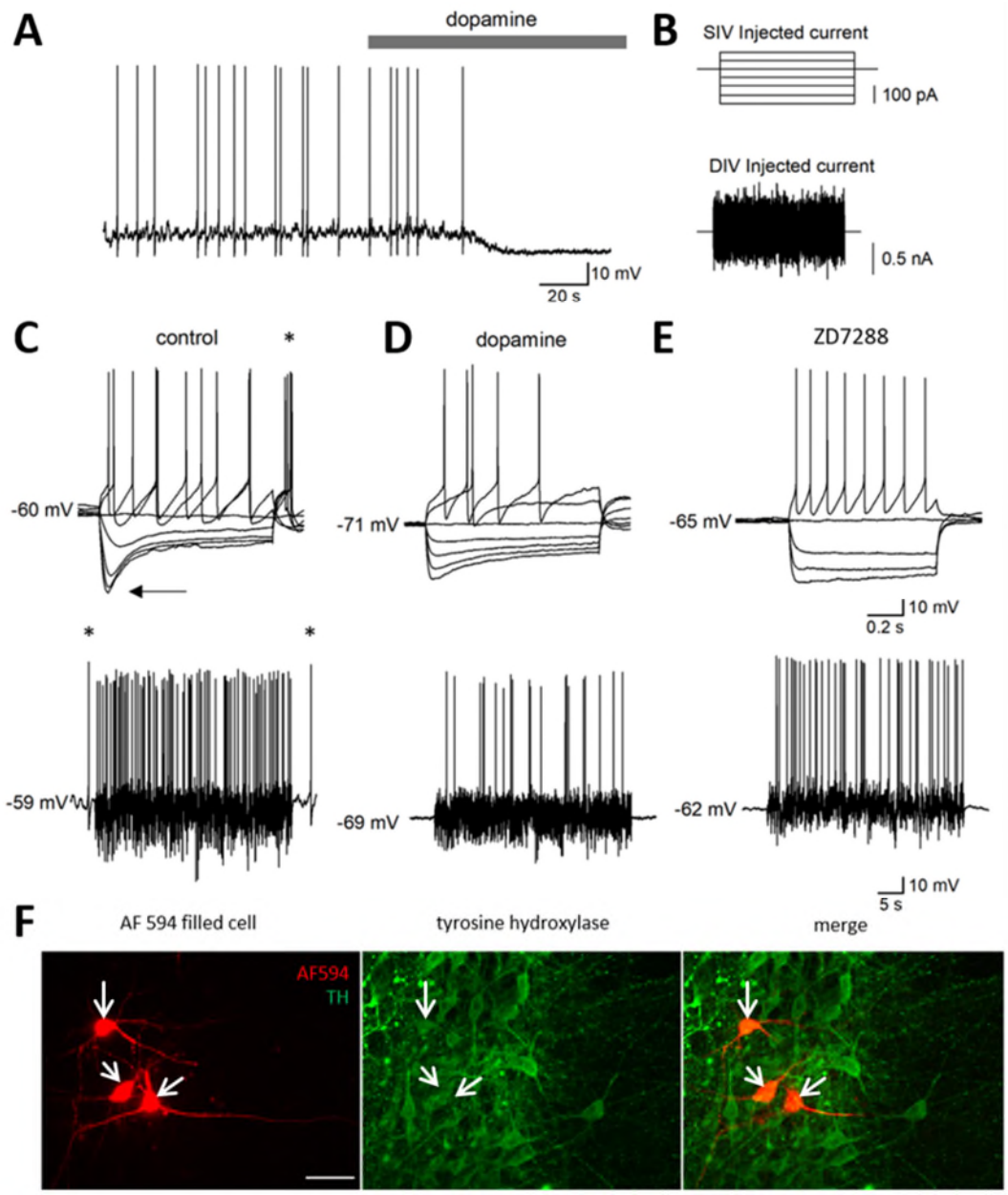

Figure 5.2: Whole-cell patch clamp of dopaminergic neurons in the SNpc, characterised by electrophysiology and immunohistochemistry.

(A) A representative membrane potential trace recorded from a putative dopaminergic neuron (DN) in the substantia nigra pars compacta (SNpc) which showed characteristic spontaneous pacemaker action potential firing. Application of dopamine hyperpolarised the neuron from -62 mV to -70 mV and also completely abolished the tonic firing. (B) The different input currents delivered to putative DNs. The standard IV (SIV) is the standard step current protocol, 3 s steps are given, starting at -200 pA and increasing by 50 pA until the neuron exhibits a regular firing pattern. The dynamic IV (DIV) protocol uses a fluctuating naturalistic noisy current trace (see Methods for more details) to elicit a more 'natural' action potential response and can be used to

give a more accurate measure of the firing rate (C) (Top) Representative membrane potential traces in response to injected current steps. The recorded neuron displays characteristic features of DNs: a large sag current in response to hyperpolarising steps (arrow) and rebound firing (*). (Bottom) The recorded membrane potential trace from the same cell in response to naturalistic current injection. The neuron can be seen to be firing at rest (*) which is also a characteristic feature. (D) (Top) Representative membrane potential traces in response to current steps following application of dopamine (30 µM). The sag current is reduced, the membrane potential hyperpolarised, the firing rate (excitability) reduced, and the rebound firing is now absent. (Bottom) Membrane potential trace from the same cell in response to the naturalistic current in dopamine (30 µM). The neuron has stopped tonic firing, fires less frequently during current application and is hyperpolarised. (E) (Top) Representative membrane potential traces in response to current steps in the presence of the I_H blocker ZD7288 (100 µM). The sag current is markedly reduced, the membrane potential is hyperpolarised, the firing rate reduced and the voltage response following the spike is altered, in line with previous studies (Harris and Constanti, 1995). (Bottom) The recorded membrane potential trace from the same cell in response to the naturalistic injected current in ZD7288 (100 µM). (F) Tyrosine hydroxylase immunohistochemistry confirms that the recorded neurons were DNs. Neurons were filled with AF594 dye (red) via the patch pipette and then slices were stained for tyrosine hydroxylase (TH; green). The merged image shows that the recorded neurons express TH and are therefore dopaminergic. The scale bar is 50 µm.

5.2.2 Characterising the structure of the alpha synuclein oligomers using transmission electron microscopy

Recombinant alpha synuclein aggregates, in the form of pre-formed fibrils (PFFs) were purchased from Abcam (ab218819) along with the monomeric form (ab218818). Negative-stain transmission electron microscopy (TEM) was used to confirm that the structure of the alpha synuclein samples were PFFs and monomers, respectively (Fig 5.3). Tau oligomers produced for Chapter 4 were analysed alongside the alpha synuclein for comparison (Fig 5.3A).

The aggregated alpha synuclein samples initially presented as small fibrils, as expected (Fig 5.3B). These fibrils would be too large to perfuse out of the end of the patch pipette and so were broken down into oligomeric form. To do this,

I added the PFFs to the filtered intracellular solution and sonicated them for 15 mins (50-60 Hz) in an ultrasonic bath (Polinski et al., 2018) to break them down to oligomers. I confirmed that this sonication successfully resulted in the breakdown from fibril form to oligomers (Fig 5.3C). Following sonication, the samples were kept on ice to ensure they remained as oligomers for the duration of the experiments (all performed within 3 hours of the initial sonication). TEM confirmed that they remained in the oligomeric form on ice for this period of 3 hours (not shown). Although the vast majority of the alpha synuclein species in the sample appeared oligomeric, I cannot rule out the possibility that there may be a small amount of other species present (for example small ~50 nm fibrils; Polinski et al., 2018) for this reason I have chosen to refer to the species as aggregates. The monomeric alpha synuclein samples displayed no signs of aggregation (Fig 5.3D).

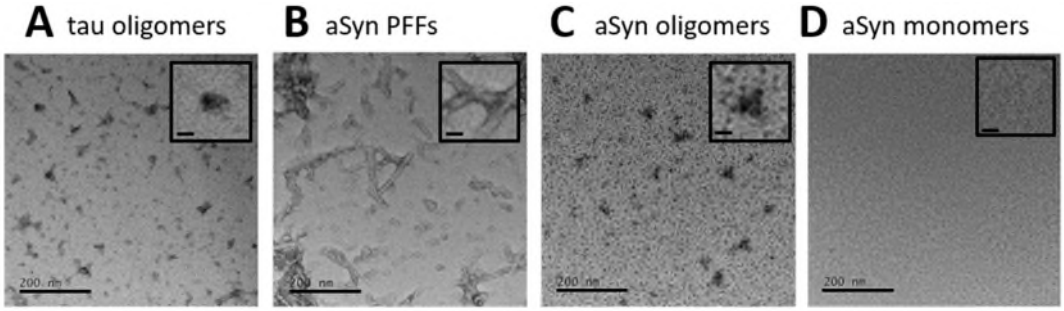

Figure 5.3: Structural analysis of alpha synuclein samples using negative-stain transmission electron microscopy.

Negative-stain-TEM of protein samples to confirm the structure of the purchased alpha synuclein. A) Tau oligomers (recombinant, from Chapter 3) for comparison of oligomeric form. B) Alpha synuclein aggregates as purchased from Abcam as pre-formed fibrils (PFFs). C) PFFs were sonicated for 15 mins (50-60 Hz) in an ultrasonic bath (Polinski et al, 2018; Dave et al, 2018) to reduce them to oligomers. This change in form can be observed by the small oligomer-like appearance. D) Monomeric alpha synuclein sample also purchased from Abcam show no aggregation. Scale bars = 200 nm, insets: higher magnification scale bar = 20 nm

5.2.3 Alpha-synuclein aggregates, but not monomers, alter the electrophysiological properties of SN dopaminergic neurons.

Monomeric or aggregated alpha synuclein samples (500 nM) were introduced into DNs and the effects on neuronal function explored over a 32-minute timeframe. This concentration was selected as it matches the concentration used in a previous alpha synuclein study conducted in the Wall lab (Kaufmann et al., 2016). This concentration was calculated from the monomeric molecular weight of alpha synuclein as it is not possible to know the exact number of monomers of alpha synuclein in each of the aggregates following sonication. This will therefore mean that the reported value is an overestimate of the actual oligomeric concentration in the patch solution (see Methods for more details). The alpha synuclein species were delivered via the patch pipette into single DNs in the SNpc of mice, and whole-cell patch clamp recordings were used to assess changes to electrophysiological properties. Both SIV and DIV current protocols were run at 8-minute intervals (for up to 32 minutes) and the voltage response to current input recorded. From this changes to input resistance, firing rate and resting membrane potential were evaluated. As a control, in a subset of neurons (termed vehicle), the same volume (2 µl) of PBS was added to the intracellular solution (200 µl) to ensure the effects were not due to dilution of the patch solution, although this is unlikely given the small volume added. At least one control recording was made at the start of each day to ensure the quality of the slices and then recordings with either vehicle, alpha synuclein monomers or alpha synuclein aggregates were interleaved to ensure that there was no recording bias.

Using this technique, the cell can act as its own internal control, which is a major advantage. Upon whole-cell breakthrough, there would be little or no time for the alpha synuclein aggregates to dialyse into the cell, therefore recordings taken immediately (time 0) are effectively ‘control’ cells. Therefore, the recordings at time 0 for all conditions should not be statistically significantly different from each other. As expected, there was no significant difference in the measured parameters from SIVs (membrane potential $p = 0.466$, input resistance $p = 0.275$ and firing rate $p = 0.851$, Table 5.1) between neurons that had received either vehicle, alpha synuclein monomers or aggregates.

	Vehicle/ control			αSyn Aggregates			αSyn Monomers			Glib + control			Glib + αSyn Aggregates		
Parameter	**Mean**	**SEM**	**SD**	**Mean**	**SEM**	**SD**	**Mean**	**SEM**	**SD**	**Mean**	**SEM**	**SD**	**Mean**	**SEM**	**SD**
RMP (mV)	-55.8	± 1.2	± 3.79	-55.4	± 1.23	± 4.10	-56.8	± 1.30	± 3.18	-53.2	± 2.14	± 5.24	-60.4	± 1.82	± 4.08
R in (MΩ)	338	± 17.6	± 55.8	312	± 17.1	± 56.8	359	± 42.2	± 103.3	386	± 25.2	± 61.7	294	± 41.9	± 93.6
Firing Rate (Hz)	1.63	± 0.39	± 0.12	2.51	± 1.57	± 0.47	2.38	± 1.14	± 0.46	2.27	± 1.15	± 0.47	2.04	± 1.29	± 0.52

Table 5.1: Electrophysiological parameters measured for dopaminergic neurons at time zero (whole-cell breakthrough) for all experimental treatments.

All recordings are made from substantia nigra pars compacta dopaminergic neurons. There was no significant difference between any of the measured parameters at time 0 minutes (whole-cell breakthrough), using Kruskal Wallis ANOVAs. Data shown as mean, SD and SEM for each experimental condition.

There were significant changes highlighted by the SIV traces over time (0 to 32 mins) for neurons where alpha synuclein aggregates were introduced via the patch pipette. After 32 mins of recording, the input resistance was significantly reduced to 63.0 ± 9.2 % of the input resistance measured at 0 mins ($p = 0.003$, $n = 11$; Fig 5.4A), reflecting the opening of a membrane channel. There was no change to the input resistance in either vehicle recordings (at 32 mins input resistance was 94.0 ± 5.0% of input resistance measured at time 0 mins, P = 0.065, n = 10, 6 animals, Fig 5.4B) or neurons with alpha synuclein monomers introduced (at 32 mins input resistance was 99.0 ± 9.0 % of input resistance measured at time 0 mins, p = 0.469, n = 6, 3 animals, Fig 5.4C). Comparing the three conditions (monomers, aggregates, and vehicle) using a Kruskal Wallis ANOVA, showed a significant difference in input resistance at 32 minutes (p = 0.0002; n = 6, 10, 11 respectively, Fig 5.4D). The change in input resistance between control and aggregated αSyn neurons first became significant at the 16-minute time point (p = 0.001; Fig 5.4D) suggesting that the opening of membrane channels occurred between 8 to 16 minutes after αSyn aggregate introduction into neurons.

The resting membrane potential at time 0 (whole-cell breakthrough) for all conditions was around -55 mV (see Table 5.1). Over the period of recording, neurons slowly depolarised by a small amount (Fig 5.4E). For vehicle, the mean depolarisation (ΔVm) was 6.2 ± 1.8 mV after 32 minutes of recording (P = 0.023, $n = 10$), for αSyn monomers ΔVm was 3.8 ± 1.2 mV (p = 0.094, $n = 6$) and for αSyn aggregates ΔVm was 6.8 ± 1.9 mV (p = 0.011, $n = 11$). This slight depolarisation was comparable between conditions and there was no significant difference over the period of recording between the membrane potential of the control neurons (vehicle and monomers) and neurons with αSyn aggregates introduced (p = 0.931).

Firing rate (FR) was measured from the voltage response to the naturalistic current injection and was used as a measure of neuronal excitability. For control neurons (vehicle), despite the slight depolarisation, there was no significant (p = 0.190) change in the firing rate (at 32 mins the FR was 124.7 ± 1.3 % of the FR at time 0 mins, $n = 10$, Fig 5.4F, G). There was also no significant change (p > 0.9999) in FR for neurons in which monomeric αSyn

was introduced (at 32 mins the FR was 120.4 ± 2.4 % of the FR at time 0 mins, *n* = 6, Fig 5.4F, G). Whereas, for the neurons that had αSyn aggregates introduced, there was a significant (p = 0.002) reduction in the firing rate (at 32 mins the FR was 42.3 ± 9.3 % of the FR at time 0 mins, *n* = 11, Fig 5.4F, G). When comparing control (vehicle and monomeric αSyn introduced cells) with cells that received αSyn aggregates, there was a significant difference in the firing rate at 32 minutes (p = 0.013). This fall in firing rate induced by αSyn aggregates is consistent with the marked reduction in input resistance.

The introduction of alpha-synuclein aggregates also affected some of the characteristic features of dopaminergic neurons including tonic and rebound firing. Tonic firing was reduced by αSyn aggregates with 64 % of neurons (7/11) initially being spontaneously active but after 32 minutes only 27 % (3/11) of neurons were still active. This is in comparison to control (vehicle) neurons, where 80 % (8/10) initially displayed tonic firing, with 60 % (6/10) still active after 32 minutes of recording. The occurrence of rebound firing (following the termination of the hyperpolarising step) also reduced with αSyn aggregates 227 % of neurons (8/11) showed rebound firing at 0 mins, but only 18 % (2/11) still showed it after 32 minutes of recording). In contrast, all the control neurons that initially displayed rebound firing (60 %, (6/10)) still showed rebound firing after 32 minutes of recording.

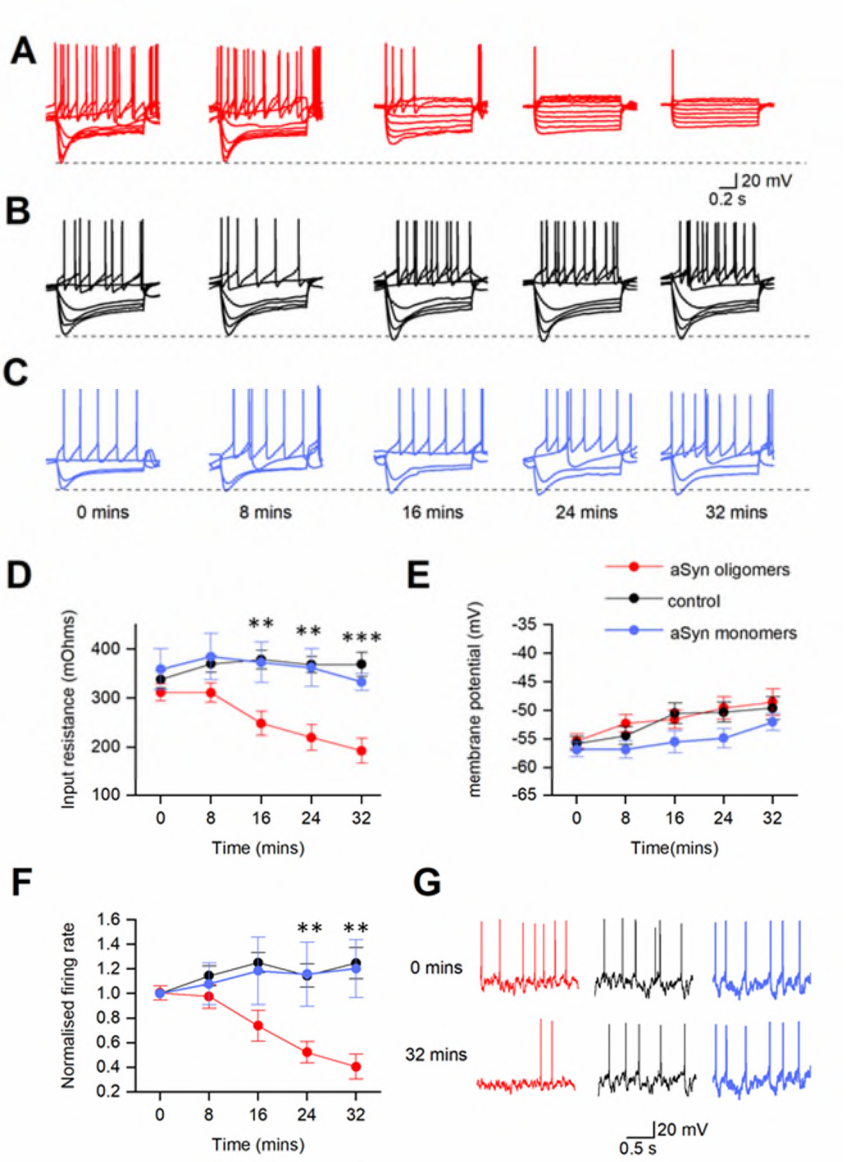

Figure 5.4: Alpha synuclein oligomers induce a time-dependent decline in firing rate and input resistance.

(A-C) Representative current-voltage relationship (SIV) traces for an example neuron injected with either alpha synuclein aggregates (A), vehicle (B) or alpha synuclein monomers (C). Current steps (1 s, starting at -200 pA and rising by 50 or 100 pA) were injected until a regular firing pattern was induced. The voltage traces are at time points at 8-minute intervals starting from whole-cell breakthrough (0 mins to 32 mins). (A) With 500 nM aggregated αSyn, a decrease in input resistance and firing rate (during positive current steps) can be observed over the 32 minutes of recording. (B) Control cells are stable throughout the period of recording. (C) With 500 nM monomeric αSyn, cells were also stable throughout the recording. (D) Mean input resistance plotted against time for control (vehicle), alpha synuclein monomers or aggregates. Alpha synuclein aggregates induced a clear reduction in input resistance

that was not observed in the control cells or those with alpha synuclein monomers introduced. (E) Mean resting membrane potential plotted against time for control (vehicle), alpha synuclein monomers or aggregates. For all three conditions, the cells slowly depolarised by comparable amounts over the 40 minutes of recording. (F) Firing rate was the only parameter that I used the voltage response to naturalistic current injection to measure (see Methods *for details). Due to the variability in firing rate between cells, firing rate was normalised to the firing rate at time 0 mins. Despite being depolarised by a comparable amount to the control and monomer-introduced cells (a corresponding increase in firing rate would be expected), alpha synuclein aggregates induced a marked reduction in firing rate that was not observed in the control cells. This is consistent with the fall in input resistance. (G) A section of the voltage response to naturalistic current injection (NT) for a representative example of a control (vehicle), alpha synuclein monomer and alpha synuclein aggregates cell at 0 mins and 32 mins. Though the firing rate of control and monomer-introduced cells are stable over time, the neuron with alpha synuclein aggregates introduced exhibits a significant reduction in firing rate over time.*

5.2.4 The decrease in conductance and firing rate caused by alpha synuclein is in part due to the opening of K_{ATP} channels

ATP-sensitive potassium channels (K_{ATP}) have well established roles in dopaminergic neurons. Previous studies have shown that in rodent models of PD, neurodegenerative effects can be at least partially rescued by either blocking them or deleting them genetically (Liss et al., 2005). A pre-print (Thakur et al., 2019) reported that alpha synuclein aggregates may act to open K_{ATP} channels within dopamine neurons and that by preventing this opening, the aggregated αSyn-mediated effects on tonic firing that they describe (reduction) can be prevented.

In my study, I have shown an aggregated αSyn-mediated increase in whole-cell conductance, indicative of the opening of a membrane channel. I therefore wanted to investigate whether this could be a K_{ATP} channel. I repeated the same set of experiments (as outlined above) following pre-incubation of the slices in 1 µM glibenclamide for at least 1 hour. Glibenclamide is a commonly used antidiabetic drug and an effective K_{ATP} channel blocker (Jiang and Haddad, 1997; Light and French, 1994). Initially, I first checked whether there were any changes to the electrophysiological properties of the SNpc DNs

produced by glibenclamide itself. I did this by comparing control cells from slices that were either preincubated or not preincubated with 1 μM glibenclamide for at least 1 hour. At 0 mins (whole-cell breakthrough), there was no significant difference between control cells from slices in normal aCSF (n = 6, 3 animals) vs control cells from slices that had been preincubated with glibenclamide (n = 6, 5 animals) for any of the parameters that I measured from SIVs (membrane potential p = 0.379, input resistance p = 0.229 and firing rate p = 0.655, Table 5.1). Over the duration of recording, glibenclamide pre-incubation did not significantly alter the input resistance (after 32 mins 99.0 ± 7.5 % of the input resistance at time 0 mins, p = 0.0.845, Fig 5.5A) or the firing rate (after 32 mins 112.1 ± 26.6 % of the FR at time 0 mins, p = 0.563, Fig 5.5A). Thus, preincubation of slices with 1 μM glibenclamide had no significant effect and should therefore not occlude any observable effects of the alpha synuclein aggregates.

I then introduced αSyn-aggregates (500 nM) into cells in slices that had been preincubated with 1 μM glibenclamide (Fig 5.5B). The fall in input resistance and reduction in firing rate that I showed previously to be induced by alpha synuclein aggregates was significantly reduced after pre-incubation (Fig 5.5B), suggesting that these effects are, at least partly, mediated through K_{ATP} channels. The input resistance at 32 mins was 90.0 ± 8.6 % of that input resistance at time 0 mins (compared to 63 % without preincubation with glibenclamide) which was not statistically significant (p = 0.250, *n* = 6) from the input resistance at time zero (Fig 5.5C). The firing rate was 80.1 ± 12.9 % of the rate at time 0 mins (compared to 42 % without preincubation with glibenclamide) which was not statistically significant from the firing rate at time zero (p = 0.353, *n* = 6, Fig 5.5 1E, F). Both sets of recorded neurons (control and αSyn aggregates) depolarised over the 32 minutes of recording to a similar degree to that of non-glibenclamide-treated slices (vehicle, ΔVm 4.7 ± 2.6 mV and αSyn aggregates, ΔVm 5.5 ± 2.1 mV, Fig 5.5D). If these changes to electrophysiological properties were solely down to the opening of K_{ATP} channels, the cells would be expected to hyperpolarise (as reported in many studies). As I did not observe this, there must be something else happening counterbalancing this effect (see Chapter 7).

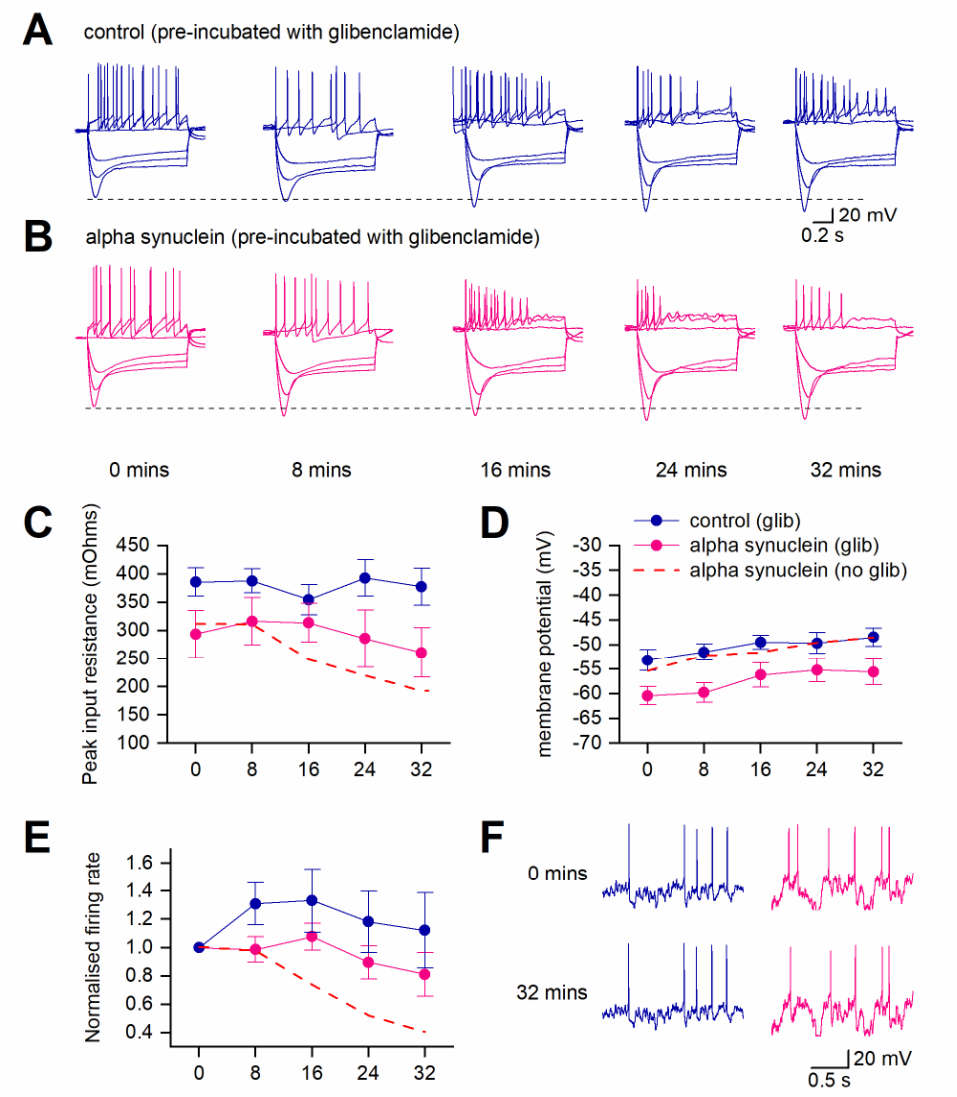

Figure 5.5: The effects of alpha synuclein aggregates on electrophysiological properties are partially prevented by pre-incubation of slices with glibenclamide.

(A) Representative current-voltage relationship (SIV) plots for an example control cell (injected with PBS as a vehicle) in the presence of glibenclamide 1 μM. Current steps (starting at -200 pA and rising by 50 pA) were injected until a regular firing pattern was induced. Recordings display time points between whole-cell breakthrough (0 mins) and 32 mins. Cells are stable throughout the period of recording, with no consistent changes to the SIV over time. (B) as in A), but with alpha synuclein 500 nM aggregates (final concentration) added to the intracellular solution. The decrease in input resistance and firing rate normally observed with alpha synuclein over the 32 minutes of recording is reduced in the presence of the glibenclamide (1 μM). (C) Mean input resistance measurements (measured at the peak deflection; before the sag) plotted against time for control (vehicle) vs alpha synuclein aggregates in the

presence of glibenclamide (1 μM). The fall in input resistance was reduced compared to that for alpha synuclein cells in normal aCSF (dashed line). (D) Mean resting membrane potential measurements plotted against time for vehicle vs alpha synuclein in the presence of glibenclamide 1 μM. Both conditions showed a slow, but comparable depolarisation over time. (E) Mean firing rate measurements plotted against time for vehicle vs alpha synuclein in the presence of glibenclamide 1 μM. The drop-in firing rate was reduced compared to that for alpha synuclein aggregate introduced into cells in normal aCSF (red dotted line for reference; data repeated from Fig 5.4 as a visual reference). Firing rate is normalised to the firing rate at time 0 mins. (G) A section of the voltage response to naturalistic current injection (NT) for a representative vehicle vs alpha synuclein cell in the presence of glibenclamide 1 μM at 0 mins and 32 mins. Under both conditions, the firing rate was stable over time.

5.3 Conclusion

I have used a combination of electrophysiological recording with detailed analysis to characterise fully the effects of introducing aggregated αSyn directly into single mouse dopaminergic neurons in the substantia nigra. Aggregates were introduced via the patch electrode during whole-cell patch clamp recordings. Aggregated αSyn caused a significant increase in conductance and decrease in firing rate without altering the resting membrane potential. Changes to conductance and firing rate occurred 8-16 minutes after whole-cell breakthrough and were specific to aggregates (they were not observed when monomeric alpha synuclein was introduced). The effects could be prevented by pre-incubating the slices in ATP-sensitive potassium channel (K_{ATP}) inhibitor glibenclamide, despite the high concentration of ATP present in the patch electrode. These data suggest that by accumulating in DNs, αSyn aggregates may chronically open K_{ATP} channels leading to a significant increase in conductance, loss of neuronal excitability and likely also a decrease in dopamine release and overall cell function.

Chapter 6:

Physiological changes in CO_2 modulate VTA and substantia nigra neuronal function

Results of this chapter have been published previously: (Hill et al., 2020a, 2020b)

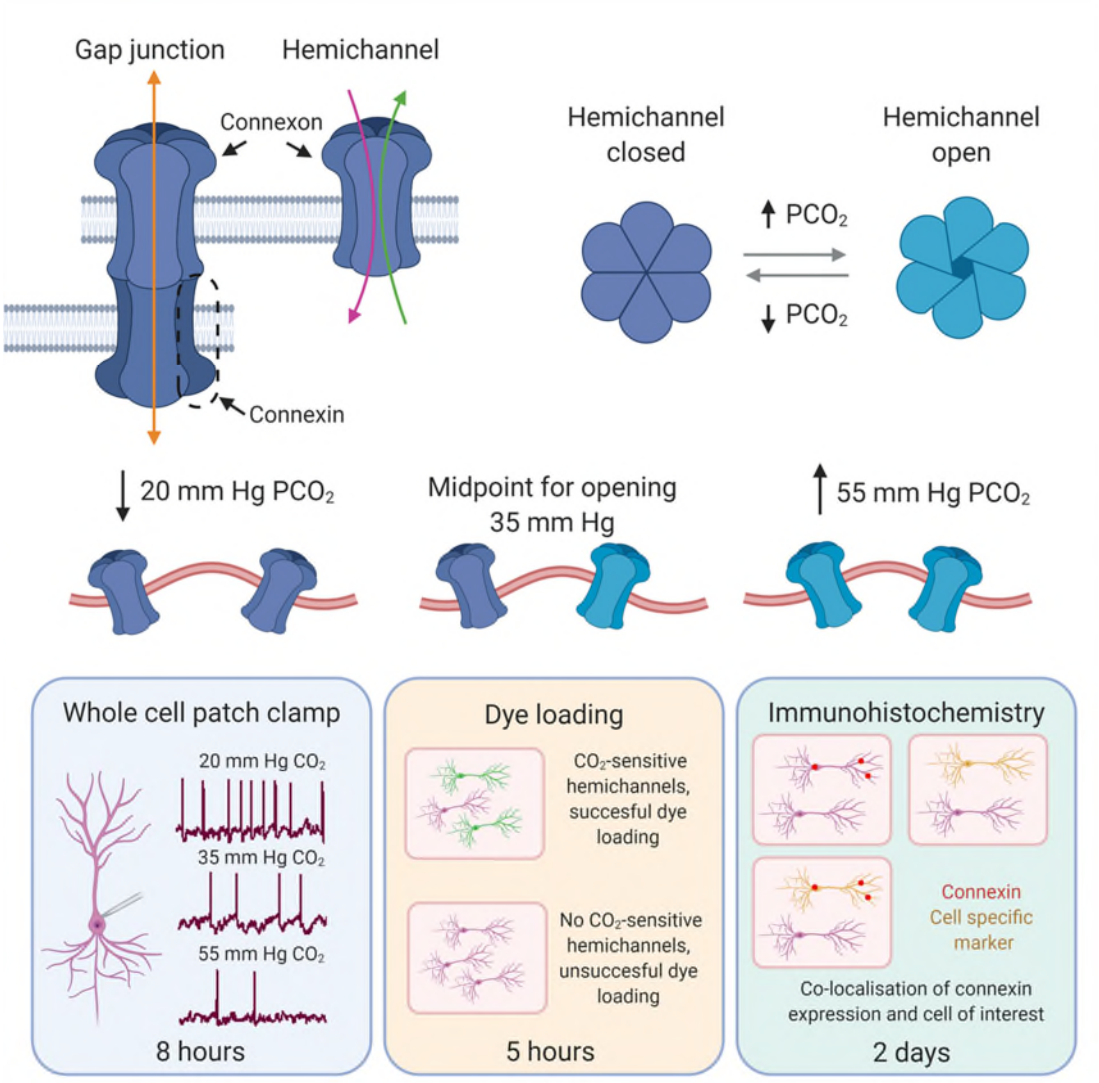

Figure 6.1: Physiological changes in the level of CO_2 alter neuronal function in the substantia nigra and ventral tegmental area through via connexin hemichannels

6.1 Introduction

Dopaminergic neurons (DNs) possess large branches of projections, have important roles in the modulation of many behaviours and have therefore been extensively studied. They have unique electrophysiological profiles (Fig 5.2) and fire at rest (tonic firing), thus making them highly energy intensive. The substantia nigra (SN) and the ventral tegmental area (VTA) represent two major dopaminergic nuclei in the mammalian brain. The SN forms a key part of the basal ganglia circuitry and its dopaminergic neurons play vital roles in the initiation and co-ordination of movement. The SN can be further divided into two regions, the *substantia nigra pars reticular* (SNpr) and the *substantia nigra pars compacta* (SNpc). The SNpc is sensitive to damage from oxidative stress and its DNs are amongst the most susceptible neurons to degeneration in Parkinson's disease (PD). Neurons in the neighbouring ventral tegmental area (VTA) play important roles in the modulation of emotion, reward and sleep- wake behaviours (Eban-Rothschild et al., 2016; Holly and Miczek, 2016; Lammel et al., 2014; Morales and Margolis, 2017; Yu et al., 2019). They are less susceptible to damage in the early stages of PD but do become affected at later stages. Important questions remain as to why dopaminergic neurons between these two regions are differentially affected and why they display varying levels of susceptibility to neurodegeneration. As complex cells, with influence on so many aspects of behaviour, it is vital to fully understand their physiology, in order to then understand how they might be implicated in pathology.

Carbon dioxide (CO_2) is a waste product of cellular metabolism, exhaled by the lungs and its levels are a key regulator of breathing. Levels will vary between people, but the average in human blood (PCO_2) at rest is around 40 mm Hg and will fluctuate around this baseline. PCO_2 is increased (hypercapnia) in diseases such chronic obstructive pulmonary disease (COPD), asthma and sleep apnoea (Owens and Malhotra, 2010). Low levels of blood PCO_2 (hypocapnia) can occur in kidney failure, diabetic acidosis and with hyperventilation (Brown, 1953; Wilson et al., 1991).

A subfamily of connexins (Cx26 and Cx30) have evolved to develop CO_2 sensitivity. The most sensitive of these is Cx26 and its sensitivity is directly mediated through the carbamylation of lysine residue 125, resulting in an increase in open probability (Huckstepp et al., 2010b, 2010a; Meigh et al., 2013). Since the physiological midpoint for hemichannel opening is ~ 40 mm Hg, there will be some connexin 26 channels open at rest. Increases in CO_2 levels will result in the opening of more Cx26 hemichannels and an increase in whole-cell conductance. Whereas a decrease in CO_2 level will result in the closing of Cx26 hemichannels and a decrease in whole-cell conductance (Huckstepp et al., 2010b, 2010a; Meigh et al., 2013). It is well established that CO_2 binding to connexin 26 on glial cells in the brainstem allows ATP to be released and that this regulates breathing (Gourine et al, 2005; Huckstepp et al 2010; Weifer et al 2010).

The discovery of gap junction coupling between dopaminergic neurons in the substantia nigra was first described by Grace and Bunney (1983) using electrophysiology. They further confirmed the coupling using Lucifer Yellow transfer between neighbouring 'coupled' cells. While reading around the vast literature on DNs electrophysiological and morphological properties, to assist in making the recordings outlined in Chapter 5, I discovered an unexpected property of SNpc DNs that I thought might be worth exploring further. Vandecasteele et al. (2005) confirmed that pairs of DNs in the SNpc are coupled by gap junctions and that they express a range of connexin proteins, as determined by single cell RT-PCR (Vandecasteele et al., 2006). They demonstrated that in young rodents (P7-10), SNpc DNs express mRNA for Cx26, Cx30, Cx32, Cx36 and Cx43 but by P17-21 a developmental switch has occurred and they now only express Cx36, Cx43 and Cx31.1 (Fig 6.2). I was particularly interested in two of these connexins which have been previously described to be directly sensitive to carbon dioxide (CO_2): connexin 26 and connexin 30 (Huckstepp et al., 2010b; Meigh et al., 2013). I set out to determine whether the mRNA profile described by Vandecasteele et al., (2006) resulted in functional hemichannel expression which could confer CO_2 sensitivity to the neurons. This would be particularly interesting as it would be the first discovery in neurons (Nagy et al., 2011). If so, I wanted to explore

whether there were functional consequences of the CO_2 sensitivity in terms of neuronal output, and whether there could be any implications of this in pathology.

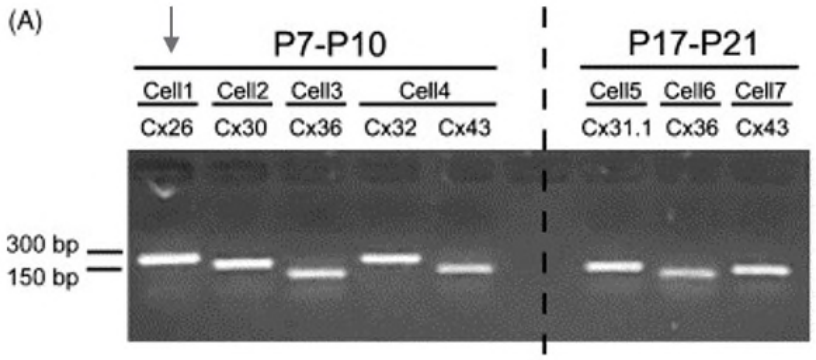

Figure 6.2: Connexin mRNA expression analysed by single-cell RT-PCR in SNpc DA neurons from P7-10 (left) and from P17-21 (right) rats.

There is a developmental shift in connexin expression in rodents. This study confirmed the presence of Cx26, Cx30, Cx36, Cx32 and Cx43 in the P7-10 rats and Cx31.1, Cx36 and Cx43 in P17-21 rats (reproduced from *Vandecasteele et al., 2006)*

Whole-cell patch clamp recordings were made from dopaminergic neurons (DNs) in the SNpc in acute coronal slices from P7-10 wild type mice. To test the sensitivity of DNs to CO_2, the level of CO_2 (35 mm Hg, basal level) was either increased to 55 mm Hg or decreased to 20 mm Hg under isohydric conditions (compensatory changes in bicarbonate concentration to maintain constant extracellular pH during the CO_2 stimulus, *see Methods*). If Cx26 hemichannels are present, then an increase in PCO_2 will cause them to open (Huckstepp et al., 2010b; Meigh et al., 2013), resulting in an increase in whole-cell conductance (decreasing excitability). By contrast, a reduction in PCO_2 would close the hemichannels, resulting in a reduction in whole-cell conductance (increasing excitability; Huckstepp et al., 2010b; Meigh et al., 2013).

6.2 Results

6.2.1 Developmental changes to SN DN electrophysiological properties

Dopaminergic neurons in the SNpc were located from their position in the slice and their characteristic electrophysiological profile (as in chapter 5). Given that mRNA for the CO_2 sensitive connexins 26 and 30 was reported to be only present in P7-10 pups and absent by P17-21 (Vandecasteele et al., 2006) I decided to test neurons for CO_2 sensitivity in both age groups, using neurons in the older mice as a control group. If the mRNA is no longer present, then any phenotype of CO_2 sensitivity (that is present in the P7-10 pups) should be lost. This comparison between age groups could potentially be complicated by developmental changes to electrophysiological properties, which are known to occur over this period. Therefore firstly, I compared the input resistance and resting membrane potential measurements from SNpc DNs of the two age groups without any intervention. There was no significant difference in input resistance between the two age groups of mice (P7-10, Rin = 380 ± 28.16 MΩ, P17-21, Rin = 290 ± 22.45 MΩ, p = 0.307; Fig 8.3). There was also no significant difference in the resting membrane potential (P7-10, RMP = -59.3 ± 1.33 mV, P17-21, RMP = -60 ± 2.08 mV, p = 0.835; Fig 8.3) or the size of the sag response, measured between the peak hyperpolarisation and steady state after I_H has activated (P7-10: 22.6 ± 2.25 mV, P17-21 20.1 ± 2.3 mV, p = 0.454). These results are consistent with expected values for these age groups of mice as reported in (Dufour et al., 2014).

6.2.2 Increase in PCO_2 significantly reduces the excitability of early postnatal substantia nigra dopaminergic neurons

Next, I wanted to check whether there were functional hemichannels in the SNpc P7-10 DNs and if so, whether they conferred sensitivity to CO_2. Whilst recording from single dopaminergic neurons, I increased the level of CO_2 from 35 mm Hg to 55 mm Hg (isohydric; constant pH) and recorded the response to single hyperpolarising (-50 pA, 100 ms) current step injections. Increasing the level of CO_2 gave a time-dependent reduction in the amplitude of the voltage response to the hyperpolarising current steps consistent with a fall in input resistance. At steady state, the voltage response to the current steps had fallen to 70.0 ± 9.6 % of control ($p = 0.002$; Fig 6.3A, B), input resistance had fallen from 380.0 ± 28.2 MΩ to 217.0 ± 27.9 MΩ ($p = 0.003$ $n = 10$) and the tonic action potential firing was abolished (Fig 6.3). All of these effects are characteristic of an increase in the resting conductance consistent with the opening of hemichannels. I observed partial recovery in a subset of recordings when the solution was returned to 35 mmHg (normal CO_2). Due to a lack of experimental repeats (n = 3), this data was not quantified, but an example demonstrating partial recovery is illustrated in Fig 6.3C. DNs in the SN of older rats (P17-21) do not express mRNA for CO_2 sensitive connexins (Vandecasteele et al., 2006) thus they should be insensitive to CO_2 if it is connexin hemichannel-dependent. When the same protocol was repeated with older (P17-21) mice, there were no significant effects of the increased PCO_2 (voltage response was 101.0 ± 0.9 % of control, $p = 0.330$, n = 4, Fig 6.3 D, E).

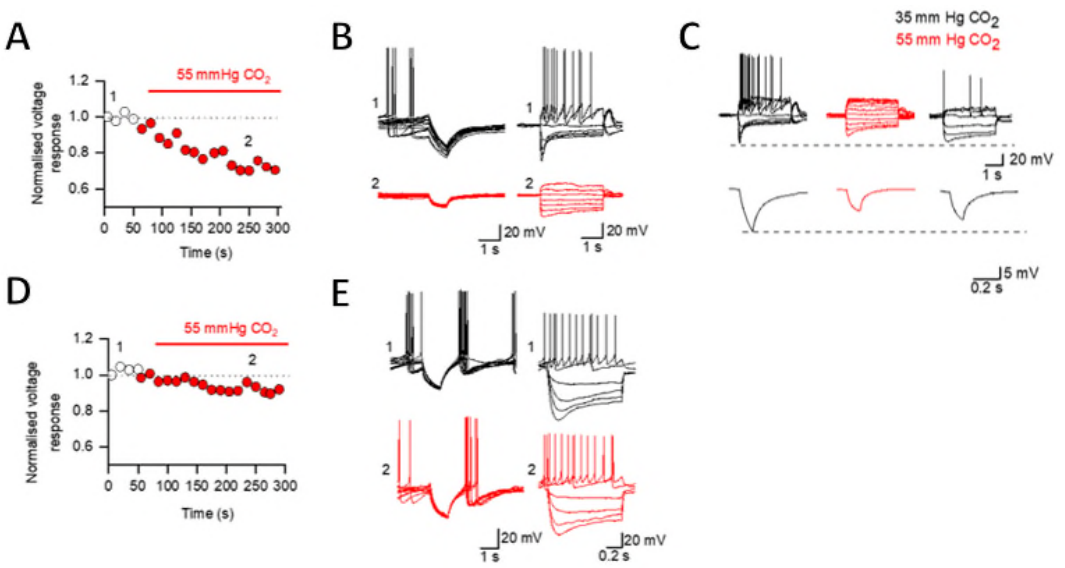

Figure 6.3: CO_2 sensitivity of dopaminergic neurons in the substantia nigra

(A) Example of a time course for changes in voltage responses to hyperpolarising current steps for a neuron from a P7-10 mouse (each point is a mean of 15 sweeps) when CO_2 was increased from 35 to 55 mm Hg (red). (B) Associated voltage traces (40 superimposed traces) and voltage responses to step currents (from -200 pA to 50pA) at the indicated time points from A. (C) Representative voltage responses (P7-10) demonstrating that input resistance and firing rate changes could be partially reversed (bottom traces are an average of 25 sweeps) when CO_2 was reduced back to 35 mmHg. (D) There was no significant change in the voltage response to hyperpolarising current steps in a dopaminergic neuron from a P17-21 mouse (each point is a mean of 15 sweeps) when CO_2 was changed from 35 to 55 mm Hg. (E) Associated voltage traces (40 superimposed traces) and voltage responses to step currents at indicated time points from D.

Figure 6.4: Example raw data traces for the full timeframe of raised CO_2 exposure.

A representative example from a P7-10 substantia nigra dopaminergic neuron. Membrane potential traces in response to -50 pA current steps in 35 mmHg CO_2 (black), then switched over to 55 mmHg CO_2 (red). Each plot represents a timepoint from Figure 6.3B and displays 9 overlaid sweeps within each 15 second time interval. A clear reduction in voltage response can be observed over time.

6.2.3 Changes in excitability are not due to the exchange of solutions or drift in recording quality over time

To confirm that the observed effects of CO_2 were not an experimental artefact, I repeated the experiment without altering the level of PCO_2 but still switched between two solutions that were both at 35 mmHg CO_2). The resting conductance and of the neurons did not significantly alter over the time course of the experiment (Fig 6.4), confirming that the observed changes are mediated by variation in the PCO_2 level rather than from an artefact resulting from the mechanical change in solution or from rundown in the quality of recordings over time.

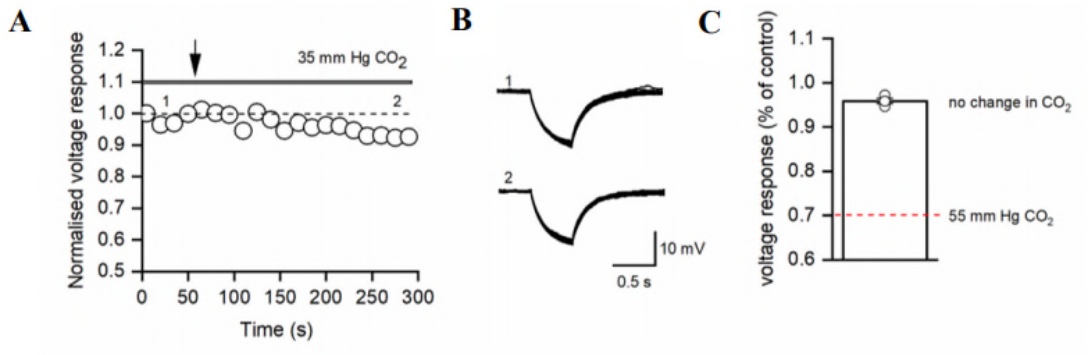

Figure 6.5: A control for solution exchange during the protocol

(A) Time course of changes in voltage response to a 50 pA hyperpolarising step current (P10 SNpc, each point is a mean of 15 sweeps) when CO_2 was maintained at 35 mm Hg, but solutions were exchanged to ensure the observations are not a result of the exchange process or loss of recording quality over time (arrow). (B) Associated voltage traces (50 superimposed traces) and voltage responses to step currents at indicated time points from A. (C) Quantification of the voltage response changes when the solution was swapped, relative to the amplitude of the response at breakthrough, data is presented as mean ± SEM. Red dashed line represents the relative level of decrease in response for cells which were exposed to high CO_2 (55 mm Hg) after an equal amount of time.

6.2.4 Changes in neuronal excitability are blocked by the hemichannel inhibitor carbenoxolone

I had now confirmed that the electrophysiological consequences of altering the level of CO_2 are not an experimental artefact, but I have not yet proved that they are mediated by connexins. The next stage was to confirm the effects were hemichannel-mediated using the blocker carbenoxolone (100 µM, n=6; Fig 6.5; Meigh et al., 2013). The level of CO_2 was raised from 35 mm Hg to 55 mm Hg CO_2 in the presence of carbenoxolone (100 µM; Fig 5.6A). The reduction in input resistance was abolished (after 5 mins in 55 mmHg CO_2, input resistance was 103.0 ± 1.4 % of the value at 0 mins, p = 0.094: Fig 6.5 B, C). There was also no change in RMP (at 40 mins, RMP was 97.0 ± 2.5 % of the value at 0 mins). Due to the wide-ranging effects reported for carbenoxolone acting directly on neuronal properties and synaptic transmission (Tovar et al., 2009), I did not examine changes to firing rate. The significant block of CO_2-mediated effects (Fig 6.5) confirms that the effects are hemichannel mediated.

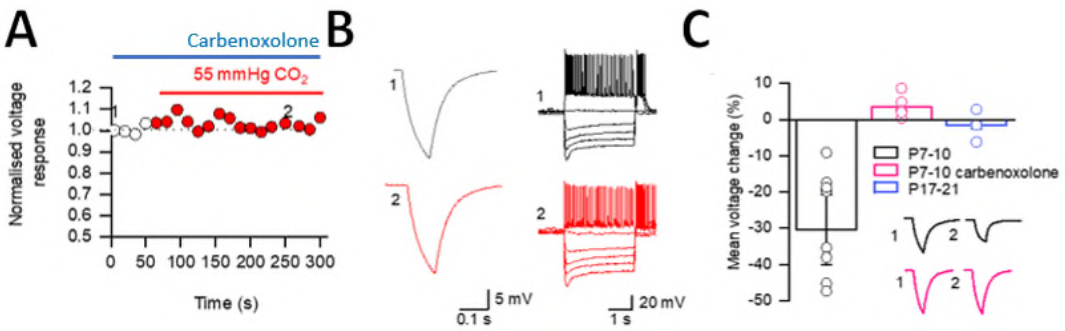

Figure 6.6: Carbenoxolone blocks changes to excitability in P71-10 SNpc DNs
(A) If slices are incubated in carbenoxolone, there is no significant change in voltage response (P7-10, each point is a mean of 15 sweeps) when the CO_2 level was changed from 35 to 55 mm Hg. (B) Associated mean voltage traces (average of 40 sweeps) and voltage responses to step currents at indicated time points from A. (C) Quantification of voltage response changes (35 to 55 mm Hg CO_2) for P7-10 mice (with and without carbenoxolone incubation) as well as P17-21 mice for reference. Inset: Example control response and response in carbenoxolone for P7-10 mice (1, 35 mm Hg and 2, 55 mm Hg).

6.2.5 Decreasing PCO_2 significantly increases the excitability of early postnatal substantia nigra dopaminergic neurons

Given that the midpoint for connexin 26 channel opening is ~ 40 mm Hg CO_2 (Huckstepp et al., 2010b), I next wanted to test whether I could increase the excitability of the SNpc DNs (in P7-10 mice) by reducing the level of PCO_2. Closing hemichannels should increase input resistance, excitability and firing rate. In a separate group of SNpc DNs cells, I decreased the PCO_2 level to evaluate this hypothesis. Reducing PCO_2 from 35 to 20 mm Hg (hypocapnia) increased the firing rate (the mean firing rate in 20 mm Hg CO_2 was 184.0 ± 28.7 % of that in 35 mm Hg CO_2, p =0.015, Fig 6.6 A, D). It also increased the amplitude of the voltage response to current steps (the mean voltage response in 20 mm Hg CO_2 was 104.0 ± 1.2 % of that in 35 mm Hg CO_2, p = 0.008; Fig 6.6 B, C, E), consistent with a decrease in conductance.

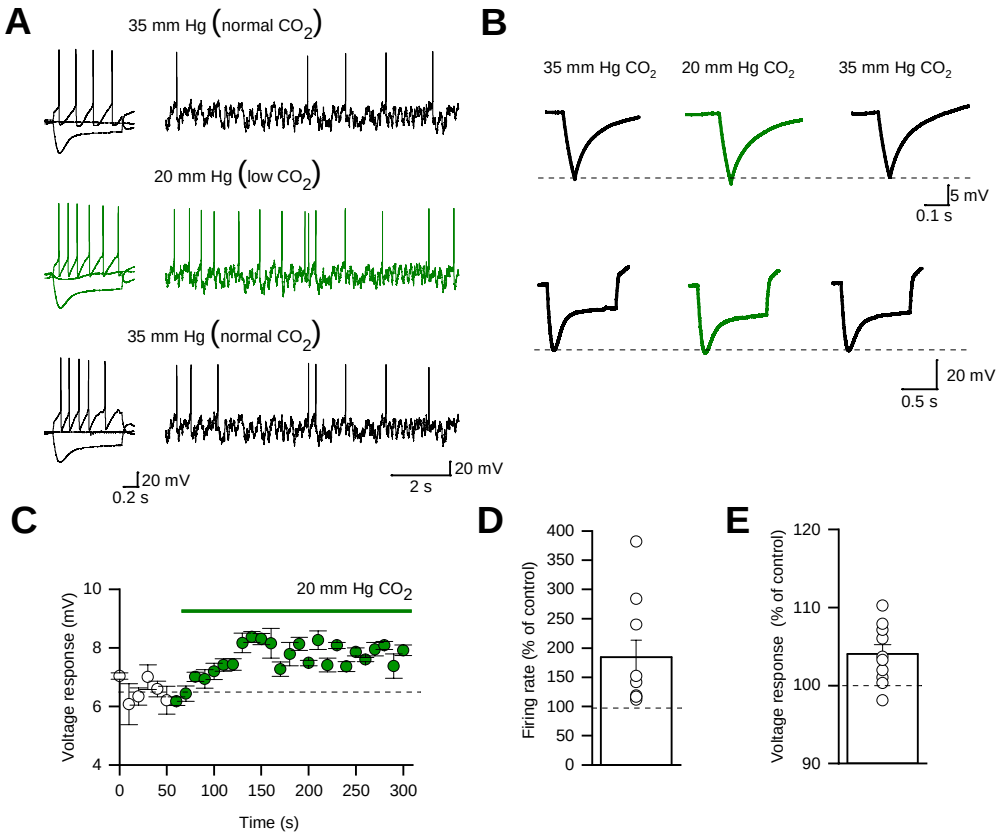

Figure 6.7: Dopaminergic neurons in the substantia nigra are sensitive to lowering CO_2.

(A) An example recording from an SN dopaminergic neuron in a P7 mouse. Black traces represent recordings in 35 mmHg (normal CO_2) and green traces represent recordings in 20 mmHg (low CO_2). An increase in firing rate can be observed from the membrane potential responses to step and fluctuating current injections (see Methods). (B) The voltage response to a 50 pA hyperpolarising step (top, traces are an average of 40 sweeps) and the membrane potential response to the -100-pA step injection (bottom). They demonstrate subtle increases to input resistance with lowered CO_2. Both the left and right panels show a partial recovery of both firing rate and input resistance after washing back into 35 mm Hg CO_2. (C) An example of the time course of changes in voltage response (for a single P7-10 slice, each point is a mean of 15 sweeps) when CO_2 was changed from 35 to 20 mm Hg. (D) Quantification of the mean change to firing rate when CO_2 was lowered from 35 to 20 mm Hg. Firing rate was measured from the voltage response to fluctuating current input. (E) Quantification of the mean change to the voltage response to hyperpolarising step input.

6.2.6 Early postnatal substantia nigra dopamine neurons dye load during hypercapnia and express connexin 26

A characteristic of hemichannels is that when they open, they allow entry of membrane-impermeant fluorescent dyes into cells, and once the hemichannels close, the dye will become trapped. Therefore, dye loading can be used as a marker for showing which cells express CO_2–sensitive hemichannels (Huckstepp et al., 2010b; Meigh et al., 2013; Fig 6.7A). When (Vandecasteele et al., 2006) attempted this with Lucifer yellow, they did not find evidence for functional hemichannels. However, this may be because the channels are heteromeric and therefore may be impermeable to this dye. I therefore used the impermeant dye, Carboxyfluorescein (CBF) that passes through open Cx26 hemichannels (Huckstepp et al., 2010b) and confirmed that neurons in the SN of P7-P10 mice could be loaded with the dye following hypercapnia (Fig 6.7A). No dye loading occurred if PCO_2 was not increased, and it did not occur in the SN of older mice (P17-21; Fig 6.7A) or in hippocampal pyramidal cells (Fig 6.11). Unfortunately, CBF cannot be fixed and so the dye-filled cells cannot be subsequently labelled with antibodies. However, I can be confident that the dye-filled cells were either SN DNs or VTA GABAergic neurons, as patch clamp recording was carried out before the dye loading (to confirm the identity of the cells from their electrophysiological properties and pharmacology) and then the same cells were subsequently dye filled.

To further confirm that early postnatal SN DNs express connexin 26 I used immunohistochemistry. The connexin 26 antibody has been used extensively in previous studies and prior publications can confirm correspondence for Cx26 immunostaining with a reporter driven from the endogenous Cx26 promoter (Huckstepp et al., 2010b; Sun et al., 2009). In slices from P7-10 mice, Cx26 expression was present in tyrosine hydroxylase positive (TH^+) neurons in SN (Fig 6.7B). However, in older mice (P17-21), Cx26 was not expressed in in TH+ neurons (Fig 6.7C) but was expressed in leptomeninges of corresponding sections, providing a positive control (Fig 6.7D; Condorelli et al., 2003).

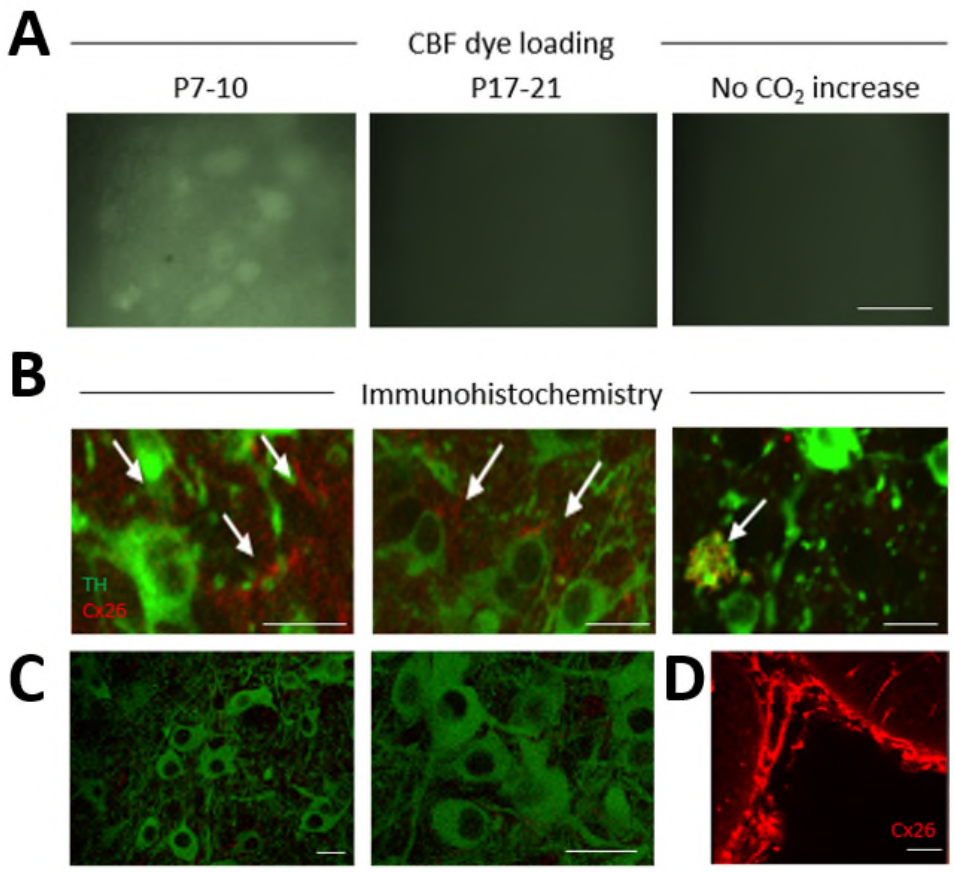

Figure 6.8: Dye loading and Cx26 expression in substantia nigra.

(A) Carboxyfluorescein (CBF) dye loading following hypercapnia (55 mm Hg CO_2) in P7-10 mouse slices. No dye loading occurred if CO_2 was not changed or if CO_2 was increased in P17-21 slices, scale bar = 50 µm. (B) Immunofluorescent staining of P7-10 SN for Cx26 (red, arrows) in TH^+ neurons (green) in single optical planes. (C) No co-localisation of Cx26 (red) in TH^+ neurons (green) in the SN at P17-21, scale bar = 30 µm. (D) Staining was deemed successful due to the positive leptomeninge staining from corresponding sections of the same mouse brain, scale bar = 30 µm.

6.2.7 FITC dye loads glial cells in high CO_2 but not neurons

Having demonstrated that cells in the region of SNpc DNs can uptake Carboxyfluorescein on exposure to high levels of CO_2, I wanted to prove definitively that they were dopaminergic. As CBF cannot be fixed (personal communication Robert Huckstepp), I instead loaded with a different dye fluorescein (FITC), which can be fixed with PFA, then counterstained with tyrosine hydroxylase. I would have expected neuronal dye loading in the P7-10 mice as there was with CBF. However, I did not see any dye loading in neurons. Depending on the profile of connexins available, they can assemble into homomers or heteromers. For example, it is known that connexin 26 and connexin 30 can form heteromeric channels that maintain their sensitivity to CO_2. I do not know whether the connexins are assembling in a homomeric or heteromeric form in my *in vitro* slice experiments. However, it is possible that FITC cannot pass through hemichannels that are not homomeric (of Cx26) and thus the presence of heteromeric channels potentially prevents the influx of the dye.

I then repeated this in P17-21 mice, expecting not to see any dye-loading. However, I observed FITC dye loading in the cells surrounding SNpc DNs (Fig 6.8A). I hypothesised that they might be glial cells. I therefore performed immunohistochemistry for connexin 26 (red) and GFAP (green) and confirmed co-localisation (Fig 6.8B). Perhaps glial cells are more likely to have homomeric Cx26 conformations than neurons. They may also have increased numbers of Cx26 hemichannels. Connexin 26 expression on glia is known to release ATP (Gourine et al, 2005; Huckstepp et al 2010; Weifer et al 2010) in response to raised CO_2. Thus, I propose here a potential developmental switch in connexin 26 action from neurons (P7-10; directly inhibitory) into glia (P17-21; indirectly excitatory). This needs to be explored further in future experiments.

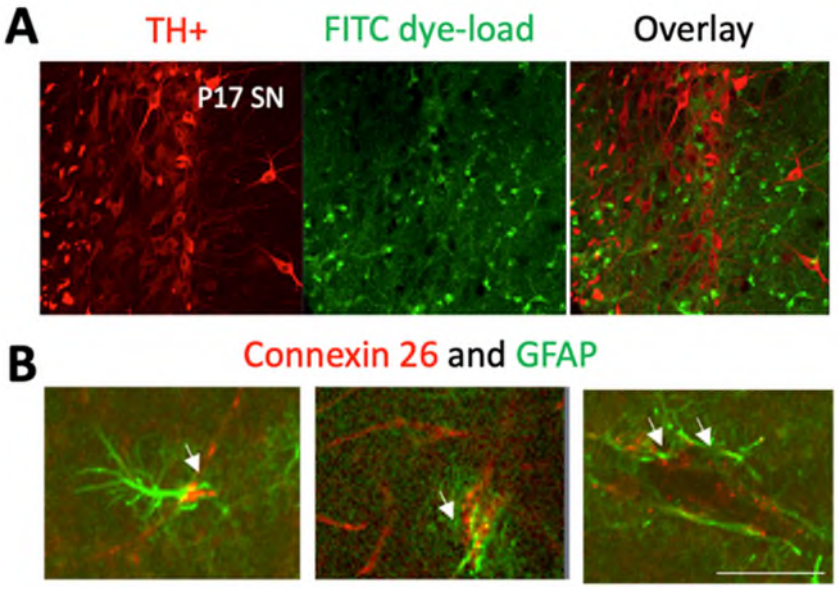

Figure 6.9: FITC dye loading suggests CO_2 presence in glial cells of P17-21 mice and is confirmed with immunohistochemistry.

No dye loading of FITC was observed in SNpc DNs of P17-21 mice. However, surrounding smaller cells were loaded with FITC. It is possible that these cells could be GABAergic neurons or glial cells (B) To test this immunohistochemistry to look for co-localisation was performed. This confirms co-localisation of connexin 26 (red) and glial fibrillary acidic protein (GFAP; green) in the SNpc of P17-21 mice. Note that the connexin 26 antibody will stain both connexin 26 (punctate appearance; white arrows) and blood vessels (long thin staining). These images are taken of single optical planes and demonstrate co-localisation of punctate Cx26 and GFAP positive glial cells.

6.2.8 Changes in PCO_2 significantly modify the excitability of neurons in the VTA

Consistent with the lack of electrophysiological changes, there was no CBF dye loading into P17-21 SNpc DNs (where there had been at younger ages). However, I observed in a neighbouring region, the ventral tegmental area (VTA) what appeared to be some neurons that loaded with the dye (Fig 6.9A). This area is another prominent nuclei for dopaminergic cells within the brain and is central to the circuits controlling reward and motivation behaviours (Morales and Margolis, 2017).

To confirm that these cells were part of the VTA, I first made recordings from a subset of the dye-filled neurons. I was surprised to discover that they were

not hyperpolarised by dopamine (30 µM) but found instead that they were hyperpolarised by application of the opioid receptor agonist [Met]-Enkephalin (10 µM). This is consistent with the neuron classification described in Johnson and North (1992); that there are a subset of neurons that are positioned close to the substantia nigra that respond in a very similar manner to SN dopaminergic neurons: a large I_H (sag) in response to hyperpolarising current steps and are hyperpolarised by dopamine. The second subgroup does not show as large I_H (sag) in response to hyperpolarising current steps and do not hyperpolarise with dopamine, but instead hyperpolarise with [Met]enkephalin (Fig 6.9B-D). The CO_2 sensitive neurons appear to belong to this second subgroup. The differences in action potential dynamics of these two different groups allows them to be distinguished from one another.

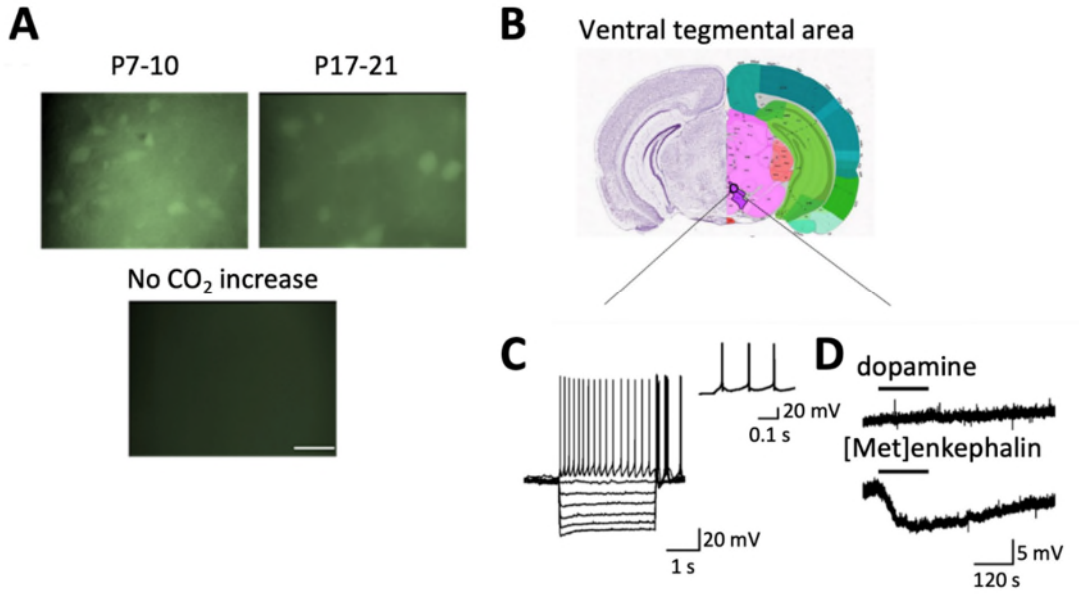

Figure 6.10: Localisation of the recorded neurons in the ventral tegmental area *(A) Carboxyfluorescein (CBF) dye loading following hypercapnia (55 mmHg CO_2) in P7-10 and P17-21 mouse slices demonstrates dye loading in putative VTA neurons. No dye loading occurred if PCO_2 was not changed scale bar = 50 µm. (B) Location of the VTA in a coronal mouse brain slice (*Adapted from Allen Mouse Brain Atlas, 2004). *(C) Membrane potential traces recorded from a putative dopaminergic neuron in the VTA in response to current steps in 35 mm Hg CO_2. Current steps (3 s duration) started at -200 pA and were increased by 50 pA until the neuron exhibited a regular firing pattern. (Inset) Membrane potential response to the injection of a +100 pA current step. There is a clear difference in the action potential dynamics of*

dopaminergic neurons in the SN and VTA regions, as previously reported (Johnson and North, 1992). (D) Membrane potential traces from a putative VTA dopaminergic neuron. Application of dopamine (30 µM) had no effect on the membrane potential whereas [Met]enkephalin (10 µM) markedly hyperpolarised the neuron. This is consistent with previous reports (Johnson and North, 1992) that DNs in this region of the VTA are not responsive to dopamine but are hyperpolarised by [Met]enkephalin.

In response to an increase in PCO_2, these (P17-21) neurons in the VTA showed similar electrophysiological changes to P7-10 SN DNs in response to changes in PCO_2: increased PCO_2 (55 mm Hg) decreased input resistance (voltage response reduced to 71.0 ± 13.2% of control p = 0.001, 335.0 ± 66.7 MΩ to 222.0 ± 39.4 MΩ, p =0.0446, before the sag n = 5;) and firing rate Fig 6.10 A-C. Reducing PCO_2 to 20 mm Hg increased input resistance (voltage response increased to 118.0 ± 6.1 % of the baseline amplitude, p = 0.043) and firing rate (193.0 ± 35.0 % of the baseline firing rate, p = 0.049, of control; Fig 6.10 D-F).

Given that the ventral tegmental area (VTA) is highly heterogenous and neurons can release dopamine, glutamate, GABA, or any combination of the three, I performed separate immunostaining protocols of connexin 26 paired with tyrosine hydroxylase for dopaminergic neurons and of connexin 26 paired with GAD65/67 for GABAergic neurons. I saw co-localisation of connexin 26 (red, AF594) with GAD65/67 GABAergic neurons which is consistent with the [Met]enkephalin sensitivity electrophysiological phenotype (Fig 6.10G). To establish whether these neurons were also dopamine releasing I looked for colocalization with tyrosine hydroxylase but saw no evidence of this (Fig 6.10G). I therefore concluded that these neurons were likely GABAergic neurons. They could either be or long-range projecting GABAergic neurons to a range of different sites or local GABAergic neurons which within the VTA are known to modulate the activity of the neighbouring dopaminergic neurons. Thus, changes in CO_2 levels could potentially indirectly modulate dopamine release into regions like the nucleus accumbens.

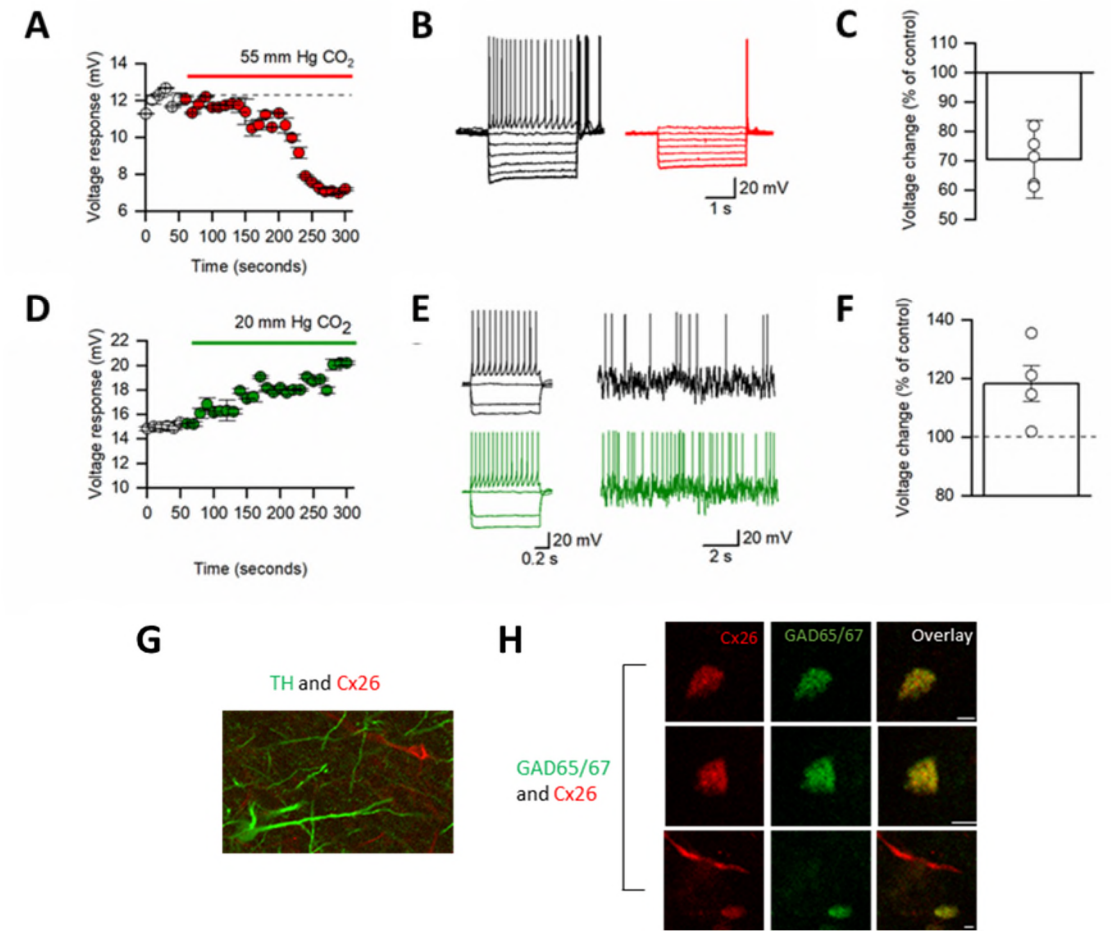

Figure 6.11: GABAergic neurons in the VTA are sensitive to CO_2.

(A) An example of the time course of changes in voltage response for a single P17-21 slice (CO_2 increased from 35 to 55 mm Hg; each point is a mean of 15 sweeps). (B) Voltage responses to step currents at indicated time points in B. (C) Quantification of changes in voltage response to increased PCO_2. (D) An example of the time course of changes in voltage response for a single P17-21 slice (CO_2 decreased from 35 to 20 mm Hg; each point is a mean of 15 sweeps). (E) Voltage responses to step and fluctuating current inputs at indicated time points in F demonstrating increased input resistance and firing rate. (F) Quantification of changes in voltage response to decreased PCO_2. (G, H) Representative single optical plane confocal microscopy immunohistochemistry images. (G), Immunofluorescent staining of P17-21 VTA for Cx26 (red) which is not expressed by TH^+ neurons (green, no co-localisation), scale bar = 50 µm. (H), co-localisation of Cx26 (red) with the soma of GAD+ neurons (green) in the VTA (scale bar 20 µm).

6.2.9 Carbon dioxide sensitivity is not present in hippocampal CA1 pyramidal neurons

To ensure that the observed CO_2 sensitivity was not a blanket response across all neurons, I recorded from pyramidal cells (PCs) in the CA1 region of the hippocampus of P7-10 mice, in slices where the DNs had responded to changes in CO_2 levels (Fig 6.11A). I chose to examine these neurons as they are easy to identify and have well-defined properties. I observed no significant change in CA1 PC electrophysiological parameters (voltage response was 100.3 ± 1.6% of control, p = 0.680, n = 6) in response to increasing the level of carbon dioxide (from 35 mmHg to 55 mm Hg CO_2; hypercapnia; Fig 6.11B-D).

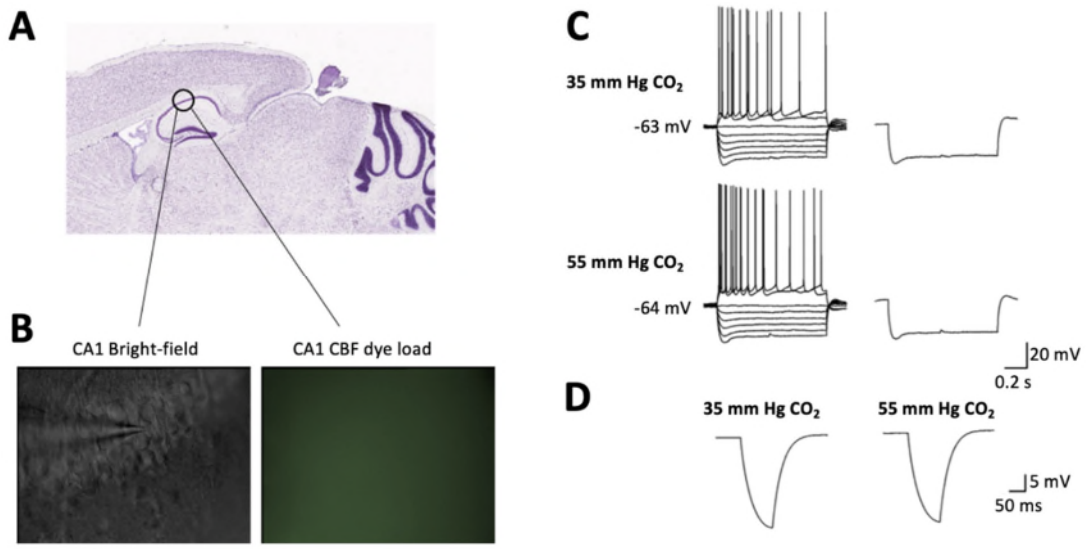

Figure 6.12: CA1 pyramidal cells show no dye loading or electrophysiological changes in response to high CO_2.

(A) The localisation of CA1 region of the hippocampus in a sagittal slice (Adapted from Allen Mouse Brain Atlas, 2004). *(B) (Left) Bright-field image of the CA1 region demonstrating the location of a recorded pyramidal cell. The slice was then subjected to carboxy-fluorescein (CBF) dye-loading (see Methods). There was no visible dye loading of the neurons (right). (C) (Top) Membrane potential traces recorded from a CA1 pyramidal neuron in response to current steps (3 s steps starting at -200 pA, increasing by 50 pA until regular firing pattern) in 35 mmHg CO_2. (Inset) Single membrane potential trace in response to the injection of -200 pA (3 s) in 35 mmHg CO_2. CO_2 levels were increased over a period of 300 seconds from 35 mm Hg to 55 mmHg CO_2, as in the SN and VTA experiments. (Bottom) Membrane potential traces*

recorded from the same CA1 pyramidal neuron in response to current steps in 55 mmHg CO_2. Single membrane potential trace in response to a -200 pA (3 s) current step in 55 mmHg CO_2. (D) Example membrane potential responses to a (100 ms) -50 pA current step. Traces (averaged from 20 sweeps) shown for 35 mmHg CO_2 (left) and 55 mmHg CO_2 (right). No difference in voltage response is observed when the level of CO_2 is increased.

6.3 Conclusion

I have demonstrated an unexpected CO_2-sensitivity phenotype for neurons in the SN and VTA, with increases in PCO_2 markedly increasing whole-cell conductance. This effect appears to occur in only specific subtypes of neurons, as for example it was not observed in hippocampal CA1 pyramidal cells. I have provided several lines of evidence that suggest that the CO_2 sensitive conductance results from the opening of Cx26 hemichannels, whose open probability increases through CO_2-mediated carbamylation of lysine residues (Meigh et al., 2013). I have shown that the effects of CO_2 in SN DNs occur over the same developmental period as they express Cx26 mRNA (measured in an independent study; Vandecasteele et al., 2006). The effects of increasing CO_2 on resting conductance could be blocked by the hemichannel inhibitor carbenoxolone. SN dopaminergic neurons and VTA GABAergic neurons could also be filled with a fluorescent dye (Carboxyfluorescein, CBF) when PCO_2 was increased (this is termed dye loading). My findings reveal an unexpected role for CO_2 in regulating the activity of these key brain regions and demonstrates a mechanism by which an CO_2 could alter complex goal-directed behaviours. There is no data in this current study on the physiological significance of CO_2 sensitivity, in particular regarding movement and reward behaviour; this will need to be examined in future studies.

Chapter 7: Discussion

I have undertaken four separate projects, three of which have focussed on quantitatively analysing the cellular and sub-cellular effects of various pathological agents on neuronal and synaptic function and the fourth on the discovery of CO_2 sensitivity in two key dopaminergic nuclei. I will now consider how my results fit in the context of their fields, discuss the limitations of the approaches I have taken and indicate how these projects could be extended in future studies to answer any remaining questions.

7.1 Chapter 3 – oTau mediated pathology

Although this is the first study of its kind for tau oligomers (oTau), the delivery of an oligomeric protein using whole-cell patch clamp has previously been published previously by my lab (Kaufmann et al., 2016). The estimated physiological concentration of tau within neurons is 2 µM (Avila, 2010) which is much higher than I have introduced here (44 - 666 nM). In this study, three different concentrations of oTau were tested to establish whether the effects were concentration-dependent. For layer V pyramidal cells (PCs), a higher concentration (666 nM) was used to give effects over a comparable timescale to that observed in CA1 neurons in the hippocampus, as they are larger neurons.

7.1.1 oTau alters action potential dynamics, input resistance and neuronal excitability

Both standard current-voltage relationships (SIV, with step current injections) and dynamic current-voltage relationships (DIV, with naturalistic current injection) were used to extract neuronal parameters and evaluate the effects of oligomer introduction at 10-minute time intervals (see Methods). As the time course for oTau to have effects varied between cells, for consistency of analysis the first and last time points of recordings were compared throughout. The last time point was selected to be 40-minutes as this is the time point in which most recordings still remained stable. I had hoped to be able to implement the dynamic IV modelling protocol (Badel et al., 2008a, 2008b;

Harrison et al., 2015) over the full time course of recording, however due to the increasing effects on action potential waveform, the protocol became less effective over time. I therefore only used it to parameterise the cells at 0 minutes to ensure that the recording quality and neuronal properties were comparable. The introduction of oTau into single cells produced significant changes to input resistance and firing rate.

With collaborators in the Zeeman Institute, I adapted and implemented a program to analyse action potential dynamics using Julia (Bezanson et al., 2017). It measures action potential amplitude (peak height), duration (full width-half max) and the rate of rise and decay from action potentials induced by the fluctuating naturalistic current input. This analysis allowed me to quantify the decrease in action potential amplitude and increase in duration as well as the slowing of both action potential rate of rise and decay. Lower concentrations of oTau took longer to achieve the same effects, thus illustrating the concentration-dependence of the effects.

A number of control experiments were used to validate the results. Firstly, no significant effect was observed when introducing the similarly sized aggregation-competent molecule BSA into cells. The effects of oTau were not due to blockage of the pipette tip as confirmed by stable series resistance measurements across the duration of the recordings and successful ‘re-patching’ experiments (Qui et al., 2014). This protocol gave stable responses in my control experiments. However, with oTau I demonstrated that the changes in action potential waveform are not simply a filtering effect and result may instead result from the modulation of specific voltage gated ion channels.

7.1.3 oTau impairs synaptic transmission and enhances synaptic depression

Next, given the effects on action potential dynamics, I wanted to investigate whether this translates into a change in transmission to neighbouring synaptically connected neurons. I made paired recordings in layer V neurons in the cortex and delivered oTau targeted to either the presynaptic or postsynaptic cell, while the rest of the network remained unaffected. In pairs where the presynaptic cell had been injected with oTau, the EPSPs were

reduced in amplitude over time even though the cells were still stable for the course of the recording. Even though the postsynaptic cell (generating the EPSPs) had no oTau introduced, the decline in transmission was clearly observed. This ruled out any changes in ligand gated ion channels (in particular AMPA receptors) in the postsynaptic cell being responsible for these changes. This is in contrast to the control cells, where the EPSP amplitude stayed constant over an hour of stable recording. There was also an enhancement of synaptic depression in the pairs when oTau was introduced into the presynaptic cell.

Though the effects on synaptic transmission could be a result of the changes to action potential waveform, it is more likely that there are two separate effects because the significant changes to the action potential waveform occurred around 30-40 minutes after whole breakthrough whereas the changes to synaptic transmission began much earlier (after 10-20 minutes). It has also been reported previously in squid giant axons that injection of human tau could directly alter synaptic transmission without changing the waveform of the action potentials. It could be that as the action potentials get smaller, they are unable to be propagated down the axon. However, this is unlikely as it has been shown that ‘spikelet’s’, which are much smaller than full size action potentials, can be fully propagated down the axons of CA1 cells (Apostolides et al., 2016). Further work could confirm this by performing paired recordings at the soma (site of oTau introduction) and the axonal bleb of the same neuron and looking at conductance of action potentials down the axon to look for branch-point failure.

The synaptic transmission deficits observed in my study match the published literature (McInnes et al., 2018; Zhou et al., 2017). In cultured hippocampal neurons, where a P301l tau construct had been delivered using an AAV viral vector, there was also enhanced synaptic depression with a train of stimuli, which resulted from the crosslinking of vesicles and actin (tau binds via the C-terminus to actin and via the N-terminus to the vesicles), this reduced vesicle mobility and the speed at which the vesicles could restock, interrupting trafficking and recycling. They were able to counteract these effects with a truncation of the N-terminal region of tau and also using a peptide that is

targeted to bind and block the N-terminus of full-length tau. Both approaches prevented the N-terminus binding to vesicles and restored vesicle motility (Zhou et al. 2017; Fig 7.1).

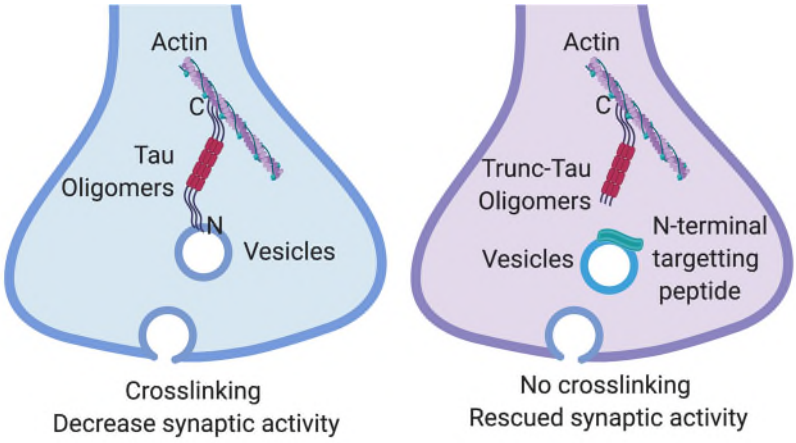

Figure 7.1: oTau crosslinks actin and vesicles, slowing vesicle recycling.
Schematic to explain the main findings by Zhou et al (2017) whereby tau binds via the C-terminus to actin and via the N-terminus to the vesicles, this reduces vesicle mobility and reduces the speed at which the vesicles can restock, interrupting trafficking and recycling. This results in enhanced synaptic depression and could be counteracted using a peptide targeting the vesicle binding region on the N terminus.

I have demonstrated a comparable increase in depression, consistent with their hypothesis of slower vesicle restock. However, this does not account for the changes to the first EPSP amplitude. Following on from the work conducted in this paper, it would be an interesting idea to test whether an N-terminal truncation of tau would rescue the effects that I observed in paired recordings, more specifically the oTau-mediated enhanced depression. This work directly complements a number of ongoing immunotherapy trials of N-terminally truncated tau in early Alzheimer's disease (e.g., BIIB092; Biogen). This study could provide evidence as to what is functionally happening in these individual neurons.

7.1.4 oTau does not affect basal synaptic transmission from postsynaptic sites

I observed no basal synaptic transmission defect when tau was introduced into the postsynaptic cell in the synaptically connected pair. In tauopathies, a high proportion of the native tau that does aggregate is hyperphosphorylated. This

is complicated to study as tau has 85 possible phosphorylation sites (Mair et al., 2016; Silva et al., 2016). Early phosphorylation of tau is known to play a role in its detachment from microtubules and mis-localisation to dendrites, but it has not been shown which residues are responsible. Teravskis et al., (2018) demonstrated that phosphorylation of Ser396 and Ser404 at the C-terminus are required for tau mis-localisation and then in order to disrupt AMPA receptor trafficking one of the following residues also needs to be phosphorylated (Ser202, Thr205, Thr212, Thr217 or Thr231), all of which can be found in the N-terminal domain. It is important to highlight that during the production of my oligomers there was no phosphorylation of the tau. However, they may be phosphorylated within the cell after introduction. I did not measure phosphorylation inside the single cells given the large number of phosphor-epitopes and that the fluorescence signal from a single phospho-epitope of introduced tau in a single cell would be too small to pick up with conventional confocal microscopy. Maybe this is because the oligomers were produced from a mechanism not reliant on hyperphosphorylation. They are however mis-localising so it would be interesting to find a way to check if Ser396 and Ser404 are being phosphorylated inside the cells from which I am recording. It is also worth noting that the sites needed for mediating the synaptic dysfunction are in the N-terminus; which fits nicely with my N-terminal truncation theory.

7.1.5 oTau impairs long term synaptic plasticity

Aggregated tau has been previously reported to impair some forms of synaptic plasticity including long-term potentiation (LTP) and long-term depression (LTD) (Fá et al 2016; Lasagna-Reeves et al, 2012; Ondrejack et al, 2018). In the next part of this project, I aimed to investigate whether impairment in LTP was a direct intracellular action of oTau rather than an extracellular action, and whether the effects were specific to the oligomeric forms of tau. I induced LTP in single cells using a high frequency tetanus stimulation. Upon receiving the stimulation, Na^+ flows in through AMPA receptors, depolarising the post synaptic compartment and activating NMDA receptors causing the influx of Ca^{2+} and an increase in the number of AMPA receptors at the membrane and potentiating transmission (Lu et al 2001, Chater and Goda, 2014). LTP was reliably induced in control cells and abolished with L689,560 confirming it to

be NMDA receptor-dependent. Tau oligomers at concentrations of 44 nM and 444 nM completely abolished long-term potentiation (and short-term potentiation) whereas monomers (444 nM) had little effect. The potentiation was slightly reduced compared to control but that could be due to reaggregation of tau inside the cell during the 45 minutes of recording.

In future experiments, I would like to investigate the mechanism of how oTau mediates this inhibition. It could be that it is increasing the threshold for eliciting LTP, and therefore as a result the depolarisation reaching the dendritic spines is not sufficiently high enough to remove the NMDA receptor Mg^{2+} block. If this were the case, a stronger stimulus would be required for the oTau cells to be potentiated, which would be a fairly simple hypothesis to test. If this was not the case, then the LTP would still be inhibited with a larger stimulus. Alternatively, it could be that oTau is directly affecting potentiation by altering some of the necessary molecular machinery or pathways required to generate plasticity. For example, tau could interrupt AMPA receptor insertion (Jurado, 2018). There is a wealth of evidence in tauopathy models showing that tau modulates AMPA trafficking and thus can alter synaptic strength in physiology (Suzuki and Kimura, 2017) and pathology, both in the presence of and independently of amyloid beta or alpha synuclein (Chang et al., 2006; Crimins et al., 2011; D'Amelio et al., 2011; Miller et al., 2014; Polydoro et al., 2009; Shrivastava et al., 2019). This would require a more in-depth pharmacological molecular approach.

A number of groups in the field have investigated other mechanisms of how tau might be mediating this reduction in LTP. To induce and maintain long-term potentiation, a number of plasticity-related genes need to be transcribed. Transcription factor cAMP response element-binding protein (CREB) can be activated by a range of kinases including mitogen- and stress-activated protein kinase 1 (MSK1), cAMP-dependent protein kinases (PKA) or mitogen-activated protein kinase/extracellular regulated kinase (MAPK/ERK) (Arthur et al., 2004; Privitera et al., 2020; Reyskens and Arthur, 2016; Teich et al., 2015). Once activated, transcription of plasticity related genes will occur, which are needed for successful long-term potentiation (Balschun et al., 2003; Barco et al., 2002; Bourtchuladze et al., 1994; Lee and Silva, 2009; Ran et al., 2012).

Thus, changes to CREB activity can alter synaptic plasticity. The level of phosphorylation of pCREB at serine 133, a key site for phosphorylation, has been shown to be considerably lower in Alzheimer's disease (Yamamoto-Sasaki et al., 1999). It was confirmed that oTau mediates a reduction in phospho-CREB and thus a reduction in the expression of immediate early genes c-fos and Arc, leading to impaired LTP (Acquarone et al., 2019). In future experiments, I would like to use RT-PCR to establish whether there are changes to these genes in my single cell assay to see if this is responsible for the reduction in potentiation. An alternative theory may be that 'non-pathological' tau could have important roles in plasticity physiologically and that oTau might bind to and sequester this native tau, removing it from the site where it normally acts at in the dendrites, thus affecting plasticity (Regan et al., 2015).

I also looked at long-term depression, another key form of plasticity at these synapses. Given that Acquarone et al., (2019) report reduced levels of ARC in the presence of tau oligomers and given that ARC is a key mediator of mGluR-LTD by causing the endocytosis of AMPA receptors (Wall et al., 2018; Waung et al., 2008), maybe ARC could be involved in the changes to LTD that I observe. This is something else that I could look at using single cell RT-PCR.

7.1.1 oTau can diffuse to synaptic sites during 30-minutes of recording

In a number of experiments Alexa fluor 594 hydrazide dye and Alexa fluor 488 labelled tau oligomers were both added to intracellular solution to look at mislocalisation of oTau within CA1 cells over 30-minutes of recording. Given the small amount of oTau introduced, it is not possible to visualise it within the recorded neuron during recordings or by using standard confocal imaging, hence the need for long timeframe AiryScan detection. Developed by Zeiss, it allows significantly better resolution and improved signal-to noise ratios (Huff, 2015). It enabled me to visualise the introduced oTau, at high resolution, determining where it had spread during the period of recording. oTau is able to travel from the site of introduction (soma) down the axon and reach distal

dendrites (beyond the bifurcation). This substantial finding is important as it is the first study to detail such rapid mislocalisation in a single neuron for tau oligomers. Given the short time frame, it is probably travelling by active transport, this could be evaluated in future studies. It would also be interesting to establish whether there is a specific region of tau required for mislocalisation and if so, what this is. It has been shown previously that tau can bind to vesicles via its N-terminus (Zhou et al., 2017). Theoretically tau might bind to vesicles in the soma and then get transported around the cell (attached to vesicles) and into the dendrites to the sites where synaptic sites can be found. If so, then a truncation of the binding region may prevent the mis-localisation. A limitation of this current study is that while I can confirm the localisation of the tau within the distal dendrites, I cannot confirm that the tau is localised specifically at post-synaptic sites without further co-staining for example with PSD-95. This approach is more complicated due to the length of time needed for imaging and the bleaching that occurs as a result of obtaining many large z-stacks as a tile scan over a period of ~24 hours across multiple wavelengths. It would finally also be beneficial to be able to visualise the oTau during my experiments to look at the time course of tau movement. In order to do this, a technique permitting the high resolution of Airyscan imaging whilst simultaneously making whole-cell patch clamp recording would be needed. This would also allow me to measure whether the introduced tau oligomers are secreted out of the introduced cell during the 30-minute timeframe.

7.1.6 Can the observations with recombinant tau be replicated with human Alzheimer's disease CSF samples?

Although recombinant tau allows precise control over what is introduced into neurons (in terms of concentration, structure, and form), it is not fully representative of the range of oligomers that are present in AD. A fraction of the toxic oTau pool in human AD brains is released into cerebrospinal fluid (CSF) in a manner that associates with pathological AD markers. CSF samples of patients with Alzheimer's disease will contain raised levels of amyloid-beta (Aβ42), total-tau and phospho-tau and can therefore be used as biomarkers

(Song et al., 2018). In future experiments, I would like to use human AD CSF samples to investigate if my single cell protocol can correlate the observed changes in neuronal and synaptic properties with the composition and concentration of oTau in CSF samples from AD patients and whether this then also correlates with patient data on disease severity.

To do this, I would first define the composition of each of the samples with a range of diagnostic parameters, including measurements of total tau, phospho-tau, amyloid beta 42, neurofilament light (a marker of neuronal damage or injury) and GFAP (glial cell marker). The samples would contain a range of tau concentrations depending on the degree of disease progression. The clinical cut off to define an AD-positive case are p-tau181 >60 ng/L, and total-tau >350 ng/L (Hansson et al., 2006). However, for advanced disease, samples will contain much higher concentrations of both tau and phospho-tau. The CSF samples will also contain other molecules e.g., amyloid beta, which could also potentially affect neuronal properties. To differentiate which effects are due to tau, a portion of each CSF sample would be immunodepleted for tau, using an established protocol (Cicognola et al., 2019) to complete removal of N-terminal region containing tau fragments (using an N-terminal antigen; confirmed with mass spectrometry imaging). In subsets of samples, a similar approach would be used to remove amyloid-beta, to explore independent and synergistic effects of tau and amyloid oligomers. I would compare the effects of introducing CSF from patients of varying pathological stages (AD, MCI, biomarker positive but cognitively normal along with age-matched healthy controls (experimenter blinded). The data I have obtained from recombinant tau gives me valuable information to guide the expected concentration-dependence of effects.

I have acquired these samples from collaborators at the University of Gothenburg. However, in initial experiments, I came across a complication in the implementation of this protocol. It would be best to introduce the same concentration of sample obtained from the patients into cells. However, it would be diluted by 50 x into patch solution. Samples will therefore need to be freeze dried and then buffer exchanged in order to concentrate the protein species without concentrating the salts, as ensuring the correct osmolarity is vital for patch clamp recording. Initially I would use standard and dynamic IV

curves to extract electrophysiological data over time as this is robust and reliable. To compliment this, I would then investigate the profiles of the CSF samples using common biomarkers for synaptic dysfunction. Established assays to measure SNAP-25, GAP-43, PSD-95 would be implemented and combined with the profiling of AD biomarkers. These samples could then be tested using my electrophysiological assay to assess effects on synaptic transmission and plasticity.

7.2 Truncating Tau Reveals Different Pathophysiological Actions of Oligomers in Single Neurons

In conditions such as Alzheimer's disease (AD), tau can dissociate from microtubules and then aggregate, with the small soluble oligomers (oTau) the most toxic species. However, the mechanisms of how oTau produces neuronal dysfunction are still not fully defined. By delivering oTau via the patch pipette (Hill et al., 2021, 2019; Kaufmann et al., 2016), I have demonstrated that full length oTau (FL-oTau) changes neuronal excitability, action potential dynamics, basal synaptic transmission and plasticity. Both labelled (Hill et al., 2019; Chapter 3) and unlabelled (this study; Chapter 4) FL-oTau had very similar effects: they both increased input resistance, increased excitability, increased action potential width and reduced action potential amplitude. This confirms that the labelling of tau and modifying the positions of the cysteine residues in tau (Hill et al., 2019) had little or no effect on the actions of oTau on neuronal properties.

7.2.1 Rationale of truncations

Since monomeric tau did not exert any oligomer-mediated toxicities, I hypothesised that the observed effects were due to conformational changes that occur to form soluble aggregates. However, given previous reports that the extreme N-terminus of tau inhibits oligomer and fibril formation (Horowitz et al., 2006; Lapointe et al., 2009), I reasoned that N-terminal and C-terminal fragments of tau should have different effects on neuronal function. The site of truncation was informed by the recent discovery of two clinically-relevant N-terminal fragments in human AD brains and CSF (N123 and N224; Cicognola et al., 2019) and the previously published evaluation of the role of the N-

terminal truncation (aa124-444) in mediating synaptic dysfunction (Largo-Barrientos et al., 2021; McInnes et al., 2018; Zhou et al., 2017). I therefore acquired recombinant versions of tau (from the University of Gothenburg) informed by a physiologically-relevant truncation at amino acid 123 that they had recently discovered in human AD brains and cerebrospinal fluid (Cicognola et al., 2019). I hypothesise that oligomers formed from N-terminal truncated tau (amino acids 124-444; C^{FRAG}) and soluble aggregates of the non-oligomer forming N-terminal fragment (amino acids 1-123; N^{FRAG}), will elicit distinct effects on single neuron physiology.

7.2.2 C^{FRAG} tau produces oligomers that increase excitability by changing spike threshold

I began investigating the mechanisms underlying the actions of FL oTau using an N-terminal truncation (C^{FRAG}). I found that C^{FRAG} tau oligomers did not replicate the effects on action potential kinetics or input resistance that I observed with FL oTau but despite this, they did increase excitability. I went on to demonstrate that this is mediated by a negative shift in rheobase (the minimum current needed to elicit an action potential), thus resulting in the neurons being more excitable. In my previous study (Hill et al., 2019; Chapter 3), I was unable to use the dynamic IV method (Badel et al., 2008a, 2008b; Harrison et al., 2015) to fully parameterise neuronal changes over the time course of the experiments due to the changes to action potential shape. As the action potential waveform was unaffected with the truncation, I was able to use the dynamic IV protocol and found that C^{FRAG} tau oligomers reduce the spike initiation threshold (making it ~ 4mV more hyperpolarised). There was no change in membrane potential and thus the difference between spike threshold and resting potential is reduced, increasing the likelihood of firing action potentials. To further confirm this observation, I used the parameters extracted from the dynamic IV curve at 0 minutes to simulate a voltage response using the exponential integrate and fire model (Fourcaud and Brunel, 2002; Fourcaud-Trocmé et al., 2003), demonstrating a comparable firing rate to the experimental traces. Then by manipulating only the spike initiation threshold by the mean reduction (4 mV), and re-running the simulation, I generated a trace which had comparable increase in firing rate as seen in the

experimental voltage recording at 40 minutes. Thus, confirming that the change in spike threshold alone is sufficient to mediate the change in neuronal excitability (Table 7).

7.2.3 The N-terminal fragment changes input resistance at high concentrations

I then investigated the fragment that had been removed to generate the truncation (amino acids 1-123; N^{FRAG}). This tau fragment has also been reported to make up a large proportion of the tau found in the CSF of Alzheimer's disease patients and it has been suggested that N-123 tau could represent a general marker of tau metabolism (Cicognola et al., 2019). N^{FRAG} does form aggregates but will not form the same structured oligomers as FL-oTau does, thus I expected it to have different effects. When the N-terminal fragment of tau was introduced into neurons at an equivalent concentration used for the FL tau (444 nM) it produced a rapid and large increase in input resistance together with a reduction in action potential amplitude and a marked slowing of action potential kinetics. These effects occurred within 5 minutes of whole-cell break-through. By measuring the neuronal time constant I found that the apparent cell capacitance had significantly decreased. This led me to hypothesise that the tau could be inferring with current flow in the cell soma and making it seem electrotonically more compact. I tested this by making double patch clamp recordings from the soma of a single neuron, introducing N^{FRAG} into one pipette and recording form both. I showed that although the input resistance had increased after 5 mins, the current flow between the two electrodes had significantly decreased. This suggests that the N^{FRAG} tau is aggregating and reducing current flow across the cell (Table 7). Given that in my original study (Hill et al, 2019; Chapter 3) I demonstrated a concentration-dependence of tau effects, I reduced the concentration of N^{FRAG} tau in order to be able to record for the full 40 minutes for comparison with the other species.

7.2.4 The N fragment changes action potential amplitude and width at low concentrations

Introducing the N^{FRAG} tau at lower concentrations (133 nM) selectively changed action potential amplitude and width without changing input

resistance. This suggests that the changes in action potential waveform are not simply due to increased filtering. To confirm this further, I tested N^{FRAG} tau monomers and observed comparable changes to action potentials. This was surprising given that tau-mediated dysfunction has been almost solely replicated with oligomers and aggregates, while monomeric versions are largely assumed not to be pathologically relevant. 133 nM N^{FRAG} tau monomers also altered the action potential waveform; thus, the effect is likely unrelated to structure and maybe instead due to a sequence in the N-terminus binding directly (Table 7). Given that both the rate of rise and decay are affected (Hill et al, 2019; Chapter 3), I hypothesised that the tau might be interacting with voltage-gated sodium channels and altering their function.

7.2.5 FL-oTau alters voltage-gated sodium currents

The neuronal function of sodium channels can be inferred from their kinetic properties as measured using whole-cell voltage clamp (Hodgkin and Huxley, 1952). Recording voltage-gated sodium currents in neurons in a brain slice is difficult because it is challenging to achieve a good voltage clamp due to the size of the neurons and resultant space clamp problems (Bar-Yehuda and Korngreen, 2008; Hartline and Castelfranco, 2003; Rall and Segev, 1985; Spruston et al., 1993; White et al., 1995). A large proportion of sodium channels are clustered in the axon initial segment (Castelli et al., 2007; Diwakar et al., 2009; Kole et al., 2008; Osorio et al., 2005; Royeck et al., 2008), and their voltage can differ significantly from that at the soma (Kole et al., 2008; Stuart et al., 1997). Therefore, when attempting to voltage clamp at the soma, these electrotonically remote sodium channels (to the site of recording) will generate unclamped action potentials, impeding the ability to measure controlled responses. To counteract this space clamp problem, most experiments looking at sodium currents are performed in reduced models such as nucleated patches, dissociated or cultured neurons. However, this is less relevant physiologically because the distribution and density of channels may not reflect the natural condition. Being able to record currents in slices provides information about channel function in their natural environment. I adapted a protocol (Milescu et al., 2010) which enabled me to make controlled voltage clamp recordings of sodium currents from neurons in acute brain slices.

Voltage-gated sodium channels are widely expressed across the CNS and PNS (de Lera Ruiz and Kraus, 2015). In the central nervous system (CNS), the channels that are the most abundant are Nav1.1, Nav1.2, Nav1.3, Nav1.5, and Nav1.6 (Wang et al., 2017). While Nav1.7, Nav1.8, and Nav1.9 are mainly found in the peripheral nervous system (PNS; Wang et al., 2017), they can also be found in certain regions of the brain. For example, Nav1.7 channels, located in the hypothalamus, are involved in the regulation of body weight (Branco et al., 2016). At the axon initial segment (AIS) of CA1 pyramidal neurons, NaV1.1, NaV1.2, and NaV1.6 channels have been detected (Akin et al., 2015; Boiko et al., 2001; Garrido et al., 2003; Hossain et al., 2005; Ogiwara et al., 2007; Van Wart et al., 2007; Van Wart and Matthews, 2006). NaV1.6 channels are highly abundant and have a more hyperpolarized voltage of activation compared with the other sodium channel isoforms, contributing to the lower activation threshold (Royeck et al., 2008). The sodium channels in the AIS probably make only a small contribution to the sodium currents I measured. This is a possible limitation of the technique that I have used. However, NaV1.6 is also present in the soma, although at less abundance than at AIS (Lorincz and Nusser, 2010). Despite this, the technique I have used allows controlled measurements of sodium channel currents in acute slices and provides more physiologically realistic information than recombinant sodium channels in cell lines.

FL-oTau had three effects on sodium channel currents: Firstly, the half activation was reduced, reflecting the increase in neuronal excitability, consistent with the effects of C^{FRAG}. Secondly, the rate of activation was reduced, underlying the slower AP rise, consistent with the effects of N^{FRAG} introduction. Finally, FL-oTau reduced $\bar{g}_{Na}$ (maximum sodium conductance) by ~ two thirds. To investigate the effects that this would have on the AP, I implemented a simplified AP model (Hodgkin and Huxley, 1952). Reducing $\bar{g}_{Na}$ had effects that matched the experimental data (reducing AP amplitude and increasing rise to threshold). Thus, this reduction in conductance alone could account for the changes in AP waveform that were observed experimentally.

From the unnormalized conductance plots, I noticed that the rate of conductance increase appeared faster for FL-oTau despite $\bar{g}_{Na}$ being reduced

(Fig 4.8) therefore, the effects are non-monotonic. Overall, it appears that there is a lower maximal conductance at 20 mins (and therefore AP height is reduced), but there is a small region at low voltages where the conductance is higher for FL-oTau, which means the model is more excitable. This means the profile of the I_{Na} activation has been changed by oTau; it is not just an issue of different maximal conductance magnitudes. It also suggests that an interaction with sodium channels could underlie both observed phenotypes. The simplest explanation for these observations is that specific a sequence in the N^{FRAG} tau is binding to the sodium channel to change the activation kinetics. Since the sodium currents are recorded in isolation, the most likely mechanism is a direct binding of the tau oligomers to the sodium channel.

The mammalian sodium channel is a molecular complex of an ~2000 amino acid α-subunit, which mediates the main channel functions and contains drug interaction sites, and smaller β-subunits, which modulate membrane expression (Catterall, 2012, 1981; Patino and Isom, 2010). The α-subunit is divided into 4 domains each with 6 segments (S1-S6). S1-4 form the voltage sensing domain (Kontis et al., 1997) and S5-6 form the pore forming domain. Upon depolarisation, S6 segments move leading to channel opening via the P-loop between S5 and S6 which forms the channel pore (de Lera Ruiz and Kraus, 2015; Fozzard et al., 2011). The S4 segments contain a high proportion of positively charged amino acid residues that make it responsive to changes in the membrane potential of the cell (Bezanilla, 2000). It is interesting to speculate on whether the tau oligomers could bind to the sodium channels to change the coupling between depolarisation and pore opening. Many studies have shown that changes in the S4 segments, associated linkers and cytoplasmic loops can all change the activation of the channels (de Lera Ruiz and Kraus, 2015; Fozzard et al., 2011).

Findings	FL- oTau (444 nM)	C^{FRAG}-oTau (444 nM)	N^{FRAG}-oTau (444 nM)	N^{FRAG}-oTau (133 nM)	N^{FRAG}-Tau (133 nM)	Mechanism?
AP height	↓	-	↓	↓	↓	Slower activation of voltage-gated sodium channels
AP width	↑	-	↑	↑	↑	
Input resistance	↑	-	↑	-	-	Aggregation in the soma impeding current flow, altering recorded capacitance.
Firing rate	↑	↑	-	-	-	Shift in spike initiation threshold (more hyperpolarised). Shift in the half activation of voltage-gated sodium channels
Rheobase	↓	↓	-	-	-	

Table 2.1: Summary of findings using recombinant truncations of tau and identified mechanisms

7.2.6 Future experiments

In future experiments, I would like to identify the minimal region of tau that is responsible for interacting with sodium channels. This could be done most efficiently using the mammalian two-hybrid system (M2H) to look for interactions between a library of fragments of the tau protein and the sodium channels expressed in CA1 neurons. This approach would permit quick identification of protein-protein interactions in a native cellular environment where post-translational modifications such as phosphorylation, acylation and glycosylation are possible (Luo et al., 1997). I could then use site-directed mutagenesis to disrupt these interactions and generate plasmids for human tau that cannot interact with sodium channels (termed $hTau^{MUT}$). Although my *in vitro* approach has provided detailed characterisation of the pathological actions of oTau; it cannot predict how these changes will modulate network function and ultimately behaviour. AAV-viral vectors provide a flexible approach to introduce tau (wild-type or mutant) via stereotaxic injection to a site of interest and then following tau expression, behaviour can be studied. This approach leaves endogenous mouse tau unaltered so there is less chance of unrelated effects (compared to transgenic approaches). Many studies using this approach have introduced versions of AAV-GFP-P301L-

hTau (a Frontotemporal dementia mutation which increases the likelihood of abnormal hyperphosphorylation; Alonso et al., 2004) and in line with the corresponding transgenic methods have highlighted neuronal dysfunction and behavioural deficits consistent with AD pathology. As my recombinant studies have been carried out with wild type (WT) full length tau, I looked instead for studies introducing AAV-GFP-hTau (non-mutant). In Yin et al., (2016), six weeks after injection with AAV-hTau expression in the CA3 region of the hippocampus of wild-type mice, there were measurable deficits in excitatory synaptic transmission, spatial and contextual memory (Yin et al., 2016). Using this experimental design, GFP-tagged AAV viral vectors for wild-type tau and for the identified mutant ($hTau^{MUT}$) could be generated and introduced into the hippocampus via stereotaxic injection to establish functional effects of binding (and lack thereof). The Barnes maze could also be used to measure spatial learning, memory retrieval, and cognitive flexibility. This would answer whether the role of the interaction with sodium channels is important in the synaptic and behavioural effects in the context of the cognitive dysfunction that typically occurs in AD.

Conclusion

I have demonstrated that by truncating tau and generating aggregates of specific regions, I am able to dissect apart a number of the effects observed with FL-oTau. This has allowed me to probe the mechanisms underlying the effects, discovering novel oTau-mediated changes to the spike initiation threshold and voltage-gated sodium channel kinetics (Table 8). Aside from providing a novel experimental tool, the findings with recombinant (but clinically-relevant) tau truncations pose an interesting hypothesis with regards to pathology too. If tau is primarily present as the C^{FRAG} form, then it will mostly affect excitability and not change action potential waveform. However, if the N^{FRAG} accumulates in the soma it will have large effects on neuronal integration and action potential waveform. Identifying the regions of tau mediating neuronal dysfunction will assist in tracking down protein-protein interactions, help design assays for interacting partners and provide a mechanistic framework for drug development.

7.3 Chapter 5 – αSyn mediated pathology

Here I have used whole-cell patch-clamp recording to introduce a known concentration and form of aggregated alpha synuclein (αSyn) into single substantia nigra pars compacta (SNpc) dopaminergic neurons in acutely isolated mouse slices.

7.3.1 Characterisation of the aggregates

Alpha synuclein was purchased as preformed fibrils (PFFs) and ultrasonication was used to break them down to oligomeric form (as in Polinski et al., 2018). While the majority of the αSyn sample displayed clear oligomeric structure, I cannot rule out the presence of other small aggregates like small ~ 50 nm fibrils (Polinski et al., 2018). A recent study has developed a new method used emerging technologies to fully isolate just the oligomeric fractions of alpha synuclein (Kumar et al., 2020), it would be interesting in future experiments to repeat these experiments with a purely oligomeric prep

7.3.2 Alpha-synuclein aggregates, but not monomers, alter the electrophysiological properties of SN DNs.

Both standard current-voltage relationships (SIV, with step current injections) and dynamic current-voltage relationships (DIV, with naturalistic current injection) were used to extract neuronal parameters and evaluate the effects of aggregate introduction. A significant increase in whole-cell conductance (fall in input resistance) was observed between 8-16 minutes after whole-cell break through, indicative of the opening of a membrane channel. This increase in conductance was paired with a reduction of both the induced and spontaneous firing rate (a measure of neuronal excitability) as well as abolishing rebound firing, which is normally characteristic of dopaminergic neurons following the input of a hyperpolarising step. These effects were only seen with the aggregated forms of alpha synuclein, but not with monomeric alpha synuclein or in the control cells. Changes to conductance and excitability began to occur between 8-16 minutes post whole-cell breakthrough. It may be that the alpha synuclein aggregates need time to reach a certain concentration before the channels can be opened. By comparison, in Chapter 3, introduction of

aggregated tau (444 nM) into pyramidal neurons started to have effects on the action potential within the first 10 minutes (Hill et al., 2019). In future experiments, I would like to evaluate whether there is a concentration-dependent effect of alpha synuclein aggregates, perhaps with lower concentrations having a slower onset (as in Chapter 3; Hill et al., 2019).

7.3.3 Modelling DNs.

I had originally hoped to be able to use the dynamic IV method to parameterise these dopaminergic neurons as it provides a good method to develop simplified, but empirically-verified models of neuronal responses based on experimental data. The protocol was originally developed for pyramidal neurons and interneurons (Badel et al., 2008a, 2008b) and has been applied in my lab to cortical layer V neurons and hippocampal CA1 neurons (Harrison et al., 2015; Hill et al., 2019; Kaufmann et al., 2016). The method is effective in these neurons as their currents are broadly linear away from the action potential threshold. Dopaminergic neurons, on the other hand express significant non-linear currents (Neuhoff et al., 2002; Richards et al., 1997), therefore the DIV curves diverge away from a standard ohmic linear response (Fig 7.2).

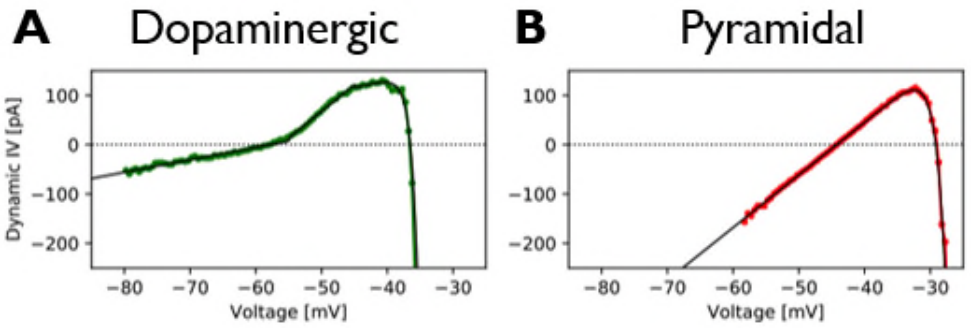

Figure 7.2: Dopaminergic neurons have non-linear dynamic IV curves.
A) Example dynamic IV curve for a dopaminergic neuron, clearly displays a non-linear form compared to the example dynamic IV curve for the pyramidal neuron in (B). The non-linearity is likely to result from their expression of significant non-linear currents (Neuhoff et al., 2002; Richards et al., 1997).

It would significantly aid the quantitative analysis of future experiments if the dynamic IV protocol could be adapted to better fit neurons that differ from the standard linear form. This would allow a greater investigation of the effects of alpha synuclein on neuronal function in dopaminergic neurons, however this modelling was outside the scope of my PhD.

7.3.4 The decrease in conductance and firing rate caused by alpha synuclein is in part due to the opening of K_{ATP} channels

K_{ATP} channels are inwardly rectifying K^+-selective ion channels that are inhibited by intracellular ATP. They provide a link between the energy state of cells and their electrical activity acting as a metabolically controlled "brake on excitation". When there is a decrease in sub-membrane ATP levels and an accompanying rise in ADP concentration (during activity), this triggers K_{ATP} channel opening, thus resulting in a drop in input resistance, K^+ moves out of the cell, inducing hyperpolarisation of the membrane potential (Haller et al., 2001; Seino, 1999; Stanford and Lacey, 1995). This mechanism protects against glutamate excitotoxicity and calcium overload and has thus important functions in neuroprotection in epilepsy or ischemia (Liss and Roeper, 2001). Conversely, when ATP levels are high, ATP binds to K_{ATP} channels and inactivates them, leading to increased neuronal firing and neurotransmitter release.

K_{ATP} channels consist of a Kir6.x (inwardly rectifying Kir6.1 or Kir6.2) pore-forming subunit and a sulfonylurea receptor (SUR1 or SUR2) subunit which binds ATP (Inagaki et al., 1995; Sakura et al., 1995). K_{ATP} channels are ubiquitously expressed across the basal ganglia and the cortex but the expression of subunits differs across regions (Liss et al., 2005; Schiemann et al., 2012). For example in the SN (an area with enhanced vulnerability to Parkinson's pathology), the expression of SUR1 is two-fold higher than in the VTA (a region less susceptible to damage), providing a potential reason for the difference in vulnerability (Han et al., 2018; Liss et al., 2005). An upregulation of SUR1 (but not SUR2B or Kir6.2) has also been confirmed in both PD brains and in alpha synuclein overexpression cultured systems suggesting that SUR1 expression will correlate well with vulnerability to pathology (Liss et al., 2005).

In dopaminergic neurons of the substantia nigra, K_{ATP} channels are more sensitive to mitochondrial complex I inhibitors, like rotenone or 1-methyl-4-phenyl- 1,2,3,6-tetrahydropyridine (MPTP), which are commonly used to induce models of oxidative stress induced Parkinson's disease pathology which may contribute to their enhanced vulnerability (Han et al., 2018; Röper and Ashcroft, 1995; Santos et al., 2019).

K_{ATP} channels also have functions outside of neuroprotection, for example in glucose sensing. Within the hypothalamus there are regions of neurons that respond to changes in nutrients and hormones and can detect fluctuations in glucose levels (Anand et al., 1964; Levin et al., 1999; Oomura et al., 1964) which is important to help regulate energy intake (Navarro et al., 1996). These neurons can be divided into subgroups that are excited by or inhibited by rises in glucose level. In the neurons that are excited by raised glucose, in low glucose conditions for example hypoglycaemia, their activity can be regulated by the activation of K_{ATP} channels, hyperpolarising them and reducing neuronal activity (Oomura et al., 1969; Trapp and Ashcroft, 1997). This can occur in the absence of any change in ATP/ADP ratio (Dadak et al., 2017). Injection of glibenclamide into the ventromedial hypothalamus confirms the role of K_{ATP} channels in neuronal defence against glucose deprivation (Evans et al., 2004).

K_{ATP} channel activity can also be regulated indirectly through glia. The subfornical organ (SFO), which is located on the anterior wall of the third ventricle, is a key region for sensing Na concentration to regulate water and salt uptake. Here there are glial cells that express Na_x channels are coupled to the Na^+/K^+-ATPase (Shimizu et al., 2007). When Na_x channels open the Na^+/K^+-ATPase is activated and consumes more ATP. Glucose is taken up into glial cells which is used in anaerobic glycolysis to produce ATP to fuel the pump. Lactate is also produced as a by-product and is then released from the glial cells. The Na_x-positive glial cells surround a population of GABAergic neurons in the SFO (Hiyama and Noda, 2016; Watanabe et al., 2006). The released lactate is taken up into these GABAergic neurons and oxidised causing an increase in intracellular ATP which closes K_{ATP} channels and thus depolarises the neurons and increases their firing rate (Hiyama and Noda, 2016).

Glibenclamide is a commonly used antidiabetic K_{ATP} channel inhibitor which can act from both sides of the membrane and its action is normally antagonised by the presence of internal MgADP (Jiang and Haddad, 1997; Light and French, 1994; Ripoll et al., 1993). 100 nM Glibenclamide can counteract the opening of K_{ATP} channels (and the subsequent conductance changes) that occur with the rotenone model of PD (Liss et al., 1999). It has also recently been demonstrated (Thakur et al., 2019), that 10 nM alpha synuclein oligomers delivered via the patch pipette mediate a reduction in tonic firing and that this could be prevented by preincubation of slices (and bath application) with 1 µM glibenclamide.

I therefore repeated my experiments (both control and alpha synuclein aggregate introduction after preincubating my slices with 1 µM glibenclamide. In control cells, there were no significant differences in any of the measured parameters between cells that had or had not been preincubated with glibenclamide, suggesting that there are very few K_{ATP} channels open physiologically. Given that they are inhibited by intracellular ATP and that my patch solution contained 2 mM ATP, the closure at rest is not surprising. However K_{ATP} channels can differ in their affinity for ATP and so there may be some channels that are not inhibited by this level of ATP (Allen and Brown, 2004). There is also evidence that local levels of ATP surrounding the K_{ATP} channel, which can be mediated by glucose transporters in close proximity to the K_{ATP} channel can influence activation, independently of the global ATP level of the neuron, which will be regulated by mitochondrial activity (López-Gambero et al., 2019; Lynch et al, 1988). Thus despite the high ATP in my patch solution K_{ATP} channels may still be able to open. It is also possible that the effects of alpha synuclein are via a direct action on the channel rather than via a reduction in intracellular ATP (as is seen with mitochondrial dysfunction in models such as rotenone and MPTP detailed above). Channel openers like diazoxide have previously been shown to directly open K_{ATP} channels in despite the presence of ATP (Schwanstecher et al., 1998), so it is possible that αSyn aggregates could have a similar direct action.

In glibenclamide-preincubated slices, cells that had alpha synuclein aggregates introduced displayed a reduction in the aggregate-mediated

changes in conductance and excitability, as would be consistent with the opening of K_{ATP} channels. However, I observed no associated membrane hyperpolarisation, which would be expected upon K_{ATP} channel activation due to the equilibrium potential for K^+ being ~ -95 mV (Allen and Brown, 2004; Stanford and Lacey, 1995). It could be that this hyperpolarisation is being counteracted by the opening of other channels which could depolarise the membrane. For example it has been reported that alpha synuclein itself can form non-selective cation channels as well as inducing local spontaneous increases in intracellular Na^+ and Ca^+ channels, depolarising neurons and stimulating the opening of K_{ATP} channels (Mironov, 2015). Dopaminergic neurons in the substantia nigra have prominent cyclic nucleotide gated HCN channels I(h) which are activated by hyperpolarisation. They have a reversal potential of ~-40 to -30 mV (Mayer and Westbrook, 1983). It is possible that the introduction of alpha synuclein oligomers only opens a relatively small number of K_{ATP} channels so is insufficient to change the membrane potential against the responsive reaction of I(h), however enough are opened to generate the changes to the input resistance/conductance of neurons. Whereas, in models where the intracellular ATP concentration is depleted or in the presence of K_{ATP} channel openers, many more K_{ATP} channels may be opened, overcoming the effects of I(h) leading to robust membrane hyperpolarisation, as is commonly reported (Stanford and Lacey, 1995). To definitively show that K_{ATP} is the channel involved in this conductance change then a transgenic mouse where the K_{ATP} gene has been deleted or using a cell line expressing the K_{ATP} channels that are normally present in the substantia nigra would be needed. These would-be good follow up experiments from this study.

In terms of pathology, it is possible that the accumulation of alpha synuclein aggregates in substantia nigra dopaminergic neurons during Parkinson's disease progression could potentially result in the prolonged activation of K_{ATP} channels which would chronically reduce electrical activity and also reduce the amount of dopamine released (Avshalumov and Rice, 2003; Patel et al., 2011), which will be detrimental to neuron function with the loss of the metabolic feedback mechanism. This is supported by retrospective epidemiological

evidence that there is a reduced risk for developing Parkinson's disease in type 2 diabetic patients that have been treated with K_{ATP} inhibitors (Brauer et al., 2015; Cereda et al., 2013; Lu et al., 2014; Schernhammer et al., 2011; Wahlqvist et al., 2012).

In future experiments, it would be good to be able to determine fully the relationship between aggregated αSyn and K_{ATP} channels. The opening of K_{ATP} channels by aggregated αSyn occurs despite the presence of 2 mM ATP and phosphocreatine in the patch pipette. Thus, it is likely to be a direct effect on the channel. To test this, I would express recombinant K_{ATP} channels and measure the effects of aggregated αSyn introduced via the patch pipette. I will also investigate whether there are smaller effects in less vulnerable regions of DNs to PD pathology (e.g., VTA) as they are known to have different K_{ATP} subunit expression (Liss et al., 2005). Single-cell RT-PCR could also be used to quantify the expression of different K_{ATP} subunits which can be correlated with changes in neuronal function.

7.3.5 Mosaic effect of aggregated alpha synuclein in layer V of the cortex

My lab had previously published a study in which oligomeric forms of alpha synuclein protein (500 nM) were introduced into single layer V neurons in the neocortex via the patch pipette (Kaufmann et al., 2016). They reported a very rapid time-dependent decrease in input resistance (occurring in the first 8 minutes of recording) and then a plateau for the remainder of the recording time. They also observed a decrease in both the firing rate of cells and the width of evoked action potentials (Kaufmann et al., 2016). In a subset of experiments, I decided to replicate this study and check that my aggregates had the same effects. I recorded from layer V pyramidal neurons in the neocortex (identified by their location, electrophysiological phenotype, and profile after being filled with Alexa fluor dye) and introduced either alpha synuclein 500 nM (n=9) or PBS (vehicle, n=9), in the internal solution to single neurons through the patch pipette. The mice were age-matched to the original study and the same concentration of oligomer was used. I observed that half of the recorded neurons exhibited a similar phenotype (decrease in input

resistance and firing rate) but that there were also a number of unaffected neurons. In the original study, two mutations commonly found in PD which make alpha synuclein more prone to aggregation had been induced (E46K,Y39W; Kaufmann et al., 2016). The alpha synuclein used in my study was wild type, so will be less prone to aggregation which might explain why the effects that I observed were less rapid.

In future studies it would be interesting to explore why only some neurons are affected. It is well established that the endogenous expression of alpha synuclein varies from cell to cell across regions like the cortex. Recently a number of important studies have indicated that the ability of alpha synuclein aggregates to seed pathology (upon spreading between neurons) is reliant on the recipient neuron expressing endogenous alpha synuclein (Courte et al., 2020; Luna et al., 2018). In cell culture models where alpha synuclein was knocked out, it was not possible to seed the pathology into the neurons (Courte et al., 2020). In two further studies, antisense oligonucleotides were used to knockdown alpha synuclein mRNA and protein, both *in vitro* and *in vivo* and this prevented the seeding of pathology and ameliorated neurological deficits (Alarcón-Arís et al., 2018; Uehara et al., 2019). A limitation of these studies is that they cannot answer whether these neurons are directly affected (after the aggregates have been up taken into the cells) or whether the uptake of the aggregates are blocked by the lack of endogenous alpha synuclein. I would like to implement my single cell delivery method to assess whether the cells are actually immune to the aggregate-mediated pathology when it is introduced directly or whether it is just blocking the uptake step. This could be done effectively using single cell RT-PCR to quantify and correlate the electrophysiological responses with the expression of endogenous alpha synuclein or by performing the experiments in a recently developed alpha synuclein GFP tagged mouse model (Caputo et al., 2020).

Therapeutically there is potential to utilise this to try to combat alpha synuclein-mediated pathology and associated degeneration. A number of different approaches are being trialled including the application CRISPR-deactivated Cas9 to downregulate the levels of SNCA in patient-derived dopaminergic neurons. This downregulation was sufficient to prevent the mitochondrial ROS

production and rescue cellular viability. As discussed in the introduction, one of the key limitations to dopaminergic neuron grafts in gene therapy is that the grafted neurons are themselves susceptible to the pathology over time. If by knocking down alpha synuclein, these new neurons are no longer susceptible to pathology, then that would be a huge advance on the potential that the treatment can give in terms of longevity of quality of life.

7.4 Chapter 6 – CO_2 sensitivity in two key dopaminergic nuclei

It is well established that Connexin 26 hemichannels are directly sensitive to physiological changes in the level of CO_2. Raised CO_2 directly mediates the carbamylation of lysine 125 (de Wolf et al., 2016; Huckstepp et al., 2010b, 2010a; Meigh et al., 2013) and increases their open probability. Therefore, an increase in CO_2 will increase whole-cell conductance. CO_2 sensitive connexins are normally found in astrocytes or oligodendrocytes, for example on the surface of the medulla oblongata (Nagy et al., 2011; van de Wiel et al., 2020).

Dopaminergic neurons were first discovered to be electrically coupled by gap junctions by Grace and Bunney, (1983) using a combination of electrophysiology and dye-coupling experiments. This was confirmed by a separate study (Vandecasteele et al., 2005) and later the same group went on to evaluate the expression profile of connexins in dopaminergic neurons using single cell RT-PCR (Vandecasteele et al., 2006). In P7-10 mice, connexins 26 and 30 were both present, but the expression is gone by P17, demonstrating a developmental switch in expression (Vandecasteele et al 2006). It is well established that Connexin 26 hemichannels are directly sensitive to physiological changes in the level of CO_2. Raised CO_2 directly mediates the carbamylation of lysine 125 (de Wolf et al., 2016; Huckstepp et al., 2010b, 2010a; Meigh et al., 2013) and increases their open probability. Therefore, an increase in CO_2 will increase whole-cell conductance. It is particularly intriguing as CO_2 sensitive connexins are normally found in astrocytes or oligodendrocytes, for example on the surface of the medulla oblongata (Nagy et al., 2011; van de Wiel et al., 2020). A limitation of single cell RT-PCR is that it does not tell you that the protein is there or that it is functional, just that there

Cx26 is expressed. I therefore used electrophysiology and dye-loading to look for the presence of functional connexin hemichannels.

7.4.1 CO_2-sensitivity in substantia nigra dopaminergic neurons is dependent on developmental stage

Dopaminergic neurons were identified by their electrophysiological profile and using immunohistochemistry. I did not find evidence of dye coupling between neurons that I had filled for identification, this is likely because Alexa Fluor 594 cannot easily pass through Cx26 channels (Weber et al., 2004). In substantia nigra DNs of P7-10 mice (but not P17-20 or control mice), when CO_2 was raised from 35 mm Hg CO_2 to 55 mm Hg CO_2, an increase in whole-cell conductance was observed (indicating the opening of a membrane channel). In the same mice, the opposite effect (decrease in whole-cell conductance) was observed when CO_2 was reduced from 35 mm Hg CO_2 to 20 mm Hg CO_2. These observations are in line with the developmental expression profile outlined in Vandecasteele's study (2006). My observations were not an artefact of the dialysis of the cell following whole-cell breakthrough as the cells were firstly allowed time to equilibrate, then standard and naturalistic currents were injected to form IV curves. In a subset of neurons, pharmacological agents were applied to characterise the cells (~30 mins to apply and wash) prior to the alteration of CO_2.

7.4.2 Comparable sensitivity to CO_2 in GABAergic neurons in the VTA

The ventral tegmental area (VTA) is highly heterogeneous and a core region of dopaminergic signalling in the brain. It has subgroups of neurons that can singularly release dopamine, glutamate or GABA or co-release a combination, allowing the VTA to function flexibly (Bouarab et al., 2019; Morales and Root, 2014; Root et al., 2018; Takata et al., 2018; Yoo et al., 2016). I have demonstrated that a subpopulation of VTA GABAergic neurons are also directly sensitive to level of CO_2 and that this is mediated via connexin 26 (Cx26) membrane hemichannels. This has potentially interesting implications in a number of VTA mediated behaviours including reward, sleep/wake and arousal (Bouarab et al., 2019, Eshel et al., 2015; Eban-Rothschild et al., 2016;

Fifel et al., 2018; Simmons et al., 2017; Tan et al., 2012; Takata et al., 2018; Yu et al., 2019; van Zessen et al., 2012).

7.4.3 Changes are not mediated by an alteration in pH

Changing the level of CO_2 experimentally (without compensation) will result in a change in pH. The role of pH-sensitive receptors in the control of breathing is well established, both in the periphery and centrally in the medullary chemosensory areas such as the retrotrapezoid nucleus and the medullary raphe (Gourine et al., 2010; Hosford et al., 2018; Kumar et al., 2014; Loeschcke, 1982; Trapp et al., 2008; Wang et al., 2013). However, there is considerable evidence that CO_2 can have additional effects that are completely independent from pH (Eldridge et al., 1985; Shams, 1985). To separate the effects of CO_2 from any effects of changing pH, I kept extracellular pH constant using isohydric solutions (an increase in pCO_2 under these conditions is often termed isohydric hypercapnia). It is also well documented that intracellular pH will transiently acidify when the level of CO_2 is raised and transiently alkalinise on its removal (Filosa et al., 2002; Putnam, 2001). In my study, I did not measure intracellular changes in pH, however, a mild intracellular acidification would be expected to result in hemichannel closure and a decrease in conductance. Thus, these transient changes in pH cannot explain the marked and sustained changes in conductance that only occur in these specific subtypes of neuron. There was also no effect of changing CO_2 (with isohydric solutions) both on dopaminergic neurons in the substantia nigra of older mice (P17-21) and in pyramidal cells in the CA1 region of the hippocampus. If the effect was due to pH change (and independent of connexin expression) then the same results would be expected in both age groups.

7.4.4 Whole-cell conductance and neuronal excitability changes are mediated by the opening and closing of hemichannels

Hemichannel function has been overlooked for a long time as focus was placed instead on understanding gap junction coupling. However, there is increasing evidence that hemichannels have important and independent roles from those mediated by gap junctions. Cx26 is a great example of this. It has opposite effects on conductance depending on whether it is assembled as part of a

hemichannel or as part of a gap junction. These effects observed in my study are unlikely to be gap junction-mediated as raised CO_2 would close Cx26 gap junctions and result in a reduction of the current that can leave the cell, therefore increasing the input resistance and neuronal excitability, which is the opposite of what was observed in my study (Nijjar et al., 2021). Whereas, if the effect of CO_2 on cell conductance is due to the opening of Cx26 hemichannels, it would be predicted, that since the midpoint of Cx26 hemichannel opening lies around the basal level of CO_2 in my experiments (Huckstepp et al., 2010b, 35 mm Hg), that a decrease in pCO_2 would close Cx26 hemichannels leading to a decrease in the resting conductance. I have presented several lines of evidence to confirm that the observed effects are through hemichannels. Firstly, the changes in conductance were blocked by carbenoxolone which is an indiscriminate hemichannel blocker. It is important to note that although carbenoxolone alone can have effects on neuronal and synaptic function (Tovar et al., 2009), they would be expected to increase the conductance rather than reduce it so the native effects will not influence my results with CO_2. To further confirm this, I observed no significant differences in electrophysiological properties of cells that had been pre-incubated in carbenoxolone compared to those that had not. In the Vandecasteele (2006) study they looked for functional hemichannels using dye loading with Lucifer yellow, in low calcium conditions and found no evidence of dye loading, therefore concluding that there are no hemichannels there. However, it could be that Lucifer yellow cannot pass through SNpc hemichannels, potentially if they are heteromeric they may not let the dye pass through. Instead, I used a dye that I knew would be able to pass through connexin 26 hemichannels – Carboxyfluorescein (CBF). SN dopaminergic neurons and VTA GABAergic neurons could be filled with CBF when pCO_2 was increased. Unfortunately, CBF cannot be fixed as it does not have the correct chemical groups and so the dye-filled cells cannot be subsequently labelled with antibodies (personal communication, Dale). However, I can be confident that the dye-filled cells were either SN DNs or VTA GABAergic neurons, as patch clamp recording was carried out before the dye loading (to confirm the identity of the cells from their electrophysiological properties and pharmacology) and then the same

region of cells were subsequently dye filled. I have also used immunohistochemistry to show that Cx26 protein is expressed in these neurons and confirm their identity. The expression pattern of Cx26 across development in SN DNs matches that reported for Cx26 mRNA expression (Vandecasteele et al., 2006). The same Cx26 antibody has extensively been used to study the role of Cx26 in breathing and recent studies have shown that there is no Cx26 labelling in Cx26 KO mice, confirming its specificity (Dale, personal observation). Cx26 staining of the leptomeninges across development was also used as a positive control. A potential limitation of the study is that I did not quantify the expression pattern of Connexin 26 in either TH+ or GAD+ neurons. In the future, tools like fluorescent in situ hybridisation (FISH) could be used to produce more accurate measurements of expression.

7.4.5 Functional implications in behaviour

I have described a novel CO_2-sensitivity phenotype of dopaminergic neurons in the substantia nigra and GABAergic neurons in the VTA. Cx26 open probability shifts when the CO_2 level changes within a physiological range, therefore neuronal excitability and potentially network output could also be affected. Given that these regions have important roles in the modulation of many behaviours, it is interesting to speculate how this sensitivity could play a role in modulating these behaviours through altering neuronal conductance and excitability. It is also potentially of interest that it is maintained in the VTA but lost in the SN. Maybe it provides some protection by inhibiting activity and this is a reason for the vulnerability of SN vs VTA neurons in PD.

Given that the substantia nigra is involved in the co-ordination of movement, in future experiments it would be interesting to evaluate whether CO_2-mediated changes to neuronal excitability alter the amount of dopamine that is released in the striatum and whether this has functional implications. Another intriguing finding was that the expression of Cx26 switches from neurons in young mice to glial cells after P17. This may be representing a shift from inhibition to excitation as in the neurons, raising CO_2 levels resulted in an inhibition of activity, whereas in glial cells that express connexin 26, when CO_2 is raised, molecules such as ATP are released (Huckstepp et al., 2010a) which would

excite dopaminergic neurons. Changes to dopamine release could be measured with fast-scan cyclic voltammetry (FSCV), using carbon fibre microelectrodes for detection as they are highly sensitive to monoamines (Puthongkham and Venton, 2020; Stamford, 1990). The age of the mice might make recording release challenging and it is not known whether connexin 26 is present at the terminals in the striatum. The sensitivity in the VTA is maintained up to P17-21 (at least). However, I have only examined a subset of GABAergic VTA neurons, which show sensitivity to [Met]enkephalin. If other VTA GABAergic or DNs are insensitive to CO_2, then exposure to CO_2 could differentially shift the output of the VTA.

VTA GABAergic neurons directly modulate the activity of neighbouring dopaminergic neurons (DNs) locally as well as have long range projections (Bouarab et al., 2019). I would like to explore whether the CO_2-mediated changes in GABAergic firing pattern that I observe *in vitro* would translate into an alteration in dopamine release *in vivo*. FSCV can be used *in vivo* (Fortin et al., 2015), however recent advances in the generation of fluorescent dopamine sensors allow for easier detection using fibre photometry (Patriarchi et al., 2018; Robinson et al., 2019). In order to determine which dopaminergic projections are affected by VTA GABAergic CO_2 sensitivity, I could make viral injections into potential DN target sites including the nucleus accumbens and prefrontal cortex to induce expression of the fluorescent dopamine sensor, dLight (Patriarchi et al., 2018; Robinson et al., 2019). Then I could use fibre photometry in a simple open field test to look for changes in dopamine release as CO_2 levels are manipulated.

GABA neurons in the VTA also have established roles in sleep/ wake and arousal behaviours (Eban-Rothschild et al., 2016; Fifel et al., 2018; Takata et al., 2018; Yu et al., 2019). Thus, modulation of their activity by changing levels the of CO_2 could potentially alter arousal and wakefulness and directly impact purposeful behaviours. To examine this, I could use a recently developed genetic tool, the viral construct $Cx26^{DN}$ (dominant negative), which allows connexin 26 to assemble into hemichannels but prevents them from opening in response to CO_2. I would target this virus into GABAergic VTA neurons to remove the sensitivity. I could then verify the loss of sensitivity using

immunohistochemistry, electrophysiology and dye loading before investigating whether Cx26 contributes to the VTA GABAergic role in arousal. To do this, I could use fibre photometry to record dopamine release while monitoring sleep states with EEG/EMG recordings and combine this with whole body plethysmography to evaluate changes to breathing as I manipulate CO_2 levels.

In the VTA, both dopaminergic neurons and the neighbouring GABAergic neurons are directly involved in reward and aversion-related behaviours (Bouarab et al., 2019; Eshel et al., 2015; McCutcheon et al., 2012; Tan et al., 2012; van Zessen et al., 2012). I could also combine fibre photometry with behavioural analysis to determine whether there is an alteration in normal reward responses (e.g., response to un-signalled sugar pellet delivery or reward-predictive stimuli) as CO_2 levels are manipulated. Drugs of abuse can act to suppress the inhibitory activity of GABAergic neurons that synapse onto dopaminergic neurons, thus increasing their activity. I could explore whether the rewarding properties of these drugs (e.g., cocaine, opiates, benzodiazepines) are altered as I manipulate CO_2 levels. This could lead to radically novel therapeutic possibilities for managing responses to these drugs.

References

Abeliovich, A., Schmitz, Y., Fariñas, I., Choi-Lundberg, D., Ho, W.H., Castillo, P.E., Shinsky, N., Verdugo, J.M., Armanini, M., Ryan, A., Hynes, M., Phillips, H., Sulzer, D., Rosenthal, A., (2000). Mice lacking alpha-synuclein display functional deficits in the nigrostriatal dopamine system. Neuron 25, 239–252. https://doi.org/10.1016/s0896-6273(00)80886-7

Abraham, W.C., Jones, O.D., Glanzman, D.L., (2019). Is plasticity of synapses the mechanism of long-term memory storage? NPJ Science of Learning. 4, 1–10. https://doi.org/10.1038/s41539-019-0048-y

Acquarone, E., Argyrousi, E.K., van den Berg, M., Gulisano, W., Fà, M., Staniszewski, A., Calcagno, E., Zuccarello, E., D'Adamio, L., Deng, S.-X., Puzzo, D., Arancio, O., Fiorito, J., (2019). Synaptic and memory dysfunction induced by tau oligomers is rescued by up-regulation of the nitric oxide cascade. Molecular Neurodegeneration 14, 26. https://doi.org/10.1186/s13024-019-0326-4

Akin, E.J., Solé, L., Dib-Hajj, S.D., Waxman, S.G., Tamkun, M.M., (2015). Preferential Targeting of Nav1.6 Voltage-Gated Na+ Channels to the Axon Initial Segment during Development. PLoS One 10. https://doi.org/10.1371/journal.pone.0124397

Alarcón-Arís, D., Recasens, A., Galofré, M., Carballo-Carbajal, I., Zacchi, N., Ruiz-Bronchal, E., Pavia-Collado, R., Chica, R., Ferrés-Coy, A., Santos, M., Revilla, R., Montefeltro, A., Fariñas, I., Artigas, F., Vila, M., Bortolozzi, A., (2018). Selective αSynuclein Knockdown in Monoamine Neurons by Intranasal Oligonucleotide Delivery: Potential Therapy for Parkinson's Disease. Molecular Therapy: The Journal of the American Society of Gene Therapy 26, 550–567. https://doi.org/10.1016/j.ymthe.2017.11.015

Albert, M.S., DeKosky, S.T., Dickson, D., Dubois, B., Feldman, H.H., Fox, N.C., Gamst, A., Holtzman, D.M., Jagust, W.J., Petersen, R.C., Snyder, P.J., Carrillo, M.C., Thies, B., Phelps, C.H., (2011). The diagnosis of mild cognitive impairment due to Alzheimer's disease: recommendations from the National Institute on Aging-Alzheimer's Association workgroups on diagnostic guidelines for Alzheimer's disease. Alzheimer's & Dementia: The Journal of the Alzheimer's Association 7, 270–279. https://doi.org/10.1016/j.jalz.2011.03.008

Alderson, T.R., Markley, J.L., (2013). Biophysical characterization of αSynuclein and its controversial structure. Intrinsically Disordered Proteins 1, 18–39. https://doi.org/10.4161/idp.26255

Allen, T.G.J., Brown, D.A., (2004). Modulation of the excitability of cholinergic basal forebrain neurons by KATP channels. Journal of Physiology 554, 353–370. https://doi.org/10.1113/jphysiol.2003.055889

Alonso, A. del C., Mederlyova, A., Novak, M., Grundke-Iqbal, I., Iqbal, K., (2004). Promotion of Hyperphosphorylation by Frontotemporal Dementia Tau Mutations. Journal of Biological Chemistry 279, 34873–34881. https://doi.org/10.1074/jbc.M405131200

Alonso, A.D., Beharry, C., Corbo, C.P., Cohen, L.S., (2016). Molecular mechanism of prion-like tau-induced neurodegeneration. Alzheimers Dementia 12, 1090–1097. https://doi.org/10.1016/j.jalz.2015.12.014

Alves-Rodrigues, A., Gregori, L., Figueiredo-Pereira, M.E., (1998). Ubiquitin, cellular inclusions and their role in neurodegeneration. Trends in Neurosciences 21, 516–520. https://doi.org/10.1016/s0166-2236(98)01276-4

Amaral, D., Lavenex, P., (2007). Hippocampal neuroanatomy, in: The Hippocampus Book. Oxford University Press, New York, NY, US, pp. 37–114.

Anand, B.K., Chhina, G.S., Sharma, K.N., Dua, S., Singh, B., (1964). Activity of single neurons in the hypothalamic feeding centers: effect of glucose. American Journal of Physiology. 207, 1146–1154. https://doi.org/10.1152/ajplegacy.1964.207.5.1146

Anderson, P., Morris, R., Amaral, D., Bliss, T., O'keefe, J., (2009). The Hippocampus Book, The Hippocampus Book. Oxford University Press, New York, NY, US.

Andorfer, C., Acker, C.M., Kress, Y., Hof, P.R., Duff, K., Davies, P., (2005). Cell-cycle reentry and cell death in transgenic mice expressing nonmutant human tau isoforms. Journal of Neurosciences 25, 5446–5454. https://doi.org/10.1523/JNEUROSCI.4637-04.2005

Andorfer, C., Kress, Y., Espinoza, M., de Silva, R., Tucker, K.L., Barde, Y.-A., Duff, K., Davies, P., (2003). Hyperphosphorylation and aggregation of tau in mice expressing normal human tau isoforms. Journal of Neurochemistry 86, 582–590. https://doi.org/10.1046/j.1471-4159.2003.01879.x

Apostolides, P.F., Milstein, A.D., Grienberger, C., Bittner, K.C., Magee, J.C., (2016). Axonal Filtering Allows Reliable Output during Dendritic Plateau-Driven Complex Spiking in CA1 Neurons. Neuron 89, 770–783. https://doi.org/10.1016/j.neuron.2015.12.040

Ar, A., Arieli, R., Shkolnik, A., (1977). Blood-gas properties and function in the fossorial mole rat under normal and hypoxic-hypercapnic atmospheric

conditions. Respiration Physiology 30, 201–219. https://doi.org/10.1016/0034- 5687(77)90031-7

Arieli, R., Ar, A., Shkolnik, A., (1977). Metabolic Responses of a Fossorial Rodent (Spalax ehrenbergi) to Simulated Burrow Conditions. Physiological Zoology. 50, 61–75. doi.org/10.1086/physzool.50.1.30155716

Arthur, J.S.C., Fong, A.L., Dwyer, J.M., Davare, M., Reese, E., Obrietan, K., Impey, S., (2004). Mitogen- and Stress-Activated Protein Kinase 1 Mediates cAMP Response Element-Binding Protein Phosphorylation and Activation by Neurotrophins. Journal of Neurosciences. 24, 4324–4332. https://doi.org/10.1523/JNEUROSCI.5227-03.2004

Atri, A., (2019). The Alzheimer's Disease Clinical Spectrum: Diagnosis and Management. The Medical Clinics of North America 103, 263–293. https://doi.org/10.1016/j.mcna.2018.10.009

Avila, J., (2010). Intracellular and Extracellular Tau. Frontiers in Neuroscience. 4. https://doi.org/10.3389/fnins.2010.00049

Avila, J., Santa-María, I., Pérez, M., Hernández, F., Moreno, F., (2006). Tau phosphorylation, aggregation, and cell toxicity. Journal of Biomedicine & Biotechnology 74539. https://doi.org/10.1155/JBB/2006/74539

Avshalumov, M.V., Rice, M.E., (2003). Activation of ATP-sensitive K+ (KATP) channels by H2O2 underlies glutamate-dependent inhibition of striatal dopamine release. Proceedings of the National Academy of Sciences 100, 11729–11734. https://doi.org/10.1073/pnas.1834314100

Baas, P.W., Qiang, L., (2019). Tau: It's Not What You Think. Trends in Cell Biology 29, 452–461. https://doi.org/10.1016/j.tcb.2019.02.007

Backlund, E.O., Granberg, P.O., Hamberger, B., Knutsson, E., Mårtensson, A., Sedvall, G., Seiger, A., Olson, L., (1985). Transplantation of adrenal medullary tissue to striatum in parkinsonism. First clinical trials. Journal of Neurosurgery 62, 169–173, doi.org/10.3171/jns.1985.62.2.0169

Badel, L., Lefort, S., Berger, T.K., Petersen, C.C.H., Gerstner, W., Richardson, M.J.E., (2008a). Extracting non-linear integrate-and-fire models from experimental data using dynamic I–V curves. Biological Cybernetics 99, 361–370. https://doi.org/10.1007/s00422-008-0259-4

Badel, L., Lefort, S., Brette, R., Petersen, C.C.H., Gerstner, W., Richardson, M.J.E., (2008b). Dynamic *I-V* Curves Are Reliable Predictors of Naturalistic Pyramidal-Neuron Voltage Traces. Journal of Neurophysiology 99, 656–666. https://doi.org/10.1152/jn.01107.2007

Badin, R.A., Binley, K., Van Camp, N., Jan, C., Gourlay, J., Robert, C., Gipchtein, P., Fayard, A., Stewart, H., Ralph, G.S., Lad, Y., Kelleher,

M., Loader, J., Hosomi, K., Palfi, S., Mitrophanous, K.A., Hantraye, P., (2019). Gene Therapy for Parkinson's Disease: Preclinical Evaluation of Optimally Configured TH:CH1 Fusion for Maximal Dopamine Synthesis. Molecular Therapy - Methods & Clinical Development 14, 206–216. https://doi.org/10.1016/j.omtm.2019.07.002

Bakshi, R., Macklin, E.A., Hung, A.Y., Hayes, M.T., Hyman, B.T., Wills, A.-M., Gomperts, S.N., Growdon, J.H., Ascherio, A., Scherzer, C.R., Schwarzschild, M.A., (2020). Associations of Lower Caffeine Intake and Plasma Urate Levels with Idiopathic Parkinson's Disease in the Harvard Biomarkers Study. Journal of Parkinson's Disease. 10, 505–510. https://doi.org/10.3233/JPD-191882

Ballard, I.C., Wagner, A.D., McClure, S.M., (2019). Hippocampal pattern separation supports reinforcement learning. Nature Communications 10, 1073. https://doi.org/10.1038/s41467-019-08998-1

Balschun, D., Wolfer, D.P., Gass, P., Mantamadiotis, T., Welzl, H., Schütz, G., Frey, J.U., Lipp, H.-P., (2003). Does cAMP Response Element-Binding Protein Have a Pivotal Role in Hippocampal Synaptic Plasticity and Hippocampus-Dependent Memory? Journal of Neuroscience 23, 6304–6314. https://doi.org/10.1523/JNEUROSCI.23-15-06304.2003

Barco, A., Alarcon, J.M., Kandel, E.R., (2002). Expression of constitutively active CREB protein facilitates the late phase of long-term potentiation by enhancing synaptic capture. Cell 108, 689–703. https://doi.org/10.1016/s0092-8674(02)00657-8

Barghorn, S., Davies, P., Mandelkow, E., (2004). Tau paired helical filaments from Alzheimer's disease brain and assembled in vitro are based on beta-structure in the core domain. Biochemistry 43, 1694–1703. https://doi.org/10.1021/bi0357006

Barker, R.A., Drouin-Ouellet, J., Parmar, M., (2015). Cell-based therapies for Parkinson disease—past insights and future potential. Nature Reviews Neurology 11, 492–503. https://doi.org/10.1038/nrneurol.2015.123

Barnard, N.D., Bush, A.I., Ceccarelli, A., Cooper, J., de Jager, C.A., Erickson, K.I., Fraser, G., Kesler, S., Levin, S.M., Lucey, B., Morris, M.C., Squitti, R., (2014). Dietary and lifestyle guidelines for the prevention of Alzheimer's disease. Neurobiol. Aging, International Conference on Nutrition and the Brain 35, S74–S78. https://doi.org/10.1016/j.neurobiolaging.2014.03.033

Barter, J.W., (2015). The Role of the Substantia Nigra in Goal Directed Behavior.

Bar-Yehuda, D., Korngreen, A., (2008). Space-Clamp Problems When Voltage Clamping Neurons Expressing Voltage-Gated Conductances. Journal

of Neurophysiology 99, 1127–1136. https://doi.org/10.1152/jn.01232.2007

Barz, S., Hummel, T., Pauli, E., Majer, M., Lang, C.J., Kobal, G., (1997). Chemosensory event-related potentials in response to trigeminal and olfactory stimulation in idiopathic Parkinson's disease. Neurology 49, 1424–1431. https://doi.org/10.1212/wnl.49.5.1424

Bateman, R.J., Xiong, C., Benzinger, T.L.S., Fagan, A.M., Goate, A., Fox, N.C., Marcus, D.S., Cairns, N.J., Xie, X., Blazey, T.M., Holtzman, D.M., Santacruz, A., Buckles, V., Oliver, A., Moulder, K., Aisen, P.S., Ghetti, B., Klunk, W.E., McDade, E., Martins, R.N., Masters, C.L., Mayeux, R., Ringman, J.M., Rossor, M.N., Schofield, P.R., Sperling, R.A., Salloway, S., Morris, J.C., (2012). Clinical and Biomarker Changes in Dominantly Inherited Alzheimer's Disease. New England Journal of Medicine 367, 795–804. https://doi.org/10.1056/NEJMoa1202753

Beharry, C., Cohen, L.S., Di, J., Ibrahim, K., Briffa-Mirabella, S., Alonso, A. del C., (2014). Tau-induced neurodegeneration: mechanisms and targets. Neuroscience Bulletin 30, 346–358. https://doi.org/10.1007/s12264-013-1414-z

Bekris, L.M., Yu, C.-E., Bird, T.D., Tsuang, D.W., (2010). Genetics of Alzheimer Disease. Journal of Geriatric Psychiatry and Neurology. 23, 213–227. https://doi.org/10.1177/0891988710383571

Berker, A.O. de, Rutledge, R.B., (2014). A Role for the Human Substantia Nigra in Reinforcement Learning. Journal of Neuroscience. 34, 12947–12949. https://doi.org/10.1523/JNEUROSCI.2854-14.2014

Berger, A.A., Winnick, A., Welschmeyer, A., Kaneb, A., Berardino, K., Cornett, E.M., Kaye, A.D., Viswanath, O., Urits, I., (2020). Istradefylline to Treat Patients with Parkinson's Disease Experiencing "Off" Episodes: A Comprehensive Review. Neurology International. 12, 109–129. https://doi.org/10.3390/neurolint12030017

Berger, T., Larkum, M.E., Lüscher, H.-R., (2001). High I h Channel Density in the Distal Apical Dendrite of Layer V Pyramidal Cells Increases Bidirectional Attenuation of EPSPs. Journal of Neurophysiology 85, 855–868. https://doi.org/10.1152/jn.2001.85.2.855

Bernheimer, H., Birkmayer, W., Hornykiewicz, O., Jellinger, K., Seitelberger, F., (1973). Brain dopamine and the syndromes of Parkinson and Huntington. Clinical, morphological and neurochemical correlations. Journal of Neurological Sciences 20, 415–455. https://doi.org/10.1016/0022-510x(73)90175-5

Bertler, Å., Rosengren, E., (1959). Occurrence and distribution of dopamine in brain and other tissues. Experientia 15, 10–11. https://doi.org/10.1007/BF02157069

Bezanilla, F., (2000). The Voltage Sensor in Voltage-Dependent Ion Channels. Physiological Reviews 80, 555–592. https://doi.org/10.1152/physrev.2000.80.2.555

Bezanilla, F. and Armstrong, C., (1977). Inactivation of the sodium channel. I. Sodium current experiments. Journal of General Physiology, 70(5), pp.549-566.

Bezanson, J., Edelman, A., Karpinski, S., Shah, V.B., (2017). Julia: A Fresh Approach to Numerical Computing. SIAM Review 59, 65–98. https://doi.org/10.1137/141000671

Bhatia, A., Lenchner, J.R., Saadabadi, A., (2021). Biochemistry, Dopamine Receptors, in: StatPearls. StatPearls Publishing, Treasure Island (FL).

Binde, C.D., Tvete, I.F., Gåsemyr, J.I., Natvig, B., Klemp, M., (2020). Comparative effectiveness of dopamine agonists and monoamine oxidase type-B inhibitors for Parkinson's disease: a multiple treatment comparison meta-analysis. European Journal of Clinical Pharmacology. 76, 1731–1743. https://doi.org/10.1007/s00228-020-02961-6

Binder, L.I., Frankfurter, A., Rebhun, L.I., (1985). The distribution of tau in the mammalian central nervous system. Journal of Cell Biology 101, 1371–1378. https://doi.org/10.1083/jcb.101.4.1371

Bland, B., (1986). The physiology and pharmacology of hippocampal formation theta rhythms. Progress in Neurobiology, 26(1), pp.1-54.

Bliss, T.V., Gardner-Medwin, A.R., (1973). Long-lasting potentiation of synaptic transmission in the dentate area of the unanaestetized rabbit following stimulation of the perforant path. Journal of Physiology 232, 357–374. https://doi.org/10.1113/jphysiol.1973.sp010274

Bliss, T.V.P., Collingridge, G.L., (1993). A synaptic model of memory: long-term potentiation in the hippocampus. Nature 361, 31–39. https://doi.org/10.1038/361031a0

Bliss, T.V.P., Lømo, T., (1973). Long-lasting potentiation of synaptic transmission in the dentate area of the anaesthetized rabbit following stimulation of the perforant path. The Journal of Physiology 232, 331–356. https://doi.org/10.1113/jphysiol.1973.sp010273

Boado, R.J., Pardridge, W.M., (2009). Comparison of Blood-Brain Barrier Transport of Glial-Derived Neurotrophic Factor (GDNF) and an IgG-GDNF Fusion Protein in the Rhesus Monkey. Drug Metabolism and Disposition. 37, 2299–2304. https://doi.org/10.1124/dmd.109.028787

Bohnen, N.I., Albin, R.L., (2011). The cholinergic system and Parkinson disease. Behavioural Brain Research 221, 564–573. https://doi.org/10.1016/j.bbr.2009.12.048

Boiko, T., Rasband, M.N., Levinson, S.R., Caldwell, J.H., Mandel, G., Trimmer, J.S., Matthews, G., (2001). Compact myelin dictates the differential targeting of two sodium channel isoforms in the same axon. Neuron 30, 91–104. https://doi.org/10.1016/s0896-6273(01)00265-3

Boluda, S., Iba, M., Zhang, B., Raible, K.M., Lee, V.M.-Y., Trojanowski, J.Q., (2015). Differential induction and spread of tau pathology in young PS19 tau transgenic mice following intracerebral injections of pathological tau from Alzheimer's disease or corticobasal degeneration brains. Acta Neuropathologica 129, 221–237. https://doi.org/10.1007/s00401-014-1373-0

Booth, C.A., Witton, J., Nowacki, J., Tsaneva-Atanasova, K., Jones, M.W., Randall, A.D., Brown, J.T., (2016). Altered Intrinsic Pyramidal Neuron Properties and Pathway-Specific Synaptic Dysfunction Underlie Aberrant Hippocampal Network Function in a Mouse Model of Tauopathy. Journal of Neurosciences 36, 350–363. https://doi.org/10.1523/JNEUROSCI.2151-15.2016

Bordia, T., Parameswaran, N., Fan, H., Langston, J.W., McIntosh, J.M., Quik, M., (2006). Partial recovery of striatal nicotinic receptors in 1-methyl-4-phenyl-1,2,3,6-tetrahydropyridine (MPTP)-lesioned monkeys with chronic oral nicotine. Journal of Pharmacology and Experimental Therapeutics. 319, 285–292. https://doi.org/10.1124/jpet.106.106997

Bouarab, C., Thompson, B., Polter, A.M., (2019). VTA GABA Neurons at the Interface of Stress and Reward. Frontiers in Neural Circuits 13. https://doi.org/10.3389/fncir.2019.00078

Bourtchuladze, R., Frenguelli, B., Blendy, J., Cioffi, D., Schutz, G., Silva, A.J., (1994). Deficient long-term memory in mice with a targeted mutation of the cAMP-responsive element-binding protein. Cell 79, 59–68. https://doi.org/10.1016/0092-8674(94)90400-6

Boutajangout, A., Ingadottir, J., Davies, P., Sigurdsson, E.M., (2011). Passive immunization targeting pathological phospho-tau protein in a mouse model reduces functional decline and clears tau aggregates from the brain. Journal of Neurochemistry 118, 658–667. https://doi.org/10.1111/j.1471-4159.2011.07337.x

Braak, H., Braak, E., (1991). Neuropathological stageing of Alzheimer-related changes. Acta Neuropathologica 82, 239–259. https://doi.org/10.1007/BF00308809

Braak, H., Del Tredici, K., Bratzke, H., Hamm-Clement, J., Sandmann-Keil, D., Rüb, U., (2002). Staging of the intracerebral inclusion body pathology associated with idiopathic Parkinson's disease (preclinical and clinical stages). Journal of Neurology 249 Suppl 3, III/1-5. https://doi.org/10.1007/s00415-002-1301-4

Braak, H., Del Tredici, K., Rüb, U., de Vos, R.A.I., Jansen Steur, E.N.H., Braak, E., (2003). Staging of brain pathology related to sporadic Parkinson's disease. Neurobiology of Aging 24, 197–211. https://doi.org/10.1016/s0197-4580(02)00065-9

Branco, T., Tozer, A., Magnus, C.J., Sugino, K., Tanaka, S., Lee, A.K., Wood, J.N., Sternson, S.M., (2016). Near-Perfect Synaptic Integration by Nav1.7 in Hypothalamic Neurons Regulates Body Weight. Cell 165, 1749–1761. https://doi.org/10.1016/j.cell.2016.05.019

Brauer, R., Bhaskaran, K., Chaturvedi, N., Dexter, D.T., Smeeth, L., Douglas, I., (2015). Glitazone Treatment and Incidence of Parkinson's Disease among People with Diabetes: A Retrospective Cohort Study. PLoS Med 12, e1001854. https://doi.org/10.1371/journal.pmed.1001854

Brotherton, D.H., Savva, C.G., Ragan, T.J., Linthwaite, V.L., Cann, M.J., Dale, N., Cameron, A.D., (2020). Conformational changes and channel gating induced by CO2 binding to Connexin 26. bioRxiv preprint 2020.08.11.243964. https://doi.org/10.1101/2020.08.11.243964

Brown, E.B., (1953). Physiological Effects of Hyperventilation. Physiological Reviews 33, 445–471. https://doi.org/10.1152/physrev.1953.33.4.445

Buchhave, P., Minthon, L., Zetterberg, H., Wallin, Å.K., Blennow, K., Hansson, O., (2012). Cerebrospinal Fluid Levels ofβ-Amyloid 1-42, but Not of Tau, Are Fully Changed Already 5 to 10 Years Before the Onset of Alzheimer Dementia. Archives of General Psychiatry 69, 98–106. https://doi.org/10.1001/archgenpsychiatry.2011.155

Bulic, B., Pickhardt, M., Mandelkow, E.-M., Mandelkow, E., (2010). Tau protein and tau aggregation inhibitors. Neuropharmacology 59, 276–289. https://doi.org/10.1016/j.neuropharm.2010.01.016

Burgoon, P.W., Boulant, J.A., (2001). Temperature-sensitive properties of rat suprachiasmatic nucleus neurons. American Journal of Physiology - Regulatory, Integrative and Comparative Physiology 281, R706-715. https://doi.org/10.1152/ajpregu.2001.281.3.R706

Burré, J., Sharma, M., Tsetsenis, T., Buchman, V., Etherton, M.R., Südhof, T.C., (2010). Alpha-synuclein promotes SNARE-complex assembly in vivo and in vitro. Science 329, 1663–1667. https://doi.org/10.1126/science.1195227

Bush, A.I., (2000). Metals and neuroscience. Current Opinions in Chemical Biology 4, 184–191. https://doi.org/10.1016/s1367-5931(99)00073-3

Buzsáki, G., (2002). Theta Oscillations in the Hippocampus. Neuron, 33(3), pp.325-340.

Caceres, A., Kosik, K.S., (1990). Inhibition of neurite polarity by tau antisense oligonucleotides in primary cerebellar neurons. Nature 343, 461–463. https://doi.org/10.1038/343461a0

Cai, X.D., Golde, T.E., Younkin, S.G., (1993). Release of excess amyloid beta protein from a mutant amyloid beta protein precursor. Science 259, 514–516. https://doi.org/10.1126/science.8424174

Calder, W.A., Schmidt-Nielsen, K., (1968). Panting and blood carbon dioxide in birds. American Journal of Physiology 215, 477–482. https://doi.org/10.1152/ajplegacy.1968.215.2.477

Caputo, A., Liang, Y., Raabe, T.D., Lo, A., Horvath, M., Zhang, B., Brown, H.J., Stieber, A., Luk, K.C., (2020). Snca-GFP Knock-In Mice Reflect Patterns of Endogenous Expression and Pathological Seeding. eNeuro 7. https://doi.org/10.1523/ENEURO.0007-20.2020

Carlsson, A., (1959). The occurrence, distribution and physiological role of catecholamines in the nervous system. Pharmacological Reviews 11, 490–493.

Castelli, L., Biella, G., Toselli, M., Magistretti, J., (2007). Resurgent Na+ current in pyramidal neurones of rat perirhinal cortex: axonal location of channels and contribution to depolarizing drive during repetitive firing. The Journal of Physiology 582, 1179–1193. https://doi.org/10.1113/jphysiol.2007.135350

Castillo-Carranza, D.L., Sengupta, U., Guerrero-Muñoz, M.J., Lasagna-Reeves, C.A., Gerson, J.E., Singh, G., Estes, D.M., Barrett, A.D.T., Dineley, K.T., Jackson, G.R., Kayed, R., (2014). Passive immunization with Tau oligomer monoclonal antibody reverses tauopathy phenotypes without affecting hyperphosphorylated neurofibrillary tangles. Journal of Neurosciences 34, 4260–4272. https://doi.org/10.1523/JNEUROSCI.3192-13.2014

Cathala, L., Paupardin-Tritsch, D., (1999). Effect of catecholamines on the hyperpolarization-activated cationic Ih and the inwardly rectifying potassium I(Kir) currents in the rat substantia nigra pars compacta. European Journal of Neurosciences 11, 398–406. https://doi.org/10.1046/j.1460-9568.1999.00452.x

Catterall, W.A., (2012). Voltage-gated sodium channels at 60: structure, function, and pathophysiology. Journal of Physiology 590, 2577–2589. https://doi.org/10.1113/jphysiol.2011.224204

Catterall, W.A., (1981). Localization of sodium channels in cultured neural cells. Journal of Neurosciences 1, 777–783.

Cereda, E., Barichella, M., Pedrolli, C., Klersy, C., Cassani, E., Caccialanza, R., Pezzoli, G., (2013). Diabetes and risk of Parkinson's disease. Movement Disorders 28, 257–261. https://doi.org/10.1002/mds.25211

Chai, X., Wu, S., Murray, T.K., Kinley, R., Cella, C.V., Sims, H., Buckner, N., Hanmer, J., Davies, P., O'Neill, M.J., Hutton, M.L., Citron, M., (2011). Passive Immunization with Anti-Tau Antibodies in Two Transgenic Models: REDUCTION OF TAU PATHOLOGY AND DELAY OF DISEASE PROGRESSION. Journal of Biological Chemistry 286, 34457–34467. https://doi.org/10.1074/jbc.M111.229633

Chang, E.H., Savage, M.J., Flood, D.G., Thomas, J.M., Levy, R.B., Mahadomrongkul, V., Shirao, T., Aoki, C., Huerta, P.T., (2006). AMPA receptor downscaling at the onset of Alzheimer's disease pathology in double knockin mice. Proceedings of the National Academy of Sciences. 103, 3410–3415. https://doi.org/10.1073/pnas.0507313103

Chaudhuri, K.R., Healy, D.G., Schapira, A.H.V., National Institute for Clinical Excellence, (2006). Non-motor symptoms of Parkinson's disease: diagnosis and management. Lancet Neurology 5, 235–245. https://doi.org/10.1016/S1474-4422(06)70373-8

Checkoway, H., Powers, K., Smith-Weller, T., Franklin, G.M., Longstreth, W.T., Swanson, P.D., (2002). Parkinson's disease risks associated with cigarette smoking, alcohol consumption, and caffeine intake. American Journal of Epidemiology 155, 732–738. https://doi.org/10.1093/aje/155.8.732

Chen, Y., Dolt, K.S., Kriek, M., Baker, T., Downey, P., Drummond, N.J., Canham, M.A., Natalwala, A., Rosser, S., Kunath, T., (2019). Engineering synucleinopathy-resistant human dopaminergic neurons by CRISPR-mediated deletion of the SNCA gene. European Journal of Neuroscience 49, 510–524. https://doi.org/10.1111/ejn.14286

Chen, H., Huang, X., Guo, X., Mailman, R.B., Park, Y., Kamel, F., Umbach, D.M., Xu, Q., Hollenbeck, A., Schatzkin, A., Blair, A., (2010). Smoking duration, intensity, and risk of Parkinson disease. Neurology 74, 878–884. https://doi.org/10.1212/WNL.0b013e3181d55f38

Chen, J.F., Schwarzschild, M.A., (2020). Do caffeine and more selective adenosine A2A receptor antagonists protect against dopaminergic neurodegeneration in Parkinson's disease? Parkinsonism Related Disorders 80, S45–S53. https://doi.org/10.1016/j.parkreldis.2020.10.024

Chen, Q., He, Y., Yang, K., (2005). Gene Therapy for Parkinson's Disease: Progress and Challenges. Current Gene Therapy 5, 71–80. https://doi.org/10.2174/1566523052997505

Choi, B.-K., Choi, M.-G., Kim, J.-Y., Yang, Y., Lai, Y., Kweon, D.-H., Lee, N.K., Shin, Y.-K., (2013). Large αSynuclein oligomers inhibit neuronal SNARE-mediated vesicle docking. Proceedings of the National Academy of Sciences 110, 4087–4092. https://doi.org/10.1073/pnas.1218424110

Chowdhury, S., Matsubara, T., Miyazaki, T., Ono, D., Fukatsu, N., Abe, M., Sakimura, K., Sudo, Y., Yamanaka, A., (2019). GABA neurons in the ventral tegmental area regulate non-rapid eye movement sleep in mice. eLife 8, e44928. https://doi.org/10.7554/eLife.44928

Cicognola, C., Brinkmalm, G., Wahlgren, J., Portelius, E., Gobom, J., Cullen, N.C., Hansson, O., Parnetti, L., Constantinescu, R., Wildsmith, K., Chen, H.-H., Beach, T.G., Lashley, T., Zetterberg, H., Blennow, K., Höglund, K., (2019). Novel tau fragments in cerebrospinal fluid: relation to tangle pathology and cognitive decline in Alzheimer's disease. Acta Neuropathologica 137, 279–296. https://doi.org/10.1007/s00401-018-1948-2

Cieślak, M., Komoszyński, M., Wojtczak, A., (2008). Adenosine A(2A) receptors in Parkinson's disease treatment. Purinergic Signal. 4, 305–312. https://doi.org/10.1007/s11302-008-9100-8

Citron, M., Oltersdorf, T., Haass, C., McConlogue, L., Hung, A.Y., Seubert, P., Vigo-Pelfrey, C., Lieberburg, I., Selkoe, D.J., (1992). Mutation of the beta-amyloid precursor protein in familial Alzheimer's disease increases beta-protein production. Nature 360, 672–674. https://doi.org/10.1038/360672a0

Citron, M., Westaway, D., Xia, W., Carlson, G., Diehl, T., Levesque, G., Johnson-Wood, K., Lee, M., Seubert, P., Davis, A., Kholodenko, D., Motter, R., Sherrington, R., Perry, B., Yao, H., Strome, R., Lieberburg, I., Rommens, J., Kim, S., Schenk, D., Fraser, P., St George Hyslop, P., Selkoe, D.J., (1997). Mutant presenilins of Alzheimer's disease increase production of 42-residue amyloid beta-protein in both transfected cells and transgenic mice. Nature Medicine 3, 67–72. https://doi.org/10.1038/nm0197-67

Clavaguera, F., Bolmont, T., Crowther, R.A., Abramowski, D., Frank, S., Probst, A., Fraser, G., Stalder, A.K., Beibel, M., Staufenbiel, M., Jucker, M., Goedert, M., Tolnay, M., (2009). Transmission and spreading of tauopathy in transgenic mouse brain. Nature Cell Bioliogy 11, 909–913. https://doi.org/10.1038/ncb1901

Cleveland, D.W., Hwo, S.Y., Kirschner, M.W., (1977). Purification of tau, a microtubule-associated protein that induces assembly of microtubules from purified tubulin. Journal of Molecular Biology 116, 207–225. https://doi.org/10.1016/0022-2836(77)90213-3

Condorelli, D.F., Trovato-Salinaro, A., Mudò, G., Mirone, M.B., Belluardo, N., (2003). Cellular expression of connexins in the rat brain: neuronal localization, effects of kainate-induced seizures and expression in apoptotic neuronal cells. European Journal of Neuroscience 18, 1807–1827. https://doi.org/10.1046/j.1460-9568.2003.02910.x

Congdon, E.E., Gu, J., Sait, H.B.R., Sigurdsson, E.M., (2013). Antibody Uptake into Neurons Occurs Primarily via Clathrin-dependent Fcγ Receptor Endocytosis and Is a Prerequisite for Acute Tau Protein Clearance. Journal of Biological Chemistry 288, 35452–35465. https://doi.org/10.1074/jbc.M113.491001

Congdon, E.E., Kim, S., Bonchak, J., Songrug, T., Matzavinos, A., Kuret, J., (2008). Nucleation-dependent tau filament formation: the importance of dimerization and an estimation of elementary rate constants. Journal of Biological Chemistry 283, 13806–13816. https://doi.org/10.1074/jbc.M800247200

Corder, E.H., Saunders, A.M., Strittmatter, W.J., Schmechel, D.E., Gaskell, P.C., Small, G.W., Roses, A.D., Haines, J.L., Pericak-Vance, M.A., (1993). Gene dose of apolipoprotein E type 4 allele and the risk of Alzheimer's disease in late onset families. Science 261, 921–923. https://doi.org/10.1126/science.8346443

Corrêa, S.A.L., Hunter, C.J., Palygin, O., Wauters, S.C., Martin, K.J., McKenzie, C., McKelvey, K., Morris, R.G.M., Pankratov, Y., Arthur, J.S.C., Frenguelli, B.G., (2012). MSK1 Regulates Homeostatic and Experience-Dependent Synaptic Plasticity. Journal of Neuroscience. 32, 13039–13051. https://doi.org/10.1523/JNEUROSCI.0930-12.2012

Cotzias, G.C., Papavasiliou, P.S., Gellene, R., (1969). Modification of Parkinsonism--chronic treatment with L-dopa. New England Journal of Medicine 280, 337–345. https://doi.org/10.1056/NEJM196902132800701

Cotzias, G.C., Van Woert, M.H., Schiffer, L.M., (1967). Aromatic Amino Acids and Modification of Parkinsonism. New England Journal of Medicine 276, 374–379. https://doi.org/10.1056/NEJM196702162760703

Coune, P.G., Schneider, B.L., Aebischer, P., (2012). Parkinson's disease: gene therapies. Cold Spring Harbor Perspectives in Medicine 2, a009431. https://doi.org/10.1101/cshperspect.a009431

Courte, J., Bousset, L., Boxberg, Y.V., Villard, C., Melki, R., Peyrin, J.-M., (2020). The expression level of alpha-synuclein in different neuronal populations is the primary determinant of its prion-like seeding. Scientific Reports 10, 4895. https://doi.org/10.1038/s41598-020-61757-x

Cowan, C.M., Chee, F., Shepherd, D., Mudher, A., (2010). Disruption of neuronal function by soluble hyperphosphorylated tau in a Drosophila model of tauopathy. Biochemical Society Transactions 38, 564–570. https://doi.org/10.1042/BST0380564

Crimins, J.L., Rocher, A.B., Peters, A., Shultz, P., Lewis, J., Luebke, J.I., (2011). Homeostatic responses by surviving cortical pyramidal cells in neurodegenerative tauopathy. Acta Neuropathologica 122, 551–564. https://doi.org/10.1007/s00401-011-0877-0

d'Abramo, C., Acker, C.M., Jimenez, H.T., Davies, P., (2013). Tau Passive Immunotherapy in Mutant P301L Mice: Antibody Affinity versus Specificity. PLOS ONE 8, e62402. https://doi.org/10.1371/journal.pone.0062402

Dadak, S., Beall, C., Vlachaki Walker, J.M., Soutar, M.P.M., McCrimmon, R.J., Ashford, M.L.J., (2017). Oleate induces KATP channel-dependent hyperpolarization in mouse hypothalamic glucose-excited neurons without altering cellular energy charge. Neuroscience 346, 29–42. https://doi.org/10.1016/j.neuroscience.2016.12.053

Dahan, A., Nieuwenhuijs, D., Teppema, L., (2007). Plasticity of Central Chemoreceptors: Effect of Bilateral Carotid Body Resection on Central CO2 Sensitivity. PLOS Medicine 4, e239. https://doi.org/10.1371/journal.pmed.0040239

Dale, N., (2008). Dynamic ATP signalling and neural development. Journal of Physiology 586, 2429–2436. https://doi.org/10.1113/jphysiol.2008.152207

D'Amelio, M., Cavallucci, V., Middei, S., Marchetti, C., Pacioni, S., Ferri, A., Diamantini, A., De Zio, D., Carrara, P., Battistini, L., Moreno, S., Bacci, A., Ammassari-Teule, M., Marie, H., Cecconi, F., (2011). Caspase-3 triggers early synaptic dysfunction in a mouse model of Alzheimer's disease. Nature Neurosciences 14, 69–76. https://doi.org/10.1038/nn.2709

Damier, P., Hirsch, E.C., Agid, Y., Graybiel, A.M., (1999). The substantia nigra of the human brain: II. Patterns of loss of dopamine-containing neurons in Parkinson's disease. Brain 122, 1437–1448. https://doi.org/10.1093/brain/122.8.1437

Danzer, K.M., Kranich, L.R., Ruf, W.P., Cagsal-Getkin, O., Winslow, A.R., Zhu, L., Vanderburg, C.R., McLean, P.J., (2012). Exosomal cell-to-cell transmission of alpha synuclein oligomers. Molecular Neurodegeneration 7, 42. https://doi.org/10.1186/1750-1326-7-42

Dawson, H.N., Ferreira, A., Eyster, M.V., Ghoshal, N., Binder, L.I., Vitek, M.P., (2001). Inhibition of neuronal maturation in primary hippocampal neurons from tau deficient mice. Journal of Cell Science 114, 1179–1187.

de Lau, L.M.L., Bornebroek, M., Witteman, J.C.M., Hofman, A., Koudstaal, P.J., Breteler, M.M.B., (2005). Dietary fatty acids and the risk of Parkinson disease: the Rotterdam study. Neurology 64, 2040–2045. https://doi.org/10.1212/01.WNL.0000166038.67153.9F

de Lau, L.M.L., Breteler, M.M.B., (2006). Epidemiology of Parkinson's disease. Lancet Neurology 5, 525–535. https://doi.org/10.1016/S1474-4422(06)70471-9

de Lera Ruiz, M., Kraus, R.L., (2015). Voltage-Gated Sodium Channels: Structure, Function, Pharmacology, and Clinical Indications. Journal of Medicinal Chemistry 58, 7093–7118. https://doi.org/10.1021/jm501981g

De Strooper, B., Saftig, P., Craessaerts, K., Vanderstichele, H., Guhde, G., Annaert, W., Von Figura, K., Van Leuven, F., (1998). Deficiency of presenilin-1 inhibits the normal cleavage of amyloid precursor protein. Nature 391, 387–390. https://doi.org/10.1038/34910

de Wolf, E., van de Wiel, J., Cook, J., Dale, N., (2016). Altered CO_2 sensitivity of connexin26 mutant hemichannels in vitro. Physiological Reports 4. https://doi.org/10.14814/phy2.13038

de Wolf, E., Cook, J., Dale, N., (2017). Evolutionary adaptation of the sensitivity of connexin26 hemichannels to CO 2. Proceedings of the Royal Society Biological Sciences 284, 20162723. https://doi.org/10.1098/rspb.2016.2723

Debanne, D., Boudkkazi, S., Campanac, E., Cudmore, R.H., Giraud, P., Fronzaroli-Molinieres, L., Carlier, E., Caillard, O., (2008). Paired-recordings from synaptically coupled cortical and hippocampal neurons in acute and cultured brain slices. Nature Protocols 3, 1559–1568. https://doi.org/10.1038/nprot.2008.147

Decker, J.M., Krüger, L., Sydow, A., Zhao, S., Frotscher, M., Mandelkow, E., Mandelkow, E.-M., (2015). Pro-aggregant Tau impairs mossy fiber plasticity due to structural changes and Ca++ dysregulation. Acta Neuropathologica Communications 3. https://doi.org/10.1186/s40478-015-0193-3

Dehay, B., Bourdenx, M., Gorry, P., Przedborski, S., Vila, M., Hunot, S., Singleton, A., Olanow, C.W., Merchant, K.M., Bezard, E., Petsko, G.A., Meissner, W.G., (2015). Targeting αSynuclein for treatment of Parkinson's disease: mechanistic and therapeutic considerations. Lancet Neurology 14, 855–866. https://doi.org/10.1016/S1474-4422(15)00006-X

Del Tredici, K., Rüb, U., De Vos, R.A.I., Bohl, J.R.E., Braak, H., (2002). Where does parkinson disease pathology begin in the brain? Journal of Neuropathology and Experimental Neurology 61, 413–426. https://doi.org/10.1093/jnen/61.5.413

DeLong, M.R., Wichmann, T., (2007). Circuits and circuit disorders of the basal ganglia. Archives of Neurology 64, 20–24. https://doi.org/10.1001/archneur.64.1.20

Deng, W., Aimone, J.B., Gage, F.H., (2010). New neurons and new memories: how does adult hippocampal neurogenesis affect learning and memory? Nature Reviews Neuroscience 11, 339–350. https://doi.org/10.1038/nrn2822

Dexter, D.T., Carayon, A., Javoy-Agid, F., Agid, Y., Wells, F.R., Daniel, S.E., Lees, A.J., Jenner, P., Marsden, C.D., (1991). Alterations in the levels of iron, ferritin and other trace metals in Parkinson's disease and other neurodegenerative diseases affecting the basal ganglia. Brain 114 (Pt 4), 1953–1975. https://doi.org/10.1093/brain/114.4.1953

Dexter, D.T., Wells, F.R., Lees, A.J., Agid, F., Agid, Y., Jenner, P., Marsden, C.D., (1989). Increased nigral iron content and alterations in other metal ions occurring in brain in Parkinson's disease. Journal of Neurochemistry 52, 1830–1836. https://doi.org/10.1111/j.1471-4159.1989.tb07264.x

Dhuriya, Y.K., Sharma, D., (2020). Neuronal Plasticity: Neuronal Organization is Associated with Neurological Disorders. Journal of Molecular Neuroscience. 70, 1684– 1701. https://doi.org/10.1007/s12031-020-01555-2

Dickson, D.W., Kouri, N., Murray, M.E., Josephs, K.A., (2011). Neuropathology of frontotemporal lobar degeneration-tau (FTLD-tau). Journal of Molecular Neurosciences 45, 384–389. https://doi.org/10.1007/s12031-011-9589-0

Dickson, D.W., Ruan, D., Crystal, H., Mark, M.H., Davies, P., Kress, Y., Yen, S.H., (1991). Hippocampal degeneration differentiates diffuse Lewy body disease (DLBD) from Alzheimer's disease: light and electron microscopic immunocytochemistry of CA2-3 neurites specific to DLBD. Neurology 41, 1402–1409. https://doi.org/10.1212/wnl.41.9.1402

Diógenes, M.J., Dias, R.B., Rombo, D.M., Miranda, H.V., Maiolino, F., Guerreiro, P., Näsström, T., Franquelim, H.G., Oliveira, L.M.A., Castanho, M.A.R.B., Lannfelt, L., Bergström, J., Ingelsson, M., Quintas, A., Sebastião, A.M., Lopes, L.V., Outeiro, T.F., (2012). Extracellular Alpha-Synuclein Oligomers Modulate Synaptic Transmission and Impair LTP Via NMDA-Receptor Activation. Journal of Neuroscience. 32, 11750–11762. https://doi.org/10.1523/JNEUROSCI.0234-12.2012

Divac, I., (1975). Magnocellular nuclei of the basal forebrain project to neocortex, brain stem, and olfactory bulb. Review of some functional correlates. Brain Research 93, 385–398. https://doi.org/10.1016/0006-8993(75)90178-X

Diwakar, S., Magistretti, J., Goldfarb, M., Naldi, G., D'Angelo, E., (2009). Axonal Na+ Channels Ensure Fast Spike Activation and Back-Propagation in Cerebellar Granule Cells. Journal of Neurophysiology 101, 519–532. https://doi.org/10.1152/jn.90382.2008

Dufour, M.A., Woodhouse, A., Amendola, J., Goaillard, J.-M., (2014). Non-linear developmental trajectory of electrical phenotype in rat substantia nigra pars compacta dopaminergic neurons. eLife 3, e04059. https://doi.org/10.7554/eLife.04059

Dufour, M.A., Woodhouse, A., Amendola, J., Goaillard, J.-M., (2014). Non-linear developmental trajectory of electrical phenotype in rat substantia nigra pars compacta dopaminergic neurons. eLife 3, e04059. https://doi.org/10.7554/eLife.04059

Eban-Rothschild, A., Rothschild, G., Giardino, W.J., Jones, J.R., de Lecea, L., (2016). VTA dopaminergic neurons regulate ethologically relevant sleep-wake behaviors. Nature Neurosciences 19, 1356–1366. https://doi.org/10.1038/nn.4377

Eftekharzadeh, B., Daigle, J.G., Kapinos, L.E., Coyne, A., Schiantarelli, J., Carlomagno, Y., Cook, C., Miller, S.J., Dujardin, S., Amaral, A.S., Grima, J.C., Bennett, R.E., Tepper, K., DeTure, M., Vanderburg, C.R., Corjuc, B.T., DeVos, S.L., Gonzalez, J.A., Chew, J., Vidensky, S., Gage, F.H., Mertens, J., Troncoso, J., Mandelkow, E., Salvatella, X., Lim, R.Y.H., Petrucelli, L., Wegmann, S., Rothstein, J.D., Hyman, B.T., (2018). Tau Protein Disrupts Nucleocytoplasmic Transport in Alzheimer's Disease. Neuron 99, 925-940.e7. https://doi.org/10.1016/j.neuron.2018.07.039

Eldridge, F.L., Kiley, J.P., Millhorn, D.E., (1985). Respiratory responses to medullary hydrogen ion changes in cats: different effects of respiratory and metabolic acidoses. The Journal of Physiology 358, 285–297. https://doi.org/10.1113/jphysiol.1985.sp015551

Emborg, M.E., Carbon, M., Holden, J.E., During, M.J., Ma, Y., Tang, C., Moirano, J., Fitzsimons, H., Roitberg, B.Z., Tuccar, E., Roberts, A., Kaplitt, M.G., Eidelberg, D., (2007). Subthalamic Glutamic Acid Decarboxylase Gene Therapy: Changes in Motor Function and Cortical Metabolism. J. Cereb. Blood Flow Metab. 27, 501–509. https://doi.org/10.1038/sj.jcbfm.9600364

Eriksen, N., Stark, A.K., Pakkenberg, B., (2009). Age and Parkinson's disease-related neuronal death in the substantia nigra pars compacta. Journal of Neural Transmission 203–213. https://doi.org/10.1007/978-3-211-92660-4_16

Eshel, N., Bukwich, M., Rao, V., Hemmelder, V., Tian, J., Uchida, N., (2015). Arithmetic and local circuitry underlying dopamine prediction errors. Nature 525, 243–246. https://doi.org/10.1038/nature14855

Evans, L.D., Wassmer, T., Fraser, G., Smith, J., Perkinton, M., Billinton, A., Livesey, F.J., (2018). Extracellular Monomeric and Aggregated Tau Efficiently Enter Human Neurons through Overlapping but Distinct Pathways. Cell Reports 22, 3612–3624. https://doi.org/10.1016/j.celrep.2018.03.021

Fá, M., Puzzo, D., Piacentini, R., Staniszewski, A., Zhang, H., Baltrons, M.A., Li Puma, D.D., Chatterjee, I., Li, J., Saeed, F., Berman, H.L., Ripoli, C., Gulisano, W., Gonzalez, J., Tian, H., Costa, J.A., Lopez, P., Davidowitz, E., Yu, W.H., Haroutunian, V., Brown, L.M., Palmeri, A., Sigurdsson, E.M., Duff, K.E., Teich, A.F., Honig, L.S., Sierks, M., Moe, J.G., D'Adamio, L., Grassi, C., Kanaan, N.M., Fraser, P.E., Arancio, O., (2016). Extracellular Tau Oligomers Produce An Immediate Impairment of LTP and Memory. Scientific Reports 6, 19393. https://doi.org/10.1038/srep19393

Fagan, A.M., Xiong, C., Jasielec, M.S., Bateman, R.J., Goate, A.M., Benzinger, T.L.S., Ghetti, B., Martins, R.N., Masters, C.L., Mayeux, R., Ringman, J.M., Rossor, M.N., Salloway, S., Schofield, P.R., Sperling, R.A., Marcus, D., Cairns, N.J., Buckles, V.D., Ladenson, J.H., Morris, J.C., Holtzman, D.M., Dominantly Inherited Alzheimer Network, (2014). Longitudinal change in CSF biomarkers in autosomal-dominant Alzheimer's disease. Science Translational Medicine 6, 226ra30. https://doi.org/10.1126/scitranslmed.3007901

Fahn,. Elton, (2003). The Unified Parkinson's Disease Rating Scale (UPDRS): Status and recommendations. Movement Disorders. 18, 738–750. https://doi.org/10.1002/mds.10473

Fan, Y., Winanto, Ng, S.-Y., (2020). Replacing what is lost: a new era of stem cell therapy for Parkinson's disease. Translational Neurodegeneration 9, 2. https://doi.org/10.1186/s40035-019-0180-x

Faraci, F.M., Fedde, M.R., (1986). Regional circulatory responses to hypocapnia and hypercapnia in bar-headed geese. American Journal of Physiology. 250, R499-504. https://doi.org/10.1152/ajpregu.1986.250.3.R499

Ferreira, D.G., Temido-Ferreira, M., Vicente Miranda, H., Batalha, V.L., Coelho, J.E., Szegö, É.M., Marques-Morgado, I., Vaz, S.H., Rhee, J.S., Schmitz, M., Zerr, I., Lopes, L.V., Outeiro, T.F., (2017). α-synuclein interacts with PrP C to induce cognitive impairment through mGluR5 and NMDAR2B. Nature Neuroscience 20, 1569–1579. https://doi.org/10.1038/nn.4648

Fifel, K., Meijer, J.H., Deboer, T., (2018). Circadian and Homeostatic Modulation of Multi-Unit Activity in Midbrain Dopaminergic Structures. Scientific Reports 8, 7765. https://doi.org/10.1038/s41598-018-25770-5

Filosa, J., Dean, J., Putnam, R., (2002). Role of intracellular and extracellular pH in the chemosensitive response of rat Locus coeruleus neurones. The Journal of physiology 541, 493–509. https://doi.org/10.1113/jphysiol.2001.014142

Fortin, S.M., Cone, J.J., Ng-Evans, S., McCutcheon, J.E., Roitman, M.F., (2015). Sampling Phasic Dopamine Signaling with Fast-Scan Cyclic Voltammetry in Awake, Behaving Rats. Current Protocols in Neuroscience 70, 7.25.1-7.25.20. https://doi.org/10.1002/0471142301.ns0725s70

Fourcaud, N., Brunel, N., (2002). Dynamics of the firing probability of noisy integrate-and-fire neurons. Neural Computation 14, 2057–2110. https://doi.org/10.1162/089976602320264015

Fourcaud-Trocmé, N., Hansel, D., Vreeswijk, C. van, Brunel, N., (2003). How Spike Generation Mechanisms Determine the Neuronal Response to Fluctuating Inputs. Journal of Neuroscience. 23, 11628–11640. https://doi.org/10.1523/JNEUROSCI.23-37-11628.2003

Fozzard, H.A., Sheets, M.F., Hanck, D., (2011). The Sodium Channel as a Target for Local Anesthetic Drugs. Frontiers in Pharmacology 2. https://doi.org/10.3389/fphar.2011.00068

Frandemiche, M.L., De Seranno, S., Rush, T., Borel, E., Elie, A., Arnal, I., Lanté, F., Buisson, A., (2014). Activity-dependent tau protein translocation to excitatory synapse is disrupted by exposure to amyloid-beta oligomers. The Journal of Neuroscience 34, 6084–6097. https://doi.org/10.1523/JNEUROSCI.4261-13.2014

Freed, C.R., Breeze, R.E., Rosenberg, N.L., Schneck, S.A., Kriek, E., Qi, J.X., Lone, T., Zhang, Y.B., Snyder, J.A., Wells, T.H., (1992). Survival of

implanted fetal dopamine cells and neurologic improvement 12 to 46 months after transplantation for Parkinson's disease. New England Journal of Medicine 327, 1549–1555. https://doi.org/10.1056/NEJM199211263272202

Friedhoff, P., von Bergen, M., Mandelkow, E.M., Davies, P., Mandelkow, E., (1998). A nucleated assembly mechanism of Alzheimer paired helical filaments. Proceedings of the National Academy of Sciences 95, 15712–15717. https://doi.org/10.1073/pnas.95.26.15712

Fujio, K., Sato, M., Uemura, T., Sato, T., Sato-Harada, R., Harada, A., (2007). 14-3-3 proteins and protein phosphatases are not reduced in tau-deficient mice. Neuroreport 18, 1049–1052. https://doi.org/10.1097/WNR.0b013e32818b2a0b

Galvan, A., Wichmann, T., (2008). Pathophysiology of Parkinsonism. Clinical Neurophysiology 119, 1459–1474. https://doi.org/10.1016/j.clinph.2008.03.017

Garrido, J.J., Giraud, P., Carlier, E., Fernandes, F., Moussif, A., Fache, M.-P., Debanne, D., Dargent, B., (2003). A targeting motif involved in sodium channel clustering at the axonal initial segment. Science 300, 2091–2094. https://doi.org/10.1126/science.1085167

George, C.H., Kendall, J.M., Evans, W.H., (1999). Intracellular trafficking pathways in the assembly of connexins into gap junctions. Journal of Biological Chemistry 274, 8678–8685. https://doi.org/10.1074/jbc.274.13.8678

Ghasemi, A., Zahediasl, S., (2012). Normality Tests for Statistical Analysis: A Guide for Non-Statisticians. International Journal of Endocrinology and Metabolism 10, 486–489. https://doi.org/10.5812/ijem.3505

Gibb, W.R., Lees, A.J., (1991). Anatomy, pigmentation, ventral and dorsal subpopulations of the substantia nigra, and differential cell death in Parkinson's disease. Journal of Neurology, Neurosurgery, and Psychiatry 54, 388–396. https://doi.org/10.1136/jnnp.54.5.388

Gibbons, G.S., Lee, V.M.Y., Trojanowski, J.Q., (2019). Mechanisms of Cell-to-Cell Transmission of Pathological Tau: A Review. JAMA Neurology 76, 101–108. https://doi.org/10.1001/jamaneurol.2018.2505

Goedert, M., Jakes, R., (2005). Mutations causing neurodegenerative tauopathies. Biochimica et Biophysica Acta 1739, 240–250. https://doi.org/10.1016/j.bbadis.2004.08.007

Goedert, M., Spillantini, M.G., Potier, M.C., Ulrich, J., Crowther, R.A., (1989). Cloning and sequencing of the cDNA encoding an isoform of microtubule-associated protein tau containing four tandem repeats:

differential expression of tau protein mRNAs in human brain. EMBO Journal 8, 393–399.

Goedert, M., Wischik, C.M., Crowther, R.A., Walker, J.E., Klug, A., (1988). Cloning and sequencing of the cDNA encoding a core protein of the paired helical filament of Alzheimer disease: identification as the microtubule-associated protein tau. Proceedings of the National Academy of Sciences 85, 4051–4055. https://doi.org/10.1073/pnas.85.11.4051

Gómez-Ramos, A., Díaz-Hernández, M., Rubio, A., Díaz-Hernández, J.I., Miras-Portugal, M.T., Avila, J., (2009). Characteristics and consequences of muscarinic receptor activation by tau protein. European Neuropsychopharmacology 19, 708–717. https://doi.org/10.1016/j.euroneuro.2009.04.006

Goodenough, D.A., Goliger, J.A., Paul, D.L., (1996). Connexins, connexons, and intercellular communication. Annual Reviews Biochemistry 65, 475–502. https://doi.org/10.1146/annurev.bi.65.070196.002355

Gorell, J.M., Johnson, C.C., Rybicki, B.A., Peterson, E.L., Kortsha, G.X., Brown, G.G., Richardson, R.J., (1997). Occupational exposures to metals as risk factors for Parkinson's disease. Neurology 48, 650–658. https://doi.org/10.1212/wnl.48.3.650

Gourine, A.V., Kasymov, V., Marina, N., Tang, F., Figueiredo, M.F., Lane, S., Teschemacher, A.G., Spyer, K.M., Deisseroth, K., Kasparov, S., (2010). Astrocytes Control Breathing Through pH-Dependent Release of ATP. Science 329, 571–575. https://doi.org/10.1126/science.1190721

Gourine, A.V., Llaudet, E., Dale, N., Spyer, K.M., (2005). ATP is a mediator of chemosensory transduction in the central nervous system. Nature 436, 108–111. https://doi.org/10.1038/nature03690

Grace, A.A., Bunney, B.S., (1983). Intracellular and extracellular electrophysiology of nigral dopaminergic neurons—3. Evidence for electrotonic coupling. Neuroscience 10, 333–348. https://doi.org/10.1016/0306-4522(83)90137-9

Grace, A.A., Onn, S.P., (1989). Morphology and electrophysiological properties of immunocytochemically identified rat dopamine neurons recorded in vitro. Journal of Neuroscience 9, 3463–3481.

Grosso, G., Godos, J., Galvano, F., Giovannucci, E.L., (2017). Coffee, Caffeine, and Health Outcomes: An Umbrella Review. Annual Reviews Nutrition 37, 131–156. https://doi.org/10.1146/annurev-nutr-071816-064941

Grover, L., Kim, E., Cooke, J. and Holmes, W., (2009). LTP in hippocampal area CA1 is induced by burst stimulation over a broad frequency range centered around delta. Learning & Memory, 16(1), pp.69-81.

Guan, Y., Ye, J.-H., (2010). Ethanol blocks long-term potentiation of GABAergic synapses in the ventral tegmental area involving mu-opioid receptors. Neuropsychopharmacology 35, 1841–1849. https://doi.org/10.1038/npp.2010.51

Guo, J.L., Lee, V.M.-Y., (2011). Seeding of normal Tau by pathological Tau conformers drives pathogenesis of Alzheimer-like tangles. The Journal of Biological Chemistry 286, 15317–15331. https://doi.org/10.1074/jbc.M110.209296

Haass, C., Schlossmacher, M.G., Hung, A.Y., Vigo-Pelfrey, C., Mellon, A., Ostaszewski, B.L., Lieberburg, I., Koo, E.H., Schenk, D., Teplow, D.B., (1992). Amyloid beta-peptide is produced by cultured cells during normal metabolism. Nature 359, 322–325. https://doi.org/10.1038/359322a0

Haaxma, C.A., Bloem, B.R., Borm, G.F., Oyen, W.J.G., Leenders, K.L., Eshuis, S., Booij, J., Dluzen, D.E., Horstink, M.W.I.M., (2007). Gender differences in Parkinson's disease. Journal of Neurology, Neurosurgery, and Psychiatry 78, 819–824. https://doi.org/10.1136/jnnp.2006.103788

Haehner, A., Hummel, T., Hummel, C., Sommer, U., Junghanns, S., Reichmann, H., (2007). Olfactory loss may be a first sign of idiopathic Parkinson's disease. Movement Disorders 22, 839–842. https://doi.org/10.1002/mds.21413

Haller, M., Mironov, S.L., Karschin, A., Richter, D.W., (2001). Dynamic activation of K(ATP) channels in rhythmically active neurons. Journal of Physiology 537, 69–81. https://doi.org/10.1111/j.1469-7793.2001.0069k.x

Hamill, O.P., Marty, A., Neher, E., Sakmann, B., Sigworth, F.J., (1981). Improved patch-clamp techniques for high-resolution current recording from cells and cell-free membrane patches. Pflügers Archive 391, 85–100. https://doi.org/10.1007/BF00656997

Hammond, C., Bergman, H., Brown, P., (2007). Pathological synchronization in Parkinson's disease: networks, models, and treatments. Trends in Neurosciences 30, 357–364. https://doi.org/10.1016/j.tins.2007.05.004

Hampel, H., Blennow, K., Shaw, L.M., Hoessler, Y.C., Zetterberg, H., Trojanowski, J.Q., (2010). Total and phosphorylated tau protein as biological markers of Alzheimer's disease. Experimental Gerontology 45, 30–40. https://doi.org/10.1016/j.exger.2009.10.010

Han, S.-S., Jiao, Q., Bi, M.-X., Du, X.-X., Jiang, H., (2018). The expression of KATP channel subunits in alpha-synuclein-transfected MES23.5 cells. Annals of Translational Medicine 6. https://doi.org/10.21037/atm.2018.04.24

Hanger, D.P., Byers, H.L., Wray, S., Leung, K.-Y., Saxton, M.J., Seereeram, A., Reynolds, C.H., Ward, M.A., Anderton, B.H., (2007). Novel phosphorylation sites in tau from Alzheimer brain support a role for casein kinase 1 in disease pathogenesis. The Journal of Biological Chemistry 282, 23645–23654. https://doi.org/10.1074/jbc.M703269200

Hantikainen, E., Lagerros, Y.T., Ye, W., Serafini, M., Adami, H.-O., Bellocco, R., Bonn, S., (2021). Dietary Antioxidants and the Risk of Parkinson Disease: The Swedish National March Cohort. Neurology 96, e895–e903. https://doi.org/10.1212/WNL.0000000000011373

Hansson, O., Zetterberg, H., Buchhave, P., Londos, E., Blennow, K., Minthon, L., (2006). Association between CSF biomarkers and incipient Alzheimer's disease in patients with mild cognitive impairment: a follow-up study. Lancet Neurology 5, 228–234. https://doi.org/10.1016/S1474-4422(06)70355-6

Harada, A., Oguchi, K., Okabe, S., Kuno, J., Terada, S., Ohshima, T., Sato-Yoshitake, R., Takei, Y., Noda, T., Hirokawa, N., (1994). Altered microtubule organization in small-calibre axons of mice lacking tau protein. Nature 369, 488–491. https://doi.org/10.1038/369488a0

Harris, K.D., Mrsic-Flogel, T.D., (2013). Cortical connectivity and sensory coding. Nature 503, 51–58. https://doi.org/10.1038/nature12654

Harris, N.C., Constanti, A., (1995). Mechanism of block by ZD 7288 of the hyperpolarization-activated inward rectifying current in guinea pig substantia nigra neurons in vitro. Journal of Neurophysiology 74, 2366–2378. https://doi.org/10.1152/jn.1995.74.6.2366

Harrison, P.M., Badel, L., Wall, M.J., Richardson, M.J.E., (2015). Experimentally Verified Parameter Sets for Modelling Heterogeneous Neocortical Pyramidal-Cell Populations. PLoS Computational Biology 11, e1004165. https://doi.org/10.1371/journal.pcbi.1004165

Hartline, D.K., Castelfranco, A.M., (2003). Simulations of Voltage Clamping Poorly Space-Clamped Voltage-Dependent Conductances in a Uniform Cylindrical Neurite. Journal of Computational Neuroscience 14, 253–269. https://doi.org/10.1023/A:1023208926805

Hatch, R.J., Wei, Y., Xia, D., Götz, J., (2017). Hyperphosphorylated tau causes reduced hippocampal CA1 excitability by relocating the axon initial segment. Acta Neuropathologica 133, 717–730. https://doi.org/10.1007/s00401-017-1674-1

He, Z., McBride, J.D., Xu, H., Changolkar, L., Kim, S.-J., Zhang, B., Narasimhan, S., Gibbons, G.S., Guo, J.L., Kozak, M., Schellenberg, G.D., Trojanowski, J.Q., Lee, V.M.-Y., (2020). Transmission of tauopathy strains is independent of their isoform composition. Nature Communications 11, 7. https://doi.org/10.1038/s41467-019-13787-x

Herantis Pharma, (2020). Herantis - Herantis Pharma Plc announces topline results of Phase 1-2 CDNF trial. Herantis. URL https://herantis.com/press_releases/herantis-pharma-plc-announces-topline-results-of-phase-1-2-cdnf-trial/ (accessed 1.25.21).

Hernán, M.A., Chen, H., Schwarzschild, M.A., Ascherio, A., (2003). Alcohol consumption and the incidence of Parkinson's disease. Annals of Neurology 54, 170–175. https://doi.org/10.1002/ana.10611

Hernán, M.A., Takkouche, B., Caamaño-Isorna, F., Gestal-Otero, J.J., (2002). A meta-analysis of coffee drinking, cigarette smoking, and the risk of Parkinson's disease. Annals of Neurology 52, 276–284. https://doi.org/10.1002/ana.10277

Hill, E., Dale, N., Wall, M.J., (2020a). Moderate Changes in CO_2 Modulate the Firing of Neurons in the VTA and Substantia Nigra. iScience 23, 101343. https://doi.org/10.1016/j.isci.2020.101343

Hill, E., Dale, N., Wall, M.J., (2020b). Detecting CO2-Sensitive Hemichannels in Neurons in Acute Brain Slices. STAR Protocols 1, 100139. https://doi.org/10.1016/j.xpro.2020.100139

Hill, E., Gowers, R., Richardson, M.J.E., Wall, M.J., (2021). αSynuclein Aggregates Increase the Conductance of Substantia Nigra Dopamine Neurons, an Effect Partly Reversed by the KATP Channel Inhibitor Glibenclamide. eNeuro 8. https://doi.org/10.1523/ENEURO.0330-20.2020

Hill, E., Karikari, T.K., Moffat, K.G., Richardson, M.J.E., Wall, M.J., (2019). Introduction of Tau Oligomers into Cortical Neurons Alters Action Potential Dynamics and Disrupts Synaptic Transmission and Plasticity. eNeuro 6, doi.org/10.1523/ENEURO.0166-19.2019

Hindle, J.V., (2010). Ageing, neurodegeneration and Parkinson's disease. Age Ageing 39, 156–161. https://doi.org/10.1093/ageing/afp223

Hirokawa, N., Shiomura, Y., Okabe, S., (1988). Tau proteins: the molecular structure and mode of binding on microtubules. Journal of Cell Biology 107, 1449–1459. https://doi.org/10.1083/jcb.107.4.1449

Hisahara, S., Shimohama, S., (2011). Dopamine Receptors and Parkinson's Disease. International Journal of Medicinal Chemistry. https://doi.org/10.1155/2011/403039

Hiyama, T.Y., Noda, M., (2016). Sodium sensing in the subfornical organ and body-fluid homeostasis. Neuroscience Research 113, 1–11. https://doi.org/10.1016/j.neures.2016.07.007

Hodges, J.L., Lehmann, E.L., (1956). The Efficiency of Some Nonparametric Competitors of the t-Test. The Annals of Mathematical Statistics. 27, 324–335. https://doi.org/10.1214/aoms/1177728261

Hodgkin, A.L., Huxley, A.F., (1952). A quantitative description of membrane current and its application to conduction and excitation in nerve. Journal of Physiology 117, 500–544.

Holly, E.N., Miczek, K.A., (2016). Ventral tegmental area dopamine revisited: effects of acute and repeated stress. Psychopharmacology 233, 163–186. https://doi.org/10.1007/s00213-015-4151-3

Hong, C.T., Chan, L., Bai, C.-H., (2020). The Effect of Caffeine on the Risk and Progression of Parkinson's Disease: A Meta-Analysis. Nutrients 12. https://doi.org/10.3390/nu12061860

Hoover, B.R., Reed, M.N., Su, J., Penrod, R.D., Kotilinek, L.A., Grant, M.K., Pitstick, R., Carlson, G.A., Lanier, L.M., Yuan, L.-L., Ashe, K.H., Liao, D., (2010). Tau mislocalization to dendritic spines mediates synaptic dysfunction independently of neurodegeneration. Neuron 68, 1067–1081. https://doi.org/10.1016/j.neuron.2010.11.030

Horowitz, P.M., LaPointe, N., Guillozet-Bongaarts, A.L., Berry, R.W., Binder, L.I., (2006). N-terminal fragments of tau inhibit full-length tau polymerization in vitro. Biochemistry 45, 12859–12866. https://doi.org/10.1021/bi061325g

Hosford, P.S., Mosienko, V., Kishi, K., Jurisic, G., Seuwen, K., Kinzel, B., Ludwig, M.G., Wells, J.A., Christie, I.N., Koolen, L., Abdala, A.P., Liu, B.H., Gourine, A.V., Teschemacher, A.G., Kasparov, S., (2018). CNS distribution, signalling properties and central effects of G-protein coupled receptor 4. Neuropharmacology 138, 381–392. https://doi.org/10.1016/j.neuropharm.2018.06.007

Hossain, W.A., Antic, S.D., Yang, Y., Rasband, M.N., Morest, D.K., (2005). Where is the spike generator of the cochlear nerve? Voltage-gated sodium channels in the mouse cochlea. Journal of Neuroscience 25, 6857–6868. https://doi.org/10.1523/JNEUROSCI.0123-05.2005

Huang, Y., (2006). Molecular and cellular mechanisms of apolipoprotein E4 neurotoxicity and potential therapeutic strategies. Current Opinions in Drug Discovery and Development 9, 627–641.

Huang, Z.-L., Qu, W.-M., Eguchi, N., Chen, J.-F., Schwarzschild, M.A., Fredholm, B.B., Urade, Y., Hayaishi, O., (2005). Adenosine A2A, but

not A1, receptors mediate the arousal effect of caffeine. Nature Neuroscience 8, 858–859. https://doi.org/10.1038/nn1491

Huckstepp, R.T.R., Bihi, R.I., Eason, R., Spyer, K.M., Dicke, N., Willecke, K., Marina, N., Gourine, A.V., Dale, N., (2010a). Connexin hemichannel-mediated CO2-dependent release of ATP in the medulla oblongata contributes to central respiratory chemosensitivity. The Journal of Physiology 588, 3901–3920. https://doi.org/10.1113/jphysiol.2010.192088

Huckstepp, R.T.R., Eason, R., Sachdev, A., Dale, N., (2010b). CO_2-dependent opening of connexin 26 and related β connexins. The Journal of Physiology 588, 3921–3931. https://doi.org/10.1113/jphysiol.2010.192096

Huff, J., (2015). The Airyscan detector from ZEISS: confocal imaging with improved signal-to-noise ratio and super-resolution. Nature Methods 12, i–ii. https://doi.org/10.1038/nmeth.f.388

Iba, M., Guo, J.L., McBride, J.D., Zhang, B., Trojanowski, J.Q., Lee, V.M.-Y., (2013). Synthetic tau fibrils mediate transmission of neurofibrillary tangles in a transgenic mouse model of Alzheimer's-like tauopathy. Journal of Neuroscience 33, 1024–1037. https://doi.org/10.1523/JNEUROSCI.2642-12.2013

Inagaki, N., Gonoi, T., Clement, J.P., Namba, N., Inazawa, J., Gonzalez, G., Aguilar-Bryan, L., Seino, S., Bryan, J., (1995). Reconstitution of IKATP: an inward rectifier subunit plus the sulfonylurea receptor. Science 270, 1166–1170. https://doi.org/10.1126/science.270.5239.1166

Ishizuka, N., Cowan, W.M., Amaral, D.G., (1995). A quantitative analysis of the dendritic organization of pyramidal cells in the rat hippocampus. Journal of Computational Neurology 362, 17–45. https://doi.org/10.1002/cne.903620103

Ittner, L.M., Ke, Y.D., Delerue, F., Bi, M., Gladbach, A., Eersel, J. van, Wölfing, H., Chieng, B.C., Christie, M.J., Napier, I.A., Eckert, A., Staufenbiel, M., Hardeman, E., Götz, J., (2010). Dendritic Function of Tau Mediates Amyloid-β Toxicity in Alzheimer's Disease Mouse Models. Cell 142, 387–397. https://doi.org/10.1016/j.cell.2010.06.036

Iwai, A., Masliah, E., Yoshimoto, M., Ge, N., Flanagan, L., de Silva, H.A., Kittel, A., Saitoh, T., (1995). The precursor protein of non-A beta component of Alzheimer's disease amyloid is a presynaptic protein of the central nervous system. Neuron 14, 467–475. https://doi.org/10.1016/0896-6273(95)90302-x

Jack, C.R., Knopman, D.S., Jagust, W.J., Petersen, R.C., Weiner, M.W., Aisen, P.S., Shaw, L.M., Vemuri, P., Wiste, H.J., Weigand, S.D.,

Lesnick, T.G., Pankratz, V.S., Donohue, M.C., Trojanowski, J.Q., (2013). Tracking pathophysiological processes in Alzheimer's disease: an updated hypothetical model of dynamic biomarkers. Lancet Neurology 12, 207–216. https://doi.org/10.1016/S1474-4422(12)70291-0

Jack, C.R., Knopman, D.S., Jagust, W.J., Shaw, L.M., Aisen, P.S., Weiner, M.W., Petersen, R.C., Trojanowski, J.Q., (2010). Hypothetical model of dynamic biomarkers of the Alzheimer's pathological cascade. Lancet Neurology 9, 119. https://doi.org/10.1016/S1474-4422(09)70299-6

Jack, C.R., Petersen, R.C., Xu, Y.C., O'Brien, P.C., Smith, G.E., Ivnik, R.J., Boeve, B.F., Waring, S.C., Tangalos, E.G., Kokmen, E., (1999). Prediction of AD with MRI-based hippocampal volume in mild cognitive impairment. Neurology 52, 1397–1403. https://doi.org/10.1212/wnl.52.7.1397

Jakes, R., Spillantini, M.G., Goedert, M., (1994). Identification of two distinct synucleins from human brain. FEBS Letters 345, 27–32. https://doi.org/10.1016/0014-5793(94)00395-5

Janelidze, S., Mattsson, N., Palmqvist, S., Smith, R., Beach, T.G., Serrano, G.E., Chai, X., Proctor, N.K., Eichenlaub, U., Zetterberg, H., Blennow, K., Reiman, E.M., Stomrud, E., Dage, J.L., Hansson, O., (2020). Plasma P-tau181 in Alzheimer's disease: relationship to other biomarkers, differential diagnosis, neuropathology and longitudinal progression to Alzheimer's dementia. Nature Medicine 26, 379–386. https://doi.org/10.1038/s41591-020-0755-1

Janson, A.M., Fuxe, K., Goldstein, M., (1992). Differential effects of acute and chronic nicotine treatment on MPTP-(1-methyl-4-phenyl-1,2,3,6-tetrahydropyridine) induced degeneration of nigrostriatal dopamine neurons in the black mouse. Clinical Investigation Journal. 70, 232–238. https://doi.org/10.1007/BF00184656

Jiang, C., Haddad, G.G., (1997). Modulation of K+ channels by intracellular ATP in human neocortical neurons. Journal of Neurophysiology 77, 93–102. https://doi.org/10.1152/jn.1997.77.1.93

Johnson, S.W., North, R.A., (1992). Two types of neurone in the rat ventral tegmental area and their synaptic inputs. Journal of Physiology 450, 455–468. https://doi.org/10.1113/jphysiol.1992.sp019136

Jouanne, M., Rault, S., Voisin-Chiret, A.-S., (2017). Tau protein aggregation in Alzheimer's disease: An attractive target for the development of novel therapeutic agents. European Journal of Medicinal Chemistry 139, 153–167. https://doi.org/10.1016/j.ejmech.2017.07.070

Jurado, S., (2018). AMPA Receptor Trafficking in Natural and Pathological Aging. Frontiers in Molecular Neuroscience 10. https://doi.org/10.3389/fnmol.2017.00446

Kachroo, A., Schwarzschild, M.A., (2012). Adenosine A2A receptor gene disruption protects in an α-synuclein model of Parkinson's disease. Annals of Neurology. 71, 278–282. https://doi.org/10.1002/ana.22630

Kajiwara, R., Wouterlood, F.G., Sah, A., Boekel, A.J., Baks-te Bulte, L.T.G., Witter, M.P., (2008). Convergence of entorhinal and CA3 inputs onto pyramidal neurons and interneurons in hippocampal area CA1--an anatomical study in the rat. Hippocampus 18, 266–280. https://doi.org/10.1002/hipo.20385

Kanaan, N.M., Morfini, G.A., LaPointe, N.E., Pigino, G.F., Patterson, K.R., Song, Y., Andreadis, A., Fu, Y., Brady, S.T., Binder, L.I., (2011). Pathogenic forms of tau inhibit kinesin-dependent axonal transport through a mechanism involving activation of axonal phosphotransferases. Journal of Neuroscience 31, 9858–9868. https://doi.org/10.1523/JNEUROSCI.0560-11.2011

Karikari, T.K., (2017). Distinct conformations, aggregation, and neuronal internalisation of different tau strains. (PhD Thesis). University of Warwick.

Karikari, T.K., Nagel, D.A., Grainger, A., Clarke-Bland, C., Crowe, J., Hill, E.J., Moffat, K.G., (2019a). Distinct Conformations, Aggregation and Cellular Internalization of Different Tau Strains. Frontiers in Cellular Neuroscience 13. https://doi.org/10.3389/fncel.2019.00296

Karikari, T.K., Nagel, D.A., Grainger, A., Clarke-Bland, C., Hill, E.J., Moffat, K.G., (2019b). Preparation of stable tau oligomers for cellular and biochemical studies. Analytical Biochemistry 566, 67–74. https://doi.org/10.1016/j.ab.2018.10.013

Karikari, Thomas K, Pascoal, T.A., Ashton, N.J., Janelidze, S., Benedet, A.L., Rodriguez, J.L., Chamoun, M., Savard, M., Kang, M.S., Therriault, J., Schöll, M., Massarweh, G., Soucy, J.-P., Höglund, K., Brinkmalm, G., Mattsson, N., Palmqvist, S., Gauthier, S., Stomrud, E., Zetterberg, H., Hansson, O., Rosa-Neto, P., Blennow, K., (2020). Blood phosphorylated tau 181 as a biomarker for Alzheimer's disease: a diagnostic performance and prediction modelling study using data from four prospective cohorts. The Lancet Neurology 19, 422–433. https://doi.org/10.1016/S1474-4422(20)30071-5

Karikari, Thomas K., Thomas, R., Moffat, K.G., (2020). The C291R Tau Variant Forms Different Types of Protofibrils. Frontiers in Molecular Neuroscience 13. https://doi.org/10.3389/fnmol.2020.00039

Karikari, T.K., Turner, A., Stass, R., Lee, L.C.Y., Wilson, B., Nagel, D.A., Hill, E.J., Moffat, K.G., (2017). Expression and purification of tau protein and its frontotemporal dementia variants using a cleavable histidine tag. Protein Expression and Purification 130, 44–54. https://doi.org/10.1016/j.pep.2016.09.009

Kasper, E.M., Larkman, A.U., Lübke, J., Blakemore, C., (1994). Pyramidal neurons in layer 5 of the rat visual cortex. II. Development of electrophysiological properties. Journal of Comparative Neurology 339, 475–494. https://doi.org/10.1002/cne.903390403

Kaufmann, T.J., Harrison, P.M., Richardson, M.J.E., Pinheiro, T.J.T., Wall, M.J., (2016). Intracellular soluble αSynuclein oligomers reduce pyramidal cell excitability. Journal of Physiology 594, 2751–2772. https://doi.org/10.1113/JP271968

Keeler, J.F., Pretsell, D.O., Robbins, T.W., (2014). Functional implications of dopamine D1 vs. D2 receptors: A “prepare and select” model of the striatal direct vs. indirect pathways. Neuroscience 282, 156–175. https://doi.org/10.1016/j.neuroscience.2014.07.021

Kefalopoulou, Z., Politis, M., Piccini, P., Mencacci, N., Bhatia, K., Jahanshahi, M., Widner, H., Rehncrona, S., Brundin, P., Björklund, A., Lindvall, O., Limousin, P., Quinn, N., Foltynie, T., (2014). Long-term clinical outcome of fetal cell transplantation for Parkinson disease: two case reports. JAMA Neurology 71, 83–87. doi.org/10.1001/jamaneurol.2013.4749

Kehr, W., (1974). A method for the isolation and determination of 3-methoxytyramine in brain tissue. Naunyn-Schmiedeberg’s Naunyn-Schmiedeberg's Archives of Pharmacology 284, 149–158. https://doi.org/10.1007/BF00501119

Kerr, M.I., Wall, M.J., Richardson, M.J.E., (2013). Adenosine A1 receptor activation mediates the developmental shift at layer 5 pyramidal cell synapses and is a determinant of mature synaptic strength. Journal of Physiology 591, 3371–3380. doi.org/10.1113/jphysiol.2012.244392

Kim, J.-I., Ganesan, S., Luo, S.X., Wu, Y.-W., Park, E., Huang, E.J., Chen, L., Ding, J.B., (2015). Aldehyde dehydrogenase 1a1 mediates a GABA synthesis pathway in midbrain dopaminergic neurons. Science 350, 102–106. https://doi.org/10.1126/science.aac4690

Kirkeby, A., Grealish, S., Wolf, D.A., Nelander, J., Wood, J., Lundblad, M., Lindvall, O., Parmar, M., (2012). Generation of regionally specified neural progenitors and functional neurons from human embryonic stem cells under defined conditions. Cell Reports 1, 703–714. https://doi.org/10.1016/j.celrep.2012.04.009

Klein, C., Westenberger, A., (2012). Genetics of Parkinson's disease. Cold Spring Harbor Perspectives in Medicine 2, a008888. https://doi.org/10.1101/cshperspect.a008888

Knierim, J.J., (2015). The hippocampus. Current Biology. 25, R1116–R1121. https://doi.org/10.1016/j.cub.2015.10.049

Kole, M.H.P., Ilschner, S.U., Kampa, B.M., Williams, S.R., Ruben, P.C., Stuart, G.J., (2008). Action potential generation requires a high sodium channel density in the axon initial segment. Nature Neuroscience 11, 178–186. https://doi.org/10.1038/nn2040

Kontis, K.J., Rounaghi, A., Goldin, A.L., (1997). Sodium Channel Activation Gating Is Affected by Substitutions of Voltage Sensor Positive Charges in All Four Domains. The Journal of General Physiology 110, 391–401.

Kontsekova, E., Zilka, N., Kovacech, B., Novak, P., Novak, M., (2014). First-in-man tau vaccine targeting structural determinants essential for pathological tau–tau interaction reduces tau oligomerisation and neurofibrillary degeneration in an Alzheimer's disease model. Alzheimer's Research & Therapy 6, 44. https://doi.org/10.1186/alzrt278

Köpke, E., Tung, Y.C., Shaikh, S., Alonso, A.C., Iqbal, K., Grundke-Iqbal, I., (1993). Microtubule-associated protein tau. Abnormal phosphorylation of a non-paired helical filament pool in Alzheimer disease. Journal of Biological Chemistry 268, 24374–24384. https://doi.org/10.1016/S0021-9258(20)80536-5

Koval, M., Molina, S.A., Burt, J.M., (2014). Mix and match: investigating heteromeric and heterotypic gap junction channels in model systems and native tissues. FEBS Letters 588, 1193–1204. https://doi.org/10.1016/j.febslet.2014.02.025

Kozloski, J., Hamzei-Sichani, F., Yuste, R., (2001). Stereotyped position of local synaptic targets in neocortex. Science 293, 868–872. https://doi.org/10.1126/science.293.5531.868

Krashia, P., Martini, A., Nobili, A., Aversa, D., D'Amelio, M., Berretta, N., Guatteo, E., Mercuri, N.B., (2017). On the properties of identified dopaminergic neurons in the mouse substantia nigra and ventral tegmental area. The European Journal of Neuroscience 45, 92–105. https://doi.org/10.1111/ejn.13364

Kriks, S., Shim, J.-W., Piao, J., Ganat, Y.M., Wakeman, D.R., Xie, Z., Carrillo-Reid, L., Auyeung, G., Antonacci, C., Buch, A., Yang, L., Beal, M.F., Surmeier, D.J., Kordower, J.H., Tabar, V., Studer, L., (2011). Dopamine neurons derived from human ES cells efficiently engraft in animal models of Parkinson's disease. Nature 480, 547–551. https://doi.org/10.1038/nature10648

Kumar, S., Tepper, K., Kaniyappan, S., Biernat, J., Wegmann, S., Mandelkow, E.-M., Müller, D.J., Mandelkow, E., (2014). Stages and Conformations of the Tau Repeat Domain during Aggregation and Its Effect on Neuronal Toxicity. The Journal of Biological Chemistry 289, 20318–20332. https://doi.org/10.1074/jbc.M114.554725

Kumar, S.T., Donzelli, S., Chiki, A., Syed, M.M.K., Lashuel, H.A., (2020). A simple, versatile and robust centrifugation-based filtration protocol for the isolation and quantification of αSynuclein monomers, oligomers and fibrils: Towards improving experimental reproducibility in αSynuclein research. Journal of Neurochemistry 153, 103–119. https://doi.org/10.1111/jnc.14955

Kumar, M.J., Andersen, J.K., (2004). Perspectives on MAO-B in aging and neurological disease: where do we go from here? Molecular Neurobiology 30, 77–89. https://doi.org/10.1385/MN:30:1:077

Kumar, N.M., Gilula, N.B., (1996). The gap junction communication channel. Cell 84, 381–388. https://doi.org/10.1016/s0092-8674(00)81282-9

Lacey, M.G., Mercuri, N.B., North, R.A., (1989). Two cell types in rat substantia nigra zona compacta distinguished by membrane properties and the actions of dopamine and opioids. Journal of Neuroscience 9, 1233–1241.

Lacey, M.G., Mercuri, N.B., North, R.A., (1987). Dopamine acts on D2 receptors to increase potassium conductance in neurones of the rat substantia nigra zona compacta. Journal of Physiology 392, 397–416. https://doi.org/10.1113/jphysiol.1987.sp016787

Lai, B.C.L., Marion, S.A., Teschke, K., Tsui, J.K.C., (2002). Occupational and environmental risk factors for Parkinson's disease. Parkinsonism Related Disorders 8, 297–309. https://doi.org/10.1016/s1353-8020(01)00054-2

Lammel, S., Lim, B.K., Malenka, R.C., (2014). Reward and aversion in a heterogeneous midbrain dopamine system. Neuropharmacology 76. https://doi.org/10.1016/j.neuropharm.2013.03.019

Lanciego, J.L., Luquin, N., Obeso, J.A., (2012). Functional Neuroanatomy of the Basal Ganglia. Cold Spring Harbour Perspectives in Medicine 2. https://doi.org/10.1101/cshperspect.a009621

Lapointe, N.E., Horowitz, P.M., Guillozet-Bongaarts, A.L., Silva, A., Andreadis, A., Binder, L.I., (2009). Tau 6D and 6P isoforms inhibit polymerization of full-length tau in vitro. Biochemistry 48, 12290–12297. https://doi.org/10.1021/bi901304u

Largo-Barrientos, P., Apóstolo, N., Creemers, E., Callaerts-Vegh, Z., Swerts, J., Davies, C., McInnes, J., Wierda, K., Strooper, B.D., Spires-Jones,

T., Wit, J. de, Uytterhoeven, V., Verstreken, P., (2021). Lowering Synaptogyrin-3 expression rescues Tau-induced memory defects and synaptic loss in the presence of microglial activation. Neuron 0. https://doi.org/10.1016/j.neuron.2020.12.016

Larson, J., Munkácsy, E., (2015). Theta-Burst LTP. Brain Research 1621, 38–50. https://doi.org/10.1016/j.brainres.2014.10.034

Lasagna-Reeves, C.A., Castillo-Carranza, D.L., Guerrero-Muoz, M.J., Jackson, G.R., Kayed, R., (2010). Preparation and characterization of neurotoxic tau oligomers. Biochemistry 49, 10039–10041. https://doi.org/10.1021/bi1016233

Lasagna-Reeves, C.A., Castillo-Carranza, D.L., Sengupta, U., Sarmiento, J., Troncoso, J., Jackson, G.R., Kayed, R., (2012). Identification of oligomers at early stages of tau aggregation in Alzheimer's disease. FASEB Journal 26, 1946–1959. https://doi.org/10.1096/fj.11-199851

Lasagna-Reeves, C.A., Sengupta, U., Castillo-Carranza, D., Gerson, J.E., Guerrero-Munoz, M., Troncoso, J.C., Jackson, G.R., Kayed, R., (2014). The formation of tau pore-like structures is prevalent and cell specific: possible implications for the disease phenotypes. Acta Neuropathologica Communications 2. https://doi.org/10.1186/2051-5960-2-56

Lashuel, H.A., Overk, C.R., Oueslati, A., Masliah, E., (2013). The many faces of αSynuclein: from structure and toxicity to therapeutic target. Nature Reviews Neuroscience 14, 38–48. https://doi.org/10.1038/nrn3406

Lavezzi, A.M., Mehboob, R., Alfonsi, G., Ferrero, S., (2020). Substantia Nigra Abnormalities Provide New Insight on the Neural Mechanisms Underlying the Sleep-Arousal Phase Dysfunctions in Sudden Infant Death Syndrome. ASN NEURO 12. https://doi.org/10.1177/1759091420962695

Lee, V.M., Goedert, M., Trojanowski, J.Q., (2001). Neurodegenerative tauopathies. Annual Review of Neuroscience 24, 1121–1159. https://doi.org/10.1146/annurev.neuro.24.1.1121

Lee, Y.-S., Silva, A.J., (2009). The molecular and cellular biology of enhanced cognition. Nature Reviews Neuroscience 10, 126–140. https://doi.org/10.1038/nrn2572

Lemay, S., Chouinard, S., Blanchet, P., Masson, H., Soland, V., Beuter, A., Bédard, M.-A., (2004). Lack of efficacy of a nicotine transdermal treatment on motor and cognitive deficits in Parkinson's disease. Prog. Neuropsychopharmacol. Biological Psychiatry 28, 31–39. https://doi.org/10.1016/S0278-5846(03)00172-6

Lesage, S., Brice, A., (2009). Parkinson's disease: from monogenic forms to genetic susceptibility factors. Human Molecular Genetics 18, R48–R59. https://doi.org/10.1093/hmg/ddp012

Levin, B.E., Dunn-Meynell, A.A., Routh, V.H., (1999). Brain glucose sensing and body energy homeostasis: role in obesity and diabetes. American Journal of Physiology 276, R1223-1231. https://doi.org/10.1152/ajpregu.1999.276.5.R1223

Lewis, J., Dickson, D.W., Lin, W.L., Chisholm, L., Corral, A., Jones, G., Yen, S.H., Sahara, N., Skipper, L., Yager, D., Eckman, C., Hardy, J., Hutton, M., McGowan, E., (2001). Enhanced neurofibrillary degeneration in transgenic mice expressing mutant tau and APP. Science 293, 1487–1491. https://doi.org/10.1126/science.1058189

LeWitt, P.A., Rezai, A.R., Leehey, M.A., Ojemann, S.G., Flaherty, A.W., Eskandar, E.N., Kostyk, S.K., Thomas, K., Sarkar, A., Siddiqui, M.S., Tatter, S.B., Schwalb, J.M., Poston, K.L., Henderson, J.M., Kurlan, R.M., Richard, I.H., Meter, L.V., Sapan, C.V., During, M.J., Kaplitt, M.G., Feigin, A., (2011). AAV2-GAD gene therapy for advanced Parkinson's disease: a double-blind, sham-surgery controlled, randomised trial. The Lancet Neurology 10, 309–319. https://doi.org/10.1016/S1474-4422(11)70039-4

Li, W., Englund, E., Widner, H., Mattsson, B., Westen, D. van, Lätt, J., Rehncrona, S., Brundin, P., Björklund, A., Lindvall, O., Li, J.-Y., (2016). Extensive graft-derived dopaminergic innervation is maintained 24 years after transplantation in the degenerating parkinsonian brain. Proceedings of the National Academy of Sciences 113, 6544–6549. https://doi.org/10.1073/pnas.1605245113

Li, Y., Li, C.-Y., Xi, W., Jin, S., Wu, Z.-H., Jiang, P., Dong, P., He, X.-B., Xu, F.-Q., Duan, S., Zhou, Y.-D., Li, X.-M., (2019). Rostral and Caudal Ventral Tegmental Area GABAergic Inputs to Different Dorsal Raphe Neurons Participate in Opioid Dependence. Neuron 101, 748-761.e5. https://doi.org/10.1016/j.neuron.2018.12.012

Li, F.-J., Ji, H.-F., Shen, L., (2012). A Meta-Analysis of Tea Drinking and Risk of Parkinson's Disease. Scientific World Journal 2012, e923464. https://doi.org/10.1100/2012/923464

Li, X., Li, W., Liu, G., Shen, X., Tang, Y., (2015). Association between cigarette smoking and Parkinson's disease: A meta-analysis. Archives of Gerontology and Geriatrics 61, 510–516. https://doi.org/10.1016/j.archger.2015.08.004

Light, P.E., French, R.J., (1994). Glibenclamide selectively blocks ATP-sensitive K+ channels reconstituted from skeletal muscle. European

Journal of Pharmacology 259, 219–222. https://doi.org/10.1016/0014-2999(94)90647-5

Lindvall, O., Brundin, P., Widner, H., Rehncrona, S., Gustavii, B., Frackowiak, R., Leenders, K.L., Sawle, G., Rothwell, J.C., Marsden, C.D., (1990). Grafts of fetal dopamine neurons survive and improve motor function in Parkinson's disease. Science 247, 574–577. https://doi.org/10.1126/science.2105529

Liss, B., Bruns, R., Roeper, J., (1999). Alternative sulfonylurea receptor expression defines metabolic sensitivity of K-ATP channels in dopaminergic midbrain neurons. EMBO Journal 18, 833–846. https://doi.org/10.1093/emboj/18.4.833

Liss, B., Roeper, J., (2001). ATP-Sensitive Potassium Channels in Dopaminergic Neurons: Transducers of Mitochondrial Dysfunction. Physiology 16, 214–217. https://doi.org/10.1152/physiologyonline.2001.16.5.214

Liss, B., Haeckel, O., Wildmann, J., Miki, T., Seino, S., Roeper, J., (2005). K-ATP channels promote the differential degeneration of dopaminergic midbrain neurons. Nature Neuroscience 8, 1742–1751. https://doi.org/10.1038/nn1570

Loeschcke, H.H., (1982). Central chemosensitivity and the reaction theory. The Journal of Physiology 332, 1–24. https://doi.org/10.1113/jphysiol.1982.sp014397

London, M., Häusser, M., (2005). Dendritic computation. Annual Review of Neuroscience 28, 503–532. doi.org/10.1146/annurev.neuro.28.061604.135703

Loomis, P.A., Howard, T.H., Castleberry, R.P., Binder, L.I., (1990). Identification of nuclear tau isoforms in human neuroblastoma cells. Proceedings of the National Academy of Sciences 87, 8422–8426. https://doi.org/10.1073/pnas.87.21.8422

López-Gambero, A.J., Martínez, F., Salazar, K., Cifuentes, M., Nualart, F., (2019). Brain Glucose-Sensing Mechanism and Energy Homeostasis. Mol. Neurobiol. 56, 769–796. https://doi.org/10.1007/s12035-018-1099-4

Lorincz, A., Nusser, Z., (2010). Molecular Identity of Dendritic Voltage-Gated Sodium Channels. Science 328, 906–909. https://doi.org/10.1126/science.1187958

Lu, L., Fu, D., Li, H., Liu, A., Li, J., Zheng, G., (2014). Diabetes and Risk of Parkinson's Disease: An Updated Meta-Analysis of Case-Control Studies. PLOS ONE 9, e85781. https://doi.org/10.1371/journal.pone.0085781

Lue, L.F., Kuo, Y.M., Roher, A.E., Brachova, L., Shen, Y., Sue, L., Beach, T., Kurth, J.H., Rydel, R.E., Rogers, J., (1999). Soluble amyloid beta peptide concentration as a predictor of synaptic change in Alzheimer's disease. The American Journal of Pathology 155, 853–862. https://doi.org/10.1016/s0002-9440(10)65184-x

Luk, K.C., Song, C., O'Brien, P., Stieber, A., Branch, J.R., Brunden, K.R., Trojanowski, J.Q., Lee, V.M.-Y., (2009). Exogenous αSynuclein fibrils seed the formation of Lewy body-like intracellular inclusions in cultured cells. PNAS 106, 20051–20056. https://doi.org/10.1073/pnas.0908005106

Luna, E., Decker, S.C., Riddle, D.M., Caputo, A., Zhang, B., Cole, T., Caswell, C., Xie, S.X., Lee, V.M.Y., Luk, K.C., (2018). Differential αSynuclein expression contributes to selective vulnerability of hippocampal neuron subpopulations to fibril-induced toxicity. Acta Neuropathologica 135, 855–875. https://doi.org/10.1007/s00401-018-1829-8

Luo, J., Kaplitt, M.G., Fitzsimons, H.L., Zuzga, D.S., Liu, Y., Oshinsky, M.L., During, M.J., (2002). Subthalamic GAD gene therapy in a Parkinson's disease rat model. Science 298, 425–429. https://doi.org/10.1126/science.1074549

Luo, Y., Batalao, A., Zhou, H., Zhu, L., (1997). Mammalian two-hybrid system: a complementary approach to the yeast two-hybrid system. Biotechniques 22, 350–352. https://doi.org/10.2144/97222pf02

Lüscher, C., Malenka, R.C., (2012). NMDA Receptor-Dependent Long-Term Potentiation and Long-Term Depression (LTP/LTD). Cold Spring Harbour Perspect. Biol. 4. https://doi.org/10.1101/cshperspect.a005710

Luth, E.S., Stavrovskaya, I.G., Bartels, T., Kristal, B.S., Selkoe, D.J., (2014). Soluble, Prefibrillar αSynuclein Oligomers Promote Complex I-dependent, Ca2+-induced Mitochondrial Dysfunction. The Journal of Biological Chemistry 289, 21490–21507. https://doi.org/10.1074/jbc.M113.545749

Ma, C., Liu, Y., Neumann, S., Gao, X., (2017). Nicotine from cigarette smoking and diet and Parkinson disease: a review. Translational Neurodegeneration 6. https://doi.org/10.1186/s40035-017-0090-8

Maeda, S., Sahara, N., Saito, Y., Murayama, S., Ikai, A., Takashima, A., (2006). Increased levels of granular tau oligomers: an early sign of brain aging and Alzheimer's disease. Neuroscience Research 54, 197–201. https://doi.org/10.1016/j.neures.2005.11.009

Magnani, E., Fan, J., Gasparini, L., Golding, M., Williams, M., Schiavo, G., Goedert, M., Amos, L.A., Spillantini, M.G., (2007). Interaction of tau

protein with the dynactin complex. EMBO Journal 26, 4546–4554. https://doi.org/10.1038/sj.emboj.7601878

Mair, W., Muntel, J., Tepper, K., Tang, S., Biernat, J., Seeley, W.W., Kosik, K.S., Mandelkow, E., Steen, H., Steen, J.A., (2016). FLEXITau: Quantifying Post-translational Modifications of Tau Protein in Vitro and in Human Disease. Analytical chemistry 88, 3704–3714. https://doi.org/10.1021/acs.analchem.5b04509

Malenka, R.C., Bear, M.F., (2004). LTP and LTD: An Embarrassment of Riches. Neuron 44, 5–21. https://doi.org/10.1016/j.neuron.2004.09.012

Marcantoni, A., Raymond, E.F., Carbone, E., Marie, H., (2014). Firing properties of entorhinal cortex neurons and early alterations in an Alzheimer's disease transgenic model. Pflugers Archives 466, 1437–1450. https://doi.org/10.1007/s00424-013-1368-z

Markram, H., Lübke, J., Frotscher, M., Roth, A., Sakmann, B., (1997). Physiology and anatomy of synaptic connections between thick tufted pyramidal neurones in the developing rat neocortex. Journal of Physiology 500, 409–440.

Markram, H., Muller, E., Ramaswamy, S., Reimann, M.W., Abdellah, M., Sanchez, C.A., Ailamaki, A., Alonso-Nanclares, L., Antille, N., Arsever, S., Kahou, G.A.A., Berger, T.K., Bilgili, A., Buncic, N., Chalimourda, A., Chindemi, G., Courcol, J.-D., Delalondre, F., Delattre, V., Druckmann, S., Dumusc, R., Dynes, J., Eilemann, S., Gal, E., Gevaert, M.E., Ghobril, J.-P., Gidon, A., Graham, J.W., Gupta, A., Haenel, V., Hay, E., Heinis, T., Hernando, J.B., Hines, M., Kanari, L., Keller, D., Kenyon, J., Khazen, G., Kim, Y., King, J.G., Kisvarday, Z., Kumbhar, P., Lasserre, S., Le Bé, J.-V., Magalhães, B.R.C., Merchán-Pérez, A., Meystre, J., Morrice, B.R., Muller, J., Muñoz-Céspedes, A., Muralidhar, S., Muthurasa, K., Nachbaur, D., Newton, T.H., Nolte, M., Ovcharenko, A., Palacios, J., Pastor, L., Perin, R., Ranjan, R., Riachi, I., Rodríguez, J.-R., Riquelme, J.L., Rössert, C., Sfyrakis, K., Shi, Y., Shillcock, J.C., Silberberg, G., Silva, R., Tauheed, F., Telefont, M., Toledo-Rodriguez, M., Tränkler, T., Van Geit, W., Díaz, J.V., Walker, R., Wang, Y., Zaninetta, S.M., DeFelipe, J., Hill, S.L., Segev, I., Schürmann, F., (2015). Reconstruction and Simulation of Neocortical Microcircuitry. Cell 163, 456–492. https://doi.org/10.1016/j.cell.2015.09.029

Masters, C.L., Simms, G., Weinman, N.A., Multhaup, G., McDonald, B.L., Beyreuther, K., (1985). Amyloid plaque core protein in Alzheimer disease and Down syndrome. Proceedings of the National Academy of Sciences 82, 4245–4249. https://doi.org/10.1073/pnas.82.12.4245

Mattsson, N., Zetterberg, H., Janelidze, S., Insel, P.S., Andreasson, U., Stomrud, E., Palmqvist, S., Baker, D., Hehir, C.A.T., Jeromin, A.,

Hanlon, D., Song, L., Shaw, L.M., Trojanowski, J.Q., Weiner, M.W., Hansson, O., Blennow, K., (2016). Plasma tau in Alzheimer disease. Neurology 87, 1827–1835. doi.org/10.1212/WNL.0000000000003246

Mayer, M.L., Westbrook, G.L., (1983). A voltage-clamp analysis of inward (anomalous) rectification in mouse spinal sensory ganglion neurones. Journal of Physiology 340, 19–45. https://doi.org/10.1113/jphysiol.1983.sp014747

Mayeux, R., (2003). EPIDEMIOLOGY OFNEURODEGENERATION. Annual Review of Neuroscience, 26(1), pp.81-104.

Mayeux, R., (2003). Epidemiology of neurodegeneration. Annual Reviews Neuroscience 26, 81–104. https://doi.org/10.1146/annurev.neuro.26.043002.094919

Mccutcheon, J.E., Ebner, S.R., Loriaux, A.L., Roitman, M.F., (2012). Encoding of Aversion by Dopamine and the Nucleus Accumbens. Frontiers in Neuroscience. 6. https://doi.org/10.3389/fnins.2012.00137

McInnes, J., Wierda, K., Snellinx, A., Bounti, L., Wang, Y.-C., Stancu, I.-C., Apóstolo, N., Gevaert, K., Dewachter, I., Spires-Jones, T.L., De Strooper, B., De Wit, J., Zhou, L., Verstreken, P., (2018). Synaptogyrin-3 Mediates Presynaptic Dysfunction Induced by Tau. Neuron 97, 823-835.e8. https://doi.org/10.1016/j.neuron.2018.01.022

McLean, C.A., Cherny, R.A., Fraser, F.W., Fuller, S.J., Smith, M.J., Beyreuther, K., Bush, A.I., Masters, C.L., (1999). Soluble pool of Abeta amyloid as a determinant of severity of neurodegeneration in Alzheimer's disease. Annals of Neurology 46, 860–866. https://doi.org/10.1002/1531-8249(199912)46:6<860::aid-ana8>3.0.co;2-m

Meigh, L., Cook, D., Zhang, J., Dale, N., (2015). Rational design of new NO and redox sensitivity into connexin26 hemichannels. Open Biology 5, 140208. https://doi.org/10.1098/rsob.140208

Meigh, L., Greenhalgh, S.A., Rodgers, T.L., Cann, M.J., Roper, D.I., Dale, N., (2013). CO_2 directly modulates connexin 26 by formation of carbamate bridges between subunits. eLife 2, e01213. https://doi.org/10.7554/eLife.01213

Meigh, L., Hussain, N., Mulkey, D.K., Dale, N., (2014). Connexin26 hemichannels with a mutation that causes KID syndrome in humans lack sensitivity to CO2. eLife 3, e04249. https://doi.org/10.7554/eLife.04249

Mercuri, N.B., Saiardi, A., Bonci, A., Picetti, R., Calabresi, P., Bernardi, G., Borrelli, E., (1997). Loss of autoreceptor function in dopaminergic

neurons from dopamine D2 receptor deficient mice. Neuroscience 79, 323–327. https://doi.org/10.1016/s0306-4522(97)00135-8

Michel, C.H., Kumar, S., Pinotsi, D., Tunnacliffe, A., St. George-Hyslop, P., Mandelkow, E., Mandelkow, E.-M., Kaminski, C.F., Kaminski Schierle, G.S., (2014). Extracellular Monomeric Tau Protein Is Sufficient to Initiate the Spread of Tau Protein Pathology. The Journal of Biological Chemistry 289, 956–967. https://doi.org/10.1074/jbc.M113.515445

Mielke, M.M., Syrjanen, J.A., Blennow, K., Zetterberg, H., Vemuri, P., Skoog, I., Machulda, M.M., Kremers, W.K., Knopman, D.S., Jack, C., Petersen, R.C., Kern, S., (2019). Plasma and CSF neurofilament light: Relation to longitudinal neuroimaging and cognitive measures. Neurology 93, e252–e260. https://doi.org/10.1212/WNL.0000000000007767

Milescu, L.S., Bean, B.P., Smith, J.C., (2010). Isolation of somatic Na+ currents by selective inactivation of axonal channels with a voltage pre-pulse. Journal of Neuroscience 30, 7740–7748. https://doi.org/10.1523/JNEUROSCI.6136-09.2010

Miller, E.C., Teravskis, P.J., Dummer, B.W., Zhao, X., Huganir, R.L., Liao, D., (2014). Tau phosphorylation and tau mislocalization mediate soluble Aβ oligomer-induced AMPA glutamate receptor signaling deficits. European Journal of Neuroscience 39, 1214–1224. https://doi.org/10.1111/ejn.12507

Mirbaha, H., Chen, D., Morazova, O.A., Ruff, K.M., Sharma, A.M., Liu, X., Goodarzi, M., Pappu, R.V., Colby, D.W., Mirzaei, H., Joachimiak, L.A., Diamond, M.I., (2018). Inert and seed-competent tau monomers suggest structural origins of aggregation. Elife 7. https://doi.org/10.7554/eLife.36584

Mironov, S.L., (2015). αSynuclein forms non-selective cation channels and stimulates ATP-sensitive potassium channels in hippocampal neurons. Journal of Physiology 593, 145–159. https://doi.org/10.1113/jphysiol.2014.280974

Mitsuoka, T., Kaseda, Y., Yamashita, H., Kohriyama, T., Kawakami, H., Nakamura, S., Yamamura, Y., (2002). Effects of nicotine chewing gum on UPDRS score and P300 in early-onset parkinsonism. Hiroshima Journal of Medical Sciences 51, 33–39.

Mondragón-Rodríguez, S., Salas-Gallardo, A., González-Pereyra, P., Macías, M., Ordaz, B., Peña-Ortega, F., Aguilar-Vázquez, A., Orta-Salazar, E., Díaz-Cintra, S., Perry, G., Williams, S., (2018). Phosphorylation of Tau protein correlates with changes in hippocampal theta oscillations and reduces hippocampal excitability in Alzheimer's model. Journal of

Biological Chemistry 293, 8462–8472. https://doi.org/10.1074/jbc.RA117.001187

Moore, A.R., Zhou, W.-L., Sirois, C.L., Belinsky, G.S., Zecevic, N., Antic, S.D., (2014). Connexin hemichannels contribute to spontaneous electrical activity in the human fetal cortex. Proceedings of the National Academy of Sciences 111, E3919-3928. doi.org/10.1073/pnas.1405253111

Morales, M., Margolis, E.B., (2017). Ventral tegmental area: cellular heterogeneity, connectivity, and behaviour. Nature Reviews Neuroscience 18, 73–85. https://doi.org/10.1038/nrn.2016.165

Morales, M., Root, D.H., (2014). Glutamate neurons within the midbrain dopamine regions. Neuroscience 282, 60–68. https://doi.org/10.1016/j.neuroscience.2014.05.032

Morgan, D.G., Finch, C.E., (1988). Dopaminergic changes in the basal ganglia. A generalized phenomenon of aging in mammals. Annals of the New York Academy of Sciences 515, 145–160. https://doi.org/10.1111/j.1749-6632.1988.tb32978.x

Morgan, C.J., (2017). Use of proper statistical techniques for research studies with small samples. American Journal of Physiology - Lung Cellular and Molecular Physiology 313, L873– L877. https://doi.org/10.1152/ajplung.00238.2017

Mountcastle, V.B., (1998). Perceptual Neuroscience: The Cerebral Cortex. Harvard University Press.

Mountcastle, V.B., (1957). Modality and topographic properties of single neurons of cat's somatic sensory cortex. Journal of Neurophysiology 20, 408–434. https://doi.org/10.1152/jn.1957.20.4.408

Mukrasch, M.D., Bibow, S., Korukottu, J., Jeganathan, S., Biernat, J., Griesinger, C., Mandelkow, E., Zweckstetter, M., (2009). Structural polymorphism of 441-residue tau at single residue resolution. PLoS Biology 7, e34. https://doi.org/10.1371/journal.pbio.1000034

Mullane, K., Williams, M., (2020). Alzheimer's disease beyond amyloid: Can the repetitive failures of amyloid-targeted therapeutics inform future approaches to dementia drug discovery? Biochemical Pharmacology 177, 113945. https://doi.org/10.1016/j.bcp.2020.113945

Müller, M.L.T.M., Bohnen, N.I., (2013). Cholinergic Dysfunction in Parkinson's Disease. Current Neurology and Neuroscience Reports 13, 377. https://doi.org/10.1007/s11910-013-0377-9

Munoz, D.G., Fujioka, S., (2018). Caffeine and Parkinson disease: A possible diagnostic and pathogenic breakthrough. Neurology 90, 205–206. https://doi.org/10.1212/WNL.0000000000004898

Muñoz, P., Huenchuguala, S., Paris, I., Segura-Aguilar, J., (2012). Dopamine oxidation and autophagy. Parkinson's Disease, 920953. https://doi.org/10.1155/2012/920953

Murphy, D.D., Rueter, S.M., Trojanowski, J.Q., Lee, V.M., (2000). Synucleins are developmentally expressed, and alpha-synuclein regulates the size of the presynaptic vesicular pool in primary hippocampal neurons. Journal of Neuroscience 20, 3214–3220.

Nabavi, S., Fox, R., Proulx, C.D., Lin, J.Y., Tsien, R.Y., Malinow, R., (2014). Engineering a memory with LTD and LTP. Nature 511, 348–352. https://doi.org/10.1038/nature13294

Nagy, J.I., Lynn, B.D., Tress, O., Willecke, K., Rash, J.E., (2011). Connexin26 expression in brain parenchymal cells demonstrated by targeted connexin ablation in transgenic mice. European Journal of Neuroscience 34, 263–271. https://doi.org/10.1111/j.1460-9568.2011.07741.x

Nagatsu, T., Sawada, M., (2006). Molecular mechanism of the relation of monoamine oxidase B and its inhibitors to Parkinson's disease: possible implications of glial cells. Journal of Neural Transmission Suppl. 53–65. https://doi.org/10.1007/978-3-211-33328-0_7

Nagy, J.I., Ionescu, A.V., Lynn, B.D., Rash, J.E., (2003). Connexin29 and Connexin32 at Oligodendrocyte and Astrocyte Gap Junctions and in Myelin of the Mouse Central Nervous System. Journal of Computational Neurology 464, 356–370. https://doi.org/10.1002/cne.10797

Narasimhan, S., Guo, J.L., Changolkar, L., Stieber, A., McBride, J.D., Silva, L.V., He, Z., Zhang, B., Gathagan, R.J., Trojanowski, J.Q., Lee, V.M.Y., (2017). Pathological Tau Strains from Human Brains Recapitulate the Diversity of Tauopathies in Nontransgenic Mouse Brain. Journal of Neuroscience 37, 11406–11423. doi.org/10.1523/JNEUROSCI.1230-17.2017

Näslund, J., Haroutunian, V., Mohs, R., Davis, K.L., Davies, P., Greengard, P., Buxbaum, J.D., (2000). Correlation between elevated levels of amyloid beta-peptide in the brain and cognitive decline. JAMA 283, 1571–1577. https://doi.org/10.1001/jama.283.12.1571

Nattie, E., (1999). CO2, brainstem chemoreceptors and breathing. Progress in Neurobiology 59, 299–331. https://doi.org/10.1016/S0301-0082(99)00008-8

Navarro, M., Rodriquez de Fonseca, F., Alvarez, E., Chowen, J.A., Zueco, J.A., Gomez, R., Eng, J., Blázquez, E., (1996). Colocalization of glucagon-like peptide-1 (GLP-1) receptors, glucose transporter GLUT-2, and glucokinase mRNAs in rat hypothalamic cells: evidence for a role

of GLP-1 receptor agonists as an inhibitory signal for food and water intake. Journal of Neurochemistry 67, 1982–1991. https://doi.org/10.1046/j.1471- 4159.1996.67051982.x

Neher, E., Sakmann, B., (1976). Single-channel currents recorded from membrane of denervated frog muscle fibres. Nature 260, 799–802. https://doi.org/10.1038/260799a0

Nelson, P.T., Abner, E.L., Schmitt, F.A., Kryscio, R.J., Jicha, G.A., Santacruz, K., Smith, C.D., Patel, E., Markesbery, W.R., (2009). Brains with medial temporal lobe neurofibrillary tangles but no neuritic amyloid plaques are a diagnostic dilemma but may have pathogenetic aspects distinct from Alzheimer disease. Journal of Neuropathology and Experimental Neurology 68, 774–784. doi.org/10.1097/NEN.0b013e3181aacbe9

Nelson, P.T., Alafuzoff, I., Bigio, E.H., Bouras, C., Braak, H., Cairns, N.J., Castellani, R.J., Crain, B.J., Davies, P., Del Tredici, K., Duyckaerts, C., Frosch, M.P., Haroutunian, V., Hof, P.R., Hulette, C.M., Hyman, B.T., Iwatsubo, T., Jellinger, K.A., Jicha, G.A., Kövari, E., Kukull, W.A., Leverenz, J.B., Love, S., Mackenzie, I.R., Mann, D.M., Masliah, E., McKee, A.C., Montine, T.J., Morris, J.C., Schneider, J.A., Sonnen, J.A., Thal, D.R., Trojanowski, J.Q., Troncoso, J.C., Wisniewski, T., Woltjer, R.L., Beach, T.G., (2012). Correlation of Alzheimer Disease Neuropathologic Changes With Cognitive Status: A Review of the Literature. Journal of neuropathology and experimental neurology 71, 362–381. https://doi.org/10.1097/NEN.0b013e31825018f7

Neuhoff, H., Neu, A., Liss, B., Roeper, J., (2002). Ih Channels Contribute to the Different Functional Properties of Identified Dopaminergic Subpopulations in the Midbrain. Journal of Neuroscience. 22, 1290–1302. https://doi.org/10.1523/JNEUROSCI.22-04-01290.2002

Neves, G., Cooke, S.F., Bliss, T.V.P., (2008). Synaptic plasticity, memory and the hippocampus: a neural network approach to causality. Nature Reviews Neuroscience 9, 65–75. https://doi.org/10.1038/nrn2303.

Neves, G., Cooke, S.F., Bliss, T.V.P., (2008). Synaptic plasticity, memory and the hippocampus: a neural network approach to causality. Nature Reviews Neuroscience. 9, 65–75. https://doi.org/10.1038/nrn2303

Niccoli, T., Partridge, L., (2012). Ageing as a risk factor for disease. Current Biology 22, R741-752. https://doi.org/10.1016/j.cub.2012.07.024

Niehaus, J.L., Murali, M., Kauer, J.A., (2010). Drugs of abuse and stress impair LTP at inhibitory synapses in the ventral tegmental area. European Journal of Neuroscience 32, 108–117. https://doi.org/10.1111/j.1460-9568.2010.07256.x

Nielsen, S.S., Gallagher, L.G., Lundin, J.I., Longstreth, W.T., Smith-Weller, T., Franklin, G.M., Swanson, P.D., Checkoway, H., (2012). Environmental tobacco smoke and Parkinson disease. Movement Disorders. 27, 293–297. https://doi.org/10.1002/mds.24012

Nijjar, S., Maddison, D., Meigh, L., Wolf, E. de, Rodgers, T., Cann, M.J., Dale, N., (2021). Opposing modulation of Cx26 gap junctions and hemichannels by CO_2. The Journal of Physiology 599, 103–118. https://doi.org/10.1113/JP280747

Nugent, F.S., Niehaus, J.L., Kauer, J.A., (2009). PKG and PKA signaling in LTP at GABAergic synapses. Neuropsychopharmacology 34, 1829–1842. https://doi.org/10.1038/npp.2009.5

Nugent, F.S., Penick, E.C., Kauer, J.A., (2007). Opioids block long-term potentiation of inhibitory synapses. Nature 446, 1086–1090. https://doi.org/10.1038/nature05726

Ogiwara, I., Miyamoto, H., Morita, N., Atapour, N., Mazaki, E., Inoue, I., Takeuchi, T., Itohara, S., Yanagawa, Y., Obata, K., Furuichi, T., Hensch, T.K., Yamakawa, K., (2007). Nav1.1 localizes to axons of parvalbumin-positive inhibitory interneurons: a circuit basis for epileptic seizures in mice carrying an Scn1a gene mutation. Journal of Neuroscience 27, 5903–5914. doi.org/10.1523/JNEUROSCI.5270-06.2007

Ondrejcak, T., Klyubin, I., Corbett, G.T., Fraser, G., Hong, W., Mably, A.J., Gardener, M., Hammersley, J., Perkinton, M.S., Billinton, A., Walsh, D.M., Rowan, M.J., (2018). Cellular Prion Protein Mediates the Disruption of Hippocampal Synaptic Plasticity by Soluble Tau In Vivo. Journal of Neuroscience 38, 10595–10606. https://doi.org/10.1523/JNEUROSCI.1700-18.2018

Oomura, Y., Kimura, K., Ooyama, H., Maeno, T., Iki, M., Kuniyoshi, M., (1964). RECIPROCAL ACTIVITIES OF THE VENTROMEDIAL AND LATERAL HYPOTHALAMIC AREAS OF CATS. Science 143, 484–485. https://doi.org/10.1126/science.143.3605.484

Oomura, Y., Ono, T., Ooyama, H., Wayner, M.J., (1969). Glucose and osmosensitive neurones of the rat hypothalamus. Nature 222, 282–284. https://doi.org/10.1038/222282a0

O'Reilly, E.J., McCullough, M.L., Chao, A., Henley, S.J., Calle, E.E., Thun, M.J., Ascherio, A., (2005). Smokeless tobacco use and the risk of Parkinson's disease mortality. Journal of Movement Disorders 20, 1383–1384. https://doi.org/10.1002/mds.20587

Osborne, J.L., Mitchell, G.S., (1978). Intrapulmonary and systemic CO2-chemoreceptor interaction in the control of avian respiration.

Respiration Physiology 33, 349–357. https://doi.org/10.1016/0034-5687(78)90061-0

Osborne, J.L., Mitchell, G.S., Powell, F., (1977). Ventilatory responses to CO2 in the chicken: intrapulmonary and systemic chemoreceptors. Respiration Physiology. 30, 369–382. https://doi.org/10.1016/0034-5687(77)90042-1

O'Shea, A., Cohen, R.A., Porges, E.C., Nissim, N.R., Woods, A.J., (2016). Cognitive Aging and the Hippocampus in Older Adults. Frontiers in Aging Neuroscience 8, 298. https://doi.org/10.3389/fnagi.2016.00298

Osorio, N., Alcaraz, G., Padilla, F., Couraud, F., Delmas, P., Crest, M., (2005). Differential targeting and functional specialization of sodium channels in cultured cerebellar granule cells. The Journal of Physiology 569, 801–816. https://doi.org/10.1113/jphysiol.2005.097022

Owens, R.L., Malhotra, A., (2010). Sleep-disordered breathing and COPD: the overlap syndrome. Respiratory Care 55, 1333–1344; discussion 1344-1346.

Palfi, S., Gurruchaga, J.M., Lepetit, H., Howard, K., Ralph, G.S., Mason, S., Gouello, G., Domenech, P., Buttery, P.C., Hantraye, P., Tuckwell, N.J., Barker, R.A., Mitrophanous, K.A., (2018). Long-Term Follow-Up of a Phase I/II Study of ProSavin, a Lentiviral Vector Gene Therapy for Parkinson's Disease. Human Gene Therapy Clinical Development 29, 148–155. https://doi.org/10.1089/humc.2018.081

Palfi, S., Gurruchaga, J.M., Ralph, G.S., Lepetit, H., Lavisse, S., Buttery, P.C., Watts, C., Miskin, J., Kelleher, M., Deeley, S., Iwamuro, H., Lefaucheur, J.P., Thiriez, C., Fenelon, G., Lucas, C., Brugières, P., Gabriel, I., Abhay, K., Drouot, X., Tani, N., Kas, A., Ghaleh, B., Le Corvoisier, P., Dolphin, P., Breen, D.P., Mason, S., Guzman, N.V., Mazarakis, N.D., Radcliffe, P.A., Harrop, R., Kingsman, S.M., Rascol, O., Naylor, S., Barker, R.A., Hantraye, P., Remy, P., Cesaro, P., Mitrophanous, K.A., (2014). Long-term safety and tolerability of ProSavin, a lentiviral vector-based gene therapy for Parkinson's disease: a dose escalation, open-label, phase 1/2 trial. Lancet 383, 1138–1146. https://doi.org/10.1016/S0140-6736(13)61939-X

Parain, K., Marchand, V., Dumery, B., Hirsch, E., (2001). Nicotine, but not cotinine, partially protects dopaminergic neurons against MPTP-induced degeneration in mice. Brain Research 890, 347–350. https://doi.org/10.1016/s0006-8993(00)03198-x

Parnetti, L., Gaetani, L., Eusebi, P., Paciotti, S., Hansson, O., El-Agnaf, O., Mollenhauer, B., Blennow, K., Calabresi, P., (2019). CSF and blood

biomarkers for Parkinson's disease. Lancet Neurology 18, 573–586. https://doi.org/10.1016/S1474-4422(19)30024-9

Patel, J.C., Witkovsky, P., Coetzee, W.A., Rice, M.E., (2011). Subsecond regulation of striatal dopamine release by pre-synaptic KATP channels. Journal of Neurochemistry 118, 721–736. https://doi.org/10.1111/j.1471-4159.2011.07358.x

Patel, S., Sharma, S., (2021). Respiratory Acidosis, in: StatPearls. StatPearls Publishing, Treasure Island (FL).

Patino, G.A., Isom, L.L., (2010). Electrophysiology and beyond: Multiple roles of Na+ channel β subunits in development and disease. Neuroscience Letters, Proteomics of Voltage-Gated Ion Channels 486, 53–59. https://doi.org/10.1016/j.neulet.2010.06.050

Patriarchi, T., Cho, J.R., Merten, K., Howe, M.W., Marley, A., Xiong, W.-H., Folk, R.W., Broussard, G.J., Liang, R., Jang, M.J., Zhong, H., Dombeck, D., von Zastrow, M., Nimmerjahn, A., Gradinaru, V., Williams, J.T., Tian, L., (2018). Ultrafast neuronal imaging of dopamine dynamics with designed genetically encoded sensors. Science 360. https://doi.org/10.1126/science.aat4422

Paulus, W., Jellinger, K., (1991). The neuropathologic basis of different clinical subgroups of Parkinson's disease. Journal of Neuropathology and Experimental Neurology 50, 743–755. https://doi.org/10.1097/00005072-199111000-00006

Pearson, R.A., Dale, N., Llaudet, E., Mobbs, P., (2005). ATP released via gap junction hemichannels from the pigment epithelium regulates neural retinal progenitor proliferation. Neuron 46, 731–744. https://doi.org/10.1016/j.neuron.2005.04.024

Pedersen, M.E.F., Fatemian, M., Robbins, P.A., (1999). Identification of fast and slow ventilatory responses to carbon dioxide under hypoxic and hyperoxic conditions in humans. Journal of Physiology 521, 273–287. https://doi.org/10.1111/j.1469-7793.1999.00273.x

Petersen, R.C., (2004). Mild cognitive impairment as a diagnostic entity. Journal of Internal Medicine 256, 183–194. https://doi.org/10.1111/j.1365-2796.2004.01388.x

Pickett, E.K., Henstridge, C.M., Allison, E., Pitstick, R., Pooler, A., Wegmann, S., Carlson, G., Hyman, B.T., Spires-Jones, T.L., (2017). Spread of tau down neural circuits precedes synapse and neuronal loss in the rTgTauEC mouse model of early Alzheimer's disease. Synapse 71. https://doi.org/10.1002/syn.21965

Pierce, J.E., Péron, J., (2020). The basal ganglia and the cerebellum in human emotion. Social Cognitive and Affective Neuroscience. 15, 599–613. https://doi.org/10.1093/scan/nsaa076

Pir, G.J., Choudhary, B., Kaniyappan, S., Chandupatla, R.R., Mandelkow, E., Mandelkow, E.-M., Wang, Y., (2019). Suppressing Tau Aggregation and Toxicity by an Anti-Aggregant Tau Fragment. Molecular Neurobiology 56, 3751–3767. https://doi.org/10.1007/s12035-018-1326-z

Poewe, W., Seppi, K., Tanner, C.M., Halliday, G.M., Brundin, P., Volkmann, J., Schrag, A.-E., Lang, A.E., (2017). Parkinson disease. Nature Reviews Disease Primers 3, 1–21. https://doi.org/10.1038/nrdp.2017.13

Polinski, N.K., Volpicelli-Daley, L.A., Sortwell, C.E., Luk, K.C., Cremades, N., Gottler, L.M., Froula, J., Duffy, M.F., Lee, V.M.Y., Martinez, T.N., Dave, K.D., (2018). Best Practices for Generating and Using Alpha-Synuclein Pre-Formed Fibrils to Model Parkinson's Disease in Rodents. Journal of Parkinson's Disease 8, 303–322. https://doi.org/10.3233/JPD-171248

Polydoro, M., Acker, C.M., Duff, K., Castillo, P.E., Davies, P., (2009). Age-dependent impairment of cognitive and synaptic function in the htau mouse model of tau pathology. Journal of Neuroscience 29, 10741–10749. https://doi.org/10.1523/JNEUROSCI.1065-09.2009

Polymeropoulos, M.H., Lavedan, C., Leroy, E., Ide, S.E., Dehejia, A., Dutra, A., Pike, B., Root, H., Rubenstein, J., Boyer, R., Stenroos, E.S., Chandrasekharappa, S., Athanassiadou, A., Papapetropoulos, T., Johnson, W.G., Lazzarini, A.M., Duvoisin, R.C., Di Iorio, G., Golbe, L.I., Nussbaum, R.L., (1997). Mutation in the alpha-synuclein gene identified in families with Parkinson's disease. Science 276, 2045–2047. https://doi.org/10.1126/science.276.5321.2045

Pooler, A.M., Phillips, E.C., Lau, D.H.W., Noble, W., Hanger, D.P., (2013). Physiological release of endogenous tau is stimulated by neuronal activity. EMBO Reports 14, 389–394. https://doi.org/10.1038/embor.2013.15

Popoli, P., Pèzzola, A., Scotti de Carolis, A., (1994). Modulation of striatal adenosine A1 and A2 receptors induces rotational behaviour in response to dopaminergic stimulation in intact rats. European Journal of Pharmacology 257, 21–25. https://doi.org/10.1016/0014-2999(94)90689-0

Privitera, L., Morè, L., Cooper, D.D., Richardson, P., Tsogka, M., Hebenstreit, D., Arthur, J.S.C., Frenguelli, B.G., (2020). Experience Recruits MSK1

to Expand the Dynamic Range of Synapses and Enhance Cognition. Journal of Neuroscience 40, 4644–4660. https://doi.org/10.1523/JNEUROSCI.2765-19.2020

Puangmalai, N., Bhatt, N., Montalbano, M., Sengupta, U., Gaikwad, S., Ventura, F., McAllen, S., Ellsworth, A., Garcia, S., Kayed, R., (2020). Internalization mechanisms of brain-derived tau oligomers from patients with Alzheimer's disease, progressive supranuclear palsy and dementia with Lewy bodies. Cell Death & Disease 11, 314. https://doi.org/10.1038/s41419-020-2503-3

Puopolo, M., Raviola, E., Bean, B.P., (2007). Roles of Subthreshold Calcium Current and Sodium Current in Spontaneous Firing of Mouse Midbrain Dopamine Neurons. Journal of Neuroscience. 27, 645–656. https://doi.org/10.1523/JNEUROSCI.4341-06.2007

Puthongkham, P., Venton, B.J., (2020). Recent advances in fast-scan cyclic voltammetry. Analyst 145, 1087–1102. https://doi.org/10.1039/C9AN01925A

Putnam, R., (2001). CO2chemotransduction in central neurons: role of intracellular pH (pHi) and extracellular pH (pHo). Respiratory Research 2, 6.4. https://doi.org/10.1186/rr122

Puzzo, D., Piacentini, R., Fá, M., Gulisano, W., Li Puma, D.D., Staniszewski, A., Zhang, H., Tropea, M.R., Cocco, S., Palmeri, A., Fraser, P., D'Adamio, L., Grassi, C., Arancio, O., (2017). LTP and memory impairment caused by extracellular Aβ and Tau oligomers is APP-dependent. eLife 6. https://doi.org/10.7554/eLife.26991

Qiang, L., Sun, X., Austin, T.O., Muralidharan, H., Jean, D.C., Liu, M., Yu, W., Baas, P.W., (2018). Tau Does Not Stabilize Axonal Microtubules but Rather Enables Them to Have Long Labile Domains. Current Biology 28, 2181-2189.e4. https://doi.org/10.1016/j.cub.2018.05.045

Qui, F., Hu, W., Yang, Z., (2014). Enhancement of GABA-activated currents by arginine vasopressin in rat dorsal root ganglion neurons. Sheng Li Xue Bao 66, 647–657.

Quik, M., Perez, X.A., Bordia, T., (2012). Nicotine as a potential neuroprotective agent for Parkinson's disease. Movement Disorders 27, 947–957. https://doi.org/10.1002/mds.25028

Quik, M., Huang, L.Z., Parameswaran, N., Bordia, T., Campos, C., Perez, X.A., (2009). Multiple roles for nicotine in Parkinson's disease. Biochem. Pharmacol. 78, 677–685. https://doi.org/10.1016/j.bcp.2009.05.003

Quik, M., Mallela, A., Chin, M., McIntosh, J.M., Perez, X.A., Bordia, T., (2013a). Nicotine-mediated improvement in L-dopa-induced dyskinesias in MPTP-lesioned monkeys is dependent on dopamine nerve terminal

function. Neurobiology of Disease 50, 30–41. https://doi.org/10.1016/j.nbd.2012.09.006

Quik, M., Mallela, A., Ly, J., Zhang, D., (2013b). Nicotine reduces established levodopa-induced dyskinesias in a monkey model of Parkinson's disease. Journal of Movement Disorders. 28, 1398–1406. https://doi.org/10.1002/mds.25594

Quik, M., Perez, X.A., Bordia, T., (2012). Nicotine as a potential neuroprotective agent for Parkinson's disease. Journal of Movement Disorders. 27, 947–957. https://doi.org/10.1002/mds.25028

Rademakers, R., Neumann, M., Mackenzie, I.R., (2012). Advances in understanding the molecular basis of frontotemporal dementia. Nature Reviews Neurology 8, 423–434. https://doi.org/10.1038/nrneurol.2012.117

Rall, W., Segev, I., (1985). Space-Clamp Problems When Voltage Clamping Branched Neurons With Intracellular Microelectrodes, in: Smith, T.G., Lecar, H., Redman, S.J., Gage, P.W. (Eds.), Voltage and Patch Clamping with Microelectrodes. Springer, New York, NY, pp. 191–215. https://doi.org/10.1007/978-1-4614-7601-6_9

Ramaswamy, S., Courcol, J.-D., Abdellah, M., Adaszewski, S.R., Antille, N., Arsever, S., Atenekeng, G., Bilgili, A., Brukau, Y., Chalimourda, A., Chindemi, G., Delalondre, F., Dumusc, R., Eilemann, S., Gevaert, M.E., Gleeson, P., Graham, J.W., Hernando, J.B., Kanari, L., Katkov, Y., Keller, D., King, J.G., Ranjan, R., Reimann, M.W., Rössert, C., Shi, Y., Shillcock, J.C., Telefont, M., Van Geit, W., Villafranca Diaz, J., Walker, R., Wang, Y., Zaninetta, S.M., DeFelipe, J., Hill, S.L., Muller, J., Segev, I., Schürmann, F., Muller, E.B., Markram, H., (2015). The neocortical microcircuit collaboration portal: a resource for rat somatosensory cortex. Frontiers in Neural Circuits 9. https://doi.org/10.3389/fncir.2015.00044

Ramón y Cajal, S., (1911). Histologie du système nerveux de l'homme & des vertébrés., Ed. française rev. & mise à jour par l'auteur, tr. de l'espagnol par L. Azoulay. ed. Maloine, Paris : https://doi.org/10.5962/bhl.title.48637

Ran, I., Laplante, I., Lacaille, J.-C., (2012). CREB-Dependent Transcriptional Control and Quantal Changes in Persistent Long-Term Potentiation in Hippocampal Interneurons. Journal of Neuroscience. 32, 6335–6350. https://doi.org/10.1523/JNEUROSCI.5463-11.2012

Raux, G., Guyant-Maréchal, L., Martin, C., Bou, J., Penet, C., Brice, A., Hannequin, D., Frebourg, T., Campion, D., (2005). Molecular diagnosis of autosomal dominant early onset Alzheimer's disease: an

update. Journal of Medical Genetics. 42, 793–795. https://doi.org/10.1136/jmg.2005.033456

Regan, P., Piers, T., Yi, J.-H., Kim, D.-H., Huh, S., Park, S.J., Ryu, J.H., Whitcomb, D.J., Cho, K., (2015). Tau phosphorylation at serine 396 residue is required for hippocampal LTD. Journal of Neuroscience 35, 4804–4812. https://doi.org/10.1523/JNEUROSCI.2842-14.2015

Ren, X., Chen, J.-F., (2020). Caffeine and Parkinson's Disease: Multiple Benefits and Emerging Mechanisms. Frontiers in Neuroscience. 14. https://doi.org/10.3389/fnins.2020.602697

Ren, Y., Sahara, N., Giasson, B., Lewis, J., (2015). Chapter 55 - Tauopathy Mouse Models, in: LeDoux, M.S. (Ed.), Movement Disorders (Second Edition). Academic Press, Boston, pp. 849–855. https://doi.org/10.1016/B978-0-12-405195-9.00055-X

Reyes, A., Sakmann, B., (1999). Developmental Switch in the Short-Term Modification of Unitary EPSPs Evoked in Layer 2/3 and Layer 5 Pyramidal Neurons of Rat Neocortex. Journal of Neuroscience. 19, 3827–3835. https://doi.org/10.1523/JNEUROSCI.19-10-03827.1999

Reyskens, K.M.S.E., Arthur, J.S.C., (2016). Emerging Roles of the Mitogen and Stress Activated Kinases MSK1 and MSK2. Frontiers in Cell and Developmental Biology 4. https://doi.org/10.3389/fcell.2016.00056

Richards, C.D., Shiroyama, T., Kitai, S.T., (1997). Electrophysiological and immunocytochemical characterization of GABA and dopamine neurons in the substantia nigra of the rat. Neuroscience 80, 545–557. https://doi.org/10.1016/s0306-4522(97)00093-6

Richardson, M.J.E., Silberberg, G., (2008a). Measurement and analysis of postsynaptic potentials using a novel voltage-deconvolution method. Journal of Neurophysiology 99, 1020–1031. https://doi.org/10.1152/jn.00942.2007

Richardson, M.J.E., Silberberg, G., (2008b). Measurement and analysis of postsynaptic potentials using a novel voltage-deconvolution method. Journal of Neurophysiology 99, 1020–1031. https://doi.org/10.1152/jn.00942.2007

Riederer, P., Konradi, C., Schay, V., Kienzl, E., Birkmayer, G., Danielczyk, W., Sofic, E., Youdim, M.B., (1987). Localization of MAO-A and MAO-B in human brain: a step in understanding the therapeutic action of L-deprenyl. Advances in neurology. 45, 111–118.

Ripoll, C., Lederer, W.J., Nichols, C.G., (1993). On the mechanism of inhibition of KATP channels by glibenclamide in rat ventricular myocytes. Journal of Cardiovascular Electrophysiology 4, 38–47. https://doi.org/10.1111/j.1540-8167.1993.tb01210.x

Roberson, E.D., Scearce-Levie, K., Palop, J.J., Yan, F., Cheng, I.H., Wu, T., Gerstein, H., Yu, G.-Q., Mucke, L., (2007). Reducing endogenous tau ameliorates amyloid beta-induced deficits in an Alzheimer's disease mouse model. Science 316, 750–754. https://doi.org/10.1126/science.1141736

Roberts, H.L., Brown, D.R., (2015). Seeking a Mechanism for the Toxicity of Oligomeric αSynuclein. Biomolecules 5, 282–305. https://doi.org/10.3390/biom5020282

Robinson, J.E., Coughlin, G.M., Hori, A.M., Cho, J.R., Mackey, E.D., Turan, Z., Patriarchi, T., Tian, L., Gradinaru, V., (2019). Optical dopamine monitoring with dLight1 reveals mesolimbic phenotypes in a mouse model of neurofibromatosis type 1. eLife 8, e48983. https://doi.org/10.7554/eLife.48983

Rocher, A.B., Crimins, J.L., Amatrudo, J.M., Kinson, M.S., Todd-Brown, M.A., Lewis, J., Luebke, J.I., (2010). Structural and functional changes in tau mutant mice neurons are not linked to the presence of NFTs. Experimental Neurology 223, 385–393. https://doi.org/10.1016/j.expneurol.2009.07.029

Romand, S., Wang, Y., Toledo-Rodriguez, M., Markram, H., (2011). Morphological Development of Thick-Tufted Layer V Pyramidal Cells in the Rat Somatosensory Cortex. Frontiers in Neuroanatomy 5. https://doi.org/10.3389/fnana.2011.00005

Root, D.H., Estrin, D.J., Morales, M., (2018). Aversion or Salience Signaling by Ventral Tegmental Area Glutamate Neurons. iScience 2, 51–62. https://doi.org/10.1016/j.isci.2018.03.008

Röper, J., Ashcroft, F.M., (1995). Metabolic inhibition and low internal ATP activate K-ATP channels in rat dopaminergic substantia nigra neurones. Pflugers Archives 430, 44–54. https://doi.org/10.1007/BF00373838

Ross, G.W., Petrovitch, H., Abbott, R.D., Tanner, C.M., Popper, J., Masaki, K., Launer, L., White, L.R., (2008). Association of olfactory dysfunction with risk for future Parkinson's disease. Annals of Neurology 63, 167–173. https://doi.org/10.1002/ana.21291

Rostami, J., Holmqvist, S., Lindström, V., Sigvardson, J., Westermark, G.T., Ingelsson, M., Bergström, J., Roybon, L., Erlandsson, A., (2017). Human Astrocytes Transfer Aggregated Alpha-Synuclein via Tunneling Nanotubes. Journal of Neuroscience 37, 11835–11853. https://doi.org/10.1523/JNEUROSCI.0983-17.2017

Roth, R.H., (1984). CNS Dopamine Autoreceptors: Distribution, Pharmacology, and Functional Annals of the New York Academy of Sciences 430, 27–53. doi.org/10.1111/j.1749-6632.1984.tb14497.x

Royeck, M., Horstmann, M.-T., Remy, S., Reitze, M., Yaari, Y., Beck, H., (2008). Role of Axonal NaV1.6 Sodium Channels in Action Potential Initiation of CA1 Pyramidal Neurons. Journal of Neurophysiology 100, 2361–2380. https://doi.org/10.1152/jn.90332.2008

Rudinskiy, N., Hawkes, J.M., Wegmann, S., Kuchibhotla, K.V., Muzikansky, A., Betensky, R.A., Spires-Jones, T.L., Hyman, B.T., (2014). Tau pathology does not affect experience-driven single-neuron and network-wide Arc/Arg3.1 response. Acta Neuropathologica Communications 2. https://doi.org/10.1186/2051-5960-2-63

Ryan, T.J., Roy, D.S., Pignatelli, M., Arons, A., Tonegawa, S., (2015). Memory. Engram cells retain memory under retrograde amnesia. Science 348, 1007–1013. https://doi.org/10.1126/science.aaa5542

Sakura, H., Ammälä, C., Smith, P.A., Gribble, F.M., Ashcroft, F.M., (1995). Cloning and functional expression of the cDNA encoding a novel ATP-sensitive potassium channel subunit expressed in pancreatic beta-cells, brain, heart and skeletal muscle. FEBS Letters. 377, 338–344. https://doi.org/10.1016/0014-5793(95)01369-5

Samii, A., Nutt, J.G., Ransom, B.R., (2004). Parkinson's disease. Lancet 363, 1783–1793. https://doi.org/10.1016/S0140-6736(04)16305-8

Santos, S.F., de Oliveira, H.L., Yamada, E.S., Neves, B.C., Pereira, A., (2019). The Gut and Parkinson's Disease—A Bidirectional Pathway. Frontiers in Neurology 10. https://doi.org/10.3389/fneur.2019.00574

Schapira, A.H.V., Emre, M., Jenner, P., Poewe, W., (2009). Levodopa in the treatment of Parkinson's disease. European Journal of Neurology 16, 982–989. https://doi.org/10.1111/j.1468-1331.2009.02697.x

Scheuner, D., Eckman, C., Jensen, M., Song, X., Citron, M., Suzuki, N., Bird, T.D., Hardy, J., Hutton, M., Kukull, W., Larson, E., Levy-Lahad, E., Viitanen, M., Peskind, E., Poorkaj, P., Schellenberg, G., Tanzi, R., Wasco, W., Lannfelt, L., Selkoe, D., Younkin, S., (1996). Secreted amyloid beta-protein similar to that in the senile plaques of Alzheimer's disease is increased in vivo by the presenilin 1 and 2 and APP mutations linked to familial Alzheimer's disease. Nature Medicine 2, 864–870. https://doi.org/10.1038/nm0896-864

Schernhammer, E., Hansen, J., Rugbjerg, K., Wermuth, L., Ritz, B., (2011). Diabetes and the Risk of Developing Parkinson's Disease in Denmark. Diabetes Care 34, 1102–1108. https://doi.org/10.2337/dc10-1333

Schiemann, J., Schlaudraff, F., Klose, V., Bingmer, M., Seino, S., Magill, P.J., Zaghloul, K.A., Schneider, G., Liss, B., Roeper, J., (2012). K-ATP channels in dopamine substantia nigra neurons control bursting and

novelty-induced exploration. Nature Neuroscience 15, 1272–1280. https://doi.org/10.1038/nn.3185

Shimizu, H., Watanabe, E., Hiyama, T.Y., Nagakura, A., Fujikawa, A., Okado, H., Yanagawa, Y., Obata, K., Noda, M., (2007). Glial Nax Channels Control Lactate Signaling to Neurons for Brain [Na+] Sensing. Neuron 54, 59–72. https://doi.org/10.1016/j.neuron.2007.03.014

Schoch, K.M., DeVos, S.L., Miller, R.L., Chun, S.J., Norrbom, M., Wozniak, D.F., Dawson, H.N., Bennett, C.F., Rigo, F., Miller, T.M., (2016). Increased 4R-Tau Induces Pathological Changes in a Human-Tau Mouse Model. Neuron 90, 941–947. https://doi.org/10.1016/j.neuron.2016.04.042

Schwanstecher, M., Sieverding, C., Dörschner, H., Gross, I., Aguilar-Bryan, L., Schwanstecher, C., Bryan, J., (1998). Potassium channel openers require ATP to bind to and act through sulfonylurea receptors. EMBO Journal 17, 5529–5535. https://doi.org/10.1093/emboj/17.19.5529

Scoville, W.B., Milner, B., (1957). LOSS OF RECENT MEMORY AFTER BILATERAL HIPPOCAMPAL LESIONS. Journal of Neurology, Neurosurgery, and Psychiatry 20, 11–21.

Seino, S., (1999). ATP-sensitive potassium channels: a model of heteromultimeric potassium channel/receptor assemblies. Annual Review of Physiology 61, 337–362. https://doi.org/10.1146/annurev.physiol.61.1.337

Seubert, P., Vigo-Pelfrey, C., Esch, F., Lee, M., Dovey, H., Davis, D., Sinha, S., Schiossmacher, M., Whaley, J., Swindlehurst, C., McCormack, R., Wolfert, R., Selkoe, D., Lieberburg, I., Schenk, D., (1992). Isolation and quantification of soluble Alzheimer's β-peptide from biological fluids. Nature 359, 325–327. https://doi.org/10.1038/359325a0

Shammas, S.L., Garcia, G.A., Kumar, S., Kjaergaard, M., Horrocks, M.H., Shivji, N., Mandelkow, Eva, Knowles, T.P.J., Mandelkow, Eckhard, Klenerman, D., (2015). A mechanistic model of tau amyloid aggregation based on direct observation of oligomers. Nature Communications 6. https://doi.org/10.1038/ncomms8025

Shams, H., (1985). Differential effects of CO_2 and H+ as central stimuli of respiration in the cat. Journal of Applied Physiology 58, 357–364. https://doi.org/10.1152/jappl.1985.58.2.357

Shoji, M., Golde, T.E., Ghiso, J., Cheung, T.T., Estus, S., Shaffer, L.M., Cai, X.D., McKay, D.M., Tintner, R., Frangione, B., (1992). Production of the Alzheimer amyloid beta protein by normal proteolytic processing. Science 258, 126–129. https://doi.org/10.1126/science.1439760

Shrivastava, A.N., Redeker, V., Pieri, L., Bousset, L., Renner, M., Madiona, K., Mailhes-Hamon, C., Coens, A., Buée, L., Hantraye, P., Triller, A., Melki, R., (2019). Clustering of Tau fibrils impairs the synaptic composition of α3-Na+/K+-ATPase and AMPA receptors. EMBO Journal 38. https://doi.org/10.15252/embj.201899871

Shulman, L.M., (2007). Gender differences in Parkinson's disease. Gender Medicine 4, 8–18. https://doi.org/10.1016/s1550-8579(07)80003-9

Sian, J., Youdim, M.B.H., Riederer, P., Gerlach, M., (1999). MPTP-Induced Parkinsonian Syndrome, in: Basic Neurochemistry: Molecular, Cellular and Medical Aspects. 6th Edition. Lippincott-Raven, Philadelphia.

Sigurdsson, E.M., (2018). Tau Immunotherapies for Alzheimer's Disease and Related Tauopathies: Progress and Potential Pitfalls. Journal of Alzheimer's Disease 64, S555–S565. https://doi.org/10.3233/JAD-179937

Silberberg, G., Gupta, A., Markram, H., (2002). Stereotypy in neocortical microcircuits. Trends in Neuroscience 25, 227–230. https://doi.org/10.1016/s0166-2236(02)02151-3

Silva, M.C., Cheng, C., Mair, W., Almeida, S., Fong, H., Biswas, M.H.U., Zhang, Z., Huang, Y., Temple, S., Coppola, G., Geschwind, D.H., Karydas, A., Miller, B.L., Kosik, K.S., Gao, F.-B., Steen, J.A., Haggarty, S.J., (2016). Human iPSC-Derived Neuronal Model of Tau-A152T Frontotemporal Dementia Reveals Tau-Mediated Mechanisms of Neuronal Vulnerability. Stem Cell Reports 7, 325–340. https://doi.org/10.1016/j.stemcr.2016.08.001

Silva, N.L., Bunney, B.S., (1988). Intracellular studies of dopamine neurons in vitro: pacemakers modulated by dopamine. European Journal of Pharmacology 149, 307–315. https://doi.org/10.1016/0014-2999(88)90661-9

Simmons, D.V., Petko, A.K., Paladini, C.A., (2017). Differential expression of long-term potentiation among identified inhibitory inputs to dopamine neurons. Journal of Neurophysiology 118, 1998–2008. https://doi.org/10.1152/jn.00270.2017

Skrabana, R., Skrabanova, M., Csokova, N., Sevcik, J., Novak, M., (2006) Intrinsically disordered tau protein in Alzheimer's tangles: a coincidence or a rule? Bratislavske Lekarske Listy 107(9-10):354-358

Smith, Y., Wichmann, T., Factor, S.A., DeLong, M.R., (2012). Parkinson's Disease Therapeutics: New Developments and Challenges Since the Introduction of Levodopa. Neuropsychopharmacology 37, 213–246. https://doi.org/10.1038/npp.2011.212

Sokolow, S., Henkins, K.M., Bilousova, T., Gonzalez, B., Vinters, H.V., Miller, C.A., Cornwell, L., Poon, W.W., Gylys, K.H., (2015). Pre-synaptic C-terminal truncated tau is released from cortical synapses in Alzheimer's disease. Journal of Neurochemistry 133, 368–379. https://doi.org/10.1111/jnc.12991

Soldner, F., Laganière, J., Cheng, A.W., Hockemeyer, D., Gao, Q., Alagappan, R., Khurana, V., Golbe, L.I., Myers, R.H., Lindquist, S., Zhang, L., Guschin, D., Fong, L.K., Vu, B.J., Meng, X., Urnov, F.D., Rebar, E.J., Gregory, P.D., Zhang, H.S., Jaenisch, R., (2011). Generation of isogenic pluripotent stem cells differing exclusively at two early onset Parkinson point mutations. Cell 146, 318–331. https://doi.org/10.1016/j.cell.2011.06.019

Sommer, U., Hummel, T., Cormann, K., Mueller, A., Frasnelli, J., Kropp, J., Reichmann, H., (2004). Detection of presymptomatic Parkinson's disease: Combining smell tests, transcranial sonography, and SPECT. Movement Disorders 19, 1196–1202. https://doi.org/10.1002/mds.20141

Song, C., Deng, P., Que, L., (2018). Rapid multiplexed detection of beta-amyloid and total-tau as biomarkers for Alzheimer's disease in cerebrospinal fluid. Nanomedicine 14, 1845–1852. https://doi.org/10.1016/j.nano.2018.05.013

Sonsalla, P.K., Wong, L.-Y., Harris, S.L., Richardson, J.R., Khobahy, I., Li, W., Gadad, B.S., German, D.C., (2012). Delayed caffeine treatment prevents nigral dopamine neuron loss in a progressive rat model of Parkinson's disease. Experimental Neurology. 234, 482–487. https://doi.org/10.1016/j.expneurol.2012.01.022

Soto, C., (1999). Plaque busters: strategies to inhibit amyloid formation in Alzheimer's disease. Molecular Medicine Today 5, 343–350. https://doi.org/10.1016/S1357-4310(99)01508-7

Spillantini, M., Schmidt, M., Lee, V., Trojanowski, J., Jakes, R. and Goedert, M., (1997). α-Synuclein in Lewy bodies. Nature, 388(6645), pp.839-840.

Spires, T.L., Orne, J.D., SantaCruz, K., Pitstick, R., Carlson, G.A., Ashe, K.H., Hyman, B.T., (2006). Region-specific dissociation of neuronal loss and neurofibrillary pathology in a mouse model of tauopathy. The American Journal of Pathology 168, 1598–1607. https://doi.org/10.2353/ajpath.2006.050840

Spruston, N., (2008). Pyramidal neurons: dendritic structure and synaptic integration. Nature Reviews Neuroscience 9, 206–221. https://doi.org/10.1038/nrn2286

Spruston, N., Jaffe, D.B., Williams, S.H., Johnston, D., (1993). Voltage- and space-clamp errors associated with the measurement of electrotonically remote synaptic events. Journal of Neurophysiology 70, 781–802. https://doi.org/10.1152/jn.1993.70.2.781

Squire, L.R., (2009). Memory and Brain Systems: 1969–2009. Journal of Neuroscience 29, 12711–12716. doi.org/10.1523/JNEUROSCI.3575-09.2009

Squire, L.R., Genzel, L., Wixted, J.T., Morris, R.G., (2015). Memory Consolidation. Cold Spring Harbor Perspectives in Biology 7. https://doi.org/10.1101/cshperspect.a021766

Stamer, K., Vogel, R., Thies, E., Mandelkow, E., Mandelkow, E.-M., (2002). Tau blocks traffic of organelles, neurofilaments, and APP vesicles in neurons and enhances oxidative stress. Journal of Cell Biology 156, 1051–1063. https://doi.org/10.1083/jcb.200108057

Stamford, J.A., (1990). Fast cyclic voltammetry: Measuring transmitter release in ‘real time.’ Journal of Neuroscience Methods 34, 67–72. https://doi.org/10.1016/0165-0270(90)90043-F

Stanford, I.M., Lacey, M.G., (1995). Regulation of a potassium conductance in rat midbrain dopamine neurons by intracellular adenosine triphosphate (ATP) and the sulfonylureas tolbutamide and glibenclamide. Journal of Neuroscience 15, 4651–4657.

Stoothoff, W.H., Johnson, G.V.W., (2005). Tau phosphorylation: physiological and pathological consequences. Biochimica Et Biophysica Acta 1739, 280–297. https://doi.org/10.1016/j.bbadis.2004.06.017

Storm, J.F., (1987). Action potential repolarization and a fast after-hyperpolarization in rat hippocampal pyramidal cells. The Journal of Physiology 385, 733–759. doi.org/10.1113/jphysiol.1987.sp016517

Stout, C.E., Costantin, J.L., Naus, C.C.G., Charles, A.C., (2002). Intercellular calcium signaling in astrocytes via ATP release through connexin hemichannels. The Journal of Biological Chemistry 277, 10482–10488. https://doi.org/10.1074/jbc.M109902200

Strang, K.H., Golde, T.E., Giasson, B.I., (2019). MAPT mutations, tauopathy, and mechanisms of neurodegeneration. Laboratory Investigation. 99, 912–928. https://doi.org/10.1038/s41374-019-0197-x

Stuart, G., Schiller, J., Sakmann, B., (1997). Action potential initiation and propagation in rat neocortical pyramidal neurons. The Journal of Physiology 505, 617–632. https://doi.org/10.1111/j.1469-7793.1997.617ba.x

Stuber, G.D., Britt, J.P., Bonci, A., (2012). Optogenetic Modulation of Neural Circuits that Underlie Reward Seeking. Biological Psychiatry 71, 1061–1067. https://doi.org/10.1016/j.biopsych.2011.11.010

Sugiyama, H., Hainfellner, J.A., Yoshimura, M., Budka, H., (1994.) Neocortical changes in Parkinson's disease, revisited. Clinical Neuropathology 13, 55–59.

Sullivan, L.M., Weinberg, J., Keaney, J.F., (2016). Common Statistical Pitfalls in Basic Science Research. J. Am. Heart Assoc. Cardiovascular and cerebrovascular diseases. 5. https://doi.org/10.1161/JAHA.116.004142

Sultan, A., Nesslany, F., Violet, M., Bégard, S., Loyens, A., Talahari, S., Mansuroglu, Z., Marzin, D., Sergeant, N., Humez, S., Colin, M., Bonnefoy, E., Buée, L., Galas, M.-C., (2011). Nuclear tau, a key player in neuronal DNA protection. The Journal of Biological Chemistry 286, 4566–4575. https://doi.org/10.1074/jbc.M110.199976

Sun, Y., Tang, W., Chang, Q., Wang, Y., Kong, W., Lin, X., (2009). Connexin30 null and conditional connexin26 null mice display distinct pattern and time course of cellular degeneration in the cochlea. The Journal of Comparative Neurology 516, 569–579. https://doi.org/10.1002/cne.22117

Suzuki, M., Kimura, T., (2017). Microtubule-associated tau contributes to intra-dendritic trafficking of AMPA receptors in multiple ways. Neuroscience Letters 653, 276–282. https://doi.org/10.1016/j.neulet.2017.05.056

Suzuki, N., Cheung, T.T., Cai, X.D., Odaka, A., Otvos, L., Eckman, C., Golde, T.E., Younkin, S.G., (1994). An increased percentage of long amyloid beta protein secreted by familial amyloid beta protein precursor (beta APP717) mutants. Science 264, 1336–1340. https://doi.org/10.1126/science.8191290

Swope, D., (2004). Rapid treatment of "wearing off" in Parkinson's disease. Neurology, 62(Issue 6, Supplement 4), pp.S27-S31.

Tai, H.-C., Wang, B.Y., Serrano-Pozo, A., Frosch, M.P., Spires-Jones, T.L., Hyman, B.T., (2014). Frequent and symmetric deposition of misfolded tau oligomers within presynaptic and postsynaptic terminals in Alzheimer's disease. Acta Neuropathologica Communications 2, 146. https://doi.org/10.1186/s40478-014-0146-2

Tai, L.-H., Lee, A.M., Benavidez, N., Bonci, A., Wilbrecht, L., (2012). Transient stimulation of distinct subpopulations of striatal neurons mimics changes in action value. Nature Neuroscience 15, 1281–1289. https://doi.org/10.1038/nn.3188

Takata, Y., Oishi, Y., Zhou, X.-Z., Hasegawa, E., Takahashi, K., Cherasse, Y., Sakurai, T., Lazarus, M., (2018). Sleep and Wakefulness Are Controlled

by Ventral Medial Midbrain/Pons GABAergic Neurons in Mice. Journal of Neuroscience 38, 10080–10092. https://doi.org/10.1523/JNEUROSCI.0598-18.2018

Takigawa, T., Alzheimer, C., (1999). G protein-activated inwardly rectifying K+ (GIRK) currents in dendrites of rat neocortical pyramidal cells. Journal of Physiology 517 (Pt 2), 385–390. https://doi.org/10.1111/j.1469-7793.1999.0385t.x

Tamagnini, F., Walsh, D.A., Brown, J.T., Bondulich, M.K., Hanger, D.P., Randall, A.D., (2017). Hippocampal neurophysiology is modified by a disease-associated C-terminal fragment of tau protein. Neurobiology of Aging 60, 44–56. https://doi.org/10.1016/j.neurobiolaging.2017.07.005

Tan, K.R., Yvon, C., Turiault, M., Mirzabekov, J.J., Doehner, J., Labouèbe, G., Deisseroth, K., Tye, K.M., Lüscher, C., (2012). GABA neurons of the VTA drive conditioned place aversion. Neuron 73, 1173–1183. https://doi.org/10.1016/j.neuron.2012.02.015

Tanemura, K., Murayama, M., Akagi, T., Hashikawa, T., Tominaga, T., Ichikawa, M., Yamaguchi, H., Takashima, A., (2002). Neurodegeneration with tau accumulation in a transgenic mouse expressing V337M human tau. Journal of Neuroscience 22, 133–141.

Tatebayashi, Y., Miyasaka, T., Chui, D.-H., Akagi, T., Mishima, K., Iwasaki, K., Fujiwara, M., Tanemura, K., Murayama, M., Ishiguro, K., Planel, E., Sato, S., Hashikawa, T., Takashima, A., (2002). Tau filament formation and associative memory deficit in aged mice expressing mutant (R406W) human tau. Proceedings of the National Academy of Sciences 99, 13896–13901. https://doi.org/10.1073/pnas.202205599

Taylor, C.J., Peacock, S., Chaudhry, A.N., Bradley, J.A., Bolton, E.M., (2012). Generating an iPSC bank for HLA-matched tissue transplantation based on known donor and recipient HLA types. Cell Stem Cell 11, 147–152. https://doi.org/10.1016/j.stem.2012.07.014

Teich, A.F., Nicholls, R.E., Puzzo, D., Fiorito, J., Purgatorio, R., Fa', M., Arancio, O., (2015). Synaptic therapy in Alzheimer's disease: a CREB-centric approach. Neurotherapeutics 12, 29–41. https://doi.org/10.1007/s13311-014-0327-5

Teravskis, P.J., Covelo, A., Miller, E.C., Singh, B., Martell-Martínez, H.A., Benneyworth, M.A., Gallardo, C., Oxnard, B.R., Araque, A., Lee, M.K., Liao, D., (2018). A53T Mutant Alpha-Synuclein Induces Tau-Dependent Postsynaptic Impairment Independently of Neurodegenerative Changes. Journal of Neuroscience. 38, 9754–9767. https://doi.org/10.1523/JNEUROSCI.0344-18.2018

Thakur, P., Luk, K., Roeper, J., (2019). Selective K-ATP channel-dependent loss of pacemaking in vulnerable nigrostriatal dopamine neurons by αSynuclein aggregates. bioRxiv 842344. https://doi.org/10.1101/842344

Thal, D.R., Rüb, U., Orantes, M., Braak, H., (2002). Phases of A beta-deposition in the human brain and its relevance for the development of AD. Neurology 58, 1791–1800. https://doi.org/10.1212/wnl.58.12.1791

Thies, E., Mandelkow, E.-M., (2007). Missorting of tau in neurons causes degeneration of synapses that can be rescued by the kinase MARK2/Par-1. Journal of Neuroscience 27, 2896–2907. https://doi.org/10.1523/JNEUROSCI.4674-06.2007

Thijssen, E.H., La Joie, R., Wolf, A., Strom, A., Wang, P., Iaccarino, L., Bourakova, V., Cobigo, Y., Heuer, H., Spina, S., VandeVrede, L., Chai, X., Proctor, N.K., Airey, D.C., Shcherbinin, S., Duggan Evans, C., Sims, J.R., Zetterberg, H., Blennow, K., Karydas, A.M., Teunissen, C.E., Kramer, J.H., Grinberg, L.T., Seeley, W.W., Rosen, H., Boeve, B.F., Miller, B.L., Rabinovici, G.D., Dage, J.L., Rojas, J.C., Boxer, A.L., (2020). Diagnostic value of plasma phosphorylated tau181 in Alzheimer's disease and frontotemporal lobar degeneration. Nature Medicine 26, 387–397. https://doi.org/10.1038/s41591-020-0762-2

Toombs, J., Zetterberg, H., (2020). In the blood: biomarkers for amyloid pathology and neurodegeneration in Alzheimer's disease. Brain Communications 2. https://doi.org/10.1093/braincomms/fcaa054

Tovar, K.R., Maher, B.J., Westbrook, G.L., (2009). Direct actions of carbenoxolone on synaptic transmission and neuronal membrane properties. Journal of Neurophysiology 102, 974–978. https://doi.org/10.1152/jn.00060.2009

Tracy, T.E., Gan, L., (2018). Tau-mediated synaptic and neuronal dysfunction in neurodegenerative disease. Current Opinion in Neurobiology 51, 134–138. https://doi.org/10.1016/j.conb.2018.04.027

Trapp, S., Aller, M.I., Wisden, W., Gourine, A.V., (2008). A Role for TASK-1 (KCNK3) Channels in the Chemosensory Control of Breathing. Journal of Neuroscience 28, 8844–8850. doi.org/10.1523/JNEUROSCI.1810-08.2008

Trapp, S., Ashcroft, F., (1997). A Metabolic Sensor in Action: News From the ATP-Sensitive K+-Channel. Physiology 12, 255–263. https://doi.org/10.1152/physiologyonline.1997.12.6.255

Tritsch, N.X., Ding, J.B., Sabatini, B.L., (2012). Dopaminergic neurons inhibit striatal output via non-canonical release of GABA. Nature 490, 262–266. https://doi.org/10.1038/nature11466

Tucker, K.L., Meyer, M., Barde, Y.A., (2001). Neurotrophins are required for nerve growth during development. Nature Neuroscience 4, 29–37. https://doi.org/10.1038/82868

Uéda, K., Fukushima, H., Masliah, E., Xia, Y., Iwai, A., Yoshimoto, M., Otero, D.A., Kondo, J., Ihara, Y., Saitoh, T., (1993). Molecular cloning of cDNA encoding an unrecognized component of amyloid in Alzheimer disease. Proceedings of the National Academy of Sciences 90, 11282–11286.

Uehara, T., Choong, C.-J., Nakamori, M., Hayakawa, H., Nishiyama, K., Kasahara, Y., Baba, K., Nagata, T., Yokota, T., Tsuda, H., Obika, S., Mochizuki, H., (2019). Amido-bridged nucleic acid (AmNA)-modified antisense oligonucleotides targeting αSynuclein as a novel therapy for Parkinson's disease. Scientific reports 9, 7567. https://doi.org/10.1038/s41598-019-43772-9

Usenovic, M., Niroomand, S., Drolet, R.E., Yao, L., Gaspar, R.C., Hatcher, N.G., Schachter, J., Renger, J.J., Parmentier-Batteur, S., (2015). Internalized Tau Oligomers Cause Neurodegeneration by Inducing Accumulation of Pathogenic Tau in Human Neurons Derived from Induced Pluripotent Stem Cells. Journal of Neuroscience 35, 14234–14250. https://doi.org/10.1523/JNEUROSCI.1523-15.2015

van de Wiel, J., Meigh, L., Bhandare, A., Cook, J., Nijjar, S., Huckstepp, R., Dale, N., (2020). Connexin26 mediates CO2-dependent regulation of breathing via glial cells of the medulla oblongata. Communications Biology 3, 521. https://doi.org/10.1038/s42003-020-01248-x

Van Den Eeden, S.K., Tanner, C.M., Bernstein, A.L., Fross, R.D., Leimpeter, A., Bloch, D.A., Nelson, L.M., (2003). Incidence of Parkinson's disease: variation by age, gender, and race/ethnicity. American Journal of Epidemiology 157, 1015–1022. https://doi.org/10.1093/aje/kwg068

Van Hook, M.J., Thoreson, W.B., (2014). Whole-Cell Patch-Clamp Recording, in: Xiong, H., Gendelman, H.E. (Eds.), Current Laboratory Methods in Neuroscience Research, Springer Protocols Handbooks. Springer, New York, NY, pp. 353–367. https://doi.org/10.1007/978-1-4614-8794-4_25

Van Thienen, R., Hespel, P., (2016). Enhanced muscular oxygen extraction in athletes exaggerates hypoxemia during exercise in hypoxia. Journal of Applied Physiology 120, 351–361. https://doi.org/10.1152/japplphysiol.00210.2015

Van Wart, A., Matthews, G., (2006). Impaired firing and cell-specific compensation in neurons lacking nav1.6 sodium channels. Journal of Neuroscience 26, 7172–7180. doi.org/10.1523/JNEUROSCI.1101-06.2006

Van Wart, A., Trimmer, J.S., Matthews, G., (2007). Polarized distribution of ion channels within microdomains of the axon initial segment. The Journal of Comparative Neurology 500, 339–352. https://doi.org/10.1002/cne.21173

van Zessen, R., Phillips, J.L., Budygin, E.A., Stuber, G.D., (2012). Activation of VTA GABA neurons disrupts reward consumption. Neuron 73, 1184–1194. https://doi.org/10.1016/j.neuron.2012.02.016

Vandecasteele, M., Deniau, J.-M., Glowinski, J., Venance, L., (2007). Electrical synapses in basal ganglia. Reviews in the Neurosciences 18, 15–35. https://doi.org/10.1515/revneuro.2007.18.1.15

Vandecasteele, M., Glowinski, J., Venance, L., (2006). Connexin mRNA expression in single dopaminergic neurons of substantia nigra pars compacta. Neuroscience Research 56, 419–426. https://doi.org/10.1016/j.neures.2006.08.013

Vandecasteele, M., Glowinski, J., Venance, L., (2005). Electrical Synapses between Dopaminergic Neurons of the Substantia Nigra Pars Compacta. Journal of Neuroscience 25, 291–298. https://doi.org/10.1523/JNEUROSCI.4167-04.2005

Villafane, G., Cesaro, P., Rialland, A., Baloul, S., Azimi, S., Bourdet, C., Le Houezec, J., Macquin-Mavier, I., Maison, P., (2007). Chronic high dose transdermal nicotine in Parkinson's disease: an open trial. European Journal of Neurology. 14, 1313–1316. https://doi.org/10.1111/j.1468-1331.2007.01949.x

Villemagne, V.L., Burnham, S., Bourgeat, P., Brown, B., Ellis, K.A., Salvado, O., Szoeke, C., Macaulay, S.L., Martins, R., Maruff, P., Ames, D., Rowe, C.C., Masters, C.L., (2013). Amyloid β deposition, neurodegeneration, and cognitive decline in sporadic Alzheimer's disease: a prospective cohort study. The Lancet Neurology 12, 357–367. https://doi.org/10.1016/S1474-4422(13)70044-9

Wahlqvist, M.L., Lee, M.-S., Hsu, C.-C., Chuang, S.-Y., Lee, J.-T., Tsai, H.-N., (2012). Metformin-inclusive sulfonylurea therapy reduces the risk of Parkinson's disease occurring with Type 2 diabetes in a Taiwanese population cohort. Parkinsonism & Related Disorders 18, 753–758. https://doi.org/10.1016/j.parkreldis.2012.03.010

Wall, M.J., Collins, D.R., Chery, S.L., Allen, Z.D., Pastuzyn, E.D., George, A.J., Nikolova, V.D., Moy, S.S., Philpot, B.D., Shepherd, J.D., Müller, J., Ehlers, M.D., Mabb, A.M., Corrêa, S.A.L., (2018). The Temporal Dynamics of Arc Expression Regulate Cognitive Flexibility. Neuron 98, 1124-1132.e7. https://doi.org/10.1016/j.neuron.2018.05.012

Walsh, D.M., Klyubin, I., Fadeeva, J.V., Cullen, W.K., Anwyl, R., Wolfe, M.S., Rowan, M.J., Selkoe, D.J., (2002). Naturally secreted oligomers of amyloid beta protein potently inhibit hippocampal long-term potentiation in vivo. Nature 416, 535–539. https://doi.org/10.1038/416535a

Walsh, D.M., Selkoe, D.J., (2016). A critical appraisal of the pathogenic protein spread hypothesis of neurodegeneration. Nature Reviews Neuroscience 17, 251–260. https://doi.org/10.1038/nrn.2016.13

Wang, G.J., Volkow, N.D., Fowler, J.S., Cervany, P., Hitzemann, R.J., Pappas, N.R., Wong, C.T., Felder, C., (1999). Regional brain metabolic activation during craving elicited by recall of previous drug experiences. Life Sciences 64, 775–784. https://doi.org/10.1016/s0024-3205(98)00619-5

Wang, F., Shi, Y., Lu, L., Liu, L., Cai, Y., Zheng, H., Liu, X., Yan, F., Zou, C., Sun, C., Shi, J., Lu, S., Chen, Y., (2012). Targeted Delivery of GDNF through the Blood–Brain Barrier by MRI-Guided Focused Ultrasound. PLOS ONE 7, e52925. https://doi.org/10.1371/journal.pone.0052925

Wang, J., Ou, S.-W., Wang, Y.-J., (2017). Distribution and function of voltage-gated sodium channels in the nervous system. Channels 11, 534–554. https://doi.org/10.1080/19336950.2017.1380758

Wang, J.-Z., Xia, Y.-Y., Grundke-Iqbal, I., Iqbal, K., (2013). Abnormal hyperphosphorylation of tau: sites, regulation, and molecular mechanism of neurofibrillary degeneration. Journal of Alzheimer's disease 33 Suppl 1, S123-139. https://doi.org/10.3233/JAD-2012-129031

Wang, S., Benamer, N., Zanella, S., Kumar, N.N., Shi, Y., Bévengut, M., Penton, D., Guyenet, P.G., Lesage, F., Gestreau, C., Barhanin, J., Bayliss, D.A., (2013). TASK-2 Channels Contribute to pH Sensitivity of Retrotrapezoid Nucleus Chemoreceptor Neurons. Journal of Neuroscience. 33, 16033–16044. doi.org/10.1523/JNEUROSCI.2451-13.2013

Wang, Y., Mandelkow, E., (2016). Tau in physiology and pathology. Nature Reviews Neuroscience 17, 5–21. https://doi.org/10.1038/nrn.2015.1

Watanabe, E., Hiyama, T.Y., Shimizu, H., Kodama, R., Hayashi, N., Miyata, S., Yanagawa, Y., Obata, K., Noda, M., (2006). Sodium-level-sensitive sodium channel Nax is expressed in glial laminate processes in the sensory circumventricular organs. American Journal of Physiology - Regulatory, Integrative and Comparative Physiology 290, R568–R576. https://doi.org/10.1152/ajpregu.00618.2005

Waung, M.W., Pfeiffer, B.E., Nosyreva, E.D., Ronesi, J.A., Huber, K.M., (2008). Rapid translation of Arc/Arg3.1 selectively mediates mGluR-

dependent LTD through persistent increases in AMPAR endocytosis rate. Neuron 59, 84–97. https://doi.org/10.1016/j.neuron.2008.05.014

Weber, P.A., Chang, H.-C., Spaeth, K.E., Nitsche, J.M., Nicholson, B.J., (2004). The Permeability of Gap Junction Channels to Probes of Different Size Is Dependent on Connexin Composition and Permeant-Pore Affinities. Biophysical Journal 87, 958–973. https://doi.org/10.1529/biophysj.103.036350

Wegmann, S., Nicholls, S., Takeda, S., Fan, Z., Hyman, B.T., (2016). Formation, release, and internalization of stable tau oligomers in cells. Journal of Neurochemistry 139, 1163–1174. doi.org/10.1111/jnc.13866

Weissman, T.A., Riquelme, P.A., Ivic, L., Flint, A.C., Kriegstein, A.R., (2004). Calcium waves propagate through radial glial cells and modulate proliferation in the developing neocortex. Neuron 43, 647–661. https://doi.org/10.1016/j.neuron.2004.08.015

White, J.A., Sekar, N.S., Kay, A.R., (1995). Errors in persistent inward currents generated by space-clamp errors: a modeling study. Journal of Neurophysiology 73, 2369–2377. doi.org/10.1152/jn.1995.73.6.2369

Whone, A., Luz, M., Boca, M., Woolley, M., Mooney, L., Dharia, S., Broadfoot, J., Cronin, D., Schroers, C., Barua, N.U., Longpre, L., Barclay, C.L., Boiko, C., Johnson, G.A., Fibiger, H.C., Harrison, R., Lewis, O., Pritchard, G., Howell, M., Irving, C., Johnson, D., Kinch, S., Marshall, C., Lawrence, A.D., Blinder, S., Sossi, V., Stoessl, A.J., Skinner, P., Mohr, E., Gill, S.S., (2019). Randomized trial of intermittent intraputamenal glial cell line-derived neurotrophic factor in Parkinson's disease. Brain 142, 512–525. https://doi.org/10.1093/brain/awz023

Widner, H., Tetrud, J., Rehncrona, S., Snow, B., Brundin, P., Gustavii, B., Björklund, A., Lindvall, O., Langston, J.W., (1992). Bilateral Fetal Mesencephalic Grafting in Two Patients with Parkinsonism Induced by 1-Methyl-4-Phenyl-L,2,3,6-Tetrahydropyridine (MPTP). New England Journal of Medicine 327, 1556–1563. https://doi.org/10.1056/NEJM199211263272203

Willecke, K., Eiberger, J., Degen, J., Eckardt, D., Romualdi, A., Güldenagel, M., Deutsch, U., Söhl, G., (2002). Structural and functional diversity of connexin genes in the mouse and human genome. Biological Chemistry 383, 725–737. https://doi.org/10.1515/BC.2002.076

Wilson, D.F., Pastuszko, A., DiGiacomo, J.E., Pawlowski, M., Schneiderman, R., Delivoria-Papadopoulos, M., (1991). Effect of hyperventilation on oxygenation of the brain cortex of newborn piglets. Journal of Applied Physiology Bethesda Md 1985 70, 2691–2696. https://doi.org/10.1152/jappl.1991.70.6.2691

Winblad, B., Palmer, K., Kivipelto, M., Jelic, V., Fratiglioni, L., Wahlund, L.-O., Nordberg, A., Bäckman, L., Albert, M., Almkvist, O., Arai, H., Basun, H., Blennow, K., Leon, M.D., DeCarli, C., Erkinjuntti, T., Giacobini, E., Graff, C., Hardy, J., Jack, C., Jorm, A., Ritchie, K., Duijn, C.V., Visser, P., Petersen, R.C., (2004). Mild cognitive impairment – beyond controversies, towards a consensus: report of the International Working Group on Mild Cognitive Impairment. Journal of Internal Medicine 256, 240–246. https://doi.org/10.1111/j.1365-2796.2004.01380.x

Winner, B., Jappelli, R., Maji, S.K., Desplats, P.A., Boyer, L., Aigner, S., Hetzer, C., Loher, T., Vilar, M., Campioni, S., Tzitzilonis, C., Soragni, A., Jessberger, S., Mira, H., Consiglio, A., Pham, E., Masliah, E., Gage, F.H., Riek, R., (2011). In vivo demonstration that αSynuclein oligomers are toxic. Proceedings of the National Academy of Sciences 108, 4194–4199. https://doi.org/10.1073/pnas.1100976108

Wischik, C.M., Harrington, C.R., Storey, J.M.D., (2014). Tau-aggregation inhibitor therapy for Alzheimer's disease. Biochemical Pharmacology 88, 529–539. https://doi.org/10.1016/j.bcp.2013.12.008

Wittmann, C.W., Wszolek, M.F., Shulman, J.M., Salvaterra, P.M., Lewis, J., Hutton, M., Feany, M.B., (2001). Tauopathy in Drosophila: neurodegeneration without neurofibrillary tangles. Science 293, 711–714. https://doi.org/10.1126/science.1062382

Wolf, M.E., Roth, R.H., (1990). Autoreceptor Regulation of Dopamine Synthesis. Annals of the New York Academy of Sciences 604, 323–343. https://doi.org/10.1111/j.1749-6632.1990.tb32003.x

Wykes, R., Kalmbach, A., Eliava, M., Waters, J., (2012). Changes in the physiology of CA1 hippocampal pyramidal neurons in pre-plaque CRND8 mice. Neurobiology of Aging 33, 1609–1623. https://doi.org/10.1016/j.neurobiolaging.2011.05.001

Xu, K., Xu, Y.-H., Chen, J.-F., Schwarzschild, M.A., (2002). Caffeine's neuroprotection against 1-methyl-4-phenyl-1,2,3,6-tetrahydropyridine toxicity shows no tolerance to chronic caffeine administration in mice. Neuroscience Letters. 322, 13–16. https://doi.org/10.1016/S0304-3940(02)00069-1

Yahr, M.D., Duvoisin, R.C., Schear, M.J., Barrett, R.E., Hoehn, M.M., (1969). Treatment of parkinsonism with levodopa. Archives of Neurology 21, 343–354. https://doi.org/10.1001/archneur.1969.00480160015001

Yamada, K., Holth, J.K., Liao, F., Stewart, F.R., Mahan, T.E., Jiang, H., Cirrito, J.R., Patel, T.K., Hochgräfe, K., Mandelkow, E.-M., Holtzman, D.M., (2014). Neuronal activity regulates extracellular tau in vivo. The Journal

of Experimental Medicine 211, 387–393. https://doi.org/10.1084/jem.20131685

Yamamoto-Sasaki, M., Ozawa, H., Saito, T., Rösler, M., Riederer, P., (1999). Impaired phosphorylation of cyclic AMP response element binding protein in the hippocampus of dementia of the Alzheimer type. Brain Research 824, 300–303. https://doi.org/10.1016/s0006-8993(99)01220-2

Yanamandra, K., Jiang, H., Mahan, T.E., Maloney, S.E., Wozniak, D.F., Diamond, M.I., Holtzman, D.M., (2015). Anti-tau antibody reduces insoluble tau and decreases brain atrophy. Annals of Clinical and Translational Neurology 2, 278–288. https://doi.org/10.1002/acn3.176

Yanamandra, K., Kfoury, N., Jiang, H., Mahan, T.E., Ma, S., Maloney, S.E., Wozniak, D.F., Diamond, M.I., Holtzman, D.M., (2013). Anti-Tau Antibodies that Block Tau Aggregate Seeding In Vitro Markedly Decrease Pathology and Improve Cognition In Vivo. Neuron 80, 402–414. https://doi.org/10.1016/j.neuron.2013.07.046

Yin, Y., Gao, D., Wang, Y., Wang, Z.-H., Wang, X., Ye, J., Wu, D., Fang, L., Pi, G., Yang, Y., Wang, X.-C., Lu, C., Ye, K., Wang, J.-Z., (2016). Tau accumulation induces synaptic impairment and memory deficit by calcineurin-mediated inactivation of nuclear CaMKIV/CREB signaling. Proceedings of the National Academy of Sciences 113, E3773-3781. https://doi.org/10.1073/pnas.1604519113

Yoo, J.H., Zell, V., Gutierrez-Reed, N., Wu, J., Ressler, R., Shenasa, M.A., Johnson, A.B., Fife, K.H., Faget, L., Hnasko, T.S., (2016). Ventral tegmental area glutamate neurons co-release GABA and promote positive reinforcement. Nature Communications 7, 13697. https://doi.org/10.1038/ncomms13697

Yoshiyama, Y., Higuchi, M., Zhang, B., Huang, S.-M., Iwata, N., Saido, T.C., Maeda, J., Suhara, T., Trojanowski, J.Q., Lee, V.M.-Y., (2007). Synapse loss and microglial activation precede tangles in a P301S tauopathy mouse model. Neuron 53, 337–351. https://doi.org/10.1016/j.neuron.2007.01.010

Yu, X., Ba, W., Zhao, G., Ma, Y., Harding, E.C., Yin, L., Wang, D., Li, H., Zhang, P., Shi, Y., Yustos, R., Vyssotski, A.L., Dong, H., Franks, N.P., Wisden, W., (2020). Dysfunction of ventral tegmental area GABA neurons causes mania-like behavior. Molecular Psychiatry 1–16. https://doi.org/10.1038/s41380-020-0810-9

Yu, X., Li, W., Ma, Y., Tossell, K., Harris, J.J., Harding, E.C., Ba, W., Miracca, G., Wang, D., Li, L., Guo, J., Chen, M., Li, Y., Yustos, R., Vyssotski, A.L., Burdakov, D., Yang, Q., Dong, H., Franks, N.P., Wisden, W.,

(2019). GABA and glutamate neurons in the VTA regulate sleep and wakefulness. Nature Neuroscience 22, 106–119. https://doi.org/10.1038/s41593-018-0288-9

Zempel, H., Luedtke, J., Kumar, Y., Biernat, J., Dawson, H., Mandelkow, E., Mandelkow, E.-M., (2013). Amyloid-β oligomers induce synaptic damage via Tau-dependent microtubule severing by TTLL6 and spastin. EMBO Journal 32, 2920–2937. https://doi.org/10.1038/emboj.2013.207

Zetterberg, H., (2019). Blood-based biomarkers for Alzheimer's disease—An update. Journal of Neuroscience Methods, Methods and Models in Alzheimer's Disease Research 319, 2–6. https://doi.org/10.1016/j.jneumeth.2018.10.025

Zetterberg, H., Bendlin, B.B., (2021). Biomarkers for Alzheimer's disease-preparing for a new era of disease-modifying therapies. Molecular Psychiatry 26, 296–308. https://doi.org/10.1038/s41380-020-0721-9

Zetterberg, H., Burnham, S.C., (2019). Blood-based molecular biomarkers for Alzheimer's disease. Molecular Brain 12, 26. https://doi.org/10.1186/s13041-019-0448-1

Zhang, J., Xia, J., Xiong, H., (2014). Techniques for Extracellular Recordings, in: Xiong, H., Gendelman, H.E. (Eds.), Current Laboratory Methods in Neuroscience Research, Springer Protocols Handbooks. Springer, New York, NY, pp. 325–345. https://doi.org/10.1007/978-1-4614-8794-4_23

Zhang, S.M., Hernán, M.A., Chen, H., Spiegelman, D., Willett, W.C., Ascherio, A., (2002). Intakes of vitamins E and C, carotenoids, vitamin supplements, and PD risk. Neurology 59, 1161–1169. https://doi.org/10.1212/01.wnl.0000028688.75881.12

Zhang, D., Bordia, T., McGregor, M., McIntosh, J.M., Decker, M.W., Quik, M., (2014a). ABT-089 and ABT-894 reduce levodopa-induced dyskinesias in a monkey model of Parkinson's disease. Journal of Movement Disorders. 29, 508–517. https://doi.org/10.1002/mds.25817

Zhang, D., McGregor, M., Decker, M.W., Quik, M., (2014b). The α7 nicotinic receptor agonist ABT-107 decreases L-Dopa-induced dyskinesias in parkinsonian monkeys. Journal of Pharmacology and Experimental Therapeutics 351, 25–32. https://doi.org/10.1124/jpet.114.216283

Zhou, L., McInnes, J., Wierda, K., Holt, M., Herrmann, A.G., Jackson, R.J., Wang, Y.-C., Swerts, J., Beyens, J., Miskiewicz, K., Vilain, S., Dewachter, I., Moechars, D., De Strooper, B., Spires-Jones, T.L., De Wit, J., Verstreken, P., (2017). Tau association with synaptic vesicles

causes presynaptic dysfunction. Nature Communications 8, 15295. https://doi.org/10.1038/ncomms15295

Zimprich, A., Biskup, S., Leitner, P., Lichtner, P., Farrer, M., Lincoln, S., Kachergus, J., Hulihan, M., Uitti, R.J., Calne, D.B., Stoessl, A.J., Pfeiffer, R.F., Patenge, N., Carbajal, I.C., Vieregge, P., Asmus, F., Müller-Myhsok, B., Dickson, D.W., Meitinger, T., Strom, T.M., Wszolek, Z.K., Gasser, T., (2004). Mutations in LRRK2 cause autosomal-dominant parkinsonism with pleomorphic pathology. Neuron 44, 601–607. https://doi.org/10.1016/j.neuron.2004.11.005

Appendix

8.1 Materials

Drug/ pharmacological agent	Company	Catalog Number
Acrylamide/bisacrylamide (30 % solution)	Sigma Aldrich	A3574
Ammonium persulfate (APS)	Sigma Aldrich	A3678
BamHI	Fisher	ER0051
Bicinchoninic Acid (BCA)	G Biosciences	786-570
Bovine Serum Albumin (BSA)	Sigma Aldrich	A7906
Carbenoxolone disodium salt	Sigma Aldrich	C4790
Chelating sepharose resin	GE Healthcare	17-0575-01
CutSmart Buffer	New England Biolabs	B7204S
D-Glucose	Fisher	0500/53
DHPG ((RS)-3,5-DHPG)	Tocris/ Biotechne	0342/1
Dopamine Hydrochloride	Sigma Aldrich	H8502
DTT (1,4-Dithiothreitol)	Sigma Aldrich	10197777001
EcoRI	Invitrogen	IVGN0116
EGTA	Sigma Aldrich	A102X
HEPES	Sigma Aldrich	H4034
Imidazole	Sigma Aldrich	I2399
IPTG (Isopropyl β-D-thiogalactoside)	Sigma Aldrich	I6758
KCl	Fisher	4280/53
KH_2PO_4	Fisher	4800/53

L-689,560	Tocris/ Biotechne	0742
Met5[enkephalin]	Merck	M6638
MgATP	Sigma Aldrich	A3377
$MgSO_4$	Fisher	1050/53
Milk powder	Marvel, Uk	NA
Monarch plasmid miniprep kit	New England Biolabs	T1010
N, N, N', N'-tetramethylethylenediamine (TEMED)	Sigma Aldrich	T-7024
NaCl	Fisher	3160/65
NaGTP	Merck	G8877
$NaHCO_3$	Fisher	4240/60
NaOAc	Fisher	2120/53
$NiCl_2$	Sigma Aldrich	339350
Phosphocreatine	Sigma Aldrich	1001244549
Picrotoxin	Sigma Aldrich	P1675
Potassium Gluconate	Sigma Aldrich	299-27-4
Protease Inhibitor tablets	Thermofisher Scientific	A32963
Site directed mutagenesis kit (Q5)	New England Biolabs	E0554S
SOC medium	Sigma Aldrich	S1797
Sodium dodecyl sulfate (SDS)	Sigma Aldrich	L3771
TCEP (Tris(2-carboxyethyl)phosphine hydrochloride)	Sigma Aldrich	C4706

Triton x100	Fisher	9002-93-1
Tween 20	Sigma Aldrich	1379
ZD 7288	Hello-Bio	HB1152

Primary antibodies

Primary Antibody	**Company**	**Catalog Number**	**Optimal concentration**
HT7 anti-human Tau Mouse	Thermo Scientific	MN1000	1:1000
T22 oligomeric tau Antibody	Merck	ABN454	1:1000
Polyclonal rabbit anti-human tau. Epitope: C terminus of 2N4R tau	Dako	A0024	1:5000
Sheep polyclonal Anti-Tyrosine hydroxylase	Merck	AB1542	1:1000
Mouse monoclonal anti-Connexin 26	Novex Life Technologies	138100	1:200
Chicken polyclonal anti-GFAP	Abcam	ab4674	1:1000
Rabbit polyclonal anti-GAD65 + GAD67	Abcam	ab49832	1:1000

Secondary antibodies

Secondary Antibody	Company	Catalog Number
Alexa Fluor 594-conjugated AffiniPure Goat anti-mouse IgG + IgM (H + L) 1:400	Jackson Immuno	115-585-044
Rabbit Anti-mouse (IgG (H+L), horseradish peroxidase 1:1000	Thermofisher	61-6520
Goat anti-rabbit IgG	Thermo Scientific	31460
Goat Anti-rabbit 1:1000 488	Invitrogen	A11008
Alexa Fluor 594 Donkey anti-rabbit 1:250	Invitrogen	A-21207
Alexa Fluor 594 Donkey anti-sheep 1:250	Invitrogen	A11016
Alexa Fluor 594 anti-mouse Connexin 26 1:250	Novex Life Technologies	138100
Donkey anti-mouse 594	Invitrogen	A21203
Donkey anti-sheep 488	Invitrogen	A-11015

Fluorescent dyes and imaging

Antibody	Company	Catalog Number
Alexa Fluor 488 C5-maleimide	Molecular Probes	A10254
Alexa Fluor 488 Hydrazide (12.5 mM stock in distilled water, stored at -20 degrees)	Thermofisher	A10436
Clarity Western ECL Substrate	BioRad	1705060
Alexa Fluor 594 Hydrazide (12.5 mM stock in distilled water, stored at -20 degrees)	Thermofisher	10072752
(6)-Carboxy-fluorescein (CBF)	Novabiochem	8.51082.001
Vectashield mounting medium	Vector Laboratories	H-5000
InstantBlue Protein Stain	Expedeon	ISB1L

Consumables

Product	Company	Catalog Number
Slide-A-Lyzer Mini Dialysis devices (10K) MWCO	Thermo Scientific	69570
Formvar/carbon coated 300 – mesh copper grids	Agar Scientific	162
ECL Nitrocellulose membrane	Amersham Biosciences	10600002
Patch pipettes: GC150F-10STD WALL W/FILAMENT 1.5mmOD	Multichannel Systems	300057

8.2 Tau DNA and protein sequences

Original full-length DNA Sequence

ATGGCTGAGCCCCGCCAGGAGTTCGAAGTGATGGAAGATCACGCTGGG
ACGTACGGGTTGGGGGACAGGAAAGATCAGGGGGGCTACACCATGCA
CCAAGACCAAGAGGGTGACACGGACGCTGGCCTGAAAGAATCTCCCCT
GCAGACCCCCACTGAGGACGGATCTGAGGAACCGGGCTCTGAAACCTC
TGATGCTAAGAGCACTCCAACAGCGGAAGATGTGACAGCACCCTTAGT
GGATGAGGGAGCTCCCGGCAAGCAGGCTGCCGCGCAGCCCCACACGG
AGATCCCAGAAGGAACCACAGCTGAAGAAGCAGGCATTGGAGACACCC
CCAGCCTGGAAGACGAAGCTGCTGGTCACGTGACCCAAGCTCGCATGG
TCAGTAAAAGCAAAGACGGGACTGGAAGCGATGACAAAAAAGCCAAGG
GGGCTGATGGTAAAACGAAGATCGCCACACCGCGGGGAGCAGCCCCT
CCAGGCCAGAAGGGCCAGGCCAACGCCACCAGGATTCCAGCAAAAACC
CCGCCCGCTCCAAAGACACCACCCAGCTCTGGTGAACCTCCAAAATCA
GGGGATCGCAGCGGCTACAGCAGCCCCGGCTCCCCAGGCACTCCCGG
CAGCCGCTCCCGCACCCCGTCCCTTCCAACCCCACCCACCCGGGAGC
CCAAGAAGGTGGCAGTGGTCCGTACTCCACCCAAGTCGCCGTCTTCCG
CCAAGAGCCGCCTGCAGACAGCCCCCGTGCCCATGCCAGACCTGAAGA
ATGTCAAGTCCAAGATCGGCTCCACTGAGAACCTGAAGCACCAGCCGG
GAGGCGGGAAGGTGCAGATAATTAATAAGAAGCTGGATCTTAGCAACGT
CCAGTCCAAGTGTGGCTCAAAGGATAATATCAAACACGTCCCGGGAGG

CGGCAGTGTGCAAATAGTCTACAAACCAGTTGACCTGAGCAAGGTGAC
CTCCAAGTGTGGCTCATTAGGCAACATCCATCATAAACCAGGAGGTGGC
CAGGTGGAAGTAAAATCTGAGAAGCTTGACTTCAAGGACAGAGTCCAGT
CGAAGATTGGGTCCCTGGACAATATCACCCACGTCCCTGGCGGAGGAA
ATAAAAAGATTGAAACCCACAAGCTGACCTTCCGCGAGAACGCCAAAGC
CAAGACAGACCACGGGGCGGAGATCGTGTACAAGTCGCCAGTGGTGTC
TGGGGACACGTCTCCACGGCATCTCAGCAATGTCTCCTCCACCGGCAG
CATCGACATGGTAGACTCGCCCCAGCTCGCCACGCTAGCTGACGAGGT
GTCTGCCTCCCTGGCCAAGCAGGGTTTGTGA

Original full-length protein

MAEPRQEFEVMEDHAGTYGLGDRKDQGGYTMHQDQEGDTDAGLKESPL
QTPTEDGSEEPGSETSDAKSTPTAEDVTAPLVDEGAPGKQAAAQPHTEIPE
GTTAEEAGIGDTPSLEDEAAGHVTQARMVSKSKDGTGSDDKKAKGADGKT
KIATPRGAAPPGQKGQANATRIPAKTPPAPKTPPSSGEPPKSGDRSGYSSP
GSPGTPGSRSRTPSLPTPPTREPKKVAVVRTPPKSPSSAKSRLQTAPVPM
PDLKNVKSKIGSTENLKHQPGGGKVQIINKKLDLSNVQSKCGSKDNIKHVPG
GGSVQIVYKPVDLSKVTSKCGSLGNIHHKPGGGQVEVKSEKLDFKDRVQS
KIGSLDNITHVPGGGNKKIETHKLTFRENAKAKTDHGAEIVYKSPVVSGDTS
PRHLSNVSSTGSIDMVDSPQLATLADEVSASLAKQGL

Truncated DNA sequence

ATGAGCCTGGAAGACGAAGCTGCTGGTCACGTGACCCAAGCTCGCATG
GTCAGTAAAAGCAAAGACGGGACTGGAAGCGATGACAAAAAAGCCAAG
GGGGCTGATGGTAAAACGAAGATCGCCACACCGCGGGGAGCAGCCCC
TCCAGGCCAGAAGGGCCAGGCCAACGCCACCAGGATTCCAGCAAAAAC
CCCGCCCGCTCCAAAGACACCACCCAGCTCTGGTGAACCTCCAAAATC
AGGGGATCGCAGCGGCTACAGCAGCCCCGGCTCCCCAGGCACTCCCG
GCAGCCGCTCCCGCACCCCGTCCCTTCCAACCCCACCCACCCGGGAG
CCCAAGAAGGTGGCAGTGGTCCGTACTCCACCCAAGTCGCCGTCTTCC
GCCAAGAGCCGCCTGCAGACAGCCCCCGTGCCCATGCCAGACCTGAA
GAATGTCAAGTCCAAGATCGGCTCCACTGAGAACCTGAAGCACCAGCC
GGGAGGCGGGAAGGTGCAGATAATTAATAAGAAGCTGGATCTTAGCAA
CGTCCAGTCCAAGTGTGGCTCAAAGGATAATATCAAACACGTCCCGGGA

GGCGGCAGTGTGCAAATAGTCTACAAACCAGTTGACCTGAGCAAGGTG
ACCTCCAAGTGTGGCTCATTAGGCAACATCCATCATAAACCAGGAGGTG
GCCAGGTGGAAGTAAAATCTGAGAAGCTTGACTTCAAGGACAGAGTCCA
GTCGAAGATTGGGTCCCTGGACAATATCACCCACGTCCCTGGCGGAGG
AAATAAAAAGATTGAAACCCACAAGCTGACCTTCCGCGAGAACGCCAAA
GCCAAGACAGACCACGGGGCGGAGATCGTGTACAAGTCGCCAGTGGT
GTCTGGGGACACGTCTCCACGGCATCTCAGCAATGTCTCCTCCACCGG
CAGCATCGACATGGTAGACTCGCCCCAGCTCGCCACGCTAGCTGACGA
GGTGTCTGCCTCCCTGGCCAAGCAGGGTTTGTGA

Truncated Protein sequence

MSLEDEAAGHVTQARMVSKSKDGTGSDDKKAKGADGKTKIATPRGAAPP
GQKGQANATRIPAKTPPAPKTPPSSGEPPKSGDRSGYSSPGSPGTPGSRS
RTPSLPTPPTREPKKVAVVRTPPKSPSSAKSRLQTAPVPMPDLKNVKSKIG
STENLKHQPGGGKVQIINKKLDLSNVQSKCGSKDNIKHVPGGGSVQIVYKP
VDLSKVTSKCGSLGNIHHKPGGGQVEVKSEKLDFKDRVQSKIGSLDNITHV
PGGGNKKIETHKLTFRENAKAKTDHGAEIVYKSPVVSGDTSPRHLSNVSST
GSIDMVDSPQLATLADEVSASLAKQGL

8.3 Production of tau truncations

I spent three months working towards producing C^{FRAG} tau (see methods for full details). I used the full length wild-type plasmid and performed site directed mutagenesis (NEB Q5 Kit) to remove amino acids 1-123. I left the initial methionine in place for structural integrity. Following mutagenesis, samples were transformed into competent cells and grown LB + ampicillin plates. Plamsid DNA was recovered using a Monarch Miniprep kit and a DNA double digest with BamHI and EcoRI performed to look for successful mutagenesis using gel electrophoresis (Figure 8.1). Undigested full-length samples should give a 1.4kb fragment and successful mutagenesis should give a 1.1kb fragment.

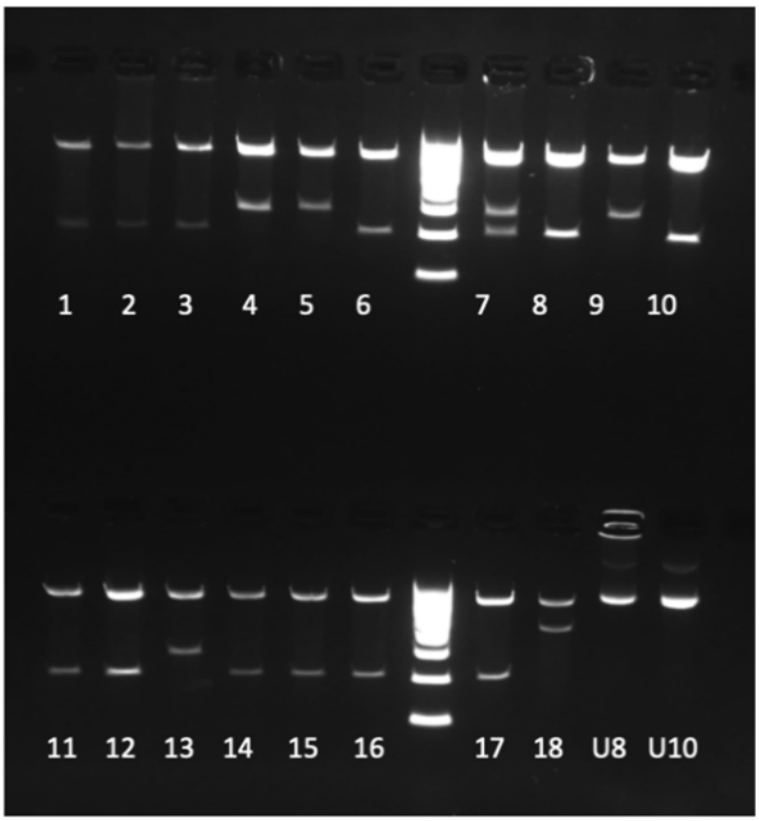

Figure 8.1: DNA gel electrophoresis following double restriction digest to look for successful site directed mutagenesis clones.

The gel confirms that 12 out of the 18 samples were successfully digested. Sample 7 was discarded as it appeared to have two bands. Samples U8 and U10 represent the undigested sample controls that were run to ensure validity of results. Ladders (middle) were used for comparison of band sizes.

Samples that had successfully been mutated were sent for sanger sequencing (Eurofins) to confirm the correct mutation, to confirm that they are in the correct frame and that the cysteine residue mutations had been maintained during the mutagenesis. These samples (that were confirmed to have correct sequences) were then transformed into competent cells and grown on LB + ampicillin plates overnight, picked and transferred directly into LB + ampicillin and allowed to grow overnight. The next morning samples began the expression and purification protocol as for FL tau (see Methods). I used hand cast SDS page gels (Fig 8.2 A, B) to look for the presence of protein for the two preparations. The only protein expected to be present is tau and therefore I was expecting one band. However, there were lots of other contaminating bands. This could be because the gradient of the column had not worked as it

should, and other contaminants had not been washed thoroughly before the eluted protein. I therefore pooled the middle fractions with the highest protein content from the samples in gel A (Fig 8.2A; black box) and re-ran the purification column, with extra wash steps of buffer A and B to ensure that any product that is not tightly bound to the column (tau: due to its his tag) should have been washed through before buffer C was used to elute the protein. This did reduce the prominence of the extra bands (Fig 8.2C) and the samples on the right hand side (Fig 8.2C; orange box) are fairly pure. I therefore ran a western blot to confirm whether it was tau (using the Ht7 monoclonal tau antibody; Fig 8.2D). This confirmed that the preparations are positive for tau, the contamination is still too prominent to isolate the tau.

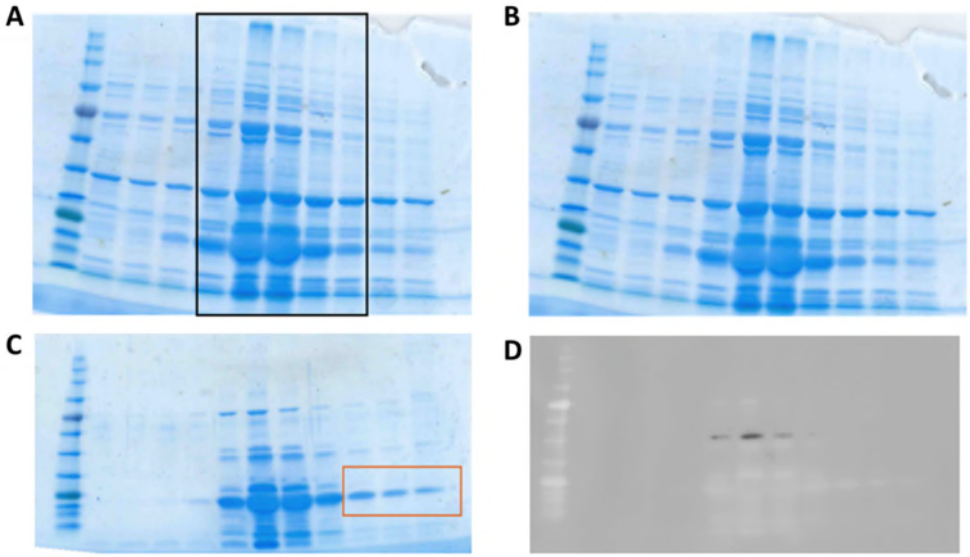

Figure 8.2: SDS-page gels confirm that the purification stage has been unsuccessful due to the presence of lots of additional contamination bands.

SDS-page gels to confirm the purity of the tau truncation preparations. There is a lot of contamination within both of the preparations (A and B), as displayed by additional bands. (C) Another run of purification with increased wash steps reduced the contamination but was unable to fully isolate the tau as was confirmed by western blot analysis (D).

Due to time constraints this preparation was abandoned, and I sourced a collaboration with a group from the University of Gothenburg who specialise in tau biochemistry to produce this mutant for me.

8.4 Comparison of P7-10 and P17-21 neuronal function

Given that connexin 26 expression was reported to be developmentally regulated. In chapter 6, I tested this using two groups of mice. P7-10 pups, where I expected it to be expressed and P17-21 juvenile mice, where I expected the expression to be gone based on previously published data (Vandecasteele et al 2006). This comparison between age groups could be complicated by the developmental changes to electrophysiological properties, which are known to occur over this period. Therefore firstly, I compared the normal input resistance and resting membrane potential measurements from SNpc DNs of the two age groups (Figure 8.3).

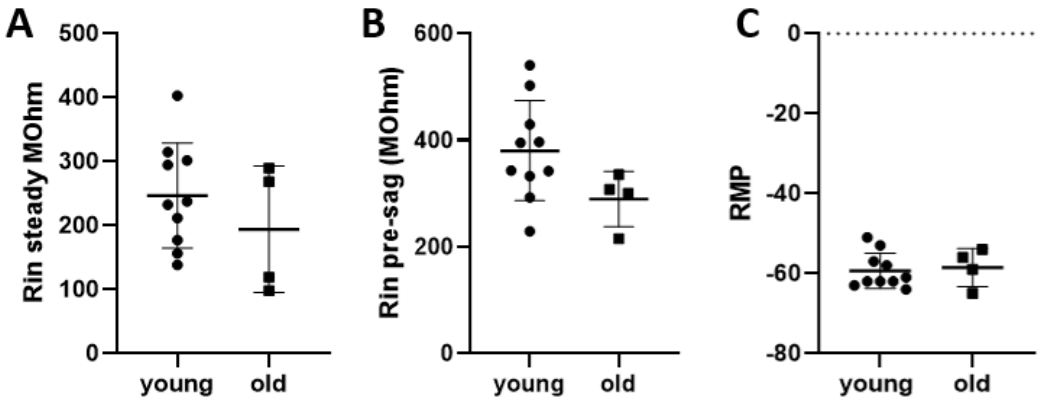

Figure 8.3: Comparison of the baseline electrophysiological parameters of P7-10 and P17-21 SNpc dopaminergic neurons.

Input resistance measurements both at 'steady state' (A) and at 'before the sag' (B) were decreased as the pups aged. This is in line with previously published work (Dufour et al, 2014). We saw no difference in the stability of recordings and there was no change to resting membrane potential (C).

There was no significant difference in input resistance (pre-sag) between the two age groups of mice (P7-10, Rin = 380 ± 28.16 MΩ, P17-21, Rin = 290 ± 22.45 MΩ, p = 0.307). There was also no significant difference in the resting membrane potential (P7-10, RMP = -59.3 ± 1.33 mV, P17-21, RMP = -60 ± 2.08 mV, p = 0.835) or the size of the sag response, measured between the peak hyperpolarisation and steady state after I_H has activated (P7-10: 22.6 ± 2.25 mV, P17-21 20.1 ± 2.3 mV, p = 0.454). These results are consistent with expected values for these age groups of mice as reported in (Dufour et al., 2014).